UNIVERSITÀ
DEGLI STUDI
FIRENZE

PhD in
Earth Sciences
CYCLE XXXIII

COORDINATOR Prof. Lorella Francalanci

Land monitoring through optical and radar remote sensing

Doctoral Candidate
Dr. Luti Tania

Supervisor
Prof. Casagli Nicola

Co-Supervisor
Prof. Munafò Michele

Coordinator
Prof. Francalanci Lorella

UNIVERSITÀ
DEGLI STUDI
FIRENZE

Firmato digitalmente da:
LORELLA FRANCALANCI
Università degli Studi di Firenze
Firmato il: 28-07-2021 01:05:49
Seriale certificato: 662347
Valido dal 29-04-2020 al 29-04-2023

Years 2017/2020

Abstract

The in-depth knowledge of spatial dynamics is an essential prerequisite for implementing sustainable natural resource management policies. In order to analyse the consequences of territorial transformations, and to prevent damage caused by natural disasters or to elaborate models of possible future climate change scenarios, it is necessary to develop analytical tools for an effective assessment of land changes.

The theme of monitoring is present in the United Nations Global Agenda for Sustainable Development and its Sustainable Development Goals (SDGs) to be achieved by 2030 or in initiatives promoted by the European community such as the Copernicus programme or Healthy soils – new European Union (EU) soil strategy, which set the target of zero net consumption to be achieved by 2050.

Thanks to the great progress made in recent decades, remote sensing is increasingly establishing itself as an economic and effective technique for land monitoring, as it allows data to be collected and processed over large areas, and updated with an ever greater frequency and spatial resolution.

Through remote sensing it is possible to classify satellite images in order to produce land cover maps that represent an accurate knowledge base to support different environmental policies related to soil protection. Most of the currently available cartographic products have been produced regionally or for specific purposes with a reduced interoperability and spatial detail. Although CORINE[1] Land Cover (CLC) has been used successfully and is the only homogeneous map at national and European level, its use is limited since it is too coarse to capture the fine details of the landscape at local and regional scale.

The present research, as outlined, starts from an analysis of current policies and data, which is presented in the first part of this dissertation, and is situated in the field of land monitoring. In this context, the study focused on the development of an innovative methodology with the aim of extracting, using remote sensing and Geographic Information System (GIS) tools, information on land cover and changes over very large areas with a good spatial and temporal frequency.

The potential of optical and radar data for land mapping was analysed, with particular attention to some critical issues, such as: soil consumption in its form mainly due to urbanization, landslide susceptibility or the rapid detection of land cover changes linked to natural disasters, in order to quickly have updated data for damage assessment and intervention planning.

The developed methodology uses the multi-temporal acquisition of Sentinel-1 and Sentienel-2 images, in order to detect land transformations in the period of 1 year, between 2017 and 2018 in Italy, chosen as study area. DT are defined to estimate changes at the 10 m pixel size by setting fixed threshold values on the composites (e.g., median, maximum, differences, etc.) of the multi-temporal images; particular attention was paid to the study of an innovative classification algorithm based on a range of spectral signatures of the optical image and the changes associated with the increase and decrease of backscattering in multi-temporal Sentinel-1, i.e. Synthetic-Aperture Radar (SAR) images.

In order to work with large areas, the Google Earth Engine was used as it provides the possibility to work on time series of satellite images and perform calculations on a free online platform, as well as develop algorithms for data processing. In this analysis, only changes visible on an annual basis have been considered, such as land consumption phenomena, some changes in the natural environment and land renaturation, through which the net land consumption can be calculated.

The methodology was satisfactory, reaching an accuracy of 83% in terms of overall accuracy, but with values reaching over 90% in the case of some specific classes. The affected areas of change related to fires showed a good alignment with the data present in the study. The European Forest Fire Information System (EFFIS), (a system to support the services responsible for protecting forests against fire in the EU, even if a direct comparison is not possible because the data are underestimated and only present for major fires.

[1] Coordination of Information on the Environment

The data obtained have allowed the elaboration of some useful indicators in order to gain a deeper knowledge of the increase of soil consumption in Italy, in the different administrative regions and in the areas with high and very high landslide and seismic risk.

Soil consumption in such areas was also analysed in greater thematic detail (land use) by processing Italian Institute for Environmental Protection and Research (ISPRA) data at the third classification level. In general, the results show a continuous increase of soil consumption, also in areas with high and very high landslide hazard subject to specific building regulations, although lower than the national average.

Soil consumption was used to map landslide susceptibility in a study area in northern Toscana. A methodology was then implemented to understand how to improve the accuracy of the susceptibility map by using, in addition to the "basic" variables widely used in the literature, four parameters derived from the elaborated artificial soil map. The results showed that the soil consumption parameters improved the susceptibility assessment. This represents an innovative contribution as the search literature showed that it is the first time that soil consumption and some variables derived from this information layer have been integrated into a susceptibility map. The use of free and easily available data makes this methodology reproducible in other contexts.

Two case studies were examined, the first one related to the consequences of the volcanic eruptions of 3 July 2019 and 28 August 2019 in Stromboli (Italy), which triggered numerous fires on the island, and the second one related to the case of storm Vaia, which caused extensive forests damages in the North-East regions of Italy. The analysis of land cover changes and the calculation of the Normalized Burn Ratio (NBR) allowed the mapping of the burned areas in Stromboli, while in the case of the Vaia event a study was carried out to select the best variables and methodologies to delimit the areas affected by the event. In both cases, the results obtained made it possible to calculate the affected areas with good accuracy and to deepen our knowledge of the potential of satellite imagery to obtain spatial data quickly.

This research has shown that the methodology developed, and the Sentinel data used in land monitoring presents promising aspects for distinguishing the various classes of cover and changes with a spatial and temporal detail useful for spatial analyses at local scale or for calculating environmental indicators. Some critical points that have emerged are related to spectral confusion in the herbaceous classes or in the case of the precise identification of the clippings, which merit further investigation.

The algorithm has the advantage of having been implemented using free data, open source tools and a classification system elaborated by EIONET[2] Action Group on Land monitoring in Europe (EAGLE) that not only meets the requirements of the EU but is easily comparable with other classification systems. Furthermore, it can be modified relatively easily and is applicable over large areas. All these aspects represent the added value of this research and make the methodology suitable for the needs of different types of users.

Keywords: Remote sensing, image classification, change detection, multispectral images, SAR images, land consumption, landslide susceptibility, soil sealing, land cover.

[2] Action Group on Land monitoring in Europe

Riassunto

La conoscenza approfondita delle dinamiche territoriali costituisce l'essenziale prerequisito per attuare politiche di gestione sostenibile delle risorse naturali. Allo scopo di analizzare le conseguenze delle trasformazioni del territorio, di prevenire i danni provocati da disastri naturali o di elaborare modelli dei possibili futuri scenari dei cambiamenti climatici, è necessario dotarsi di strumenti di analisi per un efficace stima dei cambiamenti del territorio.

Il tema del monitoraggio è presente nell'agenda globale per lo sviluppo sostenibile delle Nazioni Unite e nei relativi obiettivi di sviluppo sostenibile (SDGs) da raggiungere entro il 2030 o nelle iniziative promosse dalla comunità europea come il programma Copernicus o la Healthy soils - nuova strategia dell'Unione Europea per il suolo, che ha fissato l'obiettivo di un consumo netto pari a zero da raggiungere entro il 2050.

Il telerilevamento, grazie ai grandi progressi degli ultimi decenni, si sta sempre più affermando come una tecnica economica ed efficace per il monitoraggio del territorio poiché permette di raccogliere ed elaborare dati su vaste aree e di aggiornarli con una frequenza e una risoluzione spaziale sempre maggiore.

Attraverso il telerilevamento è possibile classificare le immagini satellitari per realizzare mappe del territorio che rappresentano un'accurata base conoscitiva a supporto delle diverse politiche ambientali legate alla protezione del suolo. La maggior parte dei prodotti cartografici attualmente disponibili sono stati prodotti a livello regionale o per scopi specifici con una ridotta interoperabilità e dettaglio spaziale. Anche se il CORINE[3] Land Cover (CLC) è stato utilizzato con successo e rappresenta l'unica mappa omogenea a livello nazionale ed europeo, il suo utilizzo è limitato a causa della bassa risoluzione, non adeguata a catturare i dettagli del paesaggio a scala locale e regionale.

Questa ricerca prende l'avvio da un'indagine sulle politiche di protezione del suolo e sui dati territoriali attualmente disponibili e si colloca nell'ambito del monitoraggio del territorio; questa analisi viene presentata nella prima parte del lavoro. Lo studio si è poi concentrato sullo sviluppo di una nuova metodologia innovativa con l'obiettivo di estrarre, tramite l'uso del telerilevamento e dei sistemi informativi geografici (GIS), informazioni sulla copertura del suolo e dei cambiamenti su aree molto grandi, con una buona frequenza spaziale e temporale.

Sono state analizzate le potenzialità dei dati ottici e radar per la mappatura del territorio con particolare attenzione ad alcune criticità che portano alla degradazione del suolo come: il consumo di suolo nella sua forma principalmente legata all'urbanizzazione, lo studio del modello di suscettibilità alle frane o il rilevamento rapido dei cambiamenti di copertura del suolo legati ai disastri naturali al fine di disporre, in tempi brevi, di dati aggiornati per la valutazione dei danni e la pianificazione degli interventi.

La metodologia sviluppata utilizza l'acquisizione multi-temporale di immagini Sentinel-1 e Sentienel-2, al fine di rilevare le trasformazioni del territorio nel periodo di un anno, tra il 2017 e il 2018 in Italia, scelta come area di studio. Gli alberi decisionali sono definiti per stimare i cambiamenti alla dimensione del pixel di 10 m, impostando valori di soglia fissi sui compositi (es. mediana, massimo, differenze, ecc.) delle immagini multitemporali; particolare attenzione è stata posta sullo studio di un innovativo algoritmo di classificazione basato su una gamma di firme spettrali dell'immagine ottica e sui cambiamenti associati all'aumento e alla diminuzione del backscattering nelle immagini multitemporali radar ad apertura sintetica (SAR) Sentinel-1.

Google Earth Engine è stato utilizzato al fine di lavorare su grandi aree, poiché fornisce la possibilità di lavorare su serie temporali di immagini satellitari ed eseguire calcoli su una piattaforma gratuita online, nonché di sviluppare algoritmi per l'elaborazione dei dati.

In questa analisi sono stati considerati solo i cambiamenti visibili su base annuale come i fenomeni legati al consumo di suolo, alcuni cambiamenti in ambiente naturale e le rinaturalizzazioni del territorio attraverso le quali è possibile calcolare il consumo di suolo netto.

[3] Coordination of Information on the Environment

La metodologia ha ottenuto buoni risultati raggiungendo un'accuratezza pari a 83% in termini di overall accuracy, ma con valori che arrivano a superare il 90% nel caso di alcune classi specifiche. Le aree di cambiamento colpite dagli incendi hanno mostrato un buon allineamento con i dati presenti nell'European Forest Fire Information System (EFFIS), un sistema a supporto dei servizi incaricati della protezione delle foreste dagli incendi nell'Unione Europea, anche se un confronto diretto non è possibile perché i dati sono sottostimati e presenti solo per incendi maggiori.

I dati ottenuti hanno permesso l'elaborazione di alcuni indicatori utili per ottenere una conoscenza più approfondita dell'aumento del consumo di suolo in Italia, nelle diverse regioni amministrative e nelle aree a pericolosità alta e molto alta di frana e sismica.

Il consumo di suolo in tali aree è stato analizzato anche ad un dettaglio tematico maggiore (uso del suolo) elaborando i dati dell'Istituto Superiore per la Protezione e la Ricerca Ambientale (ISPRA) al terzo livello di classificazione. In generale i risultati mostrano un continuo incremento del consumo di suolo, anche nelle aree a pericolosità di frana alta e molto alta soggette a specifiche regole edilizie, seppur più basso della media nazionale. Tali dati, in generale, costituisco una base conoscitiva spaziale ad alto dettaglio per ulteriori analisi e ricerche future grazie presentando un dettaglio spaziale di solo 10 m e un aggiornamento su base annuale.

È stata quindi implementata una metodologia per mappare la suscettibilità di frane in un'area studio della Toscana settentrionale, utilizzando una serie di variabili "di base" (pendio, aspect, copertura del suolo etc.) e anche alcune variabili, derivate dalla mappa del consumo di suolo. I risultati hanno mostrato che i parametri di consumo del suolo hanno migliorato la valutazione della suscettibilità. Questo rappresenta un contributo innovativo, perché dalla ricerca bibliografica, è emerso che è la prima volta che il consumo di suolo e alcune variabili derivate da questo strato informativo, siano stati integrati in una mappa di suscettibilità. L'utilizzo di dati gratuiti e facilmente reperibili rende questa metodologia riproducibile anche in altri contesti.

Sono stati esaminati due casi studio il primo relativo alle conseguenze delle eruzioni vulcaniche del 3 luglio 2019 e del 28 agosto 2019 avvenuti a Stromboli (Italia), che hanno innescato numerosi incendi nell'isola e il secondo relativo al caso della tempesta Vaia che ha causato ingenti danni ai boschi nelle regioni del Nord-Est d'Italia.

L'analisi dei cambiamenti di land cover e il calcolo del Normalized Burn Ratio (NBR) hanno permesso di mappare le aree incendiate a Stromboli, mentre nel caso dell'evento Vaia è stata eseguito uno studio per selezionare le variabili e le metodologie migliori a delimitare le aree colpite dall'evento. In entrambi i casi i risultati ottenuti hanno permesso di calcolare le aree colpite con una buona accuratezza e approfondire le conoscenze sulle potenzialità delle immagini satellitari per ottenere dati territoriali in tempi rapidi.

Questa ricerca ha mostrato che la metodologia elaborata e i dati Sentinel utilizzati per il monitoraggio del territorio presentano aspetti promettenti per distinguere le varie classi di copertura e di cambiamento con un buon dettaglio spaziale e temporale o per il calcolo di indicatori ambientali. Alcune criticità emerse, sono legate alla confusione spettrale nelle classi di vegetazione erbacea o nel caso delle della precisa individuazione delle tagliate, che meritano ulteriori approfondimenti.

L'algoritmo presenta il vantaggio di essere stato implementato utilizzando dati gratuiti, strumenti open source e un sistema di classificazione elaborato dall'EIONET[4] Action Group on Land monitoring in Europe (EAGLE) che rientra non solo nei requisiti richiesti dell'Unione Europea, ma risulta facilmente confrontabile con altri sistemi di classificazione. Inoltre, può essere modificato in maniera relativamente semplice ed è applicabile su vaste aree. Tutti questi aspetti rappresentano il valore aggiunto di questa ricerca e rendono la metodologia adatta alle esigenze di diverse tipologie di utenti.

.

Parole chiave: Telerilevamento, classificazione di immagini, change detection, immagini multispettrali, immagini SAR, consumo di suolo, suscettibilità da frana, impermeabilizzazione del suolo, copertura del suolo.

[4] Action Group on Land monitoring in Europe

Contents

List of Figures

List of Tables

Acronyms

Acronym	Description	Acronym	Description
ANN	Artificial Neural Network	MD	Minimum Distance
BI	Burned Index	MLC	Maximum Likelihood Classification
BOA	Bottom Of Atmosphere	MMU	Minimum Mapping Unit
CLC	CORINE Land Cover	MSI	Moisture Soil Index
CORINE	Coordination of Information on the Environment	NBR	Normalized Burn Ratio
DEM	Digital Elevation Model	NDCI	Normalized Difference Coniferous Index
DN	Digital Number	NDSI	Normalized Difference Snow Index
DT	Decision Tree	NDVI	Normalized Difference Vegetation Index
EAGLE	EIONET Action Group on Land monitoring in Europe	NDWI	Normalized Difference Water Index
EAP	Environment Action Programme	NIR	Near InfraRed
EC	European Commission	PGA	Peak Ground Acceleration
EEA	European Environment Agency	RF	Random Forest
EEC	European Economic Community	ROA	Roads
EFFIS	European Forest Fire Information System	SAR	Synthetic-Aperture Radar
EIA	Environmental Impact Assessment	SDGs	Sustainable Development Goals
EIONET	European environment information and observation network	SEA	Strategic Environmental Assessment
ESA	European Space Agency	SNPA	National System for Environmental Protection
EU	European Union	SOER	State of the Environment Reporting
FUA	Functional Urban Area	SRTM	Shuttle Radar Topography Mission
GIS	Geographic Information System	SS	Soil Sealing
GRD	Ground Range Detected	SSA	Soil Sealing Aggregation
HRL	High Resolution Layers	SVM	Support Vector Machine
ISPRA	Italian Institute for Environmental Protection and Research	SWIR	Short-Wave InfraRed
LC	Land Cover	TIR	Thermal InfraRed
LCC	Land Cover Components	TOA	Top Of Atmosphere
LCH	Further Characteristics	URB	Urbanization
LSM	Landslide Susceptibility Map	UTM	Universal Transverse Mercator
LUA	Land Use Attributes		

Chapter 1 Introduction

.

1.1 Background

Soil protection is one of the major environmental challenges recognised by the United Nations Environment Programme, by European policies and by national governments. The assessment and mapping extent of soil degradation, effective legislation for land monitoring and soil conservation are promoted in various relevant agreements within the International institutional framework. In order to tackle the complex problem of soil protection, the European Commission (EC) has promoted the 7th Environment Action Programme 2020 (7th EAP)(European Union, 2013) to achieve 'no net land take' by 2050 and has also defined the objectives for reducing soil erosion and loss of soil organic matter. Along with the Resources Efficiency Roadmap (European Commission, 2011) these two EU strategies have promoted the political discussion on the quality of the environment and the importance of monitoring it. Although considerable efforts have delivered significant benefits over recent years, soil degradation remains alarming and assessments of recent trends (EEA, 2019) show that policies have not been effective in protecting biodiversity and ecosystems.

Soil is generally defined as "the top layer of the earth's crust, formed by mineral particles, organic matter, water, air and living organisms. It is the interface between earth, air and water and hosts most of the biosphere" (Doula & Sarris, 2016; European Commission, 2006b). It is considered a non-renewable resource because of its very slow rate of formation: it takes several centuries just to reach a centimetre making up a thin layer of soil. It has many functions for all life cycles: it provides macro and micronutrient for the plant, it stores and transforms huge quantities of substance like water, minerals, organic matter. Indeed, soil provides various ecosystem services, among which:

- The supply of services (food and biomass, raw materials, etc.).
- Regulating and maintaining the main natural cycles (climate regulation, carbon capture and storage, control of erosion and nutrients, protection and mitigation of extreme hydrological phenomena, just to mention a few).
- Cultural services (recreational and cultural services).

Urbanization in the form of land consumption represents one of the main drivers of land degradation as referred by the Science-Policy Platform on Biodiversity and Ecosystem Services reports (Montanarella et al., 2018). It has already caused the loss or reduction of ecosystem services in the EU and at global level.
Land consumption is the process referred to an increase in artificial land cover, linked to the dynamics of settlement and infrastructures (definition is reported in the next chapter).
Scientists have long estimated the effects of land consumption on the environment and on land degradation, among which the growth of imperviousness at the expense of agriculture or other natural areas.

The sealing of soils can reduce the exchange of gas, water and energy; furthermore it leads to decreased production, more pollution and higher health risks (Salvati et al., 2011; Scalenghe & Ajmone-Marsan, 2009). The reduction of these surfaces involves a series of impacts linked, for example, to the EU's capacity of food production (Gardi et al., 2015; Imhoff et al., 2004) or to the fragmentation of the flora and fauna habitat for transport infrastructure and commercial/residential buildings. Soil sealing in urban areas increases the risk of floods and pollution. Impervious surfaces alter hydrological cycle and so less water infiltrates to the soil and more water runs off with significant soil implications (reducing groundwater recharge and increasing frequency of flood events (Ruby, 2005). Sealed surfaces absorb heat and increase air temperatures. Many organisms function like filters, degrading, catching, and detoxifying organic and inorganic pollutants, thus preventing secondary contamination of air and water (Naumann et al., 2019).

According to State of the Environment Reporting (SOER) (EEA, 2019), the long-term changes over the period 2000-2018 show that the area of artificial surfaces in Europe has changed the most, increasing by 7.1%; although in recent years this trend has been declining, during the entire period 2000-2018, 921 km²/year of land was turned into artificial surfaces which are predicted to increase by 0.7% by 2050, bringing about greater land consumption and fragmentation. At a global level the situation is not any better: “Globally, more people live in urban areas than in rural areas, with 55% of the world’s population residing in urban areas in 2018” (United Nations, 2018). United Nations Projections estimate that an urbanization process involving a gradual shift of the population from rural to urban areas is expected by 2050 with an increase of 2,5 billion of the urban population. As supported by United Nations, the sustainable development depends heavily on managing urban growth considering that “Between 1990 and 2018, the world’s cities with more than 300,000 inhabitants grew at an average annual rate of 1.8%” (United Nations, 2018).

In general land cover change and brownfield development have significant impacts on the land system (EEA, 2019). As stated by the report of the European Environmental Assessment of Soil for Monitoring (Kibblewhite et al., 2008) the following threats to soil were identified: soil erosion, decline in soil organic matter, soil contamination, soil sealing, soil compaction, decline in soil biodiversity, soil salinization, landslides and desertification. In addition, cross-cutting issues such as climate change press on the land system. Droughts, wildfires, storms and floods affect the condition of ecosystems and the food chain (EEA, 2019).

For example, landslides threaten soil functioning by removing all soil material that, as previously pointed out, is not a renewable resource – it requires thousands of years to restore its functions. A similar situation occurs with soil erosion: erosion occurs when soil is left exposed to rain or wind energy (Pimentel, 2006) producing an impact on food security and natural environment.

The land cover maps are an essential prerequisite for sustainable management of renewable natural resources, environmental protection, better preparedness for natural disasters, and more effective mitigation of their impacts, and realistic modelling of climate change scenarios.

Several user communities like decision-makers at local and regional level, non-governmental organizations, European communities, scientists and researchers require different types of land cover maps and changes for their activities and policies (Reba & Seto, 2020). For example, “Land cover and land cover change have multiple applications for evaluating progress towards various SDG targets (UNCCD, 2017). The United Nations General Assembly adopted the SDGs, including target 15.3 which contains the objective to strive towards Land Degradation Neutrality by 2030 (Wunder et al., 2018); this target requires information on the rate of land urban change to calculate the corresponding indicator.

Thanks to the significant progress of the last decades, remote sensing is increasingly asserting itself as an economic and efficient technique to extract information from the Earth surface.

Remote sensing data allow a detailed monitoring of land cover and land cover change at local and global scale, allowing to quantify land development and obtain data and statistics on the different characteristics of land cover, such as impervious surface, urban green space or trees loss; it is possible to detect damages occurring after natural or anthropogenic disasters like wildfire or earthquakes as well as perform several

kind of applications. Since 2008 the whole Landsat archive is freely accessible through the websites of the United States Geological Survey and the Global Land Cover Facility at the University of Maryland: free data archives allowed researchers to perform numerous interdisciplinary studies on land change of the Earth's surface. The launch of the Sentinel 2 constellations and previously of the Sentinel 1 SAR sensors have provided new possibilities to exploit earth observation for several applications such as land management, agriculture and forestry, disaster control, humanitarian relief operations, risk mapping and security concerns; they have also posed new challenges and offered new possibilities thanks to their high-resolution, multi-spectral imaging, a high revisit frequency of 5 days at the Equator. In addition, new free tools are available like Google Earth Engine or European Space Agency (ESA) software exploiting the combined use of Sentinel 1 SAR data and Sentinel 2.

The CLC dataset (a pan-European component of the Copernicus project, coordinated by the European Environment Agency (EEA), based on remote sensing data in its most recent version (2018) covers 39 European countries. Land cover is characterized by a 3-level hierarchy of classes (with 44 classes in total at the 3rd level). CLC dataset has represented for years the only complete mapping of homogeneous and comparable country data in Europe. It is not possible to use these data for a detailed analysis or use the dataset for some applications due to the Minimum Mappable Unit (MMU) of 25 ha and an update frequency of 6 years. In addition, the Copernicus program makes High Resolution Layers (HRL) available, a raster map describing some of the main land cover characteristics. However, just like CLC, it has accuracy problems and is only updated every three years, thus not allowing an accurate temporal analysis.

The added value of this research will then be the development of a new procedure of land cover mapping and updating for landscape monitoring that use free data and free applications, capable of extracting information on a large area with high frequency, exploiting the potentiality of both Optical and SAR time series images. Usually, the products at national or global scale suffer moderate or low resolution because of the difficulties to obtain good quality from processing satellite images on a vast area. A high spatial resolution and annual frequency map demand an enormous amount of data and an efficient processing software. These requirements make many good methods such as machine learning poorly suited to detailed mapping of large areas, because they demand a large number of training samples to perform the classification and are time consuming. For this reason, the research tries to implement a new methodology, that considers these issues by investigating the integration of Sentinel-1 and Sentinel-2 – taking advantage of multispectral optical data, traditionally used for land cover analysis together with the SAR data, making it possible to exploit different polarisations, under unfavourable weather conditions and during the night. Finally, all the procedure of mapping and updating is performed on Google Earth Engine (a cloud and free platform) able to process and handle a large amount of data and develop specific algorithms.

Taking all these aspects into account, this research programme comes within the framework of remote sensing techniques and intends to fill the technical-scientific gap in the methodology definition and in the lack of a frequently updated land cover map; innovative applications are developed to investigate the potential of optical and satellite data also in the field of landslide hazard mapping and rapid change detection of natural disaster. All these aspects could be of great help in supporting sustainable development of territory and assisting various types of user requirements, allowing land cover monitoring in an economic and automatic fashion.

1.2 Research objectives

The project research intends to meet the need for detailed information on a few relevant priorities in the environmental area, identifying issues of strategic importance in land monitoring and mapping. The aim of this research is to monitor land cover and soil consumption through the development of a methodology integrating a number of remotely sensed data and provide effective tools for soil protection.

The approach of the study is to operationally exploit free satellite data and open-source tools to provide frequent and detailed spatial characterisation of land cover, making it suitable for multidisciplinary studies and applications, as well as economically sustainable. To do this, the main objectives (summarised in the diagram in Figure 1) are addressed to:

- Define an advanced operational procedure to extract land cover classes over very large areas using free satellite data (multi-temporal Sentinel-1 (SAR) and Sentinel-2 (Optical) with a high level of accuracy to support monitoring activities and provide fundamental information to reduce soil degradation.
- Develop an efficient change detection strategy to improve the frequency and accuracy of land cover map with particular attention to land consumption and forest disturbances, by the means of an integrated use of free multi temporal optical and SAR image that can assist decision makers in evaluating the consequences of urbanization or trees lost.
- Investigate whether the soil sealing data can improve the landslide susceptibility model.
- Contribute to a deeper knowledge of the potential of remote sensing data for rapid detection of environmental damages.

Because of the variety of components influencing the transformation process of land, this research is based on a new multi-disciplinary approach, integrating optical and SAR data. In the second part of the study, some applications will be carried out on different aspects of environmental monitoring through a number of case studies, covering a range of soil degradation threats in various bio-physical and environmental contexts.

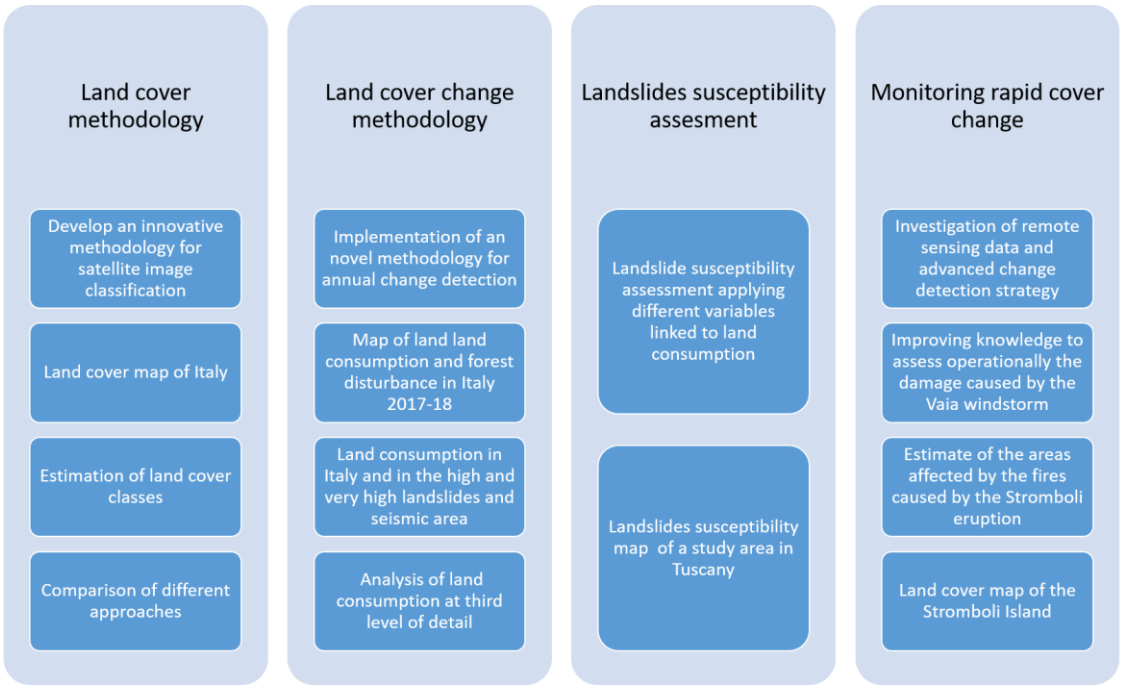

Figure 1.1 – Objectives of the research.

1.3 Outline

In accordance with the objective of a multidisciplinary approach, this PhD intends to promote a deeper knowledge on the territory through remote sensing and thesis is organized as in Fig. 1.1 and outlined as follows:

Chapter 1 Chapter 1 provides a short introduction to the thesis, along with the research objectives and the structure of the research.

Chapter 2 This chapter addresses some of the issues related to the policies of monitoring in an international context, describing some relevant strategies within soil protection adopted in interventional context. It also describes the current available data produced under the program Copernicus, the potential and limitations of these data. The chapter shows the context in which this research is taking place, the new challenges of monitoring and the need of various communities of users (stakeholders). One part is dedicated to the definitions of land cover, land consumption and land use, terms widely used in this dissertation. The second part of this chapter describes the basic principles of remote sensing in relation to mapping and monitoring environmental changes and the state of the art of different land cover classification.

Chapter 3 This chapter describes the study area, the classification system used, and the two methodologies elaborated for land cover and land cover change mapping, showing all the steps of these methodologies, evaluating the complementarity of Sentinel-1 and Sentinel-2 and understanding the added-value of these data. The last part describes the procedure for the land cover accuracy assessment.

Chapter 4 Chapter 4 presents the results of land cover classification and land cover change and some applications land cover maps for environmental monitoring. This chapter therefore discusses the methodology and analyse the accuracy of the land cover map produced and the changes occurred in Italy between 2017 and 2018; the map is also compared with the CLC to highlight the weaknesses of the two different approaches in the classification methods. Based on the data obtained, some indicators related to land consumption in landslide and seismic hazard areas are calculated. These data are presented at the third level of detail, i.e. the type of soil sealing present (roads, constructions etc.) in the different hazard areas (high, very high).

The 4.3 paragraph is addressed to monitoring of landslides and in particular to improving the landslides susceptibility map using different explanatory variables derived by soil sealing map. The test site is Norther Tuscany (3100 km^2) and the susceptibility analysis is achieved with a Random Forest algorithm. The last part of the chapter presents two studies related to the possibility of exploiting Sentinel data for short-term monitoring systems in case of damages due to natural disasters: in the first case, the areas affected by the 2018 Vaia storm in Northern Italy are mapped, and in the second case, the areas burned due to the 2019 Stromboli eruption. The methodologies are described in this section for a better understanding of the procedure adopted.

Chapter 5 In the concluding chapter, the objectives of thesis are in relation to the results obtained, highlighting their strengths and weaknesses of the methodologies developed. The peculiarities of the method and of the maps obtained in this research are also presented with a view to their use by institutions and by different types of users. At the end it presents the major findings, highlighting future challenges on land cover monitoring.

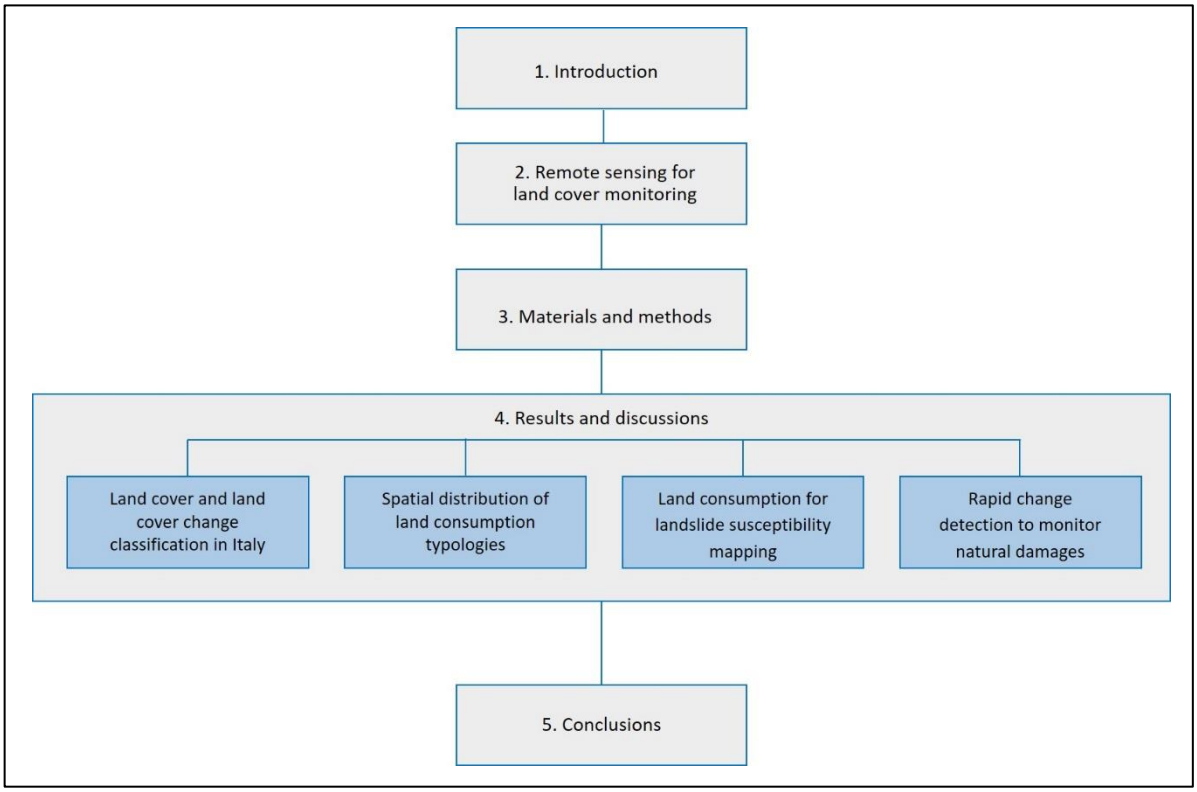

Figure 1.2 - Flowchart of the PhD thesis roadmap.

Chapter 2 Remote sensing for land cover monitoring

This chapter proposes a brief summary of policies undertaken at the international level to prevent soil degradation with the objective to contextualize the problem of soil protection and monitoring of land cover change. The main available cartographic products and their characteristics are also presented, indicating their potential and limitations for use. The second part describes the basic principles of remote sensing and reviews the current status of image classification and change detection methods.

2.1 Framework on soil protection policies

In the last years there has been a significant increase in soil degradation processes caused, among others, by urban and industrial sprawl, salinization processes, soil loss due to erosion and climate change. The importance of good land management and, soil protection and conservation have been reaffirmed by the EC with a series of initiatives that have covered more than one environmental aspect.
Some major polices that draw up a European and international level regarding soil protection are analysed below (in the section **Strategic documents and policy guidelines**), alongside with some EU publications (**Report**) which, although not covered by specific European Communications, in some way provide guidelines in relation to the measures to be taken to limit land degradation by seeking to bridge the legislative gap in this area.
None of the main initiatives analysed has a binding legislative function on the planning policies of the different Member States, and only in some cases presuppose a specific objective to be achieved.
Finally, to complete the framework, some directives will be briefly considered. They are drawn up for other purposes dealing marginally with some specific issues of soil protection but contain some binding indications to limit soil sealing and land take (**Nature conservation policies**).

All these initiatives are listed in column below and are summarised in tables 1, 2, and 3 grouped by topics; last two columns report the objectives they aim to achieve and the reference to a specific period, when expected. Except for the section on “Nature conservation policies” section, the exposition is subdivided by topic trying to follow a chronological order to better understand the evolution over time of the strategies implemented within the framework of sustainable land management.

Strategic documents and policy guidelines

- Thematic Strategy for Soil Protection (European Commission, 2006a)
- Roadmap to a resource efficient Europe (European Commission, 2011)
- Soil Sealing Guidelines (European Commission, 2012)
- 7th EAP (European Union, 2013)

- Healthy soils – New Soil Strategy (European Commission, 2020)
- The European Green Deal (European Commission, 2019c)
- Transforming our World: The 2030 Agenda for Sustainable Development Global (SDGs), (United Nations, 2015)
- EU Biodiversity strategy to 2020 (Commissione Europea, 2020)

European report on soil protection

- Towards a sustainable Europe by 2030 (European Commission, 2019a)
- Sustainable development in the European Union — Monitoring report on progress towards the SDGs in an EU context — 2019) (European Commission, 2019b)
- FUTURE BRIEF: No net land take by 2050? (European Commission et al., 2016)
- State of the Environment Reporting (EEA, 2019)

Nature conservation policies

- Floods Directive (2007/60/EC)
- Habitats Directive (92/43/EEC)
- Environmental Impact Assessment Directive (EIA, 2011/92/EU)
- Strategic Environmental Assessment Directive (SEA, 2001/42/EC)

2.1.1 Title Strategic documents and policy guidelines

Thematic Strategy for Soil Protection

As early as 2002 the EU Communication with "Towards a Thematic Strategy for Soil Protection" (European Commission, 2002) identified different soil threats relevant to the EU area, such as erosion, decline in organic matter, contamination, sealing, compaction, loss of biodiversity, salinization and landslides, but the last two have been dealt with Directive on flood risk management prevention (2007/60/EC) and are not included in the Strategy. It established a ten-year work program for the EC that at the end produced the Soil Thematic Strategy (European Commission, 2006b).

The Strategy contained an impact assessment analysing the economic, social, and environmental impacts of the proposed measures, (explained why further action is needed to ensure a high level of soil protection, setting the overall objective of the Strategy) and a proposed legislative framework for the protection and sustainable use of soil.

With respect to the latter proposal, a Soil Framework Directive, legally binding, was endorsed by the EU Parliament in 2006 alongside with the Soil Thematic Strategy. It required to the Member States to identify areas at risk for degradation (as well as already contaminated sites), define targets for soil protection and carry out programmes of measures to ensure protection. The opposition of a minority of Member States blocked this Directive grounding their opposition on the Subsidiarity Principle and because of the difficulties such a Directive would induce to industrially polluted soils, as such in 2014 the EC decided to withdraw its legislative proposal.

Roadmap to a resource efficient Europe

Concerning soil protection and land use management, in 2011 the Commission presented the Roadmap to a resource efficient Europe (European Commission, 2011), a Communication from the Commission to the European Parliament, the Council, the European Economic and Social Committee and the Committee of the Regions. It provided an overarching framework for European policies regarding sustainable management of the resources, defining medium and long-term milestones for soil protection.

For the first time an initiative contained a quantitative objective: the Roadmap, in fact, promotes 'no net land take' in EU by 2050, aiming to reduce soil erosion, increasing organic matter and mitigate the effect of urban sprawl (EEA, 2019).

Table 2.1 – Main strategic documents and policy guidelines.

Strategic documents and policy guidelines	**Year**	**Soil aspects**	**Objectives and targets**	**Target year**
Thematic strategy on the protection of soil	2006	Prevent further degradation of soil, preserve its functions and restore degraded soil + Integrate soil protection into relevant EU policies	Soil Directive	N/A
Roadmap to a resource efficient Europe	2011	Reduce soil erosion, increase soil organic matter, and promote remedial work on contaminated sites	Achieve no net land take by 2050	2050
Soil Sealing Guidelines	2012	Guidelines explicitly focus on limiting, mitigating and compensating for the effects of soil sealing.		N/A
The Seventh Environment Action Programme	2013	EU policies help to achieve no net land take by 2050	Achieve no net land take by 2050	2050
The 2030 Agenda for Sustainable Development and its 17 Sustainable Development Goals	2015	The agenda points to 17 Sustainable Development Goals, and 169 associated targets on the theme of protection, conservation and sustainable management of natural resources Goal 15.3 "land degradation neutrality" Goal 11 "Make cities and human settlements inclusive, safe, resilient and sustainable "	Target 15.3.1: by 2030 achieve a land degradation-neutral world, target 11.3.1: by 2030, the increase of a population should be aligned to the expansion of built-up area , target 11.7: by 2030 to "provide universal access to safe, inclusive and accessible, green and public spaces..."	2030
New Soil Strategy	2020	Update of the current soil strategy to address soil degradation (currently under public consultation); protect soil fertility, reduce erosion and sealing, increase organic matter, identify contaminated sites, restore degraded soils,	Achieve land degradation neutrality by 2030 Reduce the rate of land take, urban sprawl and sealing to achieve no net land take by 2050	2030 and 2050
Green Deal	2019	The European Green Deal is a response to tackle climate change growth and environmental degradation and aims of a revision of relevant legislative measures to deliver on the increased climate ambition, following the review of Land use and land use change and forestry Regulation		
EU biodiversity strategy	2020	Safeguard biodiversity and ecosystem services in the EU	To bring to 30% the surface of protected areas in EU (from the current 26%	2030

Guidelines on best practice to limit, mitigate or compensate soil sealing

In response to soil sealing issues, raised by Road map, EC published the report "Overview of best practices for limiting soil sealing or mitigating its effects" in EU-27, presenting land take and soil sealing trends in the EU. The report contains an exhaustive overview of existing Member State policies and technical measures used to reduce and mitigate soil sealing.

On the basis of this report and with the help of national soil sealing experts, the EC departments prepared the "Guidelines on best practice to limit, mitigate or compensate soil sealing" (European Commission, 2012). Actually this guide has no legal value although it establishes the policy to be followed *to limit and mitigate soil sealing*–by European countries, proposing a wide number of best practices (EU 7th EAP) and suggesting the principles of sustainable land use in regional and local spatial planning (Frelih-Larsen et al., 2017).

In other words, Member States should, as a matter of priority, ensure the reduction of imperviousness surface at the expense of agricultural and natural areas by reuse of existing infrastructure and define realistic targets to limit urban expansion and restrict urban sprawl.

The 7th EAP and the New Soil Strategy

The goal 'no net land take' in EU by 2050 was reaffirmed by EU Environment Action Programme to 2020 (European Union, 2013) adopted in 2013 by the Council and the European Parliament for the period up to 2020, under the title 'Living well, within the limits of our planet'.

The 7th EAP identifies natural capital and resource efficiency as priority areas in relation to land-related issues and requires action at EU and national levels to enhance soil protection and sustainable use of land, including forest land.

Regarding to soil protection, Priority objective 1, n. 23 refers to achieve 'no net land take' by 2050 and, more generally, to call for a 'land degradation neutral world'.

The programme plays a central role for EU environmental policies and sets instruments and guidelines for strategic initiatives and a foundation for directives on almost all environmental thematic areas.

In the context of the soil strategy, new initiatives have been promoted by the European Union, which has deemed it necessary to promote new policies more adapted to today's context, as there is a risk that the EU will fail its Green Deal (European Commission, 2019c) and international objectives; Green Deal initiatives are briefly shown in the table for what concerns the protection of the soil. In this regard, the New Soil Strategy "will provide the overarching framework and the concrete pathway towards some important objectives" (European Commission, 2020) such as "reduce the rate of land take, urban sprawl and sealing to achieve no net land take by 2050" or "achieve land degradation neutrality by 2030" (European Commission, 2020), some of which listed in Table 2.1.

Biodiversity Strategy

The Strategy's framework does not explicitly address on soil protection and is also focused to safeguard biodiversity and ecosystem services in the EU. However, it addresses a wide number of soil threats, including, compaction, contamination, erosion, flooding, to name just a few, which cause the habitat loss due to land use change and fragmentation. The Biodiversity Strategy "Bringing nature back into the our life", (Commissione Europea, 2020) adopted on 20 May 2020 includes, among others, the following elements:

- to bring to 30% the surface of protected areas in EU (from the current 26%) of these areas, one third should become strictly protected.
- an update of the EU Thematic Strategy for the soil in 2021 to address the issue of the soil and to contribute to achieve the goal of neutrality in terms of soil degradation.
- the 2021-2027 work program of the "Joint Research Centre of the European Commission" EChas including the creation of the European Observatory for Soil.

Sustainable Development Goals

In addition to the European policies, the theme of protection, conservation and sustainable management of natural resources have been addressed at global level in 2015 when United Nations Member States adopted *The 2030 Agenda for Sustainable Development* (United Nations, 2015); at the base of this Agenda are the 17 SDGs, and 169 associated targets which are an urgent call for action by all countries. Some of these targets are of particular interest to the land and the soil issues, as such they should be integrated in the national planning in the short and medium term in order to be achieved by 2030.

With the signature of the Agenda, all countries have agreed to participate in a process of monitoring these objectives managed by United Nations Statistical Commission, through a system of indicators, including some related to soil consumption.

The United Nations Sustainable Development **Goal 15.3** aims to "halt and reverse land degradation" until 2030 and has introduced the concept of "Land Degradation Neutrality". The Land Degradation Neutrality is defined as a state whereby the amount and quality of land resources which are necessary to support ecosystem functions and services and enhance food security's stability or increase within a specified temporal and spatial scales and ecosystems (UNCCD, 2016).

SDG) target 15.3 states: "By 2030, combat desertification, restore degraded land and soil, including land affected by desertification, drought and floods, and strive to achieve a land degradation-neutral world"[5]

The indicator ***15.3.1*** is the proportion of land that is degraded over total land area; it is a binary - degraded/not degraded - quantification based on the analysis of available data for three sub-indicators to be validated and reported by national authorities. The sub-indicators are: Trends in Land Cover, Land Productivity and Carbon Stocks.

Also the Goal 11 "Make cities and human settlements inclusive, safe, resilient and sustainable" is related to soil protection; in particular **Goal 11.3** aims to "by 2030, enhance inclusive and sustainable urbanization and capacity for participatory, integrated and sustainable human settlement planning and management in all countries". Associated to this goal there is the indicator ***11.3.1*** (the ratio of land consumption rate to population growth rate), which provides for a quantitative target i.e. the increase of a population should be aligned to the expansion of built-up area. Finally within this goal, the **Goal 11.7**, has the objective by 2030, to "provide universal access to safe, inclusive and accessible, green and public spaces, in particular for women and children, older persons and persons with disabilities", highlighting the importance of green spaces in cities. The Table 2.1 summarises the initiatives exposed.

2.1.2 European report on soil protection

The Agenda for SDGs (United Nations, 2015) gives a new impetus to global efforts for achieving sustainable development and actions were outlined for each SDGs. On the basis of this mandate, Eurostat has been publishing annual monitoring reports on the progresses towards the SDGs in an EU context since 2017. The first one, the publication Sustainable development in the European Union - Monitoring report on progress towards the SDGs in an EU context (European Commission, 2019b), in 2019 reached its third edition, provides a statistical presentation of trends relating to the SDGs on the basis of around 100 indicators in the EU over the past five years ('short-term') and, when sufficient data are available, over the past 15 years ('long-term').

With the paper '**Towards a sustainable Europe by 2030'** (European Commission, 2019a) the EC adopted the reflection paper to start a path involving all the member states and the citizens of the EU Member States and other stakeholders to participate in a forward-looking debate in order to work on the state and progress of SDGs (Naumann et al., 2019).

[5] https://www.unccd.int/actions/ldn-target-setting-programme.

As recommended by the '**European environment — state and outlook 2020** (EEA, 2019), in the last years Europe is not making enough progress. SOER 2020 is the most recent comprehensive environmental assessment ever undertaken on Europe published by the EEA every five years. It is providing an overview of the situation on overall environmental trends in Europe against short-term targets as well as longer term 2050. The report highlights that even if most of the 2020 targets will not be achieved, especially those on biodiversity, a better integration of environment and health are needed, in order to meet the longer-term goals and objectives for 2030 and 2050 and to avoid a further deterioration of natural resources.
Finally, the report recognizes a deteriorating past trends without meeting 2020 targets; the lack of binding, quantitative targets and polices for an efficient use of the resources and the "Key gaps relate to land and soil and an integrated framework for the environment and health, including chemicals.

FUTURE BRIEF: No net land take by 2050?
"No net land take by 2050" published by the EC within "Future Briefs" (European Commission et al., 2016) takes stock of the actions to be taken to achieve this ambitious objective. The brief report explains the meaning of "No net land take" suggesting measures for containing land take and preventing land take with brownfield development. Once again, the EU reaffirms the need to provide guidance for a soil protection policy. Table 2.2.

Table 2.2- Summary of some fundamental soil protection reports.

Report	Year	Soil aspects
FUTURE BRIEF: No net land take by 2050?	2016	take stock of the actions to be taken to achieve this ambitious objective
SOER	2019	Providing an overview of the situation in Europe on Overall environmental trends in Europe against short-term targets as well as longer term 2050
Towards a sustainable Europe by 2030	2019	It's a reflection paper to involve all the member states and the citizens to work on the state and progress of SDGs
Sustainable development in the European Union — Monitoring report on progress towards the SDGs in an EU context — 2019	2019	Annual monitoring progress towards the SDGs in an EU context.

2.1.3 Nature conservation policies

In order to provide a complete picture to this argument, it is important to point out some of the EU polices addressed forward other themes, but connected directly or indirectly to the *Sustainable Soil Management in Europe* including some elements related to soil stakes. (Table 2.3).

Floods Directive[6] is directed to flood risk management within the EU, but may support the soil protection policy, by promoting the natural water retention measures to avoid compaction of soil; it also supports land use planning rules and green infrastructure to control run-off, pluvial flooding or protection of soil by preventing the urbanization of floodplain and riparian land exposed to flooding (Frelih-Larsen et al., 2017).
Both the **Environmental Impact Assessment Directive**[7] and the **Strategic Environmental Assessment Directive**[8] involve approaches and measures that address land take and land degradation an preliminary

[6] http://data.europa.eu/eli/dir/2007/60/oj
[7] http://data.europa.eu/eli/dir/2011/92/oj
[8] http://data.europa.eu/eli/dir/2001/42/oj

depth study is required for programmes and plans, that have an impact on agriculture, forestry, town and country planning, including land use and soil.
Similarly, a project with a risk of soil sealing, requires an environmental impact assessment and mitigation measures, this is the case, for example, of a land use change that produces a land take or land degradation or significant effects on the environment and on the use of soil, land, water and biodiversity.
The **Habitats and Birds Directive**[9] has the objective of promoting the maintenance of biodiversity through the conservation of natural habitats in Europe; careful soil management in these areas allows to safeguard also its ability to support and host biodiversity.

Table 2.3- Some European Directives dealing with soil protection issues.

Nature conservation policies	Year	Soil aspects
Floods Directive	2007	Promote natural water retention measures and support land use planning rules and green infrastructure to control run-off
Habitats Directive	2007	Promote the maintenance of biodiversity through the conservation of natural habitats in Europe, supporting also soil and its biodiversity
Environmental Impact Assessment Directive (EIA)	2011	EIA and mitigation and compensation measures are required in project with significant effects on environment take into account soil, land take and land degradation
Strategic Environmental Assessment Directive (SEA)	2001	SEA is required for programmes and plans having impacts on the environment, including soil.

After this brief overview of European and global policies related to land and soil protection, it possible to verify the absence of suitable soil legislation at European level with the goal of more sustainable land use management. It is therefore important to define binding measures and establish a coherent coordination of the different existing policies to make it an effective tool for soil protection also at national and regional level.

2.1.4 Italian polices for soil protection

At the national level, the tool for the implementation of Agenda 2030 is the National Sustainable Development Strategy[10], presented to the Italian Council of Ministers in October 2017 and approved by Italian Interministerial Committee for Economic Planning in December of the same year (Munafò, 2020). The strategy is structured in five areas: People, Planet, Prosperity, Peace and Partnership, each of which is made up of a system of strategic choices (ordered by Roman numerals) divided into national strategic objectives specific to the Italian reality (complementary to the 169 targets of Agenda 2030). In order to ensure the sustainable management of natural resources, choice II ("Halting soil consumption and desertification") has been identified as one of the strategic objectives (objective II.2) which, therefore, could be brought forward to 2030. However, as in Europe, the absence of a Soil Framework Directive weighs heavily, even in Italy no law has been passed to protect soil from its progressive artificialization.

[9] http://data.europa.eu/eli/dir/1992/43/oj and http://data.europa.eu/eli/dir/2009/147/oj
[10] https://www.minambiente.it/pagina/la-snsvs

2.2 Copernicus land products

As mentioned in the short review of actions taken at European and global level to protect environmental resources and soil, land cover assessment plays a key role in understanding local pressures and to better identify the drivers behind the land cover changes. Land cover and land use data are also important for other monitoring systems that use them as a vital input factor for their data models as climate change, biomass and carbon cycle (European Environment Agency, 2017). Also, urban sprawl, landscape fragmentation and soil degradation are becoming better known and spatially localised thanks to remote sensing monitoring of territory.

In the European context many initiatives have been taken to obtain information to map the territory and his change; the most relevant is the Copernicus Land Monitoring Service[11] implemented by the EEA and the Joint Research Centre, that is one of the services released by Copernicus, the European Union's Earth observation programme which provides updated information in six thematic areas: land, marine, atmosphere, climate change, emergency management and security.

Regarding the artificial land cover information (a key theme in this thesis), it can be derived from CLC[12] data or by HRL[13], both belonging Pan-European component of Copernicus programme. A third source of information encompass Urban Atlas[14] which contains detailed information on urban characteristics and changes, although it doesn't cover all the European territory (Table 2.4).

Table 2.4– Land cover Copernicus products.

	CLC	**Imperviousness (HRL)**	**Urban Atlas (UA)**
Type of information	Land use/Land cover map (44 classes, with 3 level)	Percentage of sealed area	High-resolution Land use/Land cover map (27 classes)
Coverage	EU 39	EU 39	788 FUAS
Minimum Mapping Unit	25 ha and 5 ha (changes)	20 m (pixel), 10 m only 2018	17 urban classes 0,25 ha 10 rural classes 1 ha
Reference year	1990, 2000, 2006, 2012, 2018	2006, 2009, 2012, 2015 and 2018 (under validation)	2006, 2012, 2018

CLC has released a land cover mapping using remote sensing images for all European countries; it allows to compare data of land use/cover in a homogeneous way throughout with a very high thematic level of detail, with a legend organized in 44 classes. The first CLC map dates back to 1990 (CLC90), while subsequent updates refer to 2000, 2006, 2012, and 2018; the time series are complemented by change layers, which highlight changes in land cover with an MMU of 5 ha.

The other two layers, HRL and Urban Atlas, are also of particular importance because they directly affect urban monitoring. The HRL are produced for 39 European countries, within the framework of the Pan-European component of Copernicus (Congedo et al., 2016). They include five land cover themes: imperviousness, forests, natural grasslands wetlands and water bodies and are published every tree year. The last layers are referred to 2015, while the 2018 is under validation.

The HRL, obtained from automatic classification of satellite images and others ancillary data, have a spatial resolution of 20 m, except for Small Woody Features which have a resolution of 5 m and for the Water & Wetness with a resolution of 10 m and also envisages the realization of a product at 10 m resolution. Among

[11] https://land.copernicus.eu

[12] https://land.copernicus.eu/pan-european/corine-land-cover

[13] https://land.copernicus.eu/pan-european/high-resolution-layers

[14] https://land.copernicus.eu/local/urban-atlas

them imperviousness layer captures the spatial distribution of artificially sealed areas, including the level of sealing of the soil per area unit (the degree of imperviousness within each grid cell from 0% to 100%).
Finally, the Urban Atlas is the third important information layer produced within the project Copernicus. It is currently composed of high-resolution land use maps for 788 Functional Urban Area (FUA) and More than 300 major cities in the EU were covered by 2011. The nomenclature of the Land Cover/Land Use includes 17 urban classes with MMU 0.25 ha and 10 Rural Classes with MMU 1 ha. The minimum accuracy of the data provided is 85% for artificial surfaces and 80% for the other classes (Montero et al., 2014).
The strength of these Copernicus Land products relies in their homogeneity, repetitiveness, and objectivity. over the whole of Europe (Lefebvre et al., 2016).

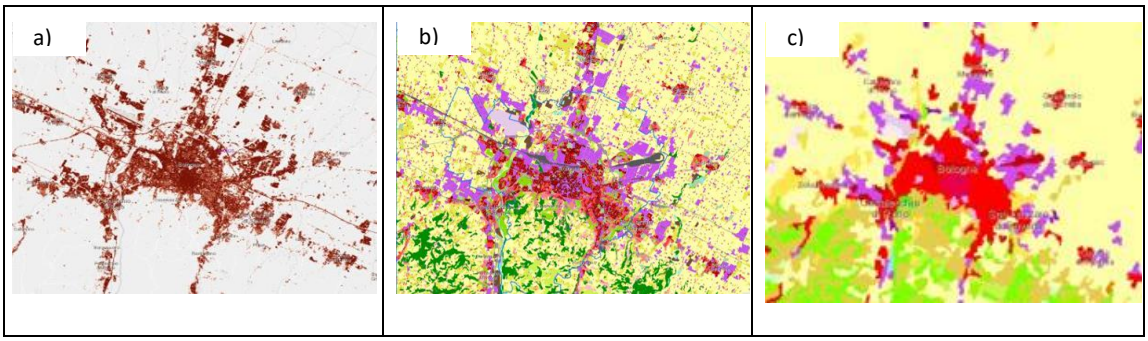

Figure 2.1 - Comparison between Imperviousness a), Urban atlas b) and CLC c) Source: ESA.

However, there are still some limits when using this data for detailed monitoring of land cover change at the national level with an annual temporal resolution. First of all, for the frequency with which they are updated: the HRL are updated every three years while CLC and Urban atlas every 6 years. A second problem lies in the accuracy of the data: in order to detect occurred after only one year, for example, it is fundamental to identify all small changes with high accuracy especially when studying changes after a short interval of time (Figure 2.1).
CLC dataset uses a MMU of 25 ha which is not enough for a precise analysis on soil sealing; also imperviousness HRL layer, that presents a valid information regarding the percentage of the sealed area, has a spatial resolution of 20 m (cell). In artificial urban areas where the changes interest small areas, 20 m are still coarse to highlight the differences occurring during a short period.

2.3 Land consumption, land cover and land use concepts

There are many definitions of land take and land consumption, often used as synonyms, sometimes used to express different concepts. This section provides an overview of the meaning of these terms considering the importance of their correct interpretation to avoid any kind of misunderstanding.
Knowledge of aspects included or excluded in a definition, for example, has consequences not only on the methodology of monitoring land cover changes, but also on policies (already quite incomplete) based on these concepts. An unequivocal interpretation of definitions therefore helps to clarify the problems behind these concepts.
Land consumption is a phenomenon associated with the loss of a fundamental environmental resource, due to the occupation of land originally agricultural, natural or semi-natural. The phenomenon refers, therefore, to an increase in artificial land cover, linked to settlement dynamics. A process mainly due to the construction of new buildings, buildings and settlements, the expansion of cities, densification, or conversion of land within an urban area, and land infrastructure. Soil consumption is, therefore, defined as a variation from non-artificial land cover (unconsumed soil) to artificial land cover (consumed soil) (Munafò, 2020). The representation of soil consumption is, therefore, given by the increasing coverage of soil by areas artificially covered by buildings infrastructure, mining areas, landfills, construction sites and other paved or

paved areas, greenhouses and other permanent roofs, airports and ports, waterproof sports areas and fields, photovoltaic panels and all other waterproofed areas, not necessarily urban. This definition therefore extends to rural and natural areas and excludes natural and semi-natural open areas in urban areas, regardless of their intended use. Within the European Union the term land take is often defined as follows:

- the land take indicator addresses the change in the area of agricultural, forest and other seminatural land taken for urban and other artificial land development. Land take includes areas sealed by construction and urban infrastructure, as well as urban green areas, and sport and leisure facilities[15].

Taking into account this definition as the official definition of EU, it is important to make some considerations. This definition refers mostly to a permanent alteration of natural and rural soil, in such a way rainwater can no longer be infiltrated, in this case, it is usually used the term “soil sealing”.
A second kind of consideration relies on the way through which land take indicators are calculated. Remote sensing tools are in general used for studying land cover and land cover change on a national level.

Table 2.5- – Definition of Land consumption, land cover and land use.

Land consumption (land take)
The replacement of a non-artificial land cover to an artificial land cover, both permanent and reversible (Strollo et al., 2020) as explained below. Artificial surfaces that have been changed by, or are under the influence of human activities resulting in a land consumption process can be sealed or non-sealed (Stephan Arnold, Barbara Kosztra, Gebhard Banko, Pavel Milenov et al., 2021). We refer to portion of territory undergoing this process as land consumed.
Land cover
The physical and biological cover of the Earth's surface including artificial surfaces, agricultural areas, forests, (semi)natural areas, wetlands, water bodies. It is an abstraction of reality as the Earth´s surface is populated with landscape elements (European Parliament, 2007).
Land use
The territory characterized according to its current and future planned functional dimension or socioeconomic purpose (e.g. residential, industrial, commercial, agricultural, forestry, recreational). Land Use is different from Land Cover, dedicated to the description of the surface of the Earth by its (bio) physical characteristics (European Parliament, 2007).

These instruments measure the soil reflectance: an object that reflect in the same way is considered belonging to the same “land cover class”; if we consider that land take class includes “urban green areas, and sport and leisure facilities”, we may confuse the concept of land use with the concept of land cover, while it is possible distinguish only the first by remote sensing earth observation. The EU definition considers the same land cover class as “urban green areas” or “sport and leisure facilities” differently, land take/not land take, depending on where it is in a natural or in an urban area. If a green urban area is considered an artificial surface every new building on this natural area will not be considered as a new land take with all the associates consequences for the regional and national legislation. It is therefore fundamental to reach a clear definition of land take since it plays an important role for the future polices in soil protection.
In this study land take is defined as the synonymous of land consumption and independently from land use. The definitions in Table 2.5 will be considered.
As for the definition of land cover and land use, these terms indicate two concepts that are closely interconnected and affect each other. In the creation of thematic maps, depending on the applications, information may be related to land use aspects compared to land cover and vice versa. For this reason, over

[15] https://www.eea.europa.eu/dataandmaps/indicators/landtake3/assessment

the years a large number of classification systems have been developed, included the CLC one, which use a mixed nomenclature in order to meet the needs of a larger number of users. This has created enormous amount of class definitions and also a considerable confusion about the meaning of classes, making these classifications not comparable to each other, not homogeneous and usable only for specific purposes or at local level.

2.4 EAGLE concept

For years CLC has been the standard for land cover and land use mapping in Europe. But this system has some limitations due to Mixed land cover and land use information such as (Kleeschulte et al., 2019):

- Ambiguous description and semantic gaps or overlaps provoke inconsistencies in class definitions.
- Only selective incorporation of temporal aspect.
- Lack of thematic content details.
- Missing option for the attribution of spatial objects.
- No flexibility to react on new appearing landscape phenomena.

This has led to the need at the European level to create a new classification system which would take account of certain fundamental principles among which: separate land cover from land use information; describe land cover in a mutually exclusive and comprehensive way, be scale-independent, allow semantic translation between classification systems. Until now, it has always been difficult to clearly and rigorously separate land cover from land use information between existing approaches. This requirement has become fundamental for land monitoring activities in order to have both a pure land cover and a pure perspective of land use on the landscape separately from each other.
EAGLE concept (Arnold et al., 2013) satisfies some of these purposes, in particular it aims at being a tool for analytic class definitions and for linking recent and future nomenclatures; moreover it allows to harmonise European land monitoring system and it can be implemented as an object-oriented base for mapping (Arnold et al., 2013) and monitoring research; finally it is not another classification system, but it is a way to unify land cover and land use information both in top-down and bottom-up approaches.
The EAGLE matrix is composed by three separate descriptors, land cover, land use and characteristics, which can be used in flexible combination with each other. Thanks to these combinations, comparisons with other systems are possible. In the EAGLE model, the basis for the description of landscape are the land cover components that make up a certain land cover class or land surface unit. The LAND COVER components (LCC) are then further characterized by using descriptors listed under “land use attributes” and “characteristics”. The EAGLE matrix itself is subdivided into three blocks standing beside each other. It contains as columns a collection of atomic landscape descriptors of (Arnold et al., 2013).

1.) LAND COVER components – LCC.
2.) LAND USE attribuites – LUA.
3.) Further characteristics – LCH.

This structure allows the user to combine LCC with LUA and LCH, in order to create a hierarchical classification which take into account every characteristics maintaining the three components independent from each other (Kleeschulte et al., 2019).
In this research, in order to make the classification comparable and adaptable to the various monitoring needs, the EAGLE classification was adopted which, in addition to distinguishing land cover from land use, takes into account the fact that the source of information is represented by remote sensing data, it is easily updating and flexible to the several applications (Stephan Arnold, Barbara Kosztra, Gebhard Banko, Pavel

Milenov et al., 2021). The classes derived from the EAGLE system are described in the chapter on methodology.

2.5 Remote sensing for land cover mapping

Remote Sensing can be defined as "the process of detecting and monitoring the physical characteristics of an area by measuring its reflected and emitted radiation at a distance (typically from satellite or aircraft)" (USGS, 2020)[16]. Remote sensing therefore allows to obtain useful information on the Earth's surface from satellite or aerial images, which are generated by exploiting the properties of electromagnetic energy emitted or reflected (Campbell & Wynne, 2011). Typical fields of application include monitoring of change, whether, land cover dynamics and classification, alerts, deforestation, fire, monitoring landslide evolution, monitoring illegal logging or biodiversity (Figure 2.2).

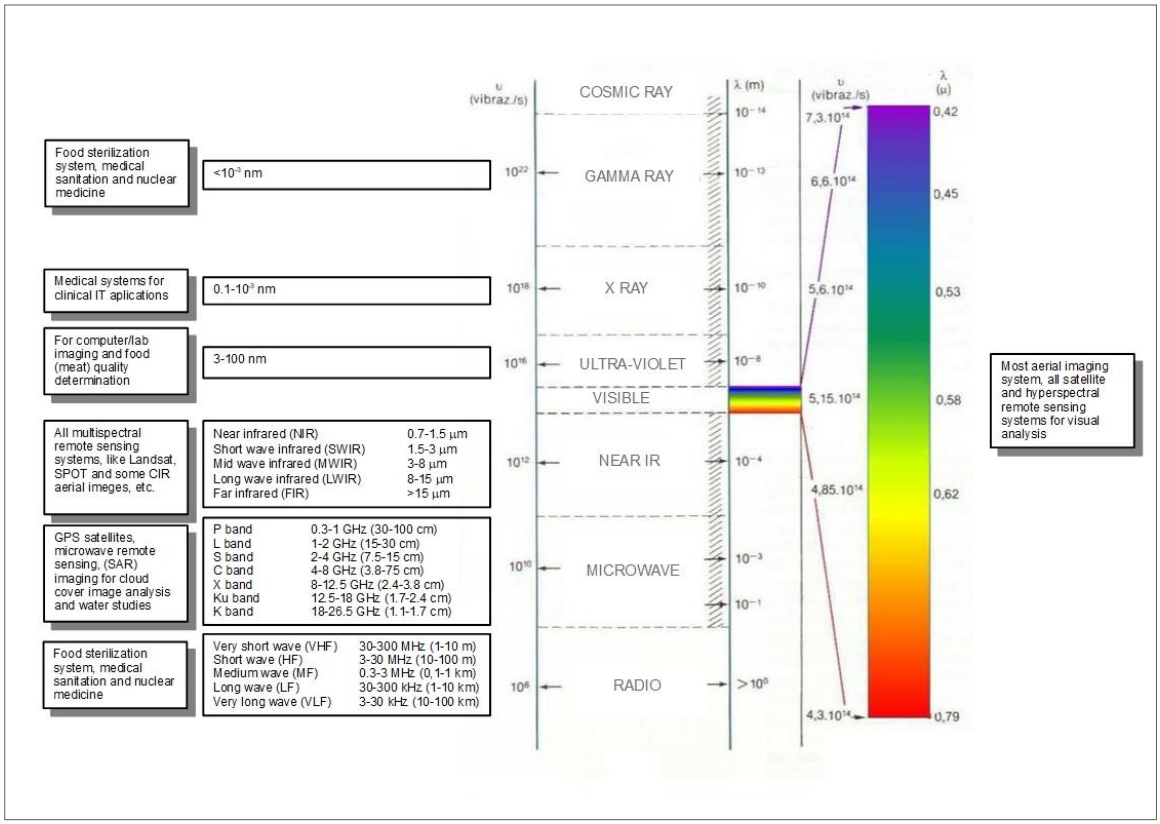

Figure 2.2 - Different bandwidth associated with electromagnetic radiation region[17].

2.5.1 Fundamentals of remote sensing

The acquisition of remote sensing data takes place thanks to special sensors that record the electromagnetic energy emitted, reflected or diffused by the bodies observed on the earth's surface (Figure 2.3). The electromagnetic energy from a source interacts with the atmosphere, then is modified according to the concentration of its components before reaching the target. The interaction between the incident energy and the natural surface leaves a "trace" called the spectral signature. The different spectral signatures of the various natural surfaces are collected and measured by sensors mounted on satellites or airplanes that

[16] https://www.usgs.gov/faqs/what-remote-sensing-and-what-it-used?qt-news_science_products=0#qt-news_science_products

[17] Source: Redesigned from Zourarakis, D.P. Remote Sensing Handbook–Volume I: Remotely Sensed Data Characterization, Classification, and Accuracies.

record from a distance. The data collected by these tools are processed to obtain information on the characteristics and the state of health of the surfaces investigated. The final outcome of the process is generally the production of maps that provide useful information for the study and management of the environment.

When the electromagnetic radiation from the Sun reaches Earth's atmosphere, it undergoes the phenomenon of scattering and absorption: scattering occurs when incident radiation is dispersed or spread out by the particles suspended in the medium unpredictably in all directions, while absorption takes place essentially by greenhouse gases and water vapour, which retains part of the incoming energy that eventually can be re-emitted from the atmosphere as heat (Figure 2.3).

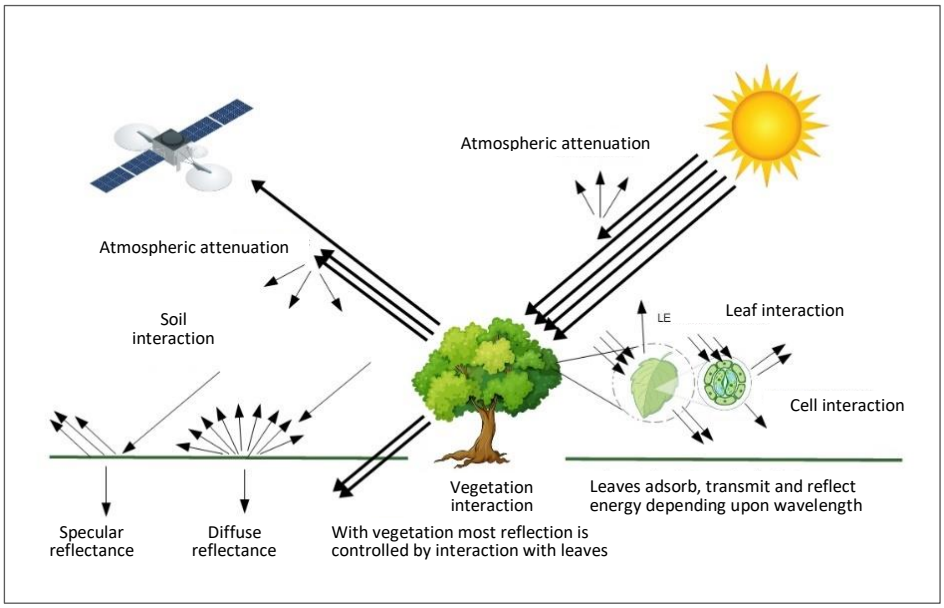

Figure 2.3 –The interaction between the incident energy and the natural surface.

.

As consequence of these processes part of energy in the electromagnetic spectrum are absorbed and effectively blocked by the atmosphere (Camps-Valls et al., 2011).

In practice, the atmosphere assumes the function of a selective filter for some spectral regions, allowing only some radiometric portions (visible, infrared, microwave) to pass (Figure 2.4). "The bands in which the atmosphere transmits radiation are called atmospheric windows". These ranges are exploited by remote sensing systems to acquire information on the earth's surface (Mårtensson, 2011).

The electromagnetic radiation, after getting through the atmosphere hits the surface and, depending on the physical nature of the object or on degree of roughness, part of the incident radiant flux is reflected by the surface, a part is absorbed, and finally the rest is transmitted. Remote sensing exploits these characteristics to extract information on the nature of earth's through the measurement of different parameters.

Remote sensing systems, which measure energy naturally available are called passive sensors. Passive sensors are used to detect energy when the naturally occurring energy is available. For all reflected energy, this occurs during the time when the sun is illuminating the Earth. Energy that is naturally emitted (such as thermal infrared) can be detected day or night.

Active sensors provide their own energy source for illumination. The sensor emits radiation which is directed toward the target to be investigated. The radiation reflected from that target is detected and measured by the sensor. Active sensors can be used for examining wavelengths that are not sufficiently provided by the sun, such as microwaves. An example of active sensor is the Synthetic Aperture Radar.

Both passive and active sensors detect the behaviour of electromagnetic radiation after its interaction with the earth surface.

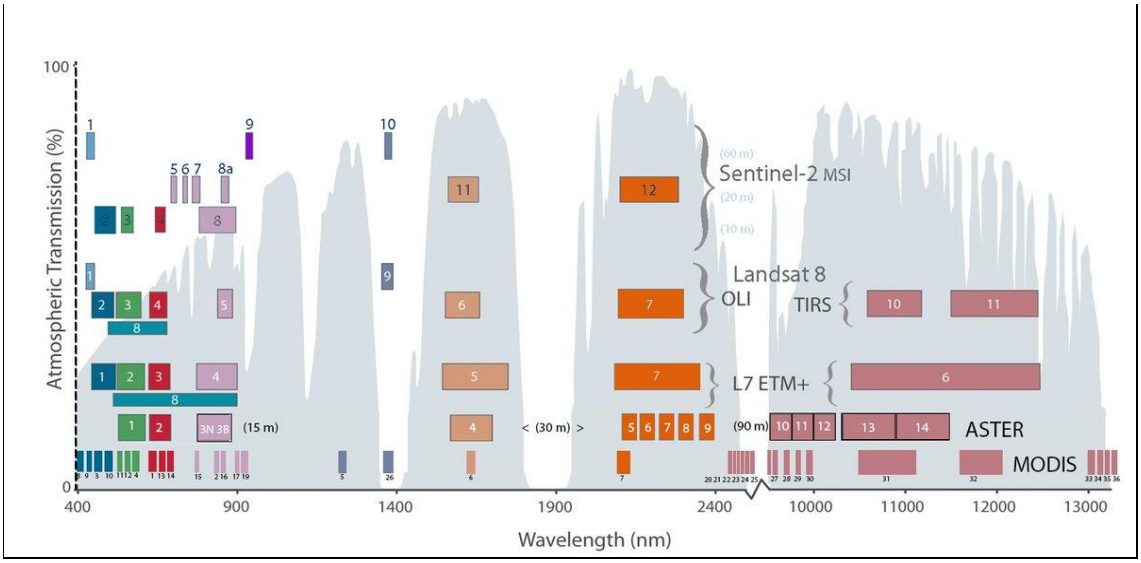

Figure 2.4 - Spectral bands of different sensors[18].

2.5.2 Optical remote sensing

Optical remote sensing uses the optical spectrum (approximately 0.3 to 14 µm) to study the Earth. Within this range are UV, visible, near- mid-, and thermal infrared wavelengths. An example of a satellite using optical sensors is the Landsat series. In the various applications of environmental interest, the spectrum is divided into various intervals called "spectral intervals" or "spectral bands" in order to classify the detected electromagnetic energy. Radiation in the visible and infrared is the data sources of greatest interest, because they are most frequently used. In the visible region, light is divided into three basic intervals: the blue, green and red bands (with λ between 380 and 750 nm), at the "longer" end there is the infrared, of which it is relevant to mention its articulation in Near InfraRed (NIR) and Thermal InfraRed (TIR).

In remote sensing, only the radiation reflected and emitted by an object are considered because the absorbed and transmitted waves cannot be measured by the sensor. In particular, the parameter measured by the sensor is the radiance which corresponds to the brightness in a certain direction towards the sensor This measure can be characterized in a quantitative: the radiance L [$W \cdot m^{-2} \cdot sr^{-1}$] is the contribution of the radiant flux dΦ incident on a unit area dA by a cone of radiation subtended by a solid angle dω at an angle θ to the surface normal.

Radiance is the “flux of energy (primarily irradiant or incident energy) per solid angle leaving a unit surface area in a given direction”, “Radiance is what is measured at the sensor and is somewhat dependent on reflectance” (https://semiautomaticclassificationmanual-v5.readthedocs.io/en/latest/index.html).

$$L\ (\theta\psi = \frac{d^2\phi(\lambda)}{cos(\theta)d\omega dA}$$

The radiance therefore depends both on instrumental characteristics (the solid angle corresponds to the opening angle of the sensor) on the geometry of the observation, and on the wavelength of the radiation considered. Furthermore, radiance is strictly correlated to another quantity known as "reflectance" which is defined as the ratio between the energy reflected by a surface compared to the total energy incident on it and can be expressed as a percentage.

[18]Source: https://gis.stackexchange.com/questions/276871/convertion-of-spectral-indices-formulas-from-landsat-to-sentinel

Images such as Landsat or Sentinel-2 are composed of several bands and a metadata file which contains information required for the conversion to reflectance.
Different sensors continuously scan the Earth's surface to produce imagery (Camps-Valls et al., 2011). An image is composed by a matrix of pixels defined by columns and rows; each pixel presents a numeric value corresponding to the intensity level of the reflected energy as discussed in previous paragraph. The image data produced by different sensors on satellite systems have unique characteristics that relate to the sensor's resolutions—spatial, spectral, radiometric, and temporal.

- **Spatial resolution** of a sensor designates the minimum size of an object that can be detected in an image. It is important not to confuse spatial resolution with pixel size, as they express different but related concepts (Weng, 2013).
- **Spectral resolution:** refers to the number and size of the bands in which the sensor is able to divide the entire spectral range it records; each band corresponds to a raster (Congedo, 2016).
- **Temporal resolution** or revisit time is the time required to complete orbital cycle, i.e. observe the same area.
- **Radiometric Resolution**: is determined by the number of discrete levels into which signal radiance can be divided. For example, 8-bit have higher contrast (0–255 digital number) than a 6-bit data that present a range between 0-63 DN (Digital Number).

2.5.3 Radar remote sensing

SAR system is an active sensor that use microwave for remote ground observation; radar transmits shorts pulses of microwave energy at regular intervals illuminating the surface obliquely at right angle to the motion of the platform. The antenna receives a portion of the transmitted energy, reflected or back scattered from various objects, and by measuring the time delay between the transmission of the pulse and the reception of the backscattered signal from different targets, it is possible to determine the distance of an object and thus his location. As that sensor platform moves forward recording and processing of the backscattered signals, the radar builds up a two-dimensional image. The figure 2.5 shows four exclusive acquisition modes of Sentinel1, which uses C-band; the wavelengths most frequently used by SAR are indicated in Table 2.6.

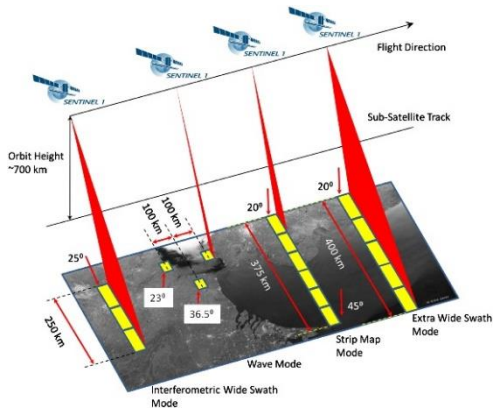

Figure 2.5 - Sentinel 1 acquisition mode[19].

Table 2.6 - Different SAR bands.

Band	Wavelength (λ), cm
Ka (0.86 cm)	0.8 – 1.1
K	1.1 – 1.7
Ku	1.7 – 2.4
X (3.0 cm)	2.4 – 3.8
C (5.0 cm)	3.8 – 7.5
S	7.5 – 15.0
L (24 cm)	15.0 – 30.0
P (68 cm) 1.0 – 0.3	30.0 – 100.0

Each pixel in the radar image represents a complex quantity of the energy formed by the phase and the amplitude: the phase is provided in radians while the amplitude is provided in decibels. In this research it was used the amplitude of radar signal.

[19] Source: https://sentinels.copernicus.eu/image

For land cover mapping is important to consider a series of the parameter that influence the characteristics of imagery produced: these are sensor parameters and surface parameters. Radar parameters which are wavelength, polarization and incidence angle, influence the transmission characteristics of the signal.

2.5.3.1 Sensor parameters

Wavelength is the distance from the peak of one wave to the peak of the next wave. Radar sensors operate at specific wavelength, for example L radar operates at a specific frequency within 15 and 30 centimeters.
The length of the wave determines the interaction with surface objects and his penetration through the medium: in general, the longer the wavelength the grater is the penetration. The wave will interact with object that are approximately its size. In vegetated area X-band is generally governed by the top of the canopy while with C-band will penetrate further and L-band penetrate even further into the vegetation canopy.

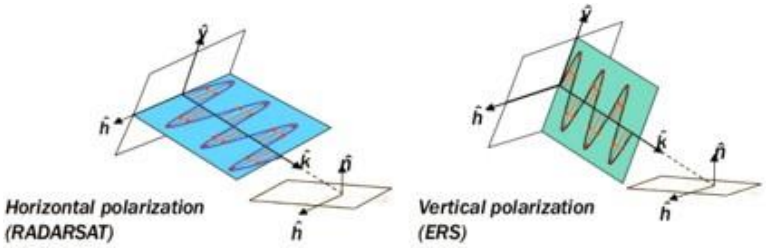

Figure 2.6 - Horizontal and vertical polarization[20].

The other radar parameter is polarization and it refers to the plane of propagation of the electric field of the signal so respect to wavelength radar signal can be transmitted and/or received in different mode of polarization (Figure 2.6). There can be four combinations of both transmit and receive polarizations for example an VV transmission means vertical transmitted and vertical receive.
Polarization is useful in providing information on structure orientation. Penetration depth is also in part influenced by polarization and in forest HH tends to be less attenuated than VV, so HH penetrates deeper into the canopy than VV or VH (Flores-Anderson et al., 2019).
The final sensor parameter is incidence angle. It is the angle between the direction of the incident wave and the earth's surface plane. In radar, incidence angle increases across the swath from the near to the far range: this mode of data acquisition influences the signal because large angles are more sensitive to surface roughness and penetrate less into the medium as opposed to small. Low incidence angles so those are perpendicular to the surface will result in higher backscatter and greater penetration; as a consequence there is less energy that is returned to the sensor moving across the swath, from near to far range and the image become increasingly darker (tone is around 3 to 5 dB difference in backscatter). This is important in classification for the choice of training area since the classes don't have the same backscatter characteristics in the far range.

2.5.3.2 Surface parameters

Unlike satellite images, which are passive remote sensing system, in active systems the brightness or darkness of the image is dependent on the portion of transmitting energy that is returned back to the radar from targets on the surface. This is what the radar measures that is known as radar backscatter (sigma naught or sigma zero). The backscattered coefficient can be a positive number, if there is a focusing of

[20] http://de.slideshare.net/EliseKoeniguer/3-sar-image-interpretation-56027271

backscattered energy towards the radar or can be a negative number (Moreira, 2013), if there is a focusing of backscattered energy way from the radar (e.g. smooth surface).
The response to radar energy by the target is primarily dependent on three factors:-*surface roughness of the target, moisture content and electrical properties of the target.*
Roughness are conditioned by the size of the components of a surface, whether a surface appears rough or smooth to a radar depend on the wavelength and incident angle. A surface is considered as smooth or rough by comparing its surface height deviation with wavelength. For example, a smooth surface occurs if the high variations are much smaller than the radar wavelength (Figure 2.7 a).

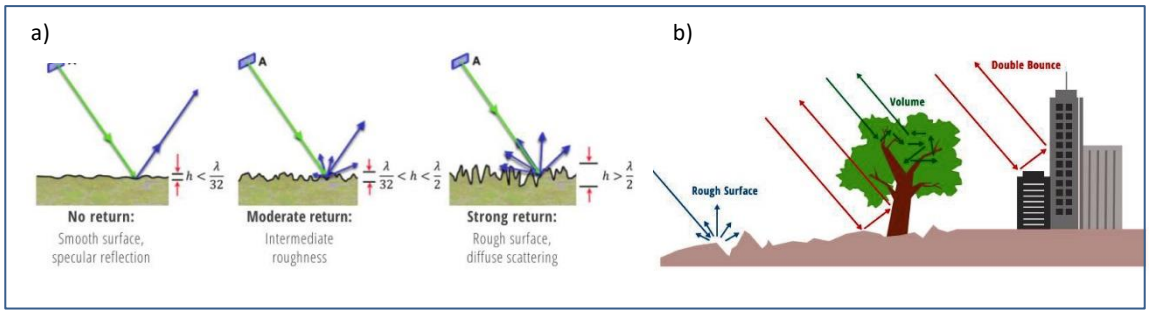

Figure 2.7 - Radar backscatter depends on surface roughness as a function of wavelength (a) and different characteristic of object (b)[21].

The smooth surface is also known as specular reflection. A smooth surface acts as a mirror to the incidence radar pulse, and most of the incident radar energy is reflected away from the sensor. Open water surface tends to be specular reflector and the energy is reflected away from the radar, in this way the surface tends to look very dark in radar images. When the surface height variations begin to approach the size of the wavelength, the surface will appear rough and the incident beam is scattered. There is different scatter mechanism: rough surface scatters, volume scatters double-bounce scatters (Figure 2.7 b).
In rough surface, energy is dispersed approximately equally in all direction and a portion of that energy is back scattered to the radar. An example is an open water when there are ripples: if the size of small ripple is large enough to be approximately similar to size of the length of the wave, the surface appears rough. In that case part of energy reach the satellite and the surface appear even brighter.
Volume scattering occurs when the radar energy is scattered within a volume or medium and it usually consists of multiple bounces and reflections from different components within the volume. There is volume scattering within a snowpack or within the vegetation.
Finally, there is double bounce when two smooth surfaces form a right angle facing the radar beam, where the beam bounces twice off the surfaces and most of the energy is reflected to the radar sensor. Double bounce is commonly seen in urban areas such as high buildings or also in flooded vegetation areas.
In general, areas that have low vegetation fields, bare soils or roads have rough surface scattering and they are characterized by a very low backscatter.
In forested area the dominant scattering mechanism is volume scattering that can be co-polarized or cross polarized. This second mechanism such as HV or VH will have a higher return then co-polarized in case of volume scattering, thus, for forest degradation studies or for changes detection, cross-polarized observations with SAR imagery are fundamental. In a deforested area there is a change from volume to surface scattering, this means a lower backscatter, as typical after the deforestation event.
The oblique observations geometry inherent to all imaging radar systems, result in geometric distortions in SAR data acquisition; they are known as foreshortening, layover, and shadow and illustrated in Figure 2.8. A cause of foreshortening the slopes oriented to the SAR appear compressed in radar imagery; in the case

[21] Source: elaborated from SAR handbook, http://www.SERVIRglobal.net

of layover, the signal come from the higher portion of an object, is received before the return from the lower part, causing backscatter distortion. Shadow indicates those areas not illuminated by the radar beam, so they appear very dark because not return signal is received.

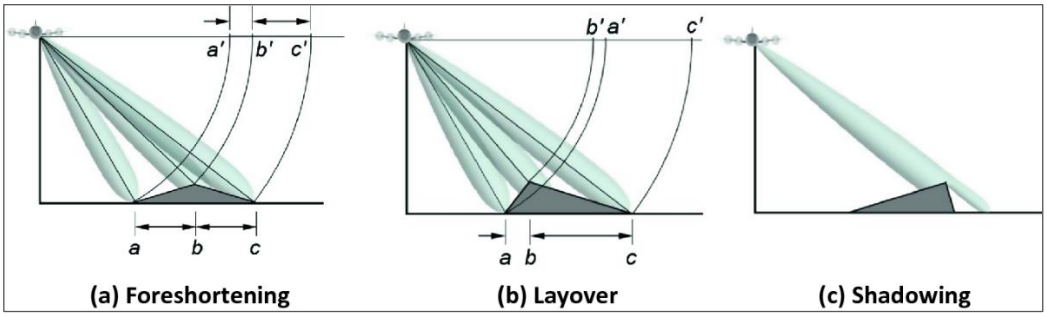

Figure 2.8 - Geometric distortions in SAR data acquisition[22].

SAR image are characterized by spackle noise that is grainy salt and pepper texture in an image. It is caused "by random constructive and destructive interference from multiple scattering returns that occur within each resolution cell"[23]. In order to reduce the spackle, it necessary to apply a filter or performing a multi looking processing where range and/or azimuth resolution cells are averaged. In both situation the result is a reduction of spatial resolution (Flores-Anderson et al., 2019).

2.6 Spectral analysis of optical image

Image correction, enhancement or transformation are always devoted to the preparation of a data set useful for the extraction of required information.
Analysis of remote sensing imagery involves the identification of various targets in an image, which may be environmental as well as artificial features. Targets can be defined in terms of the way they reflect or emit radiation, i.e. in terms of their spectral behaviour. Image analysis permit to translate the spectral behaviour of different surfaces into classes and to classify the image.

2.6.1 The spectral signature

As illustrated in paragraph 2.5.2, the spectral reflectance of surface is defined by the ratio between the incident and reflected radiant energy in a certain wavelength. Such ratio varies according to the considered wavelength range; thus, spectral characteristics of different surfaces can be described graphically by means of the spectral reflectance curves. The Figure 2.9 shows a couple of examples for soil and vegetation: the differences in absorption and reflection in the various spectral intervals are evident.
For the main surface types, the following general statements can be done:

[22] http://www.radartutorial.eu/20.airborne/ab07.en.html. Accessed 03/02/20
[23] https://www.nrcan.gc.ca, 25/11/2015

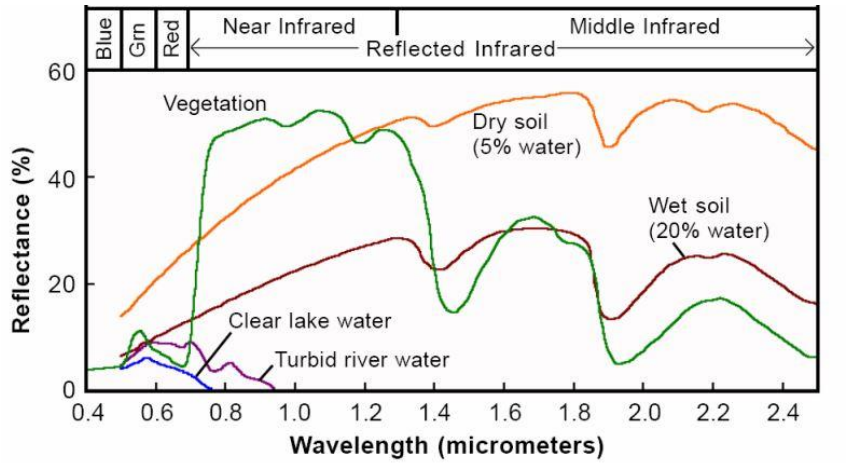

Figure - 2.9 Spectral signature of different objecs[24].

- Clear deep water absorbs most part (more than 90%) of the incident radiation in the visible; absorption can reach 100% in the infrared portion of the spectrum; the reflectance increases, especially at shorter wavelength, when suspended material (sediments) is present and for very shallow waters.
- Bare, dry soil reflectance increases with wavelength; the presence of humidity can cause absorption peaks at 1.4, 1.9 and 2.7 µm.
- The behaviour of vegetation is quite more complex, having two absorption peaks in the blue (0.40 – 0.50 µm) and red (0.63 – 0.70 µm) wavelength and two reflection peaks in the green (0.50 – 0.63 µm) and in the near infrared wavelength (0.7 – 1.1 µm).

In principle, various kinds of surface materials can be recognised and distinguished from each other by these differences in relative reflectance, provided there is some suitable method for measuring these differences as a function both of wavelength and of intensity of reflected radiation. Satellite multispectral sensors measure reflectance in different portions of the spectrum, one for each spectral band; each image pixel is therefore characterised by a sequence of digital numbers which record information on a specific band. In a multispectral image, recorded values of reflectance for a certain surface will vary according to the wavelength investigated, while for the same wavelength different surfaces can behave in very different ways with respect to incident radiation.

The various approaches to computer-aided image classification aim at the identification and description of spectral characteristics of different clusters (representing land use/land cover and biophysical information) to be classified, by means of statistical parameters of such clusters; once each group has been statistically defined, every pixel of the image will be assigned to its most probable class.

2.6.2 Spectral indices

Spectral indices are mathematical equations applied to image bands to derive information about the composition and characteristics of land surface. Many indices are developed to highlight the behaviour of vegetation: they are called vegetation indices which are the most commonly used.

Net photosynthesis is directly related to the amount of photosynthetically active radiation that plants absorb. In short, the more a plant is absorbing visible sunlight (during the growing season), the more it is photosynthesizing and the more it is being productive. More in detail, absorption and reflectance effects of

[24] Source: https://www.hatarilabs.com/ih-en/land-cover-spectral-signatures-determination-with-qgis-3-and-semi-automatic-classification-plugin-scp-6-tutorial

vegetation are the following: absorption by chlorophyll pigment in green leaf chloroplasts is maximal at 0.65 µm (red) and, and to a similar extent, in the blue wavelength (Figure 2.10). Conversely, the predominant reflectance is in the green wavelength (thus, most vegetation is characterised by green leafy colour). Also, reflectance is strong between 0.7 and 1.0 µm in the leaf mesophyll cells; the intensity of this reflectance is commonly greater (higher percentage) than from most inorganic materials, so that vegetation is described as "bright" in the NIR. These properties of vegetation account for their tonal signatures on multispectral images: darker tones in the blue and especially red bands, somewhat lighter in the green band, and notably light tones in the NIR bands.

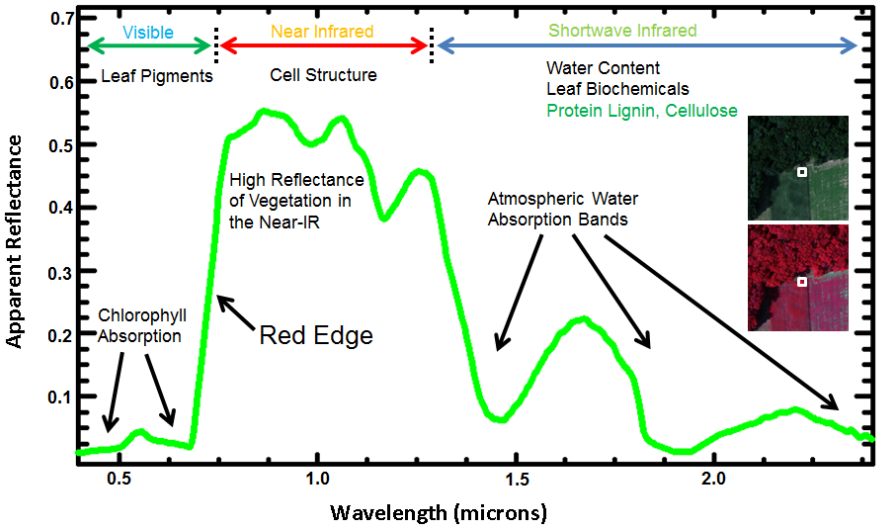

Figure 2.10 - Details of an example vegetation spectral signature [25].

This spectral behaviour of green, healthy vegetation can be used in image processing to process multispectral data in order to extract useful information about vegetation cover.

Since chlorophyllian activity is responsible for high absorption of red (R) radiation and high reflection of NIR radiation, it is clear that the total amount of reflected radiation in these two wavelengths (which is measured by the sensor) is function of the amount of chlorophyll and, therefore, of the total green biomass covering the soil at a certain location. So, linear combinations of NIR and R bands of multispectral images allow exalting these strong differences in spectral behaviour of vegetation with respect to the other types of surfaces.

One widely used index is the Normalized Difference Vegetation Index (NDVI) which has been used to monitor vegetation conditions (Rouse Jr, 1973).

The value of this index can vary within a range between -1 and +1 a: it increases with vegetation density and presents low values in the case of surfaces covered by water. Threshold values as 0.2 can be considered the limit above which the presence of vegetation begins to occur.

$$NDVI= (B8 - B4) / (B8 + B4)$$

NDVI is usually preferred to the simple ratio for global vegetation monitoring because it helps to compensate for changing illumination conditions, surface slope, aspect and other extraneous factors.

Many indexes have been proposed in literature to study specific land cover class or to extract information to distinguish the characteristics of surfaces.

[25] Source: Mark Elowitz

The following are only ones that have been used in this research for image classification and the bands are referred to Sentinel-2 sensor.
NBR (Key & Benson, 1999) can be calculated with the following formula:

$$NBR = (B8 - B12) / (B8 + B12)$$

This index is normally used to identify areas burned by fire or to establish the state of the vegetation. Vegetation shows high reflectance values in NIR band and low reflectance values in the Short-Wave InfraRed band (SWIR) in case of fire this situation is reversed. Therefore, the NBR index assumes high values at vigorous vegetation and low values in burnt areas.
The Normalized Difference Water Index (NDWI) was proposed to detect surface waters in wetland environments and to allow for the measurement of surface water extent. It was designed mainly to maximize the reflectance of the water body in the green band and to minimize the reflectance of water body in the NIR band. McFeeters's NDWI (McFEETERS, 1996) is calculated as:

$$NDWI = (B2 - B8) / (B2 + B8)$$

To distinguish the surfaces covered by ice it was used the Normalized Difference Snow index (NDSI) (Dozier, 1989)

$$NDSI = (B3 - B11) / (B3 + B11)$$

The NDSI reflect the fact that only snow surface present high spectral value in visible range and very low in the short-wave infrared. Finally, the last index used is the Normalized Difference Coniferous Index (NDCI):

$$NDCI = (B6 - B12) / (B6 + B12) * (B8 - B11) / (B8 + B11)$$

This index was proposed in the context of this research and it is used to characterize the behaviour of Coniferous and better distinguish them from broadleaved trees. This index exploits the properties of red edge and those of SWIR bands where Coniferous have higher spectral values than broadleaved trees in winter.
The Table 2.7 summarizes the indexes used.

Table 2.7 - Indices used in the methodology for land cover classification and their formula.

Satellite	Index name	Formula	Reference
Sentinel 2	Normalized Difference Vegetation Index	NDVI= (B8 - B4) / (B8 + B4)	(Rouse et al., 1973)
	Normalized Burn Ratio	NBR = (B8 - B12) / (B8 + B12)	(Key & Benson., 1999)
	Normalized Difference Water Index	NDWI = (B2 - B8) / (B2 + B8)	(McFeeters, 1996)
	Normalized Difference Snow Index	NDSI = (B3 - B11) / (B3 + B11)	(Dozier, 1989)
	Normalized Difference Coniferous Index	NDCI = (B6 - B12) / (B6 + B12) * (B8 - B11) / (B8 + B11)	
	Burned Index	BI = (1 - (B3 + B4 + B8) / (1 + (B3 + B4 + B8)	

The last index used is the Burned Index (BI), which, like the previous one, was developed as part of this research. The index contributes to discrimination between areas affected by fire and those subject to other types of forest disturbances. The index exploits the different behaviour of vegetation that shows a low

reflectance in the visible, in the case of fires (linked to the presence of generally dark bare soil), and a higher reflectance in the visible of spectrum for the areas that have suffered a loss of forest vegetation but have not been burned. These areas are generally characterised by vegetation regrowth or soil with low reflectance compared to forest vegetation, but higher reflectance compared to burnt areas.

$$BI = (1 - (B3 + B4 + B8) / (1 + (B3 + B4 + B8$$

2.7 Land cover classification methods

Analysis of remote sensing imagery involves the identification of various targets in an image, and those targets may be environmental as well as artificial features. Digital image analysis can be performed following two completely different approaches:

Manual interpretation:

This approach consists of observing the differences between objects and their backgrounds comparing different objects based on the visual elements of tone, shape, size, pattern, texture, shadow, and association. Using these visual elements and an interpretation legend, it is possible to classify features in an image, i.e. to identify homogeneous groups of pixels which represent various features or land cover classes of interest. In this study visual interpretation was used in order to collect reference data or to define the training area to set the threshold in land cover classification process.

Automated classification:

Unlike the manual interpretation, the extraction of land cover information can be obtained automatically (as opposed to manual extraction), using computing devices. In this context, the traditional subdivision of classifications into supervised and unsupervised can be overcome by the concept of automatic classification to which both fall.

This approach uses the spectral information represented by pixel value in one or more spectral bands and attempts to classify each individual pixel, based on this spectral information. The objective is to assign all pixels in the image to classes or themes (e.g. water, coniferous forest, deciduous forest, corn, wheat, etc.). The result is a thematic "map" of the original image, i.e. a mosaic of pixels, each of them belonging to a specific theme according to a specific legend chosen.

Actually, a more recent research has focused on automated non-parametric methods both supervised ad unsupervised. Many of these methods belong to the non-parametric statistic domain that differs from parametric systems because they do not require any assumption on the probability distribution of variables (Figure 2.11). The most advantage of these methods is their ability to better label classes that are not perfectly divided into clusters. The parametric systems assume that the distribution of pixels in the image comes from a known probability distribution and make inferences about the parameters of the distribution. The most common non-parametric methods are Minimum distance, K-means clustering, ISODATA and the Maximum likelihood classification. These methods have the advantage of being simple and work even better than the most modern systems if the distribution conditions are met.

From the above, it is possible to divide the classification systems in different ways: either according to the assumptions about the pixel distribution and therefore in parametric and non-parametric, or more traditionally on type of learning used by the algorithm to classify the pixel. In the letter case they are distinguished in supervised and unsupervised classification system.

In this research classification methods are described according to second criteria to better describe the procedure.

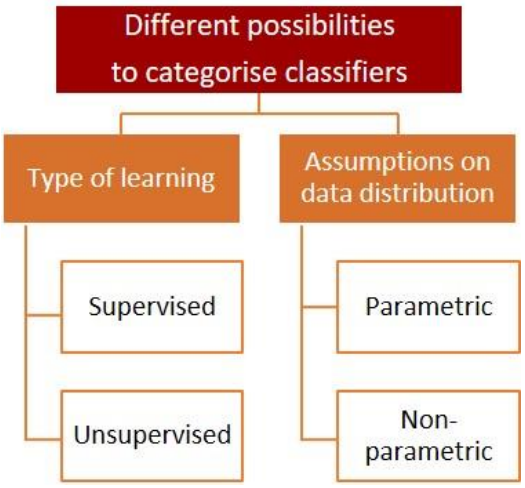

Figure 2.11 – Different approaches to images classification.

2.7.1 Unsupervised classifications

Unsupervised classifications can be considered almost completely automatic procedures; with this category of functions, the analyst plays, in the first phase, a quite passive role; one main advantage which is commonly reported of this approach is that, unlike the supervised approach, no *a priori* knowledge of the area under study is required. This statement is only partially true, since classified images resulting in output from this type of classifications still require to be interpreted. In general, this approach achieves an accuracy lower then supervised methods.

This family of classifiers involves algorithms that examine pixels in the n spectral bands used and aggregate them into a certain number of classes based on natural groupings (or clusters) present in the image values. The basic concept is that values of pixels belonging to a certain land cover type should be close together in the feature space, while data of different classes should be comparatively well separated.

One common form of clustering, called the K-means approach, is a self-iterative procedure that follows several steps. In K-Means method, at the beginning, it is necessary to decide how many classes are expected and define the number of clusters, then each pixel is assigned to their nearest cluster location. The result of such automatic procedures is simply the identification of spectrally distinct classes in image data: the analyst must translate each spectral class into a land cover class, according to a pre-established legend. This last phase has important implications in the unsupervised classification procedure. ISODATA is like K-means, except that the number of clusters can vary. The algorithm eventually indicates the number of clusters.

2.7.2 Supervised classifications

The supervised classification is a common classification procedure to generate land cover maps from remotely sensed data. It is based on the use of training data to define the typical pixel values of each land cover class or, in other words, to identify the regions of the feature space that contain the points belonging to classes that must be recognised in the image. Such regions will be described in terms of mean value of the class in each spectral band and its standard deviation. With this operation, the analyst determines the spectral signature of a land cover class:

Once the spectral signatures of each class have been determined, pixels are assigned to a class by comparing their digital values with the various spectral signatures; such operation can be accomplished by using different algorithms (or classifiers) that will be briefly discussed later.

The classification strategy is quite simple and can be described in three basic phases:

1. The training stage: it includes the selection of desired land cover classes, the preparation of the classification legend and the selection of groups of pixels (training data set) representative of each class in the legend. The training stage's quality is extremely important, because it directly determines the quality of the final result.
2. The classification stage: digital values of selected pixels are used to calculate the spectral signatures of each class; then, spectral signatures are used as input parameters of the classification algorithm used to perform image classification.
3. The accuracy assessment stage: an independent set of pixels representative of each class is used to estimate the classification accuracy.
Numerous supervised classification methods have been developed: these algorithms range from more traditional system to advanced machine learning algorithms. In the next section a brief overview of the different systems is provided, briefly describing the concepts on which they are based and highlighting the disadvantages and strengths.

Maximum Likelihood Classifier (MLC)
Within supervised system, MLC is a widely used classifier and as previous methods, fall in the category of parametric approach.
MLC quantitatively evaluates both the variance and covariance of each sample class when classifying an unknown pixel. To do this, an assumption is made that the distribution of clusters forming the training data set for each category is Gaussian (normally distributed).
This assumption of normality is generally reasonable for common spectral response distributions. Under this assumption, the distribution of a category response pattern (i.e., the shape of the region in the feature space for that cluster) can be completely described by the mean vector and the covariance matrix. Through these parameters, it is possible to compute the statistical probability of a given pixel value, to be a member of a particular land cover class.
After evaluating the probability in each category, the pixel will be assigned to the most likely class (highest probability value) or it will be labelled "unknown" if the probability values are all below a minimum threshold set by the analyst.

Artificial Neural Network (ANN)
A certain kind of supervised algorithm is ANN so here the objective of this algorithm is to mimic the human brain which is able to see and analyse a lot of information coming from different sources and making link between this data sets. It is a non-parametric classifier, i.e. it does not require any assumption about the statistical distribution of the data, and it can incorporate *a priori* knowledge as a realistic constraint including input data of area of interest. The advantage is that it is much more accurate then MLC when are related dataset. The main drawback is that is a like black box, and it is very difficult to understand why a pixel is in one class or in another one.

Support Vector Machine (SVM)
This is a non-parametric statistical learning technique for solving a quadratic optimization problem. SVM instead of using the dataset is based on training samples, defined support vectors, to determine the best threshold to maximize the separation between two vectors. In this way SVM is a binary classification, but it is applied to the classifier to all possible combination to increase the number of classes.

Decision tree (DT)
“A tree classifier is determined by a finite set of decision rules that are connected and sequentially applied according to a tree topology” (L Breiman et al., 1984). The decision tree graph assigns to each node a feature of the instance to be classified and to each branch a value among those that the node can assume. The

instances are classified from the "root" of the tree and divided gradually according to the values of the characteristics (Kotsiantis et al., 2007). The result is a graphical representation of a set of *if - then* rules, which proves to be particularly clear and easily interpretable (Mitchell, 1997). Normally a decision tree belongs to learning techniques and use reference data set divided in training set on the basis of which the tree structure is created and validation datasets to evaluate the results.

Random forest (RF)

RF algorithm, originally proposed by Braiman (Leo Breiman, 2001), is a machine learning technique based on the decision tree classification model. In this model several DT are created, and the response is calculated based on the outcome of all DT. RF takes its name from the characteristic tree structure, in which each branch (node) represents a binary choice (yes/no), and in which the leaves at the bottom are the result obtained from the concatenation of these decisions. RF can overcome the drawbacks associated with single DT by creating many (usually several hundreds) different DT using random subsets of the data (bootstrap dataset) and variables. Once the forest has been created, the accuracy of the model can be determined by processing all the data not included in the bootstrap dataset (Out-Of-Bag data) and performing a validation.

Table 2.8 - Advantages and disadvantages of different classification methodologies[26].

Algorithm	Strengths/characteristics	Weaknesses
Maximum Likelihood (Parametric)	• Simple application • Easy to understand and interpret • Predicts class membership probability	• Parametric • Assumes normal distribution of data • Large training sample necessary
Artificial Neural Networks (Non-parametric)	• Manages large feature space well • Indicates strength of class membership • Generally, classification accuracy • Resistant to training data deficiencies – requires less training data than Decision Trees	• Needs parameter for network design • Tends to overfit data • Black box (rules are unknown) • Computationally intense • Slow training
Support Vector Machines (Non-parametric	• Manages large feature space well • Insensitive to Hughes effect • Works well with small training data set • Does not overfit	• Needs parameters: regularization and kernel • Poor performance with small feature space • Computationally intense • Designed as binary, although variations exist
Decision Trees (Non-parametric)	• Non need for any kind of parameter • Easy to apply and interpret • Handless missing data • Handless data of different types (e.g. Continuous, categorical) and scales • Handless non-linear relationships • Intensive to noise	• Sensitive to noise • Tends to overfit • Does not perform as well as others in large feature spaces • Large training sample required
Randon Forests (Non-parametric)	• Capacity to determinate variable importance • Robust to data reduction • Does not overfit • Produces unbiased accuracy estimate • Higher accuracy than DTs	• Decision rules unknown (black box) • Computationally intense • Requires input parameters (trees and variables per node)

During the last years the supervised classification techniques have increased (Thanh Noi & Kappas, 2018) thanks to the availability of ancillary data, which provide accurate information on ground truth (Colditz, 2015). Parametric supervised classifiers (MLC, minimum distance) are difficult to use for classifying large

[26] Source: https://eo4society.esa.int/

multi-temporal datasets, because they are not characterized by a large flexibility in decision boundaries. Since these classifiers assume a normal data distribution, they furnish excellent results when data distribution is unimodal, but they could be difficult to apply for multi-modal dataset analysis (Belgiu & Drăguţ, 2016; Gómez et al., 2016).

Machine learning approaches are largely used in land cover mapping, thanks to their capacity to model class signatures, to elaborate many input data and to produce higher accuracy compared to traditional parametric classifiers, especially for complex data with many predictor variables (Maxwell et al., 2017). For example, DT and neural networks are machine learning which focus on decision rules and on class boundaries which improve the classification of land cover types with unknown distribution and frequency (Foody & Mathur, 2006).
On the other hand RF (an implementation of DT) allows a higher classification accuracy (Ma et al., 2019), but it is characterized by a higher computational intensity, unknown decision rules (black box) and the need of input parameters (Gómez et al., 2016; Rodriguez-Galiano et al., 2012). Table 2.8 shows the advantages and weaknesses of the most common image classification methods.
One of the objectives of this research is the development of a methodology to create a new map covering the entire Italian territory. To overcome some of the limitations of the classification techniques previously presented, the method proposed in this research is the "decision rule". This method makes it possible to analyse and interpret "large continuous amounts of data" over vast areas and in a short time, allowing at the same time to achieve good levels of accuracy. Since it is not a “closed box”, it is also possible to better analyse the weak points and the behaviour of the variables used and understand where to intervene to improve the classification results. A new "change detection" technique was also developed to update the land cover map, so as to guarantee the sustainability of the system over time. The following paragraph gives an overview of the available change detection techniques and the problems related to their use.

2.8 Review of change detection algorithm

Change detection consists in two principal approaches: the first one directly detects changes from satellite data in a unique step, the second performs two single classifications and then identifies the changes by comparison of the two classified data.
Below is a brief review of the main research progress on algorithms specifically used to detect land cover changes, some of which are also used for image classification; the principles on which the latter are based have been set out in the previous section.
Researchers have made enormous efforts in developing various change detection methodologies and have published several change detection reviews, based on satellite remote sensing data (Ban & Yousif, 2016; Coppin et al., 2004; Hansen & Loveland, 2012; Hussain et al., 2013; Karantzalos, 2015; Lu et al., 2004, 2014; Radke et al., 2005; Reba & Seto, 2020; Singh, 1989; Tewkesbury et al., 2015; Z. Zhu, 2017). Change detection methodologies have focused on different fields of applications, including desertification studies, flood mapping (Li et al., 2019) and disaster monitoring (Bovolo & Bruzzone, 2007; Gamba et al., 2007), however, due to the complexity of the problem, most authors agree that a universal technique does not yet exist (Ehlers et al., 2014). Many of these studies and reviews stress the difficulty of identifying common guidelines for the choice of the most suitable methodology algorithm. Likewise comparing the accuracy of different technique is a very hard task for several reasons: it depends, among the others, on the spatial, spectral and temporal resolution of the sensor used and on the objective of the research.
The pixel (resolution) represents the base unit of image analysis (Hussain et al., 2013) and it is one of the most important factors because it is directly connected with the ability to discriminate small objects.
By literature change detection methods can be grouped according different principle, into pre-classification and post-classification analysis, in object-based or pixel-based techniques or supervised and unsupervised.

Object based are more suitable when very high resolution data are utilized, while the latter are preferable with images with medium-high resolution, as they better exploit the information available at a pixel level; however, many change detection technique that could be implemented to pixels can also be used to object (Warner et al., 2009)

The most commonly used algorithms are based on image differencing (Bovolo & Bruzzone, 2007), image ratioing (Moser & Serpico, 2006), regression analysis, vegetation index differencing, CVA (Bovolo & Bruzzone, 2007; He et al., 2011; Thonfeld et al., 2016), transformation (as principal component analysis) (Deng et al., 2008) and tasselled cap transformation, machine-learning (such as ANN, SVM or DT) (Nemmour & Chibani, 2006; Tewkesbury et al., 2015; Volpi et al., 2013), or hybrid i.e. those using more than one system. Image differing or ratioing are best suited for change/no-change (binary) information. Most of these techniques are based to threshold value to discriminate area changed /no changed; the selection of the best threshold determines the accuracy of the technique used. In order to improve the performance, it is possible to combine different fusion techniques or apply automated threshold algorithms.

Another method of image transformation widely used in literature is the CVA. It is a multivariate change detection technique where the algorithm produces two information vectors: change vector direction and multispectral change magnitude. Changed areas are derived as the difference between these two vectors through a threshold to distinguish changed from unchanged pixels. Johnson and Kasischke (Johnson & Kasischke, 1998) described the capability of CVA as an effective method to capture all changes and his potential was illustrated in several applications and researches (Bovolo & Bruzzone, 2007; S. Liu et al., 2017; Saha et al., 2019; Ye et al., 2016). Nevertheless, the performance and accuracy are affected by image acquisitions at different dates (atmospheric conditions, solar angle) and by the definition of single threshold that could be insufficient for detecting magnitudes of change.

Several classification systems are based on direct image classification. The process consists in a classification of multitemporal images where, in a single step, a classifier labels both the stable classes and the change classes and, as highlighted previously; these systems can be supervised and unsupervised. They were used for forest change detection and they are widely used in machine learning systems. For example, Schneider (Schneider, 2012) used SVM and DT in urban detection using a series of 50 Landsat images while other researchers highlighted the potential machine learning techniques for change detection analysis (Bovolo et al., 2008; Nemmour & Chibani, 2006; Volpi et al., 2013; Z. Zhu & Woodcock, 2014). However, these methods have some disadvantages such as the difficulty to find a sufficient number of training areas, the user-defined parameters to set the algorithm and the effectiveness of variable used. On the other hand, unsupervised systems which do not need ground truth, may not detect small changes, of crucial importance for short-term changes (Warner et al., 2009) in urban context. To overcome these difficulties, some authors have tried to develop semi-unsupervised change classification systems (X. J. Zhu, 2005). These systems are based on the idea of extracting unlabelled samples from a previously acquired image (Zanotta et al., 2015) in order to increase the number of training areas and then use this information for developing any supervised method (Ghosh et al., 2014).

Another line of research has focused on the combined use of radar and optical sensors: from these two kinds of sensors is possible to extract a larger amount of information, exploiting the different physical principles of electromagnetic waves.

Ban *et al.* (Ban et al., 2017) used both these two sensors for urban land cover mapping using an object-based classification method; (Pesaresi et al., 2016) used fused data for improving the results of urban settlement map; Jan Haas & Yifang Ban (Haas & Ban, 2017) segmented the combination of Sentinel SAR and Multi-spectral image stack for classify the Zürich metropolitan area using SVM algorithm; Goldbatt *et al.* (Goldblatt et al., 2018) mapped built up changes in Ho Chi Minh City, Vietnam, Celik and Sun *et al.*(Celik, 2018; Sun et al., 2019) performed extracted urban land cover information from Sentinel-1A SAR data and Sentinel-2 Multi-spectral image based on Google Earth Engine.

The analysis carried out shows that a significant progress has been made to analyse land cover changes and no one algorithm can be considered suited for all the change detection applications. Besides this, most of the methodology elaborated in literature are applied to small areas and their reproducibility over large areas is much more problematic because of the complexity of landscape. In order to solve classification issues, many authors have used hybrid methods that allow a certain flexibility and take advantages offered by more than one system; instead, few methods, in literature use a specific algorithm for each class to be extracted. Using this latter approach, it is possible to identify *ad hoc* procedures depending on the class to be obtained and intervening only on the classes that present major problems. In this research it has been considered a technique of this type through decision rules, in which each rule represents an algorithm aimed at classifying a single class; in addition it has been investigated the integration of multispectral optical data, which were traditionally used for land cover classification and change detection analysis together with the data SAR. These latter data make the exploiting different polarisations possible, under unfavourable weather conditions, for developing a new methodology that will be illustrated in the next chapter.

Chapter 3 Materials and methods

This chapter provides a detailed description of the method developed for mapping Italy through the classification of satellite images. It also describes the methodology to identify the changes occurred between 2017 and 2018, considering those transformations that can be identified after one year, such as land consumption or burned areas. Finally, the procedure to obtain the reference dataset needed for validation and to perform the accuracy analysis is explained.

3.1 Study area

The study area is represented by the entire Italian territory for a total surface of 301,338 km². Most of Italy consists of mountainous areas (35%) or hills (41.6%) and plains (23.2%)[27]. The mountain belts extend in the northern area, forming the Alps with peaks reaching over 4000 m in the western part. The Appenini Mountains extends over the whole peninsula reaching its highest peak with the Gran Sasso (2912 m), located in Abruzzo. Finally, the insular area includes Sardinia, Sicily and numerous smaller islands. With these characteristics the northern sector and the central chain are often covered by clouds or affected by perturbations that make it difficult to find free-clouds optical images for various periods of the year.
The Italian geological profile is very complex and is the result of numerous geodynamic events that have led to the formation of the Alpine and Apennine mountain chains, and to the presence of several active volcanic zones and extensive seismic, hydraulic and hydrogeological risk zones. The landslides recorded in the ISPRA Inventory of Landslides in Italy are 620,808 and affect an area of 23,700 km^2, equivalent to 7.9% of the national territory (Trigila A. et al., 2018). As a result, 1,224,000 inhabitants are resident in areas with very high landslide hazard and high landslide hazard according to the ISPRA 2018 report. For what concerns the hydraulic hazard, it emerges, for example, that areas with high hydraulic hazard cover 12,405 km^2 of the territory (4.1% of the national territory) and a resident population of 1,915,236 inhabitants (3.2%), considering the scenario of high hydraulic hazard P3 (return time between 20 and 50 years).
Finally, due to its particular geographical position, in the area of convergence between the African and Eurasian plates, Italy has a high "seismicity", characterized by areas where earthquakes often occur, but are of low energy (for example: Colli Albani south of Rome, Vesuvian area, Etnean area), and other areas, where earthquakes occur more rarely, but are of high energy (for example Calabrian Apennines and eastern Sicily).

[27] https://www.istat.it/it/archivio/137001

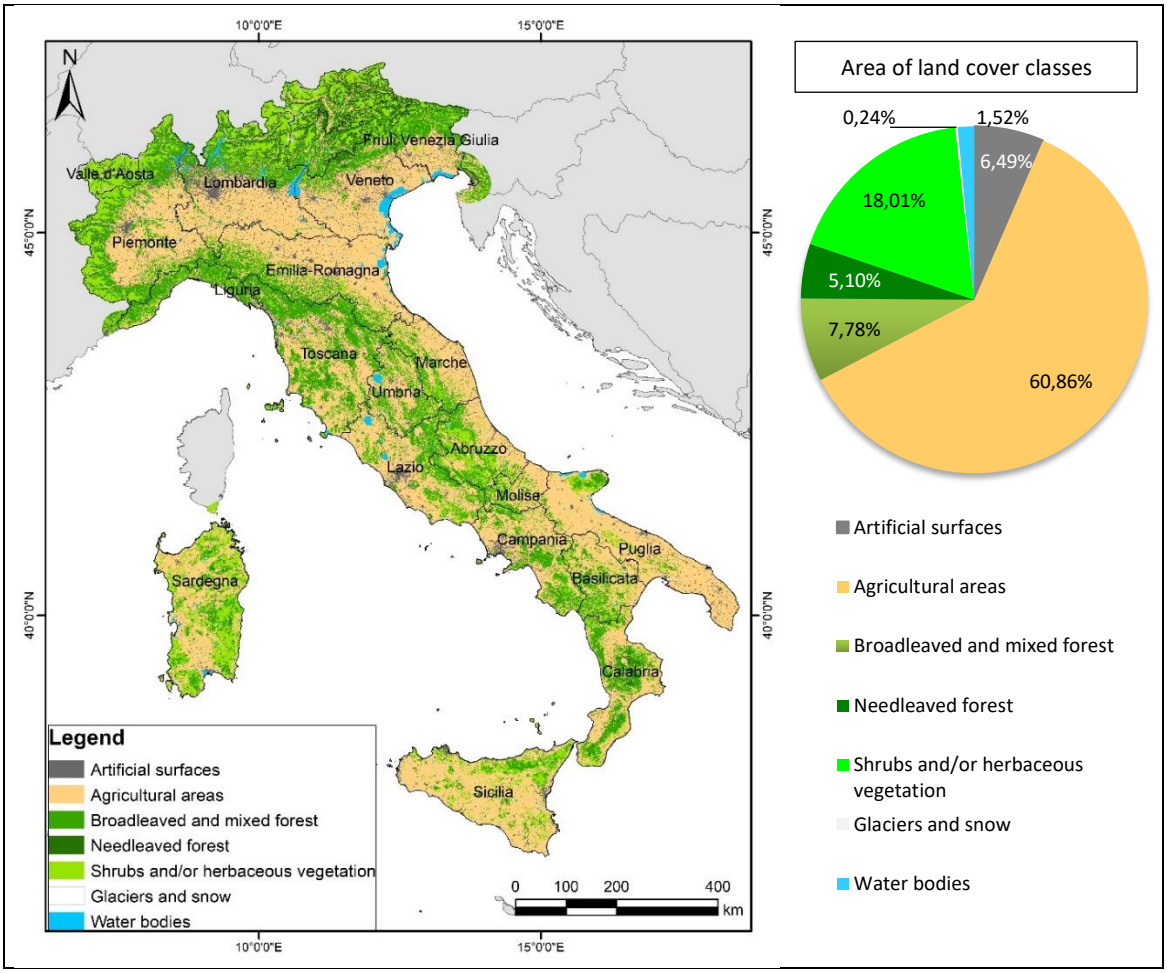

a) b)

Figure 3.1 – Study area: (a) Map of land cover classes. (b) Area of land cover classes in %[28].

Administratively Italy is divided into 20 regions of which one, the Trentino Alto Adige divided into the autonomous provinces of Trento and Bolzano (often the environmental indicators take into account this subdivision). The territory is also further subdivided into provinces and municipalities (93 and 7 904 respectively.

According to the data collected by ISPRA (ISPRA, 2018), the Italian territory is characterized by tree cover for 45,95% of the surface (considering also trees in urban areas and those in agricultural areas) and by herbaceous and shrub vegetation for 38,7 and 4,6 % respectively. Artificial surfaces occupy 7.65% while natural non-vegetated surfaces amount to 1.63%. Finally, the water and wetlands class represent only 1.47% of the national territory. The orographic conformation of the territory heavily affects the geography of urbanization, which is concentrated in the foothills (such as the Lombardy-Venetia), in the plains and coastal areas; the largest density in Italy are located in the main metropolitan areas like Rome, Milan, Naples; the main roads are privileged axes of urban development, especially in northern Italy.

The largest areas of vegetation cover are occupied by trees and grasses (shrub areas are instead the least extensive vegetation cover): the former extend with higher percentages in Tuscany, Piedmont and Sardinia, the latter, dominated mainly by agricultural activities, are very extensive in Sicily, in Emilia-Romagna with in Lombardy and in Piedmont. Waters and wetlands extend mainly in the northern regions due to the presence of large lakes (Garda, Como and Maggiore) (ISPRA, 2018).

[28] Source: CORINE 2018 aggregated.

3.2 Data and materials

One of the added values of this research was the use of free data, software and tools. Below is a brief description of the satellite sensors exploited and the tools used for data pre-processing and for developing the methodology.

3.2.1 Sentinel 1

The Sentinel-1 mission is the European Radar Observatory for the Copernicus joint initiative of EC and the ESA. Copernicus, previously known as Global Monitoring for Environment and Security, is a complex Earth observation program launched in 1998 for the implementation of information services dealing with environment and security. It is based on observation data received from Earth Observation satellites and ground-based information. Each Sentinel missions aiming to provide data on different thematic areas Atmospheric, Oceanic, and Land monitoring that can be used in many applications. Table 3.1 shows the characteristics of missions Sentinel-1 and Sentnel-2.

Table 3.1 - Sentinel1 and Sentinel 2 characteristics.

	Datasets	Characteristics	Spatial Resolution (m)	Temporal Resolution (Day)	Data availability in GEE
Sentinel-1	Sentinel-1 SAR GRD	C-band Synthetic Aperture Radar Ground Range Detected, log scaling	10	6	2014-10-3_present
Sentinel-2 Multispectral Instrument	Surface Reflectance	Level-2A orthorectified atmospherically corrected surface reflectance.	10, 20, 60	5	2017-03-28_present
	Top-of-Atmosphere Reflectance	Level-1C orthorectified top-of-atmosphere reflectance.	10, 20, 60	5	2015-06-23_present

The Sentinel-1 mission is composed of a constellation of two satellites, Sentinel-1A and Sentinel-1B, sharing the same orbital plane and providing, between the two of them coverage over the equator every six days. Sentinel-1 includes C-band imaging operating in four exclusive imaging modes with different resolution (down to 5 m) and coverage (up to 400 km) (Table 3.1). It provides dual polarisation capability, very short revisit times and rapid product delivery. For each observation, precise measurements of spacecraft position and attitude are available.

SAR has the advantage of operating at wavelengths not impeded by cloud cover or a lack of illumination and can acquire data over a site during day or night-time under all weather conditions.

3.2.2 Sentinel 2

Sentinel-2A was launched in 2015 and followed by Sentinel-2B in 2017. Sentinel-2C and Sentinel-2D are under construction and will be ready for launch in 2020/2021

The Sentinel-2 Multi-spectral Instrument sensors provide high spatial resolution images over the global surface, at high revisit time (5 days at the Equator with two satellites in orbit) with 13 bands in the optical NIR, SWIR parts of the electromagnetic spectrum, four bands at 10 m, six bands at 20 m and three bands at 60 m spatial resolution (Figure 3.2 c). The images are produced at different levels, for orthorectified products (Level-1C and Level-2A, see Figure 3.2 b) the granules (also called tiles) consist of 100 km by 100 km ortho-images in UTM/WGS84 projection. Tiles are approximately 500 MB in size (Tiles can be fully or partially covered by image data. Partially covered tiles correspond to those at the edge of the swath, Figure 3.2 a.).

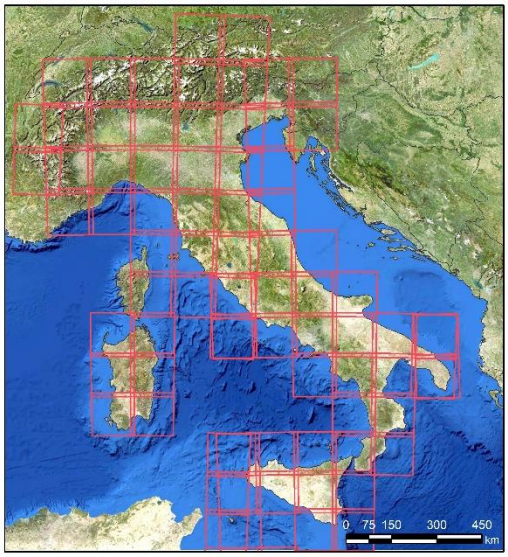

(a) About 80 Sentinel-2 tiles of size 100x100 km^{2}cover the entire Italian territory.

(b) The difference between the L1C and L2A products: on the left L1C products provide the top of atmosphere reflectance, on the right the Level-2A includes an atmospheric correction process to provide an orthoimage bottom of atmosphere corrected reflectance product.

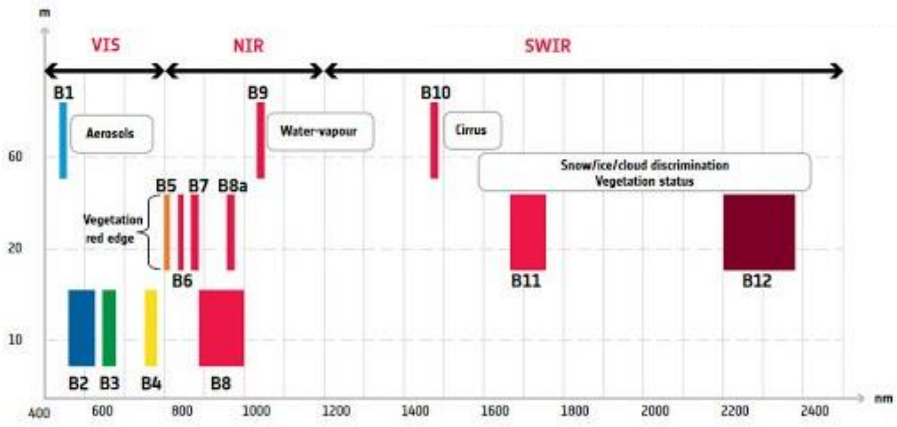

(c) Sentinel 2 bands: the ordinate axis shows the spatial resolution of the bands expressed in m, the abscissa axis the wavelength of the different Sentinel-2 bands.

Figure 3.2 - Sentinel-2 characteristics[29].

The Level-1C are provided in Top of Atmosphere (TOA) reflectance with all parameters to transform pixel values into radiances while the Level-2A product provides Bottom Of Atmosphere (BOA) reflectance images. This resolution and mission coverage permit many applications such as land management, agriculture and forestry; in addition, the high revisit frequency permits supports to natural disasters (e.g. floods, forest fires, landslides, earthquakes and volcanic eruptions), risk mapping and security concerns and information at local, regional, national and international scales.

3.2.3 GIS and processing software

In this research mainly open source software were used: QGIS as a GIS tool and Google Earth Engine for image processing and methodology elaboration.

[29] Source: http://esamultimedia.esa.int/docs/EarthObservation/Sentinel-2_ESA_bulletin161.pdf

QGIS is an open-source software that enables to perform GIS processing and spatial analysis. Like any GIS application, QGIS permits to superimpose various cartographic layers, raster or vectoral, and extrapolate new useful information.
In addition to the normal functions for geographic data analysis, it allows to visualize two windows together and to shows Google Earth™ images in one of these windows. It is also possible to check the date of the displayed images and visualize the same area displayed in QGIS and, in Google Earth™ tool with the advantage of being able to analyse all series of images available for the interested zone. This characteristic permits to photo-interpret the points used as reference data, using the high detailed images provided by Google Earth™ and the tools available in QGIS, at the same time.
« Google Earth Engine is a cloud-based platform that makes it easy to access high-performance computing resources for processing very large geospatial datasets » (Gorelick et al., 2017) and allows to manage a huge amount of georeferenced date. In this research, Google Earth Engine was used to implement the whole methodology, to perform analysis on multi temporal images over large area, to create time series and to calculate various indices and extract statistical information. The platform consists of an interface where it is possible to insert programming codes, in Java script language, and a window where visualize the results of processing on a cartographic support. In addition, within the platform, there is a wide and publicly accessible catalogue of satellite data and images, from which can be selected those of interest for data elaboration and processing analysis, without the need to download them.

3.2.4 Thematic classes

This section includes a brief description of land cover classification system, based on the EAGLE concept, as specified in the first chapter. According to this system three main land cover classes were defined: *Abiotic Non-Vegetated Surfaces and Objects, Biotic Vegetated Surfaces and Water surface.* The Table 3.2 shows a summary of the nomenclature adopted; the last column shows the classes identified in the land cover map. A description of these classes is given in Table 3.3.
The first class encompasses any unvegetated surfaces, either covered with man-made artificial structures, as built-up areas or bare soil consolidated or unconsolidated unvegetated. It is then distinguished into *artificial* and *natural abiotic surface*.

Table 3.2 – Land cover and land cover change classes.

Land Cover classes				**Scheme classification**
Abiotic surfaces	Artificial		11	Artificial
	Natural abiotic		12	Natural abiotic
Biotic vegetated surfaces	Woody vegetation	Broadleaf trees	121	Broadleaf trees
		Needleaved trees	122	Coniferous
	Herbaceous vegetation	Periodic herbaceous	221	Periodic herbaceous
		Permanent herbaceous	222	Permanent herbaceous
Water surfaces	Water		31	Water bodies
	Ice and Snow		32	Ice and snow
Land Cover change classes				
Soil consumption			**4**	Soil sonsumption
Restoration			5	Restoration
Burned area			6	Burned area
Others disturbances			7	Others disturbances

Table 3.3 - Land cover classes based on EAGLE system.

Abiotic Non-Vegetated Surfaces and Objects		
Artificial surfaces and constructions	Any unvegetated surfaces, either covered with man-made artificial structures, building, paved roads	
Natural abiotic surfaces	Any kind of surface material that remains in its natural consistence or form, consolidated and unconsolidated: bare rock, sands, Pebble, gravel, clay etc	
Biotic Vegetated Surfaces - herbaceous		
Permanent herbaceous	Herbaceous areas characterized by a continuous vegetation cover throughout a year. No bare soil occurs within a year.	
Periodically herbaceous	Herbaceous areas characterized by at least one land cover change between bare soil and herbaceous vegetation within one year. Often these areas are managed as arable areas	

Biotic Vegetated Surfaces - woody vegetation		
Broadleaved trees	woody vegetation characterized by predominant broadleaved trees or shrubs	
Needleleaved trees	Woody vegetation characterized by predominant needle leaved trees or shrubs	
Water Surfaces		
Water	Natural or artificial water surface; rivers, channels, non-flowing water, mainly lakes and ponds	
Ice and snow	Snow cover that persists throughout the year, persistent ice cover formed by accumulation of snow.	

In the next (for the calculation of some environmental indicators) soil consumption class is further subdivided into *permanent abiotic surfaces* (i.e. covered by Impervious and sealed surfaces in an irreversible way), such as buildings and roads, and *reversible surfaces*, (i.e. consisting by man-made material or where natural material has been removed, forming a non-impermeable and undeveloped surface), as unpaved roads, construction sites or courtyards or sports fields, permanent deposits of material, photovoltaic fields, quarries.
Although the EAGLE system (EAGLE, 2020) includes quarries and extraction sites in the natural abiotic class, in the nomenclature adopted in this thesis they are included in the artificial class and on the second level, in the reversible artificial class, since this type of cover strongly modifies the soil structure and causes strong compaction (Strollo et al., 2020).

Natural vegetation includes areas covered by vegetation, both natural and artificial such as crops or urban parks. This class has been further subdivided into *Woody vegetation* from *Herbaceous vegetation* and in a third level of detail that distinguishes the woody class into *Needleaved* and *Broadleaved* and *Herbaceous vegetation* in into permanent and periodic. *Permanent herbaceous* areas are characterized by a grass cover throughout a year. No bare soil occurs within a year. These areas can be either unmanaged or extensively managed natural grasslands, or arable areas with a permanent vegetation cover or even set-aside land in agriculture. *Periodically herbaceous* areas are characterized by at least one land cover change between bare soil and herbaceous vegetation within one year.
The third class includes liquid and solid form of water. This class is also divided into *Water* (liquid) as basins, rivers, streams, stagnant waters, both artificial and natural origin and *Ice and snow*, in the case of ice and snow cover during the whole year.
The classes of change are:

- Soil consumption (= land consumption): the replacement of a non-artificial land cover to an artificial land cover, both permanent and reversible.
- Restoration: replacement of an artificial and reversible land cover with a semi-natural land cover.
- Burned area: the class includes natural woody vegetation affected by recent fires.
- "Other disturbances" identifies the removal of all or most of the trees in a surface following a disturbance event, identified most of the time as forest harvesting.

3.3 Land cover classification methodology

The methodology presented in this study uses Sentinel-1 Ground Range Detected (GRD) and Sentinel-2 images to detect land cover and land cover change in Italy on a yearly basis, through multitemporal indices and decision rules. Sentinel-1 imagery allows the calculation of backscatter in the polarizations VV and VH; backscatter values are influenced by several factors such as geometry, dielectric properties, and roughness of surfaces (Nezry, 2014). Sentinel-2 images enable the evaluation of spectral characteristics of land surface, which are determined by land cover materials.

Decision rules are defined to identify land cover classes at pixel size of 10 m, setting fixed threshold values on composites (e.g. median, maximum) of multitemporal images. In particular, three sets of decision rules were defined that allowed the identification of three macro-classes (abiotic, natural vegetation and water). The macro-classes were subsequently detailed through the definition of further rules (Figure 3.4).

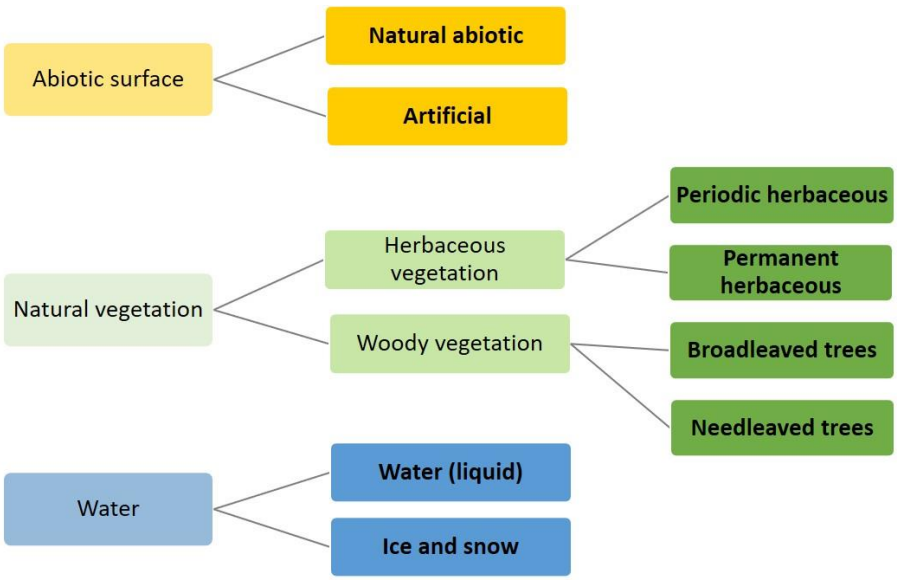

Figure 3.3 – Decision rules to define three macro-classes, in bold the classes used for the classification.

The rules developed for land cover classification and land cover change are based on experience and reasoning. Specifically, these rules are based on deep knowledge of literature and on previous analysis of temporal trend of spectral signatures, (Spadoni et al., 2020) indexes and backscatter coefficients of each class. These studies permitted to identify some thresholds while others thresholds were established on the base of training areas collected for specific classes (manly vegetation classes).
The methodology was developed on Google Earth Engine (Javascript language program).
The output classifications were validated through the photointerpretation of very high-resolution images that permitted the identification of land cover classes and changes (see change detection methods). The methodology includes a series of steps each identifying a type of land cover.
The workflow illustrated in Figure 3.4 describes the main steps of the land cover classification methodology.

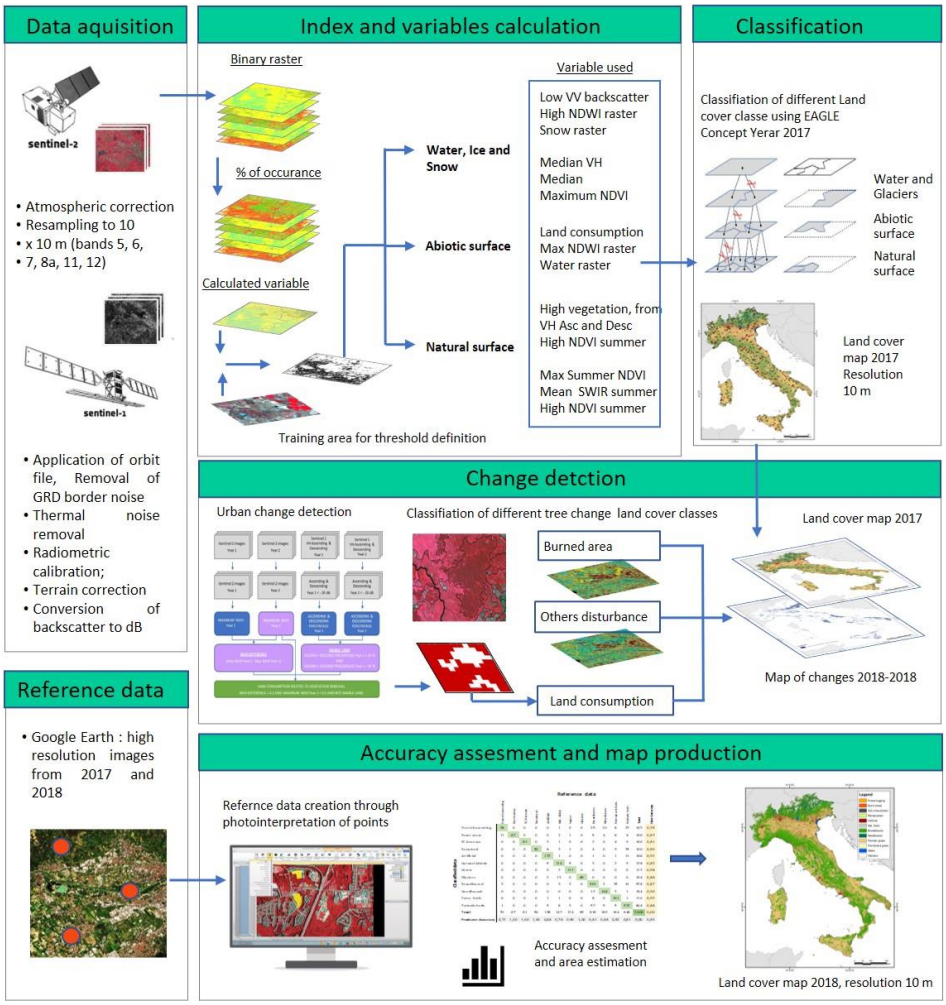

Figure 3.4 Workflow of the land cover classification methodology.

3.3.1 Acquisition and pre-processing of images

The use of Sentinel-1 GRD and Sentinel-2 images requires a few pre-processing steps in order to obtain the backscatter values and reflectance values. Sentinel-1 GRD and Sentinel-2 grids are not aligned and have different spatial resolution: in particular, the Sentinel-1 GRD have ground range geometry, and the pre-processing involves the geocoding to map coordinates. Sentinel-2 images are provided in WGS 84 UTM coordinates and cover the Italian territory with about 80 granules. In order to use both images in the same workflow, the spatial resampling to a common coordinate reference system and same spatial resolution

were performed, in particular, Sentinel-2 grid alignment and the WGS 84 UTM coordinates were used also for Sentinel-1 images at resolution of 10 m.

Google Earth Engine provides Sentinel-1 GRD images already converted to backscatter values, following the steps described in the website (https://developers.google.com/earth-engine/sentinel1), which are showed in Figure 3.5**.** In addition, the platform offers access to Sentinel-2 images L1C and L2A, however the L2A historical archive was not complete at the time of the research, thus not allowing calculations based on the whole years 2018 and 2019. Therefore, L1C images were used in this study, masking clouds with a simple algorithm based on the quality assessment band as described in Google Earth Engine website (https://developers.google.com/earth-engine/datasets/catalog/COPERNICUS_S2). It is worth highlighting that cloud mask products provided with Sentinel-2 images generally underestimate clouds (Coluzzi et al., 2018). Therefore, the input images affected by clouds are not involved in calculations. However, the atmospheric disturbance affecting L1C pixels can increase the uncertainty of spectral signatures, therefore decreasing classification accuracy.

Photointerpretation was required to collect training areas for the land cover classes of broadleaved and needleleaved trees, which are used in the methodology illustrated in the following paragraphs.

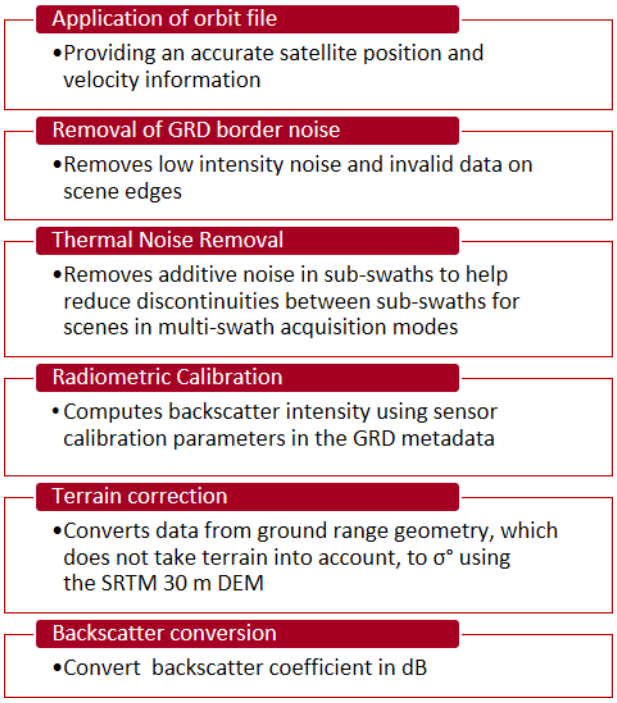

Figure 3.5 Sentinel-1 Pre-processing.

3.3.2 Water classes

The classification of water and ice classes is a required input for the abiotic land cover classes, therefore this class must be defined before the others.

The workflow requires both Sentinel-1 and Sentinel-2 input images for the whole year and Sentinel -2 during Summer (July 1st to September 30th). Every image was processed in order to calculate NDWI index (Figure 3.6), NDSI (Dozier, 1989) and NDVI. In particular, median and maximum values of NDVI (per pixel) were calculated, obtaining two raster used later for liquid and solid conditions respectively.

3.3.2.1 Liquid Water

Five conditions were considered in order to identify water surfaces, each of them contributes to reduce possible mistakes between the spectral signature of water and other classes. These conditions are illustrated below:

1) High NDWI raster >= 5%.
2) Median NDVI < 0.3.
3) Snow raster < 20%.
4) Median VH polarization < -20 dB and
5) Low VV backscatter < -15%

1) High NDWI raster >= 5%:

It was observed by (McFEETERS, 1996) that a cover type is water if NDWI > 0 and it is non-water if NDWI < 0; since in some cases the built up area and other surfaces have positive values of this index, but always lower than the water surfaces, a more appropriate threshold value of 0.3 of NDWI was considered to better isolate water surfaces from those without detectable water surfaces (McFeeters, 2013). A binary raster was calculated for every NDWI raster, according to the previous condition at pixel level, the presence of water was indicated if NDWI ≥ 0.3 where pixel assumes a value = 1. Therefore, the percentage of occurrences verifying the above conditions was calculated as the sum of every binary raster divided by the number of valid acquisitions, generating "High NDWI raster". It should be highlighted that the number of valid acquisitions can be lower or equal to the total number of satellite acquisitions, depending on the cloud cover. The percentages obtained from the binary raster will always be calculated in this way unless otherwise specified: $P_{class}=(N_{occur}/N_{free\text{-}cloud})*100$.
Then it was considered all the pixels of "High NDWI raster" with occurrence high more then 5%: this percentage permit to exclude outliers pixels from the time series.

2) Median NDVI < 0,3

The condition "Median NDVI" < 0.3 excludes vegetated pixels from liquid water.

3) Snow raster < 20%

A peculiar algorithm developed by ESA[30] is used for the detection of solid water (snow), which is identified by pixels that have band reflectance lower than threshold values reported in italics below:

$$((\text{band 3} - \text{band 11}) / (\text{band 3} + \text{band 11})) \geq \textit{0.2}$$
$$\text{and band 8} > \textit{0.15} \text{ and band 2} > \textit{0.28} \text{ and (band 2 / band 4)} > \textit{0.85}$$

First binary raster, where value 1 identifies pixels verifying the above conditions (no snow) was generated, and then the percentage of occurrence in temporal series was calculated: all pixels with a percentage < 20% were considered water. When this condition is only partially verified during the year (< 20%) it is likely that it will not be perennial snow: this condition helps to define water class.

4) Median VH polarization < -20 dB and 5) Low VV backscatter < -15%

The backscatter values used in this classification are derived from tests carried out on sample areas and from values reported in the literature (Gulácsi & Kovács, 2020; Mansaray et al., 2017; Zhou et al., 2017).

[30] https://sentinels.copernicus.eu/web/sentinel/technical-guides/sentinel-2-msi/level-2a/algorithm

In general, the VH band discriminates quite well the different classes presenting backscatter values around -20 db, which remains constant throughout the year. Variations can be due to the wind that makes the water surface rougher and modifies its backscatter.
The VV values are generally higher as highlighted by Zhou et al., 2017, Mansaray et al, 2016 (Mansaray et al., 2017; Zhou et al., 2017); in the case of VV backscatter the value -10dB was determined as a good threshold for identifying water (the threshold was identified by trial and error). A raster was produced starting from the monthly median (i.e. divided 12): above -10 decibels the pixels assume a value equal to 1, below -10 decibels a value equal to 0 (probably water). Pixels that verify the condition for less than 15% of the observations are classified as water. Given the process described above, the class 3.1 Liquid waters is identified when (Figure 3.6):

High NDWI raster ≥ 5% and Low VV backscatter < 15% and Median NDVI < 0.3
and Median VH polarization < -20dB and Snow raster < 20%

3.3.2.2 Ice and snow

The snow identification is based on three inputs data: NDSI, NDVI indices and the reflectance of single bands of blu (band 2), of red (band 4) and of infrared (band 8).
For snow cover detection the follows conditions were considered:

1) Snow raster ≥ 10%.
2) Snow raster summer > 1%.
3) Maximum NDVI < 0.4.

1) Snow raster ≥ 10% and 2) Snow raster summer > 1%

As specified before, “Snow raster” derives from the methodology elaborated from ESA to detect snow surface. The algorithm elaborated, is based on NDSI index, and it is useful as it highlights the characteristics that only snow surfaces are very bright in the visible and dark in shortwave infrared (cloud and snow reflectance are similar in band 3 but band 11 reflectance for clouds is very high while it is low for snow). This index allows to detect snow and differentiate it from clouds; as NDVI, presents values varying from -1 to 1. As a general rule, positive values define probable areas with snow. In addition to the NDSI, three successive "filters” were exploited on band 2, band 8 reflectance values and on the ratio between band 2 and band 4. The thresholds are those indicated by ESA analysis. Band 8 threshold permits to eliminate pixels that have high NDSI values and low band 8 (NIR) reflectance: pixels with values over 0,15 are considered as snow. Threshold on band 2 eliminates pixels that have high NDSI values and low band 2 (blue) reflectance; finally, Ratio Band 2 / Band 4 eliminates pixels that have high NDSI values and low Band 2/Band 4 reflectance ratio which usually corresponds to water bodies. Two outputs derive from this process: “Snow raster” and “Snow raster summer” representing the percentage of times in the period considered under which all the conditions are satisfied. For the whole year it was assumed a threshold value over 10%; a less conservative threshold of 1% was considered for the summer. In both situation the percentages permit to eliminate outliers’ pixels (Figure 3.6).

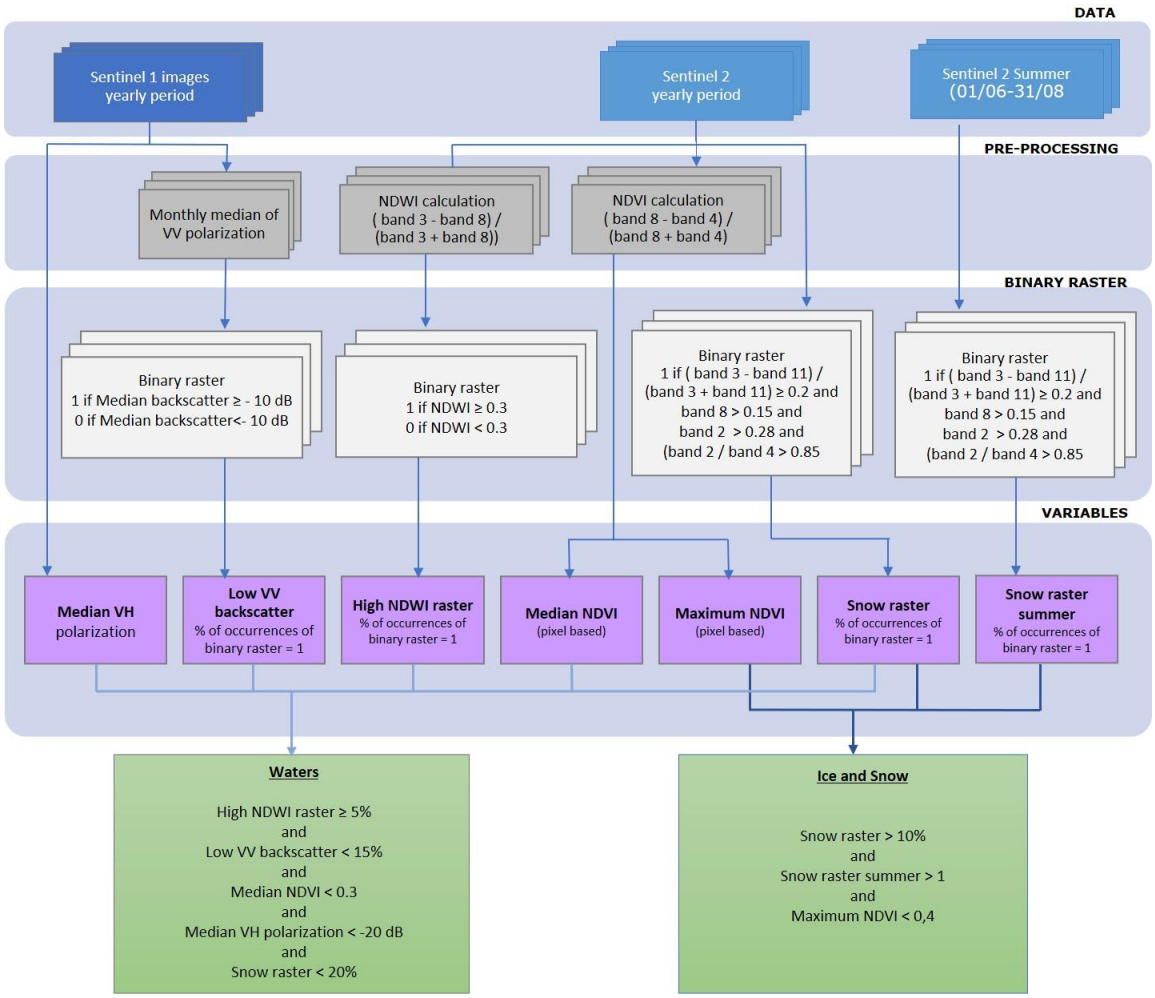

Figure 3.6 - Workflow for *Water* and *Ice and Snow.*

3) Maximum NDVI < 0.4

It was used a threshold of 0.4, a conservative threshold to exclude vegetation.
The class 3.2 Solid waters is identified by the following conditions:

Snow raster ≥ 10% and Snow raster summer > 1% and Maximum NDVI < 0.4

The class 3 Water is therefore the combination of classes 3.1 Liquid waters and 3.2 Ice and snow, and it is used as input raster in the conditions for the classification of abiotic classes, as described in the following paragraphs.

3.3.3 Abiotic classes

The workflow for A*biotic classes* requires only Sentinel-2 input images for the whole year. From the NDVI multitemporal series, the maximum value per pixel was calculated, obtaining the "Maximum NDVI" raster. This calculation is in common with the processing of water classes, therefore, the same data were calculated only once. Since abiotic surfaces have low NDVI values, similar to water surfaces, this could cause classification errors (water classified as abiotic class); thereby, class 3 Water, previously described, is used as input raster to exclude this kind of commission errors, resulting in the following condition for classifying class 1 *Abiotic / Non vegetated surfaces* (Figure 3.7):

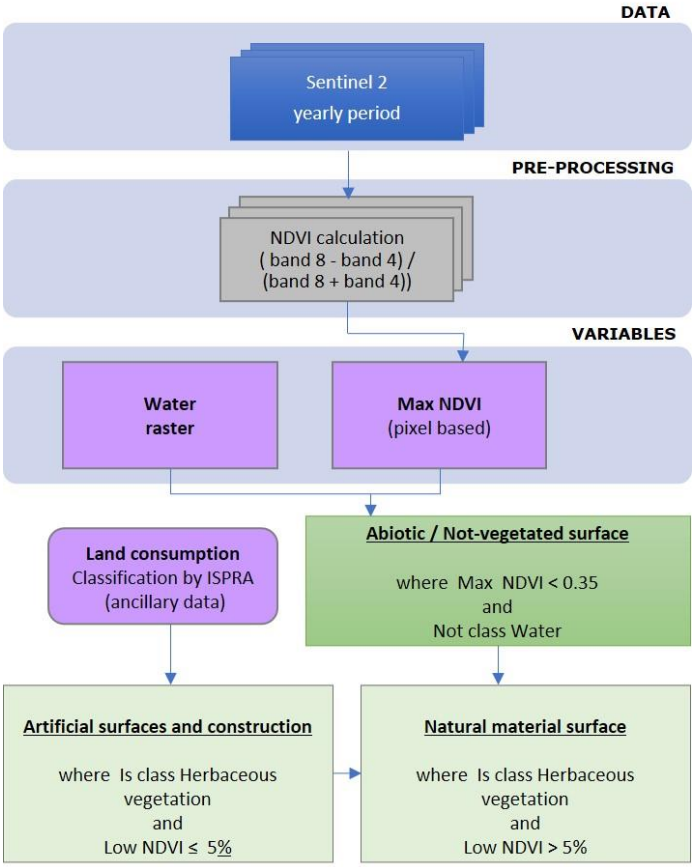

Figure 3.7 - Workflow for *Artificial surface* and *Natural material surface.*

1) **Maximum NDVI ≤ 0.35 and 2) is Not Class 3 Water**

3.3.3.1 Natural material surface and Artificial surfaces and constructions

The distinction between artificial and natural surfaces using only satellite data is very difficult because of spectral similarities between artificial materials (e.g. asphalt, concrete, etc.) and natural soils. In this study, the class 1.1. *Artificial Surfaces and Constructions* are derived from ancillary data, because of the availability of a very accurate map of land consumption classification by ISPRA (Munafò, 2020) that is updated yearly. The artificial surface classification is a raster where value 1 identifies land consumption with 10 m spatial resolution. The methodology developed in this research for updating land consumption is part of the process that leads to the update of the map to 2017 for the realization of 2018 land cover map.
The class 1.2. *Natural material surfaces* is derived, therefore, from the difference between the class 1 Abiotic and class 1.1. as in the following condition:

1) **is Class 1 Abiotic and**
2) **Not Class 1.1 Artificial Surfaces and Constructions**

3.3.4 Biotic classes

The characteristics of Sentinel-1 and Sentinel-2, as well as the results of the analysis conducted on the training areas were used to identify woody vegetation
The woody vegetation is obtained from three different input data:

- Pre-processed Sentinel-2 in summer.
- Pre-processed Sentinel-2 in winter.
- Pre-processed Sentinel-1 GRD over one year.

The various thresholds and indices derive from a series of analyses based on temporal trend of vegetation index and spectral signature of different vegetation classes (Spadoni et al., 2020).
The outputs of this part of the methodology are two raster, Broadleaved and Needleaved trees.
In order to perform a correct classification of tree cover, the temporal behaviour of the spectral signatures related to the different natural land classes was investigated.

3.3.4.1 Woody vegetation

The woody vegetation was distinguished through the following conditions (Figure 3.8):

1) High NDVI summer ≥ 70% (percentage of occurrences where the raster assumes a value ≥ 0.5).
2) Maximum NDVI summer ≥ Threshold Maximum NDVI summer.
3) High vegetation < 2% (percentage of occurrence where raster assumes a value < -20 dB).

1) High NDVI summer ≥ 70%

First, the NDVI was calculated for every image, covering the period between from June 1st to August 31st, which is the period when the differences between the various biotic classes are greater. Then, a binary raster that considers equal to 1 all pixels exceeding the value of 0.5 was created; the value of 0 was given to the other pixels of the temporal series. Finally, it was established that the condition probably trees is met when the percentage of occurrences in over 70%. This condition allows to consider woody vegetation only for those situations where the value is above the threshold for 70% of the cases, this threshold is a more conservative approach than 100% condition.
Output of this elaboration is the raster

- High NDVI summer: pixels take the value of the percentage of times they have exceeded the value of 0.5.

2) Maximum NDVI summer ≥ Threshold minimum value of the Maximum NDVI summer

Another condition always exploits the behaviour of the NDVI, but utilizes a threshold deriving from the reflectance values collected on the training samples area. In these areas the minimum value of the maximum NDVI summer is calculated, and this threshold is used to identify woody vegetation raster:

- Maximum NDVI summer: pixels take the value of NDVI maximum during the summer.

3) High vegetation

The backscatter of VH polarization of Sentinel-1 was used as it can partially improve the detection between high vegetation (trees) and low vegetation (e.g. crops) (Holtgrave et al., 2020). Since the acquisition orbit influences the angle of view, the ascending and descending orbits are considered separately. For ascending and descending orbits separately, two binary raster were calculated with the following condition: if backscatter ≤ -20dB then raster = 1

The value -20dB was used as a threshold for distinguishing low vegetation and fallow land that generally have backscatter values lower than -11 dB (Formaggio et al., 2001), from trees that generally have higher backscatter values (-20dB represents a more conservative threshold). Then it was calculated the percentage of times that this condition is verified, crating others two raster.

Outputs of this elaboration are two binary raster for both orbits:

- VH ascending pixels take the value of the percentage of times they assume a value less then -20dB.
- VH descending pixels take the value of the percentage of times they assume a value less then -20dB.

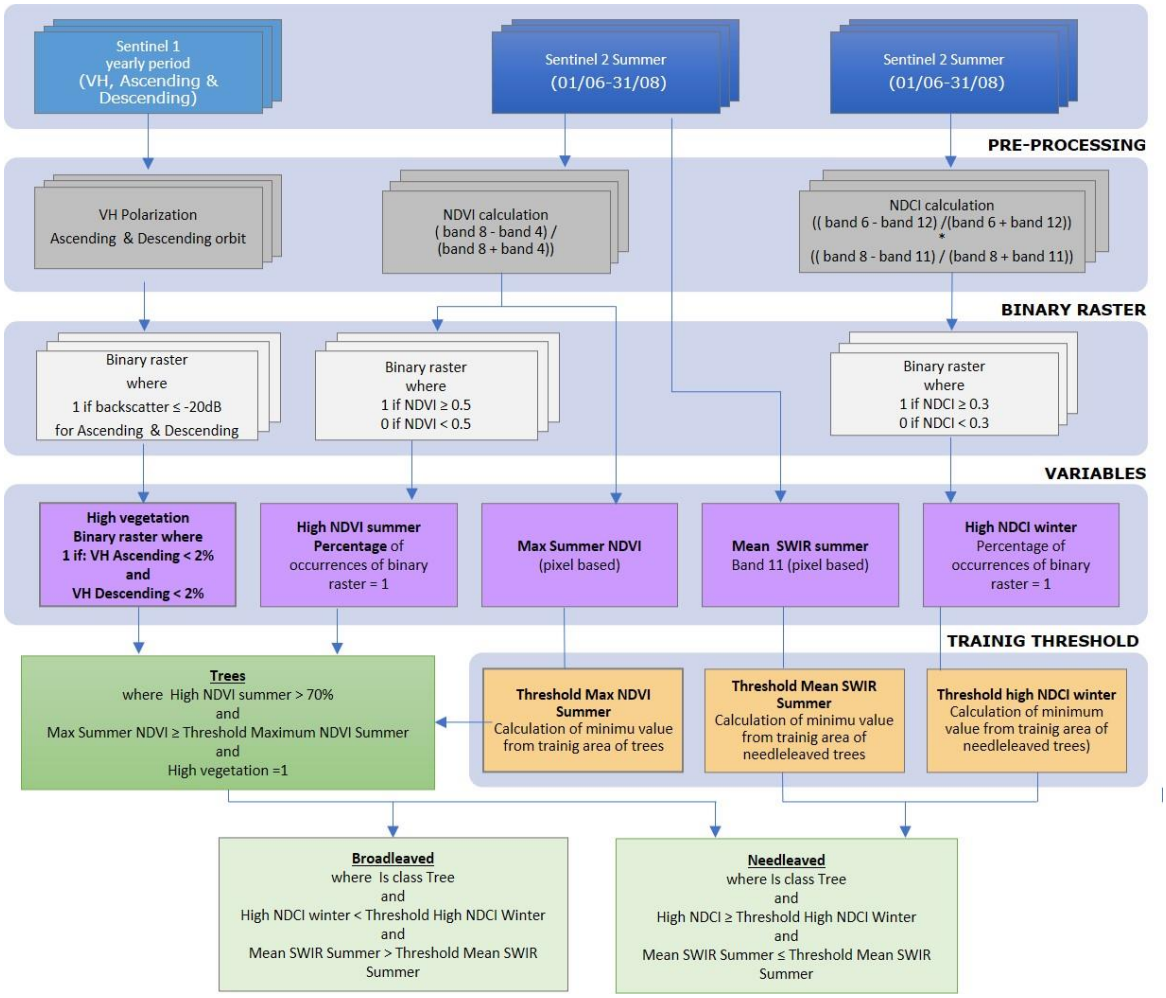

Figure 3.8 - Workflow for *Broadleaved* and *Needleaved.*

It is considered "High vegetation" if VH ascending < 2% and VH descending < 2% then raster = 1. The 2% threshold is used to exclude possible outliers from time series of backscatter values.

In synthesis Woody vegetation is when:

High NDVI summer ≥ 70% and Maximum NDVI summer ≥ Threshold Maximum NDVI summer and High vegetation = 1

BROADLEAVED AND NEEDLEAVED

For this last elaboration two inputs data were used: the "Mean SWIR summer" (i.e mean of band 11.) from the summer subset of Sentinel-2, and a new index, the NDCI (described in the paragraph 2.6.2) calculated on winter subset of Sentinel-2 images, that was elaborated within this research.

The distinction between Broadleaved and Needleaved is based on the condition that must be woody vegetation and have to satisfy the others two following requirements:

1) Mean SWIR summer > Threshold Mean SWIR summer.
2) High NDCI winter > Threshold high NDCI winter.

1) Mean SWIR summer > Threshold Mean SWIR summer

Infrared band short wave is very important because of the differences in reflection between Needleaved and Broadleaved. This behaviour was exploited calculating the minimum value of "Mean SWIR summer"

raster extracted from Needleaved training area. The minimum value of "Mean SWIR summer" was used as threshold in the first condition.

2) High NDCI winter > Threshold high NDCI winter

The second condition uses the NDCI: this index is a multiplication between two normalized difference index: the first is based on band 6 (red edge, 740 nm) and band 12 (short wave infrared band, 2190 nm), the second is based on band 8 (infrared, 842 nm) and band 11 (short wave infrared band, 1610 nm). The multiplication is done in order to highlight the effect of a single ratio.

NDCI = ((band 6 - band 12) / (band 6 + band 12)) * ((band 8 - band 11) / (band 8 + band 11))

These bands show a more pronounced difference between Needleaved and Broadleaved in winter than in summer. This is probably due to the drastic fall in the spectral response of Broadleaved trees compared to Needleaved ,which don't drop their leaves in senescence period (Persson et al., 2018a).
A binary raster was calculated considering the percentage of times each pixel is over 0.3 in the temporal series (the raster pixels give this percentage). Then a "Threshold high NDCI" raster was created considering the minimum value of this percentage obtained from the coniferous training area. This threshold constitutes the second condition: over this value there are Needleaved.

Broadleaved is mapped where:

is class Woody vegetation and High NDCI winter < Threshold high NDCI winter and
Mean SWIR summer > Threshold Mean SWIR summer.

Needleleaved is mapped where:

is class Woody vegetation and High NDCI winter > Threshold high NDCI winter and
Mean SWIR summer < Threshold Mean SWIR summer.

3.3.4.2 Herbaceous vegetation

Herbaceous vegetation considers two condition

1) **Maximum NDVI > 0.35 and**
2) **Not class Woody vegetation**

Basically, the condition "Maximum NDVI" > 0.35 identifies all vegetated areas, and herbaceous vegetation is calculated by subtracting the Woody vegetation class.

PERMANENT AND PERIODIC HERBACEOUS

The distinction between permanent and temporary herbaceous classes consider the following condition, in addition to the fact that both must belong to the herbaceous vegetation class. (Figure 3.9).

Mean SWIR summer > Threshold Mean SWIR summer

Herbaceous vegetation was divided in continuous and periodic vegetation considering the NDVI only for the summer period. Then it was calculated the frequency in which the pixel has a value greater than the threshold value. In this case, a binary raster was created, "Low NDVI" considering a threshold of 0.3: above this value the pixel assumes a value of 0, under this value the pixel assumes a value of 1.
Outputs of this elaboration is a raster

- Low NDVI: pixels take the value of the percentage of times the condition is verified.

Permanent herbaceous is classified with the following conditions:

is class Herbaceous Vegetation and Low NDVI ≤ 5%.

The condition "Low NDVI" ≤ 5% implies a very constant presence of vegetation during the year, such as permanent grass.

Periodically herbaceous is identified by the conditions:

is class Herbaceous Vegetation and Low NDVI > 5%.

In this case, the condition "Low NDVI" > 5% implies that vegetated cover was replaced by non-vegetated cover for several periods of the year (i.e. more than 5% of valid acquisitions). It is worth noticing that non-vegetated cover could also be snow cover.

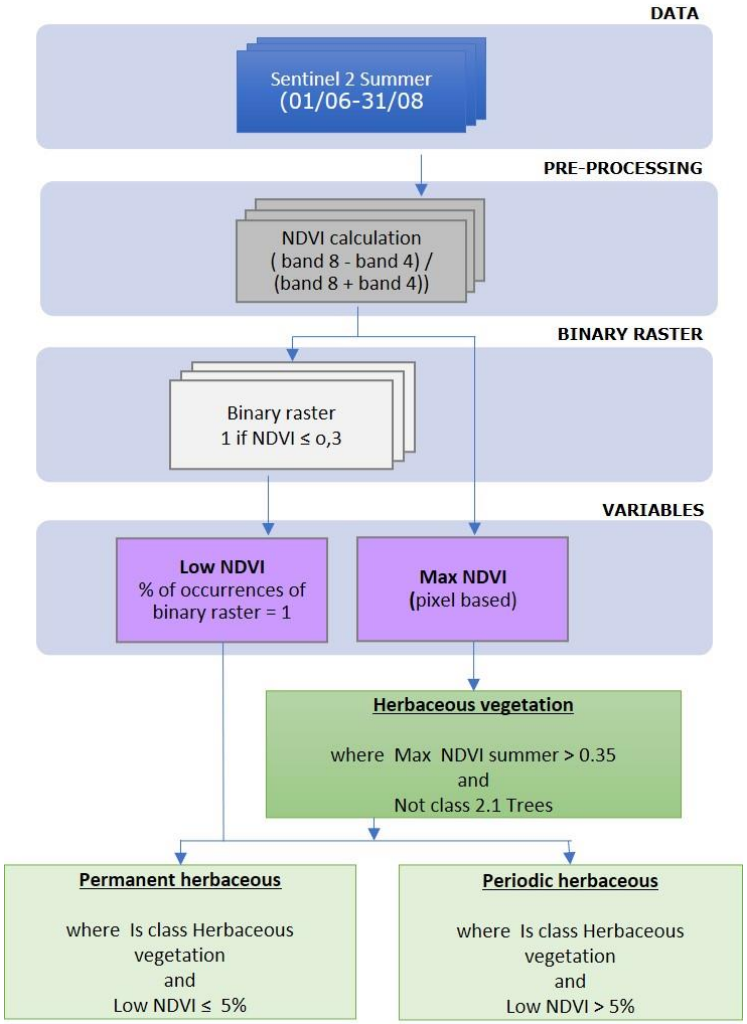

Figure 3.9 - Workflow for *Permanent herbaceous* and *Ice and Snow.*

3.4 Land cover changes methodology

The land cover map for the year 2018 is elaborated updating the changes between 2017 and 2018. In this study two types of changes are considered: the transformations taking place in the woody vegetation class,

generally characterized by *burned area* and *other disturbances* as forest harvesting, and the changes in *soil consumption* (=land consumption) between 2017 and 2018 and vice-versa (r*estoration* the replacement of artificial surface by natural land cover). Therefore, changes that occur within the herbaceous class are not considered because, in the short period of one year, it is not possible, through remote sensing, to determine exactly whether a change between permanent and periodic herbaceous classes has occurred or if the change is due to the natural phenological period of grassland.
Two different methods were, therefore, developed: the first one identifies the changes occurred in the natural environment, while the second one identifies the changes in the artificial environment. The procedures generate a raster of forest changes classified into “other disturbances” and “burned area”, and a second raster, which is a mask that defines the areas of possible land consumption. This mask was used to support the photo-interpretation of land consumption, conducted by a group of experts (ISPRA). From these masks two products were derived, the soil consumption (which ISPRA uses to update the map) and the third level characterisation of the changes occurred, according to the legend adopted by ISPRA since 2018 (see chapter 4). It should be pointed out that the masks are intended to reduce manual work, so the methodology is specifically designed to search for all possible areas of change by allowing errors of commission but preventing as much as possible errors of omission. In this way the photo-interpreter will be able to search for changes only within the areas (thus avoiding verification of the areas throughout the Italian territory) with significant time saving. About the "other disturbances" class, in many cases the algorithm detected changes related to forest harvesting, even if it was designed to identify any changes other than the burned areas. Considering the importance of this class in a forest context, the effectiveness of the method in identifying this type was tested, although it was not based on this single objective. The accuracy results are therefore affected by this choice.

3.4.1 Monitoring natural disturbances

A specific methodology for mapping forest disturbance was developed, also for distinguishing burned areas from other kinds of changes like forest harvesting. The input data are the Sentinel-2 images acquired during summer (from June 1th to August 31th) and Woody vegetation raster (developed in previous process), which are reference data for the year 1 (before the changes) and Sentinel-2 images acquired during summer (from June 1th to August 31th) as reference data for the year 2 (after changes).
Every image was processed calculating a few spectral indexes:

- the NDVI for all the images of Year 1 and Year 2;
- the NBR of Year 1 and Year 2, defined as:

$$NBR = ((band\ 8 - band\ 12) / (band\ 8 + band\ 12))$$

Compared to the NDVI, the NBR uses NIR and shortwave-infrared (SWIR) portions of the electromagnetic spectrum.
Pre-fire, healthy vegetation has very high near-infrared reflectance and low reflectance in the shortwave infrared portion of the spectrum. Recently burned areas have a relatively low reflectance in near infrared and a high reflectance in the short-wave infrared band. The trend of spectral signatures is shown in Figures 3.10. To calculate the burned area, it was subtracted the post-fire NBR raster from the pre-fire NBR according to the following steps.

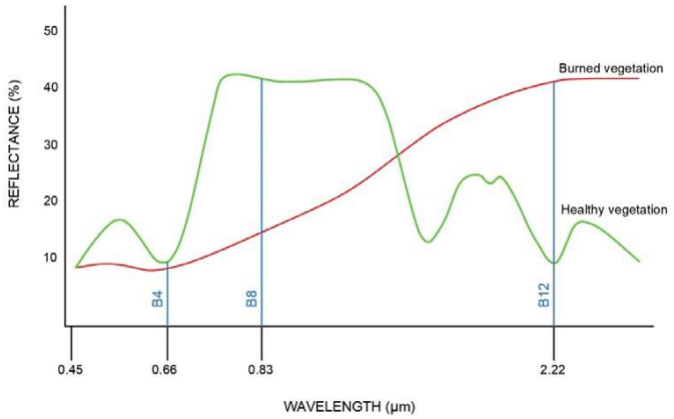

Figure 3.10 Reflectance values in electromagnetic spectrum[31].

1. The pixel-based median of NDVI and NBR was calculated respectively for Year 1 and Year 2, obtaining the raster: “Median NDVI Year 1”, “Median NDVI Year 2”, “Median NBR Year 1”, and “Median NBR Year 2”.

NDVI Difference = Median NDVI Year 1 - Median NDVI Year 2
NBR Difference = Median NBR Year 1 - Median NBR Year 2

1. The land cover change class “Tree loss” was determined by the following conditions:
is Class 2.1 Trees Year 1 and (NDVI Difference ≤ -0.2 or NBR Difference ≤ -0.2).

The above conditions imply that tree loss is mapped only if the classification of Year 1 resulted in Woody vegetation. The second part of the expression identifies tree loss if NDVI median of Year 1 is greater than 0.2 of NDVI median of Year 2, or NBR median of Year 1 is greater than 0.2 of NBR median of Year 2. The threshold value 0.2 was identified empirically (on training area by trial and error method) as optimal value for detecting tree loss and avoiding errors caused by phenological variations between years (Figure 3.11).

The distinction between “burned trees” and “other disturbances” was derived through an innovative burned index defined as:

BI = ((1 - (band 3 + band 4 + band 8)) / (1 + (band 3 + band 4 + band 8)))

The above index is higher when the pixel is dark or brown (false colour composite as 8, 3, 2), as it is in case of forest fires. The index was calculated for all the Sentinel-2 images of Year 2, and the median was calculated, obtaining the raster “Median Burned index Year 2”. The conditions for distinguish burned areas from the other disturbances are:

1. **Other disturbances**
if Class Trees loss and Median Burned index Year 2 < 0.45.

2. **Burned trees**
if Class Trees loss and Median Burned index Year 2 ≥ 0.45.

The threshold value 0.45 was determined empirically as optimal value for distinguishing burned areas and avoiding errors due to shadow areas where pixels tend to be dark. As specified before, “other

[31] *Source* M. Pepe, 2020

disturbances" consisted of forest harvesting and other trees changes due to loss of forest, since most of these changes are forest trimmed, in the following this change will be defined as "forest harvesting".

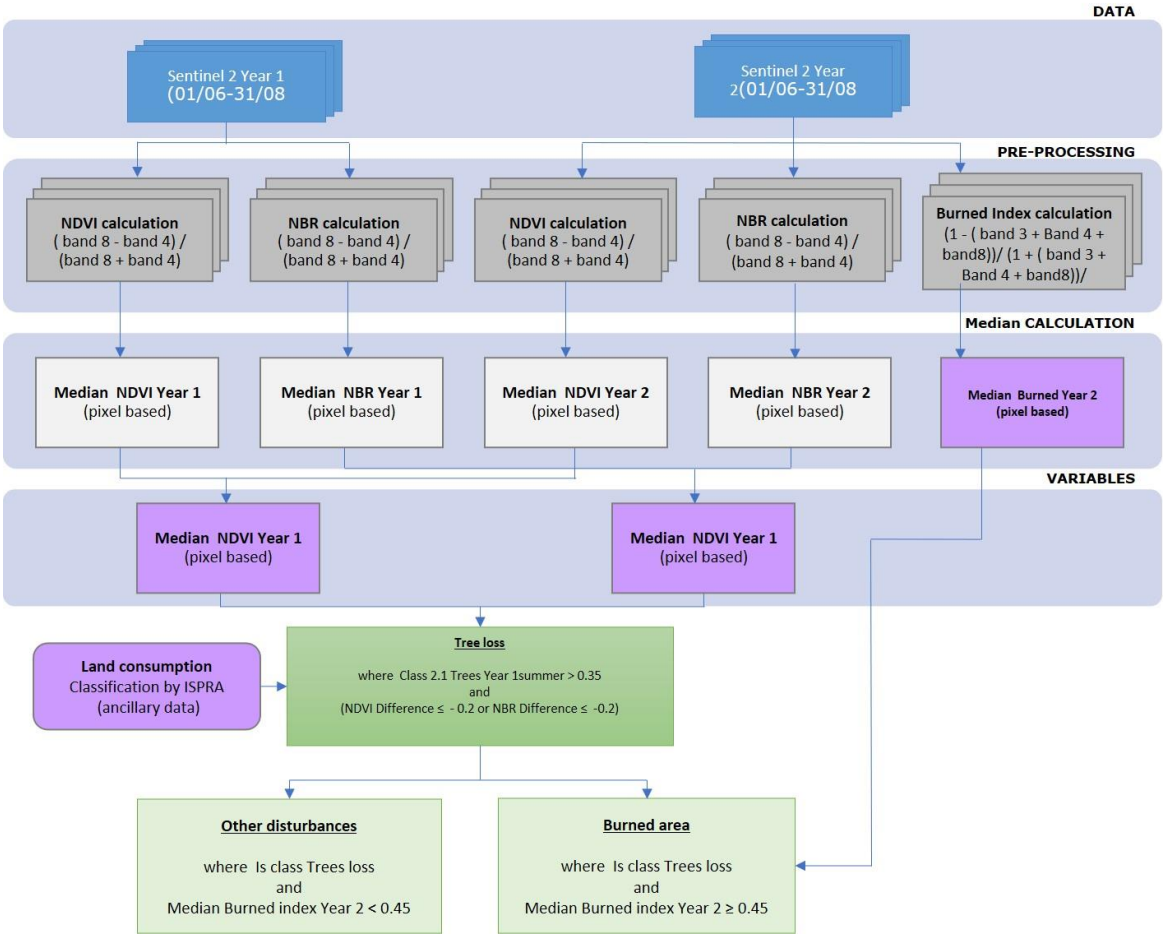

Figure 3.11 - Workflow for *Permanent herbaceous* and *Ice and Snow.*

2. The pixel based difference was calculated for both NDVI and NBR medians, as follows:

3.4.2 Monitoring land consumption

This part of the research mainly concerned to the identification of areas potentially affected by the presence of new soil consumption, based on the variations in NDVI and backscatter throughout the year. These areas were used to create the masks, which support the photointerpretation of the new land consumption, through which the National Land Consumption Map is updated.

This methodology of change detection involves the acquisition of multitemporal Sentinel-1 GRD and Sentinel-2 images, already pre-processed as explained in the previous paragraph, and acquired in 2 years, (2017 and 2018); Figure 3.12 shows the main steps of the methodology.

This methodology for identifying land consumption changes is based on the following assumptions, depending on observation of test areas and literature knowledge; according to these assumptions different satellite data were used, (underlined in the list):

1. Land consumption can be a consequences of vegetation cover removal, therefore cause a decrease of vegetation indices, such as NDVI.
   Sentinel-2 images were used for calculating NDVI differences in the two years; Sentinel-1 GRD was also used to improve the detection.

2. Built-up areas such as buildings, are characterized by high backscattering values related to double-bounce effect; therefore, land consumption can increase the backscatter if the land cover before the change was particularly smooth or constituted by bare soil.
   Sentinel-1 GRD were used for calculating differences in backscatters caused by buildings, infrastructures, or construction sites.
3. Land consumption can be detected if at least one of the above assumptions is verified.

In line with these hypotheses, a fully automatic workflow was developed. For the sake of simplicity, these two methods are explained in two separate paragraphs, but this is actually a unique model.

A set of specific thresholds and decision rules are used to determine the artificial changes at 10 m resolution. The thresholds are defined empirically through several test in sample areas within various land cover classes and adopting training and error system. A digital terrain model was used to calculate the slope and refine the calculation in order to avoid errors related to the morphology of mountain area. It is worth pointing out that these classifications of changes are intended to be used to support the ISPRA monitoring of land consumption, in order to reduce the time of manual photointerpretation work.

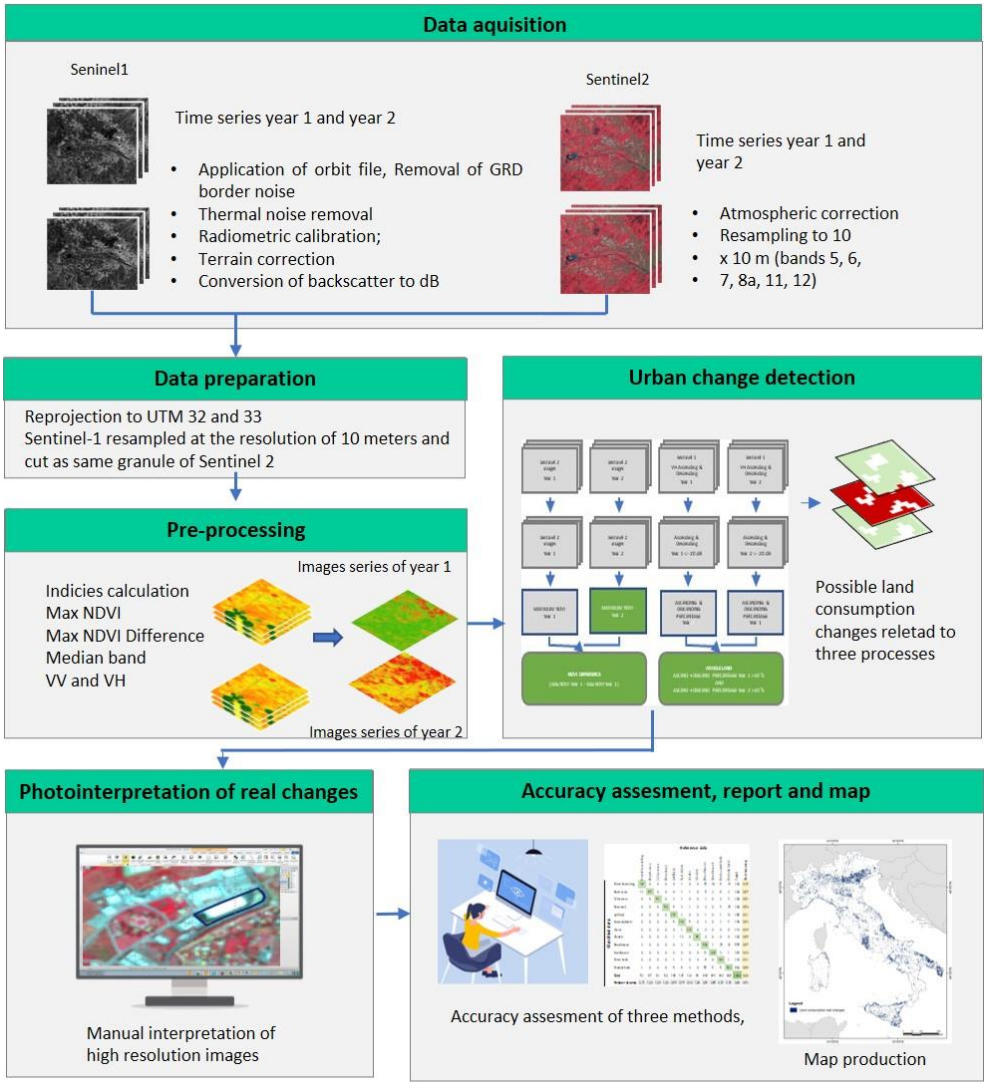

Figure 3.12 - Methodology scheme of change detection methodology.

3.4.2.1 Land consumption related to the removal of vegetation

The workflow illustrated in figure 3.13 focuses the changes related to the removal of vegetation. Three experimental versions were developed and tested in order to assess the benefit of different periods and thresholds, although these versions all share the same basic approach.

In order to produce the composites, the acquisition periods must be the same in the 2 years; in detail, for Sentinel-2 the period between March and July was selected because the growth of vegetation favours the distinction between land consumption and bare soil (Strollo et al., 2020), and cloud cover is low. For Sentinel-1 a narrow period from 1st March to 31st March was used because cloud cover is not an issue, allowing to process fewer images.

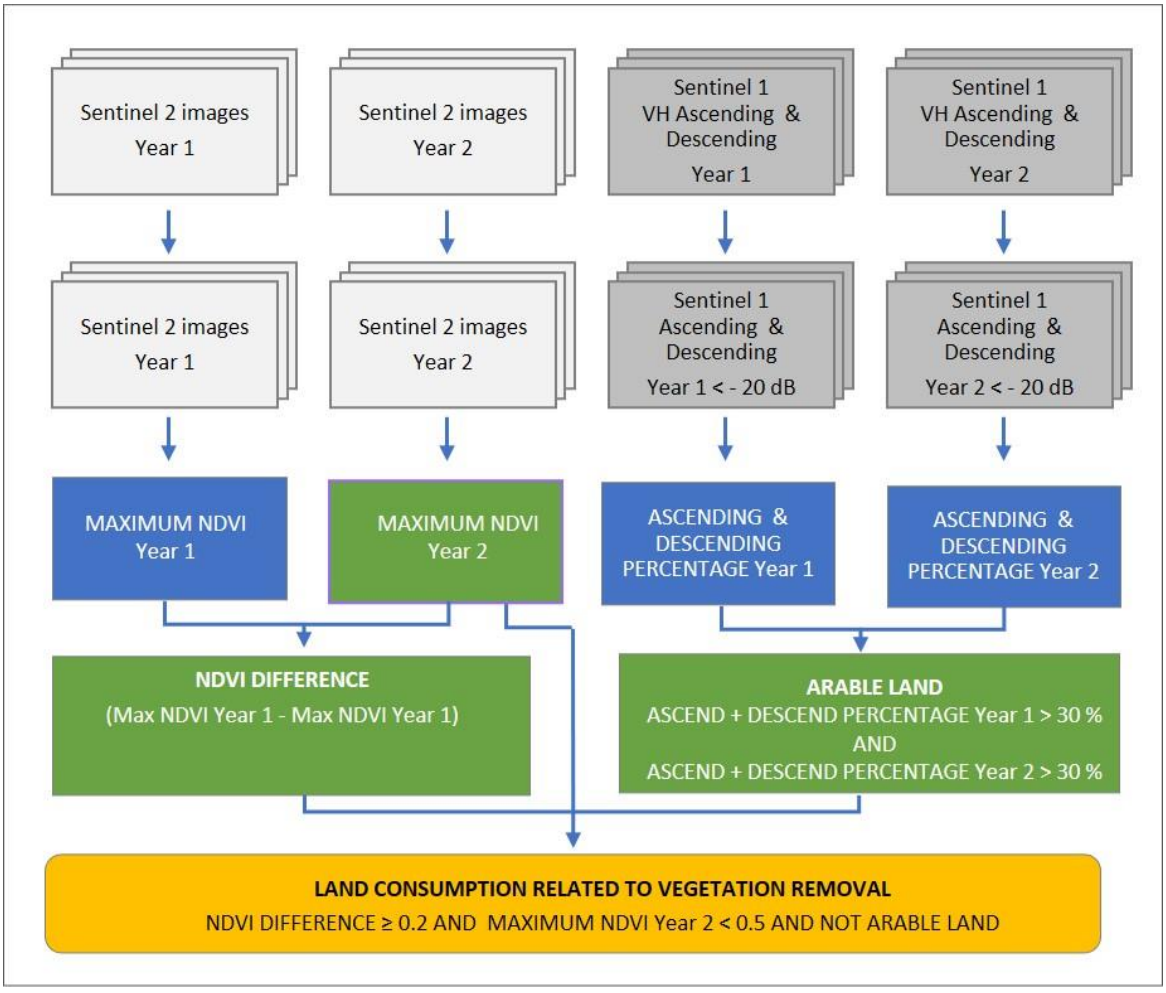

Figure 3.13 - Workflow of the methodology of land consumption related to vegetation removal.

Processing

Since Sentinel-2 images are provided as granules (the minimum partition of the image with size 100x100km^2), the steps in the workflow are intended to be performed for each granule. Italy is covered by about 80 granules in the WGS 84 UTM 32 and UTM 33 coordinates.

Land consumption related to removal of vegetation was calculated considering 3 different scenarios according to the Table 3.4.

The first scenario identifies potential changes starting with the definition of two NDVI-based rules and the addition of a filter to exclude agricultural areas. The second scenario excludes the filter on agricultural areas, in order to allow an analysis of the potential changes identified through only the two conditions of NDVI. Finally, the third scenario takes into consideration an additional observation period, in addition to the standard one which runs from 1st March to 31st July. This period is called the "shift period" and runs from 1st

June to 31st December. In the third scenario, the two conditions on the NDVI are considered to identify changes, while the filter on agricultural areas is excluded.

I. In the first scenario Sentinel-2 images were used for NDVI calculation and Sentinel 1 for exploiting VH backscatter. The requirements to be soil consumption, are the following, the must be satisfied at the same time.

1. **NDVI difference ≥ 0.2**
2. **Maximum NDVI year 2 < 0.5**
3. **Not arable land**

The first condition implies a reduction of vegetation cover (by NDVI difference: MAX NDVI Year 1 - MAX NDVI Year 2), while the second condition i.e. MAXIMUM NDVI Year 2 < 0.5 (calculated on temporal series of year 2) verifies the scarce presence of vegetation. The third condition (i.e. NOT ARABLE LAND) verifies that the changes are not in arable land raster. For the latter requirement Sentinel-1 images with VH polarization were used since, fallow land is characterized by low backscatter, generally lower than -11 dB (Formaggio et al., 2001); therefore, this characteristic was exploited to calculate the percentage of acquisitions where pixels show a backscatter lower than -20 dB, according to the following steps:

Table 3.4 - The table summarises the three tests carried out to identify land consumption related to the removal of vegetation. The conditions of experiment 2 are (in blue).

also used in the other two tests **Land consumption related to the removal of vegetation**			
Test	Data	Processing	Conditions
1	Sentinel 2: *1st March to 31st July of Year 1 and Year 2*	• MAX NDVI year 2 • NDVI DIFFERENCE = MAX NDVI Year 1 - MAX NDVI Year 2	• NDVI DIFFERENCE ≥ 0.2 • MAX NDVI Year 2 < 0.5
	Sentinel 1: *1st March to 31st March*	• Ascending backscatter < -20 db, Raster Perc ASC year1 • Descending backscatter < -20 db, Raster Perc DESC year1 • Ascending backscatter < -20 db, Raster Perc ASC year2 • Descending backscatter < -20 db; Raster Perc DESC year2 ARABLE LAND when: (Perc ASC 1year + Perc DESC 1year) > 30% AND (Perc ASC 2year + Perc DESC 2year) > 30%	• NOT ARABLE LAND
2	Sentinel 2:*1st March to 31st July of Year 1 and Year 2*	• MAX NDVI year 2 • NDVI DIFFERENCE = MAX NDVI Year 1 - MAX NDVI Year 2	• NDVI DIFFERENCE ≥ 0.2 • MAX NDVI Year 2 < 0.5
3	Sentinel 2: *March and July of Year 1 and Year 2*	• MAX NDVI year 2 • NDVI DIFFERENCE = MAX NDVI Year 1 - MAX NDVI Year 2	• NDVI DIFFERENCE ≥ 0.2 AND • MAX NDVI Year 2 ≤ 0.3 • MAX NDVI Year 2 shift < 0.4 • NDVI DIFFERENCE SHIFT ≥ 0.2 AND • MAXIMUM NDVI Year 2 shift ≤ 0.3
	Sentinel 2: *1st June to 31st December of Year 1 and Year 2*	• MAX NDVI Year 2 shift • NDVI DIFFERENCE shift	• NDVI DIFFERENCE ≥ 0.2 AND • 0,3< MAX NDVI Year 2 ≤ 0.4 AND • MAXIMUM NDVI Year 2 shift < 0.4 • NDVI DIFFERENCE SHIFT ≥ 0.2 AND • MAXIMUM NDVI Year 2 shift ≤ 0.4

For every image the condition Backscatter < -20 dB was verified, creating a binary raster (1 = true, 0 = false) and obtaining 4 collections of raster related to ascending and descending backscatter for the two periods. The percentage of acquisitions verifying the above condition was calculated as the sum of every raster in the collection divided by the number of acquisitions ($Perc_{class}$= (N_{true}/$N_{acquisition}$) *100). For instance, if a pixel has value 1 (i.e. Backscatter < -20 dB) in all the images of the collection, the percentage is 100%.

Four raster were obtained: Ascending Percentage Year 1, Descending Percentage Year 1, Ascending Percentage Year 2, Descending Percentage Year 2.

Finally, ARABLE LAND raster is calculated according to the following condition:

(Ascending Percentage Year 1 + Descending Percentage Year 1) > 30%
And
(Ascending Percentage Year 2 + Descending Percentage Year 2) > 30%

This layer ARABLE LAND is a binary raster where pixels have the value 1 if the above conditions is verified, otherwise value 0. It is worth pointing out that the scope of this layer is not the classification of arable land, but the detection of the portion of arable land that can be confused with land consumption because of the temporary removal of vegetation. This could fail the detection of fallow land that exhibits low backscatter values in 1 year only, but it is coherent with the intention of preferring commission to omission errors.

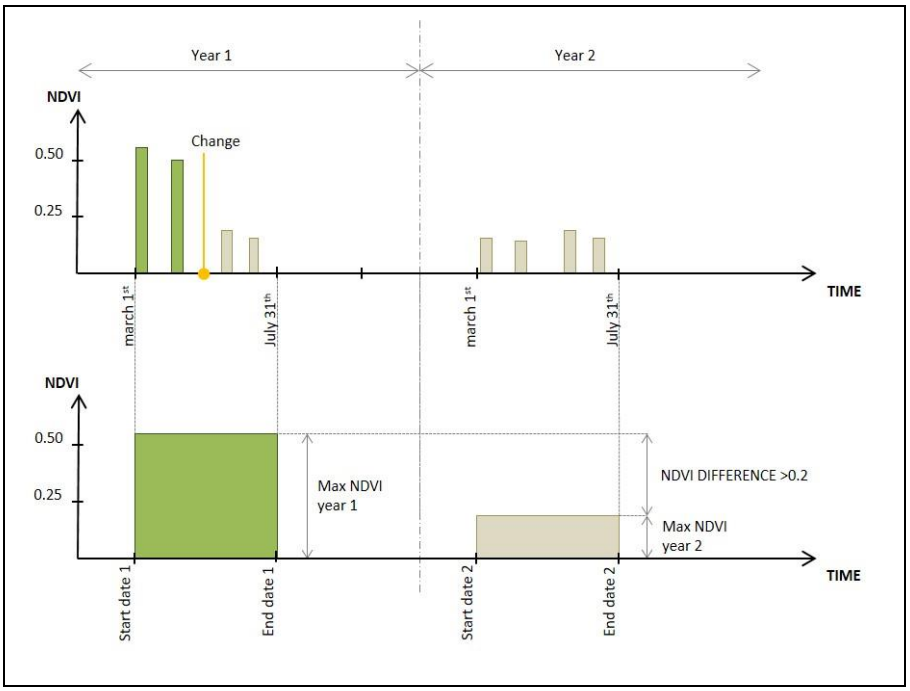

Figure 3.14 - Scheme of change occurred between Start date 1 and Start date 2 and detected by the methodology, the upper chart represents the NDVI values of a pixel at different acquisition times; the lower chart represents the Maximum NDVI value resulting from the acquisition periods of the 2 years.

A change occurred after the start of year 2 (i.e. between March and June) (Figure 3.14), is not detected because even if the NDVI values decrease during the second year, the MAXIMUM NDVI year 2 is affected by the NDVI values before the change, and the difference between the two MAXIMUM NDVI raster is lower than the threshold. This change will be detected in the following year (e.g. comparing Year 2 and Year 3) because the change happens between the start of year 2 and the start of year 3 as illustrated in the previous example.

This third experiment aimed to detect also the changes occurred after the start of year 2. The same methodology was applied to a "shifted period" starting from June (Year 1 SHIFT and Year 2 SHIFT) which should allow to measure NDVI variations (i.e. MAXIMUM NDVI Year 1 shift and MAXIMUM NDVI Year 2 shift) occurred between March (i.e. Start date 2) and June (i.e. Start date 2 shift), as illustrated in Figure 3.15.

Moreover, a different set of NDVI thresholds was applied, in order to differentiate the most probable changes from NDVI variations more probably due to agricultural areas.

For the identification of changes occurred before March of the second year, a third condition was defined, based on the information provided by the shift period. This condition confirms the persistence of the change after the 1st March.

The most probable changes where identified according to the following conditions:

NDVI DIFFERENCE ≥ 0.2
AND
MAXIMUM NDVI Year 2 ≤ 0.3
AND
MAXIMUM NDVI Year 2 shift < 0.4

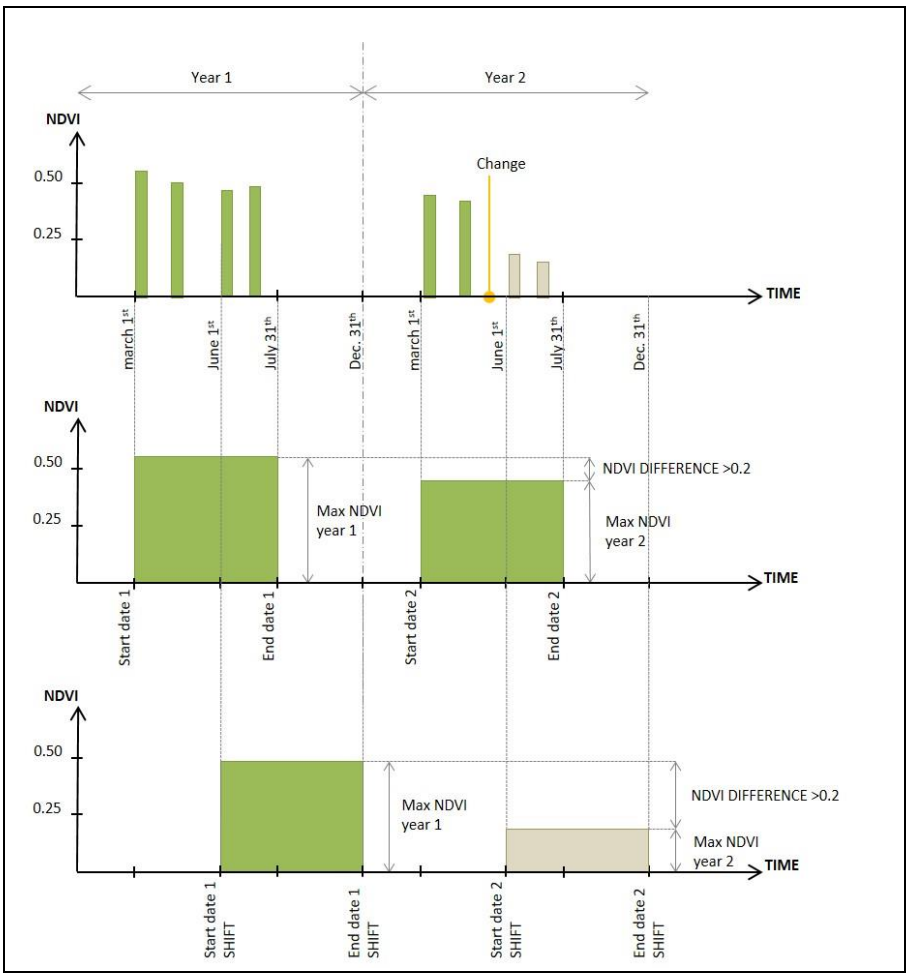

Figure 3.15 - Scheme of change occurred after Start date 2 that can be identified with the Shift period.

The changes occurred between March and July of the second year are detected thank to the shift period, introducing the following conditions:

NDVI DIFFERENCE SHIFT ≥ 0.2
AND
MAXIMUM NDVI Year 2 shift ≤ 0.4

The less probable changes occurred before March are determined using an additional range of NDVI thresholds using the following conditions (Figure 3.16):

NDVI DIFFERENCE ≥ 0.2
AND
0.3 < MAXIMUM NDVI Year 2 ≤ 0.4
AND
MAXIMUM NDVI Year 2 shift < 0.4

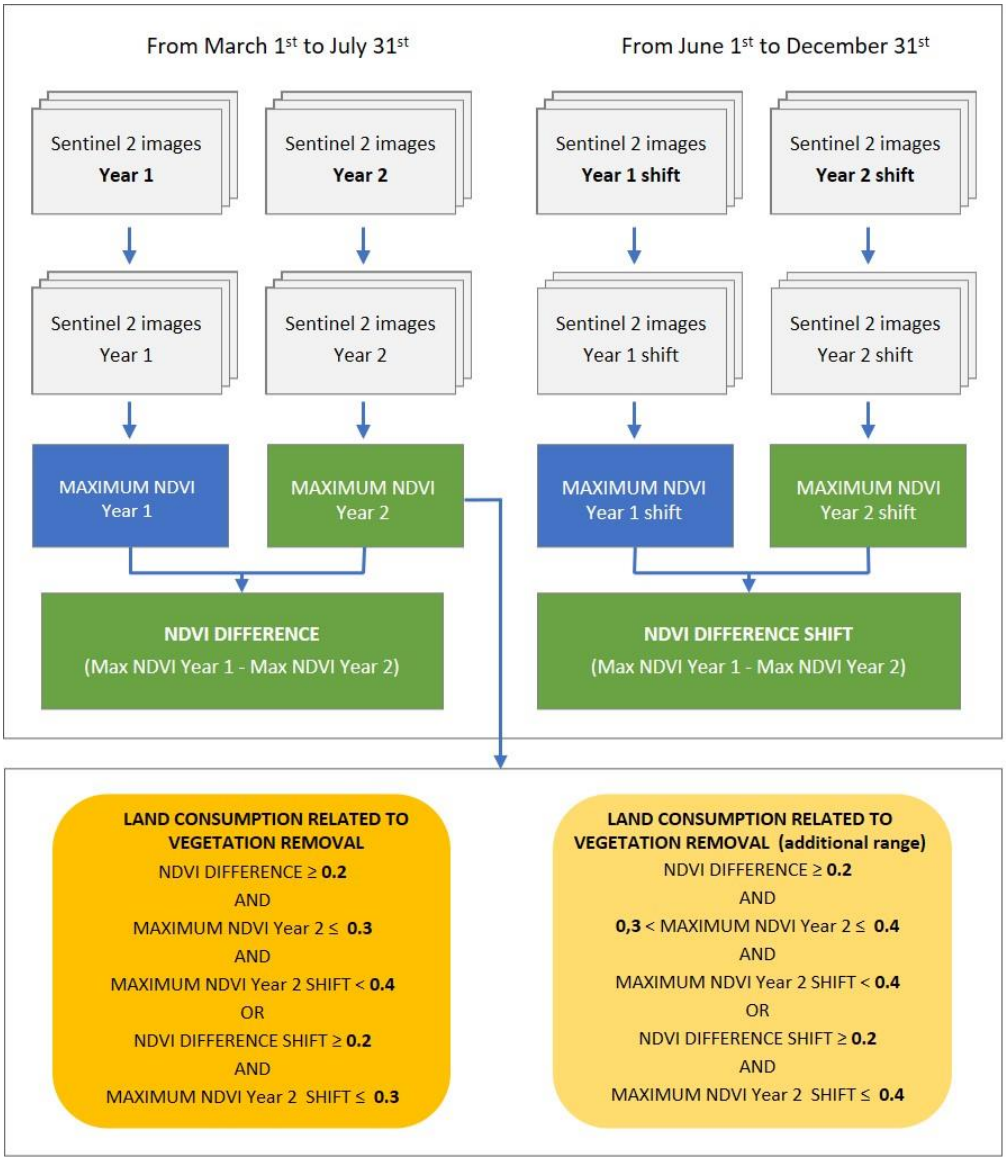

Figure 3.16 - Workflow of the methodology of land consumption related to vegetation removal.

3.4.2.2 Land consumption related to buildings and infrastructures

Land cover changes related to buildings and infrastructures (Table 3.5) can increase the backscatter values, although these values are influenced by several factors such as height and orientation of buildings (Koppel et al., 2017). The developed workflow tries to exploit the availability of Sentinel-1 images in order to compare backscatter variations of two periods (Figure 3.17). It is worth highlighting that roads or squares without buildings have generally low backscatter values, therefore are not detected with this method. VV

polarization of Sentinel-1 images was used since building backscatter emerge from the background more than VH polarization (Koppel, et al., 2017), therefore being better suited for building detection.
From the ascending and descending Sentinels in the two years, the median was calculated, and the dB values were converted to natural values, obtaining four raster:

- ASCENDING MEDIAN Year 1
- ASCENDING MEDIAN Year 2
- DESCENDING MEDIAN Year 1
- DESCENDING MEDIAN Year 2

Table 3.5 - The table summarises the steps to detect land consumption related to buildings and infrastructures

Land consumption related to buildings and infrastructures			
Test	Data	Processing	Conditions
1	Sentinel 1	• Ascending Median year1 • Descending Median year1 • Ascending Median year2 • Descending Median year2 Ascending Median Difference = Ascending Median Year2 – Ascending Median Year 1 Descending Median Difference = Descending Median Year2 – Descending Median Year 1	• Ascending Median Difference >= 0.1 and • Ascending Median year 1 < -9 db and • Descending Median Difference >= 0.1 and • Descending median year 1 < -9 db and • Slope < 20 and • Maximum NDVI year 2 < 0.5
	Sentinel 2	• MAX NDVI year 2	
	SRTM DEM	• Slope in degrees from SRTM DEM	

The differences between the median values of the two years were calculated for the ascending orbit and for the descending orbit:

- ASCENDING MEDIAN DIFFERENCE = ASCENDING MEDIAN Year 2 – ASCENDING MEDIAN Year 1
- DESCENDING MEDIAN DIFFERENCE = DESCENDING MEDIAN Year 2 – DESCENDING MEDIAN Year 1

Difference values greater than 0 mean that backscatter values increased in the period.
Slope in degrees was calculated from the SRTM DEM (Shuttle Radar Topography Mission) Version 4 (Jarvis et al., 2008), in order to exclude areas whose backscatter values are influenced by high slope.
The following conditions were evaluated for producing the map of land consumption related to buildings and infrastructures:

- ASCENDING MEDIAN DIFFERENCE >= 0.1 and
- ASCENDING MEDIAN Year 1 < -9 dB and
- DESCENDING MEDIAN DIFFERENCE >= 0.1 and
- DESCENDING MEDIAN Year 1 < -9 dB and
- SLOPE < 20 and
- MAXIMUM NDVI Year 2 < 0.5

The threshold values 0.1 and -9 dB were evaluated as optimal values to distinguish real changes after several trial and errors system. The concurrent conditions for ascending and descending orbits aim to exclude partial increase of backscatter values related to variations of vegetation and the particular geometry of objects at the ground.
The condition ASCENDING (DESCENDING) MEDIAN Year 1 < -9 dB is intended to exclude areas that are already built in the first year (therefore having high backscatter values), such as buildings under construction or restoration that could verify the condition ASCENDING (DESCENDING) MEDIAN DIFFERENCE >= 0.1. This could potentially exclude land consumption over forested areas (characterized by high backscatter values), nevertheless these changes should be detected in the methodology described in the previous paragraph considering the NDVI difference.

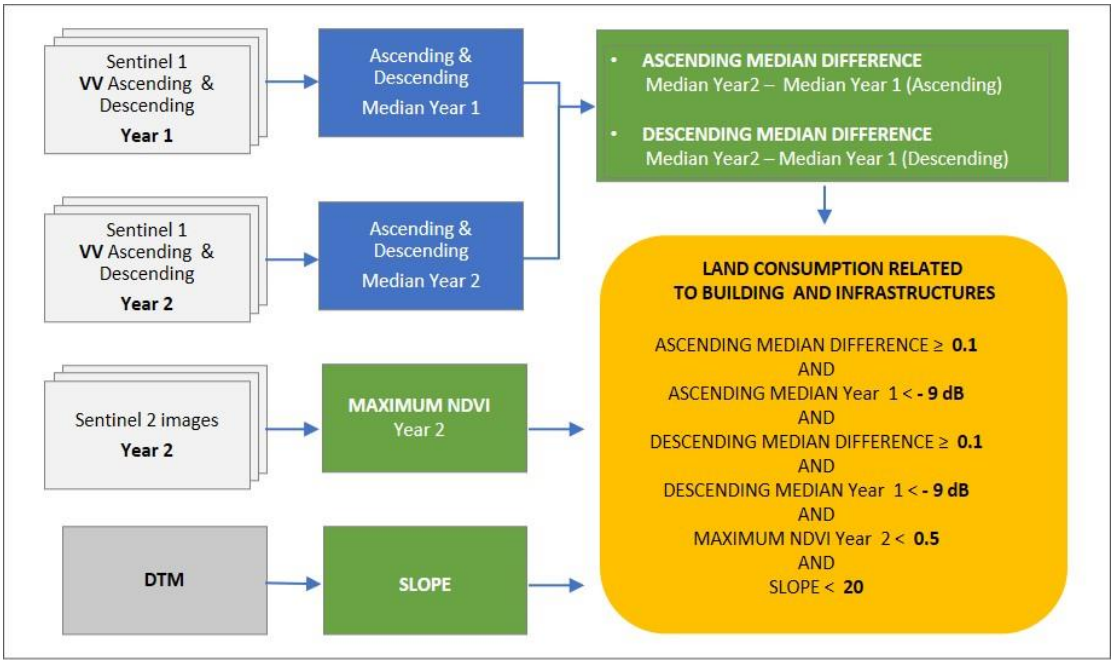

Figure 3.17 - - Workflow of the methodology of land consumption related to building and infrastructures.

In addition, areas having slope values greater than 20 degrees were excluded from the detection because usually flat land is urbanized, and backscatter values are badly affected by high slope.
The last condition (MAXIMUM NDVI Year 2 < 0.5) uses the NDVI calculation from Sentinel-2 described in the previous paragraph, with the scope of excluding from the classification vegetated pixels that had a backscatter increase, for instance because of forest growth.
The changes derived with this method are therefore combined with the changes identified in the previous paragraph using Sentinel-2, producing a unique map of possible changes related to land consumption.

3.4.2.3 Validation of Land consumption mask

The three experiments were compared to land consumption monitored by ISPRA SNPA (National System for Environmental Protection) in the frame of the annual report 2018-2019. About 33,000 real changes where classified by ISPRA, covering about 57 km^2 of land consumed between 2018 and 2019 (Munafò, 2020). It should be noted that the photo-interpretation was performed for the whole Italian territory, also in absence of detected possible changes, in order to classify all the real changes and assess the omission errors of the experiments.
The first experiment produced the lowest number of detected pixels and in terms of area, only a small portion of consumed land (i.e. 424 ha) was correctly classified. However, considering the whole changes as patch entities, and defining detected a change that was identified in at least one pixel, it is possible to count the number of real changes identified by the methodology and supporting the photo-interpretation. In this case, the first experiment detected 31% of total changes (Table 3.6). The second experiment resulted in a higher detection of soil consumption (about 50.7% of real changes). The third experiment provided the highest detection of soil consumption (about 59.8% of real changes).

Table 3.6 – Results obtained from the three experiments.

Experiment	Not detected changes	Detected changes	Total	Percentage of detection
First	22742	10205	32947	31.0
Second	16245	16702	32947	50.7
Third	13257	19690	32947	59.8

Considering only the changes larger than 100 m^2 (i.e. one pixel), the first experiment detected the 37.6% of changes (Tab 3.6). The second experiment resulted in 58.9% of changes detected. The highest percentage of detection was provided by the third experiment (i.e. 70.4%). Table 3.7 confirms that single pixels are omitted because of several causes, such as mixed pixel, while larger changes are detected by at least one pixel.

Table 3.7 - Results obtained from the three experiments where single pixels are omitted.

Experiment 2	Not detected changes	Detected changes	Total	Percentage of detection
First	15426	9309	24735	37.6
Second	10163	14572	24735	58.9
Third	7332	17403	24735	70.4

To better understand the relation between detected changes and change area, changes were grouped in classes based on the area (i.e. ≤ 100 m^2, between 100 m^2 and 500 m^2, between 500 m^2 and 1,000 m^2, between 1,000 m^2 and 1,500 m^2, between 1,500 m^2 and 2,000 m^2, > 2,000 m^2). Table 3.8 illustrates the changes identified by the third experiment, showing that very high percentage of detection is reached for larger changes, while only 48.5 of pixel size changes are detected.

Table 3.8 - Changes identified by the third experiment: very high percentage of detection is reached for larger changes.

Class of area	Not detected changes	Detected changes	Percentage of detection
≤ 100 m^2	11983	11304	48.5
between 100 m^2 and 500 m^2	1126	6236	84.7
between 500 m^2 and 1,000 m^2	113	1205	91.4
between 1,000 m^2 and 1,500 m^2	22	420	95.0
between 1,500 m^2 and 2,000 m^2	3	188	98.4
> 2,000 m^2	10	337	97.1

3.5 Accuracy assessment of remotely sensed map

All maps derived from a classification of remote sensing image are never correct (remote sensing results are never perfect) because of classification errors, so it is always necessary to implement an analysis that takes the classification errors into account providing an estimate of the map precision.
Accuracy assessment has the objective to evaluate the correctness of an image classification and involves the comparison of a classified map to a reference dataset assumed to be true. Through this process is possible to evaluate the errors in quantitative terms in order to determine the quality of a map created from remotely sensed data and to identify, measure and then correct map errors (Congalton & Green, 2019). Accuracy analysis also allows researchers to compare various techniques or to verify which algorithms provide the best result and improve the quality of data products. Finally, accuracy measures are fundamental information to mostly decision-making process and represent an essential part of a mapping project (Strahler et al., 2006) or of any scientific study.

3.5.1 Accuracy assessment methodology

The methodology adopted for the accuracy assessment is based on some fundamental steps according to a procedure amply documented in literature (FAO, 2016; Olofsson et al., 2014; Stephen V. Stehman & Foody, 2019; S V Stehman & Czaplewski, 1998) and in particular it refers to the publication of Olofsson et al., 2014. The key components are described in this section and include:

- ✓ Sampling design: the protocol for selecting the samples.
- ✓ Response design which encompasses all aspects of map and reference data.
- ✓ Analysis which comprehend the formulas and inference for estimating accuracy and area.

Before sampling designs a preliminary qualitative control should be conducted. The control consists in a systematic visual check to identify macroscopic errors, e.g. a river labelled as vegetation, and it is an important step because in most mapping products there are macro-errors which are not visible in the quantitative metrics.

Sampling design

In this phase is defined the procedure for obtaining a subset of population that must be representative of the population, in this case the pixels. In such way it possible to analyse just a small sample and make inference from it.

The definition of reference sample design is needed to establish sample unit and size and to determine where allocate them in the different strata: for a correct evaluation of accuracy, all strata must be sampled. The strategy for the sampling design also considers some important criteria: it should be easy to implement, cost effective and precise (i.e. the estimates should have small standard errors) and spatially well distributed across the study area.

Sample size

The number of samples must be statistically significant and attempt to meet precision requirements of more than one purpose. It is important to highlight that only the probabilistic samples ensure the possibility of knowing the measure of the inaccuracy that is inevitably committed in selecting the units.

Furthermore, the greater the collection of reference data, the greater the efforts to be made in terms of costs and labour. It is therefore essential to calculate the correct number of samples and find a right balance between these conditions. There is a wide bibliography about sample size notably (Brooner, 1976; Congalton, 1991; Hay, 1979); many researchers have published formulas useful for determining the appropriate sample size. One of the formulas more commonly used is that one proposed by Cochran in 1977 and applied in this study:

$$\frac{(\sum W_i S_i)^2}{[S(\hat{O})]^2+(\frac{1}{N})\sum {W_i S_i}^2} \approx \frac{(\sum W_i S_i)^2}{[S(\hat{O})]^2}$$

The number of the samples depends on the expected user accuracy of each class, the standard error of the expected overall accuracy and area information. These variables are not known prior to the assessment, determining the choice of size an inexact science (FAO, 2016). On the other hand, when the size of the sample exceeds a few percent of the total population the mathematics of probability prove that the size of the population is not a determining factor, as can be seen from the formula.

Sample allocation

Once the number of samples was determined, a second order of problems is to allocate the samples in the different strata. There are different sampling methods, the most used are:

- ✓ Simple random sampling, where the sample is selected randomly in the area.
- ✓ Simple systematic, when observations are placed at equal intervals according to a strategy.
- ✓ Stratified random sampling, when a minimum number of points are randomly located in each stratum.

This last method of sampling is usually very powerful especially in the context of land cover change class such as land consumption or burnt areas. In fact, changes took at a very small proportion of the area, so this method ensures a specified minimum number of observations randomly placed in each class. This study uses random stratified sampling method where the strata are map classes, as this method improves the precision of the accuracy and area estimates by increasing the numbers of test points in the change classes.
Usually it is possible to allocate the sample to strata in equal, optional and proportional manner. In equal allocation the overall sample size is distributed equally between the strata and it is used when all classes are considered equally important; this method favours the estimation of user's accuracy. When the sample size is allocated proportionally to the area, rare strata receive a small proportion of the overall sample size and they usually correspond in a smaller error for overall accuracy. "As a compromise, it is suggested to use a proportional allocation, but guaranteeing a minimum number of sample size per stratum". (FAO 2016).

Response design

Response design defines how to collect the information from the reference data. The reference data is used to compare a classified point on the map with what should presumably represent the ground truth. This data could be an existing map, an inventory data (Falkowski et al., 2009; McRoberts, 2011; Wulder et al., 2007), aerial photo (Skirvin et al., 2004), satellite imagery (Cohen et al., 2010) or ground collected; in this project ground survey screen interpretation based on Google Earth has represented the process to collect the reference data. Some considerations must be made with respect to their use. For example, in the case of Google Earth images used in this project, they have the advantage of being freely accessible, but they do not offer a review time comparable to those of the "sentinels", which is a few days. This aspect creates difficulties for the validation of land cover change classes over a short period of time or for distinguishing classes that vary the reflectance during the year due to phenological changes.
In some cases, the reference data may show some shifts with respect to the classified map because the data was captured by different satellite platforms. This results in a different position of the control points respect to classified map, with a consequent error in the accuracy assessment. Additionally, reference should be collected in the same period respect to the map, in order to avoid errors caused the land cover transformations.
Spatial unit represent the unit at which the reference data is collected and the base for the comparison of two dataset. Due to the project's land cover map having pixel-level detail, this dimension is chosen as the spatial unit.
In this step the rules for defining agreement between classified and reference data are also defined, especially when the data does not have the same classification system.

Analysis

In the analysis phase, the information coming from the classified map and the reference data are compared. These analyses, normally used to assess the accuracy and to estimate the area of each class are based on the error matrix or confusion matrix (Olofsson et al., 2013; Stephen V. Stehman et al., 2012).

Error Matrix

It is one of the most popular tools for the evaluation of the accuracy of a classification process. It is a square matrix, in which the number of rows and columns is given by the number of classes considered in the land cover map and reference data (Table 3.9). The elements of the matrix are the number of pixels corresponding to the test points chosen for the accuracy assessment. In this error matrix, the rows represent the map classification and the columns represent the reference classification.
The elements on the main diagonal represent the correctly classified pixels; the elements on the rows represent the number of test pixels incorrectly entered by the classification within a given class; the other

elements along the columns represent the omission error, i.e. the number of test pixels of a given class assigned by the classification to the other classes. The accuracy for each class is given by the ratio between the number of correctly classified test pixels (indicated on the main diagonal) and the total number of test pixels considered. The overall accuracy is given by the ratio between the total of the elements of the main diagonal and the total number of test pixels considered.

Table 3.9 – Example of error matrix.

		Reference data				Row total
	Class	**A**	**B**	**C**	**D**	
Classified data	**A**	$p_{1,1}$	$p_{1,2}$	$p_{1,3}$	$p_{1,k}$	p_{1+}
	B	$p_{2,1}$	$p_{2,2}$	$P_{2,3}$	$p_{2,k}$	p_{2+}
	C	$p_{3,1}$	$p_{3,2}$	$p_{3,3}$	$p_{3,k}$	p_{3+}
	D	$p_{k,1}$	$p_{k,2}$	$p_{k,3}$	$p_{k,k}$	p_{k+}
	Column total	p_{+1}	p_{+2}	p_{+3}	p_{+k}	n

- Overall accuracy (OA) $$OA = \sum_{i=1}^{k} \frac{p_{ii}}{n}$$
- User's accuracy (UA) $$UA_i = \frac{p_{ii}}{p_{+1}}$$
- Producer's accuracy (PA) $$PA_i = \frac{p_{ii}}{p_{i+}}$$

3.5.2 Accuracy assessment of land cover map

The validation process is based on a comparison between the land cover map and reference dataset derived from-Google Earth images. This set of points constitutes the reference data set. The accuracy analysis was carried out with the aim of estimating the overall and class accuracies and to evaluate their area and confidence intervals. In this research, accuracy estimation is carried out. The process involves the following steps according to (Olofsson et al., 2014).

- ✓ Sampling design.
- ✓ Response design.
- ✓ Analysis and results.

3.5.2.1 Sampling design

The first step is a general analysis of the classification to highlight inconsistencies or macro errors. This has not highlighted any critical issues in the classified map. The number of samples was determined according to the formula below, Table 3.10 shows the results:
Land cover map was divided into 12 strata that correspond to the land cover classes defined in the legend. 4 are change (in italic in Table 3.10) classes and 8 are stable classes; the size of each stratum is calculated using the pixel as the unit.

The sample size (n) calculation was performed using the formula reported by Olofsson et al. 2014 and referred to Equation 5.25 in (Cochran, 2007).

$$n = \frac{(\sum W_i S_i)^2}{[S(\hat{O})]^2}$$

Where:

W_i = is area proportion of each classes derived from the map classification

S_i= are areas proportions is the standard deviation of stratum i, SI = $\sqrt{Ui(1-Ui)}$ (Cochran, 1977, Eq. 5.55)

$S(\hat{O})$= is the standard target standard error that we aim to achieve.

$S(\hat{O})$ influences the sample size and his value depends from Ui of the classes that is an unknown value; for this reason the worst case scenario was considered in the calculation; in particular the range of Ui is 0 to 1, and therefore the range of $Ui(1-Ui)$ is 0 to 1. Consequently, since there is no information available to approximate Ui, the value of 0,6 was used to generate a conservative setting, with a very large sample size. The target standard error for overall accuracy was assumed to be 0.01 as suggested by Olofsson et al. (2014), that corresponds to a confidence interval of 0,01. The Table 3.10 shows size calculation.

Table 3.10 - Sample size calculation according Olofsson et al. (2014). The required inputs are the map areas and the expected user's accuracy for the sample.

Classes (strata)	*Area in m²*	*Wi (Mapped proportion)*	*Ui (Expected user's accuracy)*	*Si (Standard deviation)*	*Wi*Si*
Artificial	21279989200	0.071	0.6	0.490	0.035
Nat. Abiot.	9535740300	0.032	0.6	0.490	0.015
Broadleaves	1,20065E+11	0.398	0.6	0.490	0.195
Needleaved	16075824100	0.053	0.6	0.490	0.026
Perm. herb.	1,26579E+11	0.420	0.6	0.490	0.206
Periodic herb.	2398340300	0.008	0.6	0.490	0.004
Water	3377369300	0.011	0.6	0.490	0.005
Ice and Snow	1117731200	0.004	0.6	0.490	0.002
Forest disturb.	784903200	0.003	0.6	0.490	0.001
Burned areas	111060600	0.000	0.6	0.490	0.000
Soil consum.	66003200	0.000	0.6	0.490	0.000
Restoration.	9060400	0.000	0.6	0.490	0.000
Total	301399739400				1
S(O) overall accuracy		0.01			
Total number of samples		2400			

Once the total number of points to be sampled was established, the samples were allocated using "stratified random sampling" method that presents the advantage that all strata (i.e., map classes), no matter how small, will be included in the sample (Table 3.11).

The number attributed to each class is equal to the average of equal and proportional distribution (see https://fromgistors.blogspot.com/2019/09/Accuracy-Assessment-of-Land-Cover-Classification.html); from the calculations performed, each class was assigned a minimum number of samples equal to 100; in this way all classes have a statistically significant number of samples.

Table 3.11 – Distribution of samples (Final allocation column).

Classes	Equal	Proportional	Final Allocation
Artificial	200	169	185
Nat. Abiot.	200	76	138
Broadleaves	200	956	578
Needleaved	200	128	164
Perm. herb.	200	1008	604
Periodic herb.	200	19	110
Water	200	27	113
Ice and snow	200	9	104
Forest disturb.	200	6	103
Burned areas	200	1	100
Soil consum.	200	1	100
Restoration.	200	0	100
Total	**2400**	**2400**	**2400**

3.5.2.2 Response design

In order to assess the map accuracy, the reference data must be of good quality and independent; in this case, high resolution orthophotos were used from Google Earth, acquired at the same year as the classified image. These data present the advantage to have a resolution of less than 1 m and are free. For the period considered (2017-2018), most of the territory is covered by images. When no image was available, Sentinels were used through a manual photo-interpretation process (Figure 3.18).

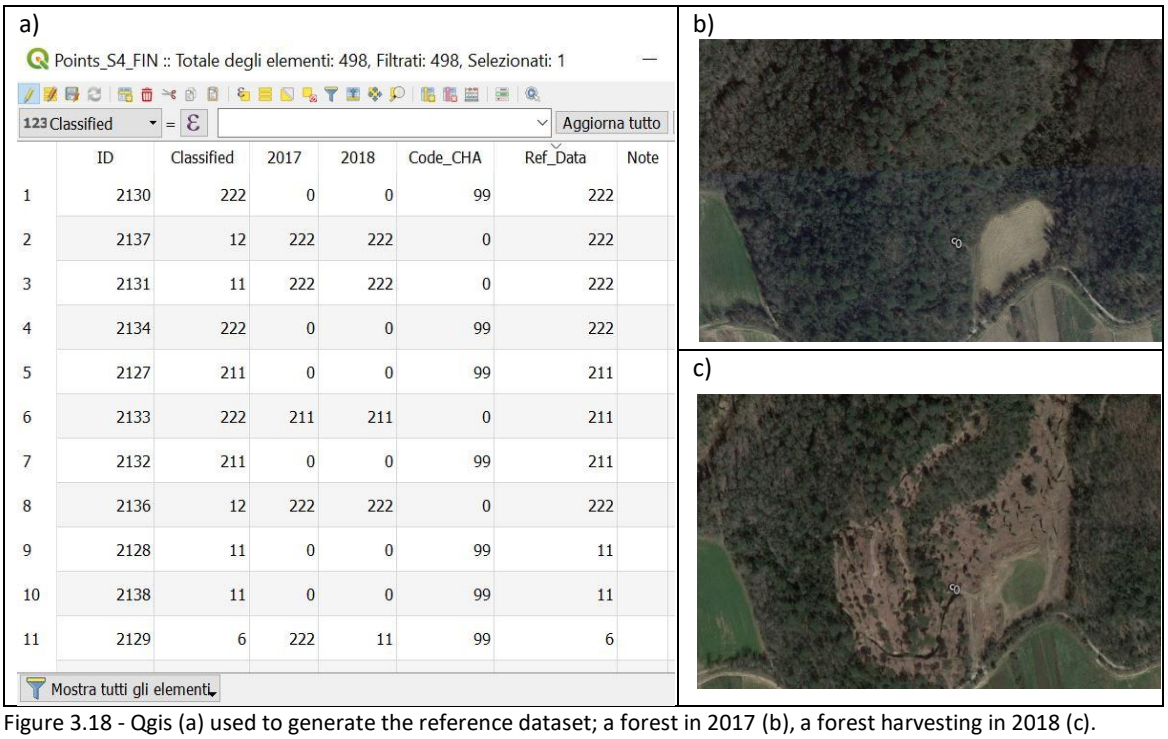

	ID	Classified	2017	2018	Code_CHA	Ref_Data	Note
1	2130	222	0	0	99	222	
2	2137	12	222	222	0	222	
3	2131	11	222	222	0	222	
4	2134	222	0	0	99	222	
5	2127	211	0	0	99	211	
6	2133	222	211	211	0	211	
7	2132	211	0	0	99	211	
8	2136	12	222	222	0	222	
9	2128	11	0	0	99	11	
10	2138	11	0	0	99	11	
11	2129	6	222	11	99	6	

Figure 3.18 - Qgis (a) used to generate the reference dataset; a forest in 2017 (b), a forest harvesting in 2018 (c).

QGIS software was used to randomly distribute the points over all classes. A raster obtained from map classification was used, after applying a shrink that reduces the patch edges. This operation avoids the selection of points at the border between two homogeneous areas, preventing uncertain interpretation

especially in the presence of geolocation error (this error is defined as a mismatch between the location of point on the classified map and the reference data). Once a given set of points was selected, the classification value was assigned to each point using Qgis tool, (Rankings field), then, through a manual photointerpretation work, the 2400 sample points was classified, attributing the corresponding class to each of them, based on Google Earth images. Below are the criteria adopted to translate information derived from the photointerpretation into reference labels (classification).
The fields 2017 and 2018 were used as follows: if there wasn't any change the class is confirmed by adding 99 in the field Code_Cha; if there was a change, in 2017 and 2018 fields, it was inserted the code of the observed classes. Classified field refers to the land cover classification.
In general, code 99 confirms the classification while code 0 indicates an error. In order to compare the two classifications Ref_Data was compiled by entering Ref_Data =_Classified in presence of 99 in the Code_Cha field, while Ref_Data = 2018 in case of error, by entering in the field the class observed in 2018.
In all uncertain situations (points on isolated pixel within a different cluster, points at the edges, points probably positioned in an incorrect place due to resampling or geolocation error) the criteria adopted is pixel based and the points were interpreted by assigning to the point the class on which it falls exactly.
The field Note was used to indicate unclear situations or contexts to be reviewed. It is the case for example of a point over an isolated pixel, surrounded by another type of land cover class.

3.5.2.3 Analysis

Data interpretation was performed defining the confusion matrix, which collects data on the accuracy of each class and on the map in general. It's always a square matrix, where the columns represent the reference data and the rows represent the classification data. The validation was carried out on the individual points according to the procedure described in the previous chapter and related to *response design*.

The Error Matrix
The error matrix obtained is made up of 12 classes, the first four are change classes, while the other eight are stable classes referring to 2018 period. Through the error matrix it is possible to understand how many of the real points of a class were included in another type of land cover and how many were wrongly classified in that same class. From the confusion matrix in Table 3.12 is possible to extract three indicies to evaluate quantitatively the accuracy that characterizes the different classes.
As explained in the previous paragraph:
Overall accuracy (OA) is the sum of the diagonals divided by the total. The Land cover map has produced a result equal to 0.83. User Accuracy (UA) is computed by dividing the number of correctly classified points in each category by the total number of points that were classified in that category (the row total); its complementary measures commission error of class *i,* (1 – $\frac{p_{ii}}{p_{+1}}$).
The values obtained depend on the class examined: the lowest values correspond to forest disturbances while the highest values correspond to the waters class.
Producer's accuracy (PA) results from dividing the number of correctly classified points in each class (on the major diagonal) by the number of reference points (the column total). Its complementary measures omission error of class, (1 - $\frac{p_{ii}}{p_{+1}}$). For this value, the 2018 map has produced, good results ranging from 0.62 to 1.

Table 3.12 – Error matrix.

		Reference data													
		Forest disturb.	Burned areas	Soil consumption	Renatural.	Artificial	Nat. Abiot.	Water	Ice and snow	Broadleaves	Needleaved	Permanent herb.	Periodic herb.	**Total**	**User Accuracy**
Classified data	Forest disturbances	36	0	0	0	0	1	0	0	25	10	8	23	103	0.35
	Burned areas	11	67	0	0	0	2	1	0	5	4	6	4	100	0.67
	Soil consum.	0	0	81	0	3	1	0	0	2	0	4	9	100	0.81
	Renatural.	0	0	0	50	8	3	1	0	4	0	9	25	100	0.50
	Artificial	0	0	0	0	172	1	0	0	1	0	1	11	186	0.92
	Natural Abiotic	0	0	0	0	5	114	5	0	3	0	2	9	138	0.83
	Water	0	0	0	0	0	2	111	0	0	0	0	0	113	0.98
	Ice and snow	0	0	0	0	2	13	0	89	0	0	0	0	104	0.86
	Broadleaved	3	0	0	0	0	3	3	0	501	2	25	41	578	0.87
	Needleaved	0	0	0	0	0	0	0	0	12	148	3	1	164	0.90
	Perm. herb.	0	0	0	0	1	1	0	0	6	0	101	1	110	0.92
	Periodic herb.	1	0	0	0	5	6	3	0	57	5	5	522	604	0.86
	Total	51	67	81	50	196	147	124	89	616	169	164	646	2400	0.00
	Producer Accuracy	0.71	1.00	1.00	1.00	0.88	0.78	0.90	1.00	0.81	0.88	0.62	0.81	0.00	0.83

In the next chapter, the accuracy of land cover classification and land cover change are examined and interpreted; in addition, the results obtained by this research are discussed together with the transformations of land cover at national and regional level.

Chapter 4 Results and discussion

This chapter presents the results derived from implemented methodology for land cover and land cover change classification of Italy, discussing the strengths and weaknesses of the map produced.
In particular, the accuracy of different classes and their estimated areas will be analysed as well as the territorial distribution of land cover and land cover changes; the discussion of the results of the land cover map concludes with the comparison between the map obtained through this methodology and the CLC map, highlighting the limits and advantages of these two different approaches.
The other part of the chapter is dedicated to main findings from practical applications: the second paragraph presents a series of environmental indicators useful to better understand the transformations of the territory. They are processed by the land cover change map and they show the evolution of changes occurred in areas with seismic and landslide hazard, with attention to land consumption in areas classified as more hazards.
The next two sections focus on two case studies, which explore the potential of remote sensing data for land monitoring, presenting the results related to Objectives 3 and 4. The methodologies used in the case studies are described in the respective sections to give greater continuity to the exposition.
In the paragraph 4.3 four new indicators were elaborated using the soil consumption map as additional parameters within a landslide susceptibility assessment in order to investigate their efficacy to enhance the model performances, the last part shows the results of this new approach to derive the Landslide Susceptibility Map (LSM).
The last paragraph presents the main findings in the case of monitoring rapid changes linked to environmental disasters. In these situations, the importance of obtaining short-term data is crucial in order to organise not only rescue interventions and damage assessment, but also the actions necessary for a "return to normality" and define planning strategies. The case studies refer to two events occurred in Italy: the Vaia storm on October 2018 in North-Est of Italy and the eruptions on the island of Stromboli on July and August 2019.

4.1 Land cover and land cover change classification of Italy

4.1.1 National scale

The overall accuracy obtained from the accuracy assessment (0.83) is presented in Table 4.1; it offers a general estimation of the map accuracy, but is influenced by the distribution of the error between the classes and in particular in change classes (classes 4-7). As regard producer's accuracy, this value corresponds to omission errors: 4 classes have values equal to 1 and others 7 classes out of 12 have values over 0.88; the only *Permanent herbaceous* class achieved lower value.

Water (0.98), *Artificial* (0.92) and *Permanent herbaceous* (0.92) are the classes with the best User's accuracy, while the classes of change present the highest misclassification, except for *Soil consumption* which achieves a user accuracy of 0.81. Figure 4.1 shows an example of land cover in a predominantly artificial area.

Table 4.1. Accuracy of land cover map and changes.

Code map	Class name	User's accuracy	Producer's accuracy	Overall accuracy
4	Forest disturbances	0.35	0.71	0,83
5	Burned areas	0.67	1.00	
6	Soil consumption	0.81	1.00	
7	Restoration	0.50	1.00	
11	Artificial	0.92	0.88	
12	Natural abiotic	0.83	0.78	
31	Water	0.98	0.90	
32	Ice and snow	0.86	1.00	
211	Broadleaves	0.87	0.81	
212	Needleaved	0.90	0.88	
221	Perm. herb.	0.92	0.62	
222	Periodic herb.	0.86	0.81	

Artificial surface and artificial changes

Since the artificial component derives from the manual photo-interpretation carried out by ISPRA on the areas (masks) produced according to the methodology presented in previous chapter, it has a high accuracy due to periodic updates and improvement (Munafò, 2019); the presence of omission errors is linked to the use of masks to support photo-interpretation. This is because, although the masks have been designed using conservative criteria, aimed at limiting this type of error, they could contain some omissions.

The *Restoration*, *Natural abiotic* and in certain circumstances (senescence period) *Herbaceous periodic* classes, are characterised by reflectance values similar to the artificial class and can be confused with it, producing the omission errors observed in the confusion matrix (Table 4.1).

In the *Natural abiotic* class, there are some omissions errors for the ice and perennial snow classes, essentially due to the seasonal variation of the glacier profile in high altitude areas.

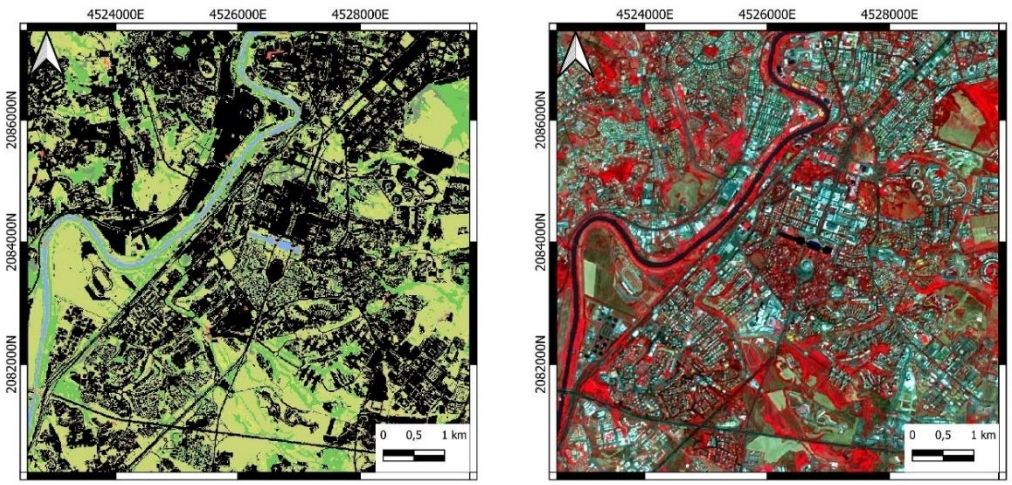

Figure 4.1 - Land cover map 2018 on the left, example of artificial surface class, Sentinel-2 (false colour) on the right.

Water, Ice and snow

The *Water* class has provided good results since it has characteristics that can be easily discriminated through the optical and radar instruments used in this research: user and producer accuracy values are above 0.9 (Figure 4.2).

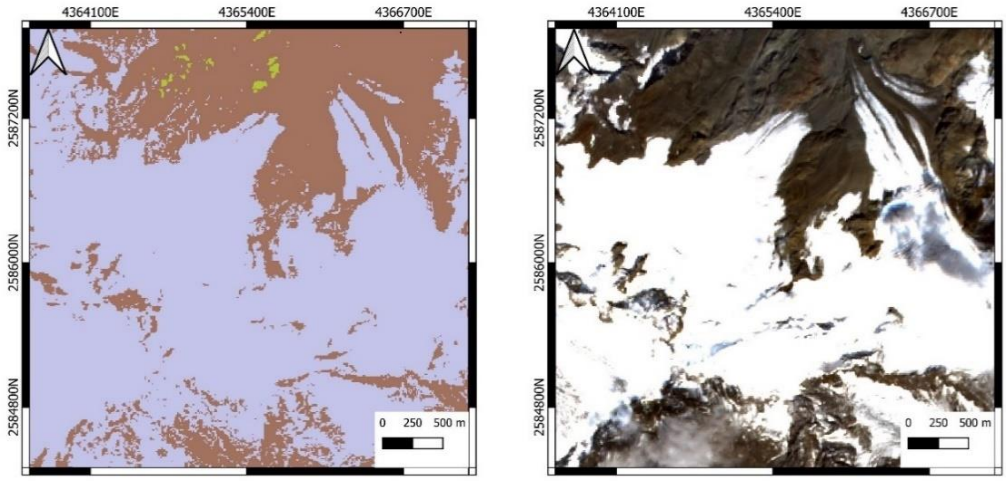

Figure 4.2 - Land cover map 2018 on the left, example of water class, (orthophoto on the right).

The class *Ice and snow* (ice and perennial snows) has lower user accuracy than water (0.86). The commissions errors are related to the N*atural abiotic* and they are consistent with the errors of omission analysed for the N*atural abiotic* itself. In general, the errors related to both these two classes (Water and Ice and snow) depend on the seasonal fluctuation of the flow of the water bodies or to melting of the ice, during summer (Figure 4.3).

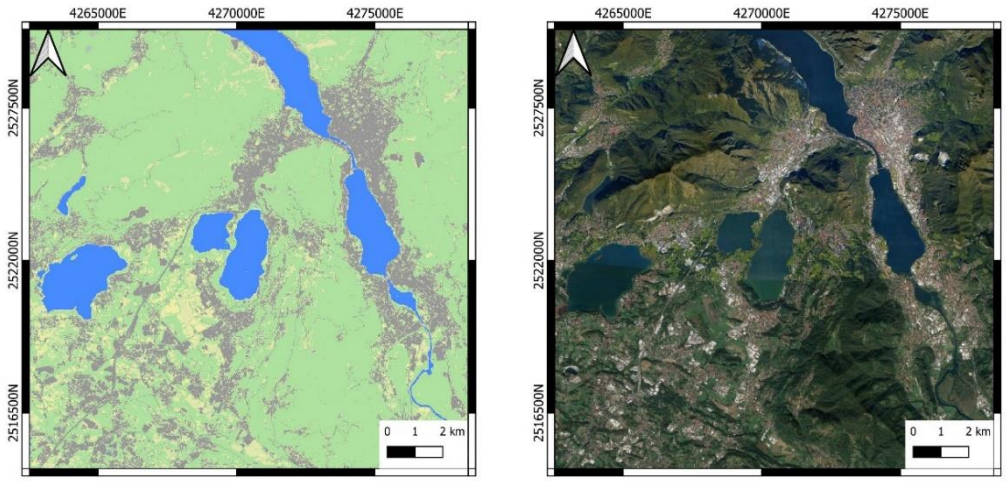

Figure 4.3 - Land cover map 2018 on the left, example of *Ice and snow* class, (orthophoto on the right).

Vegetation

The woody vegetation class has generally given good results, allowing conifers to be fairly well separated from broadleaf trees. However, broadleaves present lower accuracy values than conifers. Both errors of the omission and commission for the trees are due to the absence of a shrubs subclass, that often covers the areas between tree and herbaceous vegetation. In fact, the errors refer to transition areas between wooded and herbaceous areas. Areas with sparse or very discontinuous herbaceous vegetation are a first source of uncertainty as they can be misclassified as natural abiotic surfaces (Figure 4.4).

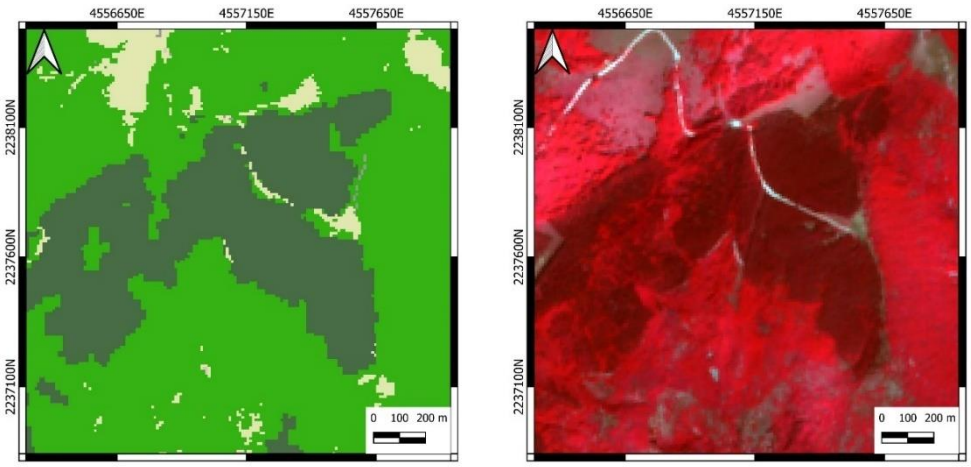

Figure 4.4 - Land cover map 2018 on the left, example of and tree classes in Sentinel-2 False colour imagery RGB (8,4,3). In this band combination Needleaved appear dark red and Broadeleaved light red.

Forest disturbances

The adoption of wide thresholds for the identification of the cases of interest in the field of forest disturbances allowed very limited errors of omission to be obtained. On the other hand, the commission error values are among the highest found among all the classes analysed. Since permanent crops frequently have a spectral behaviour that can be confused with disturbances over the year, commissions errors regard the inclusion of permanent crop in the disturbance class. A distinction must be made between the two classes of disturbance: *Burned areas* obtain a User accuracy equal to 0.67 and a Producer accuracy equal to 1.00, where the indices used identified very well the areas affected by fire; while lower results derive from *Other disturbances* class.

This class was validated by assimilating the disturbance to "*Forest harvesting*" and this is a further cause of the low accuracy for this class. The choice was made with the objective of evaluating the effectiveness of the algorithm for detecting this type of disturbance. The identification of forest disturbances due to forest harvesting provided different results depending on the areas: it is more effective in central Italy, while it is more difficult in areas, such as the Alps, where the selective logging method is used. In this areas the spectral signature between the disturbances areas and the intact ones does not allow a clear distinction (Chirici et al., 2020) and, consequently, it is not always possible to associate this disturbance with changes clearly and unambiguously by remote sensing (see also discussion section).

Land cover classes in Italy

Analysing the land cover data on a national scale for 2018 (Table 4.2), 10.28% of the area is represented by the abiotic, of which about 3/4 are artificial surfaces (7.08%). The land cover map with the changes is showed in Figure 4.5.

Table 4.2. Area (ha) and (%) of land cover classes in Italy (2018).

Land Cover classes 2018	ha	%
Abiotic surfaces	**3099370**	**10.28**
Artificial	2134599	7.08
Natural	964771	3.20
Woody vegetation	**13614233**	**45.17**
Broadleaved	12006647	39.84
Needleaved	1607586	5.33
Herbaceous vegetation	**12976861**	**43.06**
Periodic herbaceous	12658527	42.00
Permanent herbaceous	318335	1.06
Water and ice	**449510**	**1.49**
Water	337737	1.12
Glaciers	111773	0.37
Italy	**30139974**	**100.00**

Most of the territory is divided between woody vegetation (45.17%, with a prevalence of broadleaved trees) and herbaceous vegetation (43.06%, with a prevalence of periodic herbaceous). The remaining 1.49% is represented by water bodies (1.12%) and perennial ice and snow (0.37%).

The analysis of the changes between 2017 and 2018 (Table 4.3 and Table 4.4) shows that: the areas most affected by S*oil consumption* are those with *Periodic herbaceous* cover (4231 ha, equal to 64.11% of total *Soil consumption*) and those with *Natural abiotic* cover (about 20% of the total). The percentage of 15.89% of the total *Soil consumption*, equal to 1048.9 ha, took place in forests, especially with respect to broadleaved trees.

Table 4.3 - Cross tabulation between land cover 2017 and 2018 in ha.

	2018								
2017	Artificial	Nat. Abiot.	Broad-leaved	Need-leaved	Periodic herb.	Perman. herb.	Water	Ice and snow	Total
Artificial	2127998	90	165	3.1	636	10	0	0	2128904
Nat. Abiot.	1311	800608	0	0	152914	50	0	0	954885
Broadleaved	1018	6609	12006481	0	0	71096	0	0	12085206
Needleaved	30	4496	0	1607582.4	0	7394	0	0	1619502
Periodic herb.	4231	54229	0	0	12603660	3	0	0	12662124
Permanent herb.	8	0	0	0	0	239830	0	0	239839
Water	0	0	0	0	0	0	337736	0	337736
Ice and snow	0	0	0	0	0	0	0	111773	111773
Total	2134599	866035	12006647	1607585	12757211	318385	337736.	111773	0

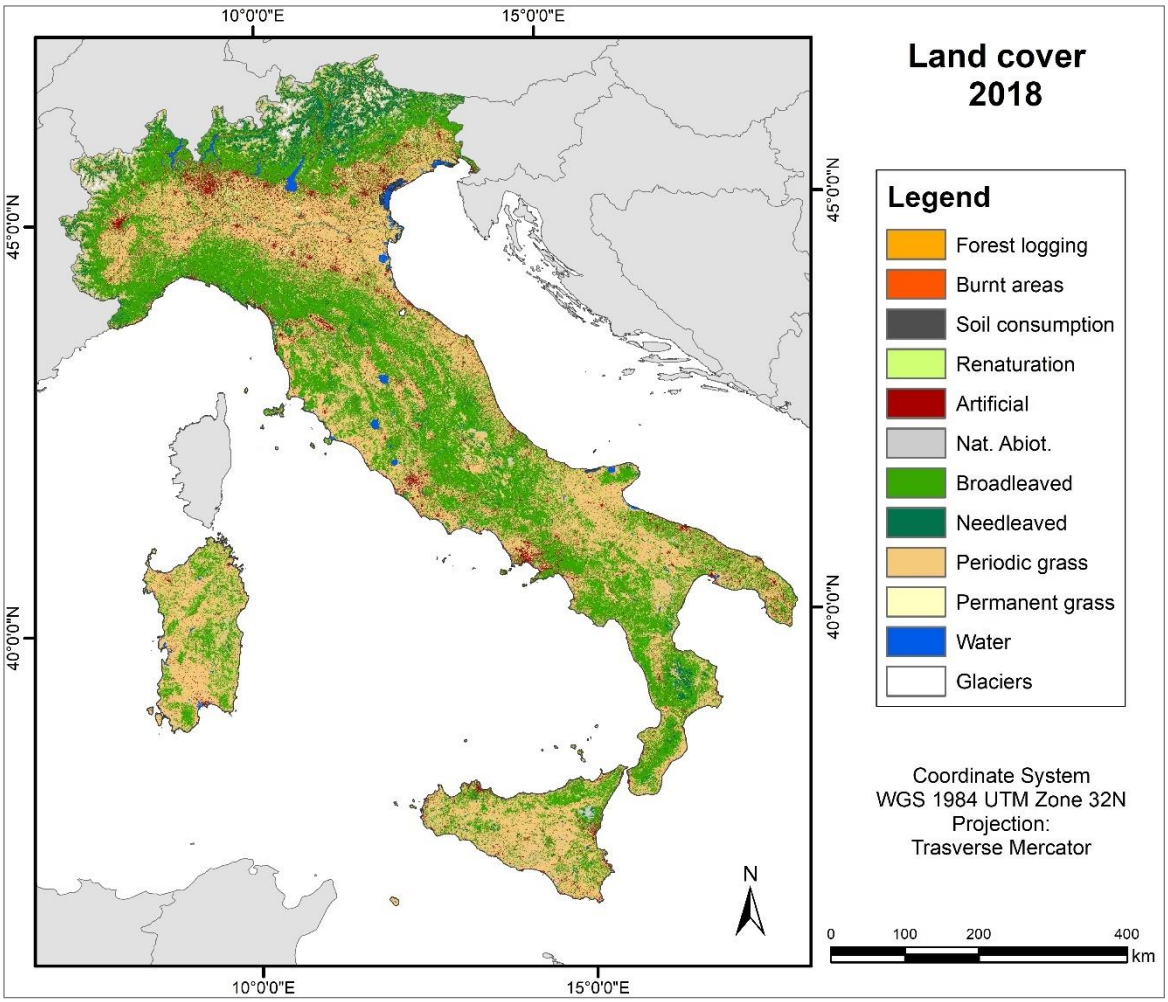

Figure 4.5 - Land cover 2018.

The Table 4.4 shows the changes related to the transformation that have led to an increase in land consumption.

Table 4.4 - Land consumption distribution in the different land cover classes in (ha) and (%) between 2017 and 2018).

Reference period - 2017-18	ha	%
Artificial	-	-
Natural abiotic	1311	19.86
Abiotic surfaces	1311	19.86
Broadleaved	1019	15.44
Needleaved	30	0.46
Woody vegetation	1049	15.89
Periodic herbaceous	4231	64.11
Permanent herbaceous	9	0.13
Herbaceous vegetation	4240	64.24
Water	0	0.00
Ice and snow	0	0.00
Water, Ice and snow		
Italy	6600	100.00

The changes in tree vegetation affected a total of 89,596.38 ha (Table 4.5) and 12.40% (11,106 ha) were caused by fires, while 87.60% (78,490 ha) had other causes (such as forest harvesting).
The "*Other disturbances*" class was further analysed, showing that more than half of the disturbance are attributable to forest harvesting. However, since cuttings are conducted with different systems, which vary according to the geographical location, in this class, not all cuttings carried out in the study area between 2017 and 2018 are present.

Table 4.5 - Changes relating to fires and others disturbance.

Land cover class	2017-18	ha	%
Burned areas	*Broadleaved trees*	*6610*	*59.51*
	Needleaved trees	*4496*	*40.49*
	Total	**11106**	**12.40**
Other disturbances	*Broadleaved trees*	*71096*	*90.58*
	Needleaved trees	*7394*	*9.42*
	Total	**78490.32**	**87.60**
Total disturbances		**89596.38**	**100**

4.1.2 Regional scale

An analysis has also been carried out at regional level, taking as reference for each region, the composition of the territory and the distribution of each land cover class in the different regions.

4.1.2.1 Distribution of land cover classes

Distribution of Land cover classes between the regions
Analysing the distribution of land cover classes among the regions, the following aspects are highlighted:
Lombardia is the region with the highest value for *Artificial abiotic* areas with 2863.9 km^2 (Table 4.6), equal to 13.5% of total *Artificial* surface (Table 4.7). These values are comparable to the sum of A*rtificial* surface in Valle D'Aosta (0.3%), Trentino Alto Adige (2.0%), Friuli (2.9%), Liguria (1.8%), Umbria (2.1%), Abruzzo (2.5%), Molise (0.8%) and Basilicata (1.5%), (Table 4.7).
Veneto accounted for 10.1% of total *Artificial* surface; 52.7% of the total *Natural abiotic* is concentrated mainly in the regions of the Alps (Piemonte, Lombardia, Valle D'Aosta, Veneto, Trentino Alto Adige and Friuli V. G.) on the North. High values are also present in Sicily (10.9% of the total N*atural abiotic*, concentrated mainly near Etna) and Apulia, while this class is almost absent in Molise and Liguria, both with 0.6%.
Toscana and Piemonte are the regions with the highest percentage of B*roadleaved trees* cover with 10.2% and 9.6% of total broadleaved trees. In Trentino-Alto Adige, on the other hand, *Needleaved trees* are mainly concentrated (31.8% of the total). 48.2% of the *Herbaceous* vegetation is concentrated in the southern regions and islands, particularly in Sicily (11.9%) and Sardinia (12%), which are also the regions with the richest areas of *Periodic herbaceous* coverage (12.2% and 12.1% respectively), while P*ermanent herbaceous* vegetation is mainly present in the northern regions (Lombardia, with 19%, Veneto with 14.4% and Emilia Romagna with 11.1%).

Table 4.6 - Land cover class distribution in km^2.

Region	Other disturb.	Burned areas	Soil consum	Restoration	Artificial	Natural Abiotic	Broadleaved	Needleaved	Periodic herb.	Perm. herb.	Water	Ice and Snow	Total
Piemonte	88.3	17.7	5.4	1.4	1699.9	1124.9	11579.3	1368.1	9123.4	79.9	177.7	135.3	25401.3
Valle d'Aosta	5.0	0.4	0.3	0.1	69.8	693.9	539.0	619.6	1008.0	0.6	2.7	322.9	3262.2
Lombardia	51.9	2.6	7.1	0.7	2863.9	1063.5	7680.4	1766.1	9165.7	456.0	674.1	146.6	23878.7
Trentino A.A.	41.9	8.7	1.4	0.4	431.1	1344.2	3426.4	5113.4	2768.9	8.0	58.8	401.7	13604.9
Veneto	48.4	9.0	11.4	2.8	2157.0	503.5	5730.4	1430.7	7167.6	345.8	848.6	81.9	18337.0
Friuli V. G.	28.4	2.6	2.8	0.3	627.9	298.7	3560.6	722.6	2370.6	86.0	204.9	14.1	7919.6
Liguria	8.7	1.2	0.4	0.0	391.2	54.2	3966.0	481.2	496.8	14.1	5.8	0.2	5420.0
Emilia R.	30.6	1.4	6.2	1.1	1988.5	283.7	8265.0	216.1	11129.0	267.0	256.5	0.0	22445.1
Toscana	67.5	9.3	2.9	0.3	1409.2	402.2	12253.3	753.0	7738.1	252.0	100.1	0.0	22987.9
Umbria	28.5	1.9	1.2	0.4	441.6	81.5	4438.0	286.4	2966.1	68.6	139.7	0.0	8454.0
Marche	6.1	0.3	1.9	0.1	642.8	140.7	3927.7	246.8	4347.2	58.1	10.0	0.8	9382.4
Lazio	42.1	8.7	4.5	0.6	1381.9	217.4	7984.4	378.0	6710.6	231.2	243.1	0.5	17203.0
Abruzzo	16.1	2.0	3.1	0.1	530.2	273.3	5602.3	458.9	3819.0	61.0	27.4	3.8	10797.1
Molise	17.8	0.5	0.5	0.0	171.4	53.8	2239.4	83.8	1821.1	39.2	12.5	0.3	4440.2
Campania	30.9	4.2	2.5	0.0	1395.7	193.6	6678.0	106.9	5056.9	101.7	28.2	1.1	13599.5
Puglia	80.9	6.7	4.9	0.1	1560.4	662.6	5970.3	235.7	10633.2	6.4	193.7	0.0	19355.0
Basilicata	31.7	1.0	1.8	0.2	312.3	270.6	4570.1	125.9	4598.8	45.1	33.9	0.6	9992.0
Calabria	94.4	13.9	1.0	0.1	757.5	286.2	7912.5	942.2	4945.2	82.5	42.0	5.2	15082.8
Sicilia	60.0	13.7	4.7	0.2	1660.4	1042.2	6907.5	533.8	15391.8	16.3	86.3	2.0	25718.9
Sardegna	5.4	5.2	2.0	0.1	787.5	545.0	6834.1	206.9	15320.9	178.9	231.4	0.8	24118.1

Table 4.7 - Land cover class distribution between the region in %.

Region	Other disturb	Burned areas	Soil consum	Restoration	Artificial	Natural Abiotic	Broadleaved	Needleaved	Periodic herb.	Perm. herb.	Water	Ice and snow
Piemonte	11.25	15.94	8.24	15.78	7.99	11.8	9.64	8.51	7.21	3.33	5.26	12.1
Valle d'Aosta	0.64	0.34	0.41	1.4	0.33	7.28	0.45	3.85	0.8	0.03	0.08	28.89
Lombardia	6.62	2.38	10.77	8.2	13.46	11.15	6.4	10.99	7.24	19.01	19.96	13.12
Trentino A.A.	5.34	7.81	2.16	4.85	2.03	14.1	2.85	31.81	2.19	0.33	1.74	35.93
Veneto	6.16	8.08	17.2	30.97	10.14	5.28	4.77	8.9	5.66	14.42	25.13	7.32
Friuli V. G.	3.62	2.36	4.24	3.84	2.95	3.13	2.97	4.5	1.87	3.58	6.07	1.26
Liguria	1.11	1.04	0.64	0.29	1.84	0.57	3.3	2.99	0.39	0.59	0.17	0.02
Emilia R.	3.9	1.3	9.35	11.99	9.34	2.97	6.88	1.34	8.79	11.13	7.6	0
Toscana	8.6	8.41	4.4	3.1	6.62	4.22	10.21	4.68	6.11	10.51	2.96	0
Umbria	3.63	1.7	1.86	4.68	2.08	0.85	3.7	1.78	2.34	2.86	4.13	0
Marche	0.78	0.3	2.82	0.92	3.02	1.48	3.27	1.53	3.43	2.42	0.3	0.07
Lazio	5.37	7.82	6.86	6.22	6.49	2.28	6.65	2.35	5.3	9.64	7.2	0.04
Abruzzo	2.05	1.84	4.66	0.91	2.49	2.87	4.67	2.85	3.02	2.54	0.81	0.34
Molise	2.27	0.45	0.74	0.12	0.81	0.56	1.87	0.52	1.44	1.64	0.37	0.02
Campania	3.94	3.76	3.72	0.37	6.56	2.03	5.56	0.66	4	4.24	0.84	0.1
Puglia	10.31	6.04	7.46	0.85	7.33	6.95	4.97	1.47	8.4	0.27	5.74	0
Basilicata	4.04	0.9	2.79	1.66	1.47	2.84	3.81	0.78	3.63	1.88	1	0.06
Calabria	12.03	12.49	1.48	1.34	3.56	3	6.59	5.86	3.91	3.44	1.24	0.47
Sicilia	7.65	12.36	7.19	1.71	7.8	10.93	5.75	3.32	12.16	0.68	2.56	0.18
Sardegna	0.69	4.66	3	0.79	3.7	5.72	5.69	1.29	12.1	7.46	6.85	0.07
Total	100	100	100	100	100	100	100	100	100	100	100	100

The presence and extent of permanent *Water bodies* is linked to the spatial resolution (in the case of river) of the data and the periodicity of the water bodies. They are concentrated in the northern regions, especially in Veneto (25.1%, thanks to Lake Garda and the Lagoon of Venice) and Lombardia (20%, thanks to the presence of the large lakes and the Po). In Valle d'Aosta, Trentino, Liguria, Marche, Abruzzo, Molise,

Campania, Basilicata and Calabria there are values lower than 2%. *Perennial ice and snow* are concentrated in the Alpine regions and in particular in Trentino (35.9%) and Valle d'Aosta (28.9%).

Composition of regional land cover

If we take as reference the land cover classes considered in this research, the composition of the regions presents the prevalence of vegetation classes. In 18 out of 20 regions the woody vegetation exceeds 30% of the regional area (Table 4.8), and in the remaining 2, it is just under 30% (28.9% in Sicily and 29.2% in Sardinia). *Broadleaved* class covers 73% of the Liguria's surface and more than 50% of the territory in Toscana, Umbria, Molise, Abruzzo and Calabria. *Needleaved* class covers high surface in the North and have lower percentages descending towards the South. In Trentino it occupies 37.6% and in Valle D'Aosta 19% of the surface; in the other regions *Needleaved* class remains below 10% and reaches values lower than 1% of the regional surface in Sardinia, Campania and Emilia Romagna. Sardinia, with 1549976.15 ha (64.3%) is the region with the largest herbaceous surface area. *Herbaceous* class cover over 50% of the regional territory in Emilia Romagna (50.8%), Puglia (55%) and Sicily (59.9%).

Table 4.8 - Land cover class distribution in the region in %.

Region	Other disturb	Burned areas	Soil consum	Restoration	Artificial	Natural Abiotic	Broadleaved	Needleaved	Periodic herb.	Perm. herb.	Water	Ice and Snow	Total
Piemonte	0.35	0.07	0.02	0.01	6.69	4.43	45.59	5.39	35.92	0.31	0.70	0.53	100
Valle d'A.	0.15	0.01	0.01	0.00	2.14	21.27	16.52	18.99	30.90	0.02	0.08	9.90	100
Lombardia	0.22	0.01	0.03	0.00	11.99	4.45	32.16	7.40	38.38	1.91	2.82	0.61	100
Trent. A.A.	0.31	0.06	0.01	0.00	3.17	9.88	25.19	37.58	20.35	0.06	0.43	2.95	100
Veneto	0.26	0.05	0.06	0.02	11.76	2.75	31.25	7.80	39.09	1.89	4.63	0.45	100
Friuli V G.	0.36	0.03	0.04	0.00	7.93	3.77	44.96	9.12	29.93	1.09	2.59	0.18	100
Liguria	0.16	0.02	0.01	0.00	7.22	1.00	73.17	8.88	9.17	0.26	0.11	0.00	100
Emilia R.	0.14	0.01	0.03	0.00	8.86	1.26	36.82	0.96	49.58	1.19	1.14	0.00	100
Toscana	0.29	0.04	0.01	0.00	6.13	1.75	53.30	3.28	33.66	1.10	0.44	0.00	100
Umbria	0.34	0.02	0.01	0.01	5.22	0.96	52.50	3.39	35.09	0.81	1.65	0.00	100
Marche	0.07	0.00	0.02	0.00	6.85	1.50	41.86	2.63	46.33	0.62	0.11	0.01	100
Lazio	0.24	0.05	0.03	0.00	8.03	1.26	46.41	2.20	39.01	1.34	1.41	0.00	100
Abruzzo	0.15	0.02	0.03	0.00	4.91	2.53	51.89	4.25	35.37	0.56	0.25	0.03	100
Molise	0.40	0.01	0.01	0.00	3.86	1.21	50.44	1.89	41.01	0.88	0.28	0.01	100
Campania	0.23	0.03	0.02	0.00	10.26	1.42	49.10	0.79	37.18	0.75	0.21	0.01	100
Puglia	0.42	0.03	0.03	0.00	8.06	3.42	30.85	1.22	54.94	0.03	1.00	0.00	100
Basilicata	0.32	0.01	0.02	0.00	3.13	2.71	45.74	1.26	46.03	0.45	0.34	0.01	100
Calabria	0.63	0.09	0.01	0.00	5.02	1.90	52.46	6.25	32.79	0.55	0.28	0.03	100
Sicilia	0.23	0.05	0.02	0.00	6.46	4.05	26.86	2.08	59.85	0.06	0.34	0.01	100
Sardegna	0.02	0.02	0.01	0.00	3.27	2.26	28.34	0.86	63.52	0.74	0.96	0.00	100

While *Ice and snow* occupy a significant percentage of the territory only in Valle D'Aosta (9.9%) and Trentino (2.9%), *Permanent water bodies* occupy more than 1% of the regional territory in 8 of the 20 regions, with a maximum of 4.65% of the regional territory in Veneto due to Garda Lake; Lombardy and Friuli Venezia Giulia follow with 2.8% and 2.6% respectively.

4.1.2.2 Distribution of land cover changes

Distribution of land cover changes between the regions

The distribution of changes was also analysed at regional level, with reference to *Burned area* and *Other disturbances*; the discussion of the data concerning the *Restoration* change class and *Soil consumption* will be addressed in paragraph 4.3, where reversible and irreversible soil changes in Italy and in the individual regions will also be presented, labelled with greater thematic detail.

Burned areas

The region most affected by forest fires is Piemonte (Table 4.9), with 1770.5 ha (15.9% of the total), followed by Calabria and Sicilia (in these two regions a quarter of the total fires are concentrated, respectively 12.5% and 12.4%) and Tuscany (8.4%). Together these 4 regions account for about half (49.2%) of the burned areas recorded in the period 2017-2018. Valle d'Aosta (0.3%), Marche (0.3%) Molise (0.5%) and Basilicata (0.9%) (Table 4.7), have less than 1% of the burned area and are the regions least affected by the phenomenon. In the 4 regions with the highest presence of burned areas, the West area of Turin in Piemonte, the central-southern area of the province (sub-regional level) of Cosenza in Calabria, south of the province of Enna in Sicilia and between Grosseto and Siena in Toscana are the provinces most affected by fires. The regions with the highest presence of forest, Piemonte, Calabria and Toscana, are among the three regions with the largest damaged surface area. In Sicily, on the other hand, there are fewer burned area, but fires affecting larger areas than in the other regions considered.

Table 4.9 - Percentage of the total forest covered by burned areas and disturbances.

Region	Other disturb.	Needleaved	Tot Woody (ha)	O. disturb./ Tot Woody (%)	Burned area/ Tot Woody (%)
Piemonte	8831.4	136813.0	1294745.3	67.7	13.6
Valle d'Aosta	499.4	61955.9	115852.8	42.9	3.2
Lombardia	5192.9	176605.8	944648.9	54.7	2.8
Trentino-Alto Adige	4193.1	511337.4	853981.2	48.8	10.1
Veneto	4836.9	143067.5	716111.9	67.0	12.4
Friuli Venezia Giulia	2837.6	72264.8	428326.7	65.8	6.1
Liguria	874.9	48118.2	444722.1	19.6	2.6
Emilia-Romagna	3064.4	21609.9	848107.3	36.0	1.7
Toscana	6751.2	75296.8	1300631.7	51.6	7.1
Umbria	2850.9	28639.1	472441.7	60.0	4.0
Marche	613.5	24675.3	417442.2	14.7	0.8
Lazio	4212.7	37800.3	836244.2	50.1	10.3
Abruzzo	1609.7	45890.3	606118.5	26.5	3.4
Molise	1779.5	8380.5	232323.0	76.0	2.1
Campania	3089.0	10687.3	678482.4	45.3	6.1
Puglia	8093.4	23566.0	620591.5	128.6	10.7
Basilicata	3173.8	12593.2	469604.1	67.1	2.1
Calabria	9438.7	94216.8	885465.0	105.3	15.5
Sicilia	6002.8	53377.0	744128.6	79.9	18.3
Sardegna	544.5	20687.5	704094.8	7.7	7.3
Total	78490.3	1607582.4	13614063.9	57.3	8.1

Other disturbances

As with fires, about half of the *Other disturbances* class (49.8%) is concentrated in a few regions: Piemonte, Calabria (11.3% and 12% of the total respectively), also, Puglia, Toscana and Sicilia are at the top of the list The regions least affected by the phenomenon are Valle D'Aosta (0.6%), Sardinia (0.7%) and Marche (0.8%).

Composition land cover changes in the regions

Calabria is the region with the largest extent of fires and other disturbances in relation to the regional surface (cuttings account for 0.6% and fires for 0.09%) (Table 4.9). In general, in terms of extension compared to the regional area, 19 of the 20 regions have other disturbances of less than 0.5% of the regional area, while fires remain below 0.1%. Due to the reduced extent of the phenomena, the incidence of burned area and forest harvesting in relation to the total forest area was expressed in terms of m^2 of burned area and forest harvesting per ha of total forest area (Table 4.9). The national average value for the forest

disturbances is 57.3 $m^{2/}$ha of woodland. The highest value is in Puglia (128.6 $m^{2/}$ha) and Calabria (105.3 $m^{2/}$ha) and in another 7 of the 20 regions. The lowest values are in Sardegna (7.7 $m^{2/}$ha) and in Marche (14.7 $m^{2/}$ha) while all the other regions have values higher than 20 $m^{2/}$ha. The fires occurred in Italy between 2017 and 2018 have the highest values, in terms of burned area, in Sicilia (18.3 $m^{2/}$ha), Calabria (15.5 $m^{2/}$ha), Piemonte (13.6 $m^{2/}$ha) and Veneto (12.4 $m^{2/}$ha). Trentino Alto Adige, Lazio and Puglia have values close to 10 $m^{2/}$ha, while the other regions remain below the national average (8.1 $m^{2/}$ha for each ha of forest), with a minimum in the Marche region, where each ha of forest corresponds to only 0.8 $m^{2/}$ha of burned area.

4.1.3 Comparison of two different approaches: Land cover map 2018 and CLC

The 2018 Land cover classification (derived from the methodology developed in this research - hereinafter referred to as LC) and Copernicus CLC 2018 were compared in order to assess the points of agreement between the two approaches, to conduct a critical analysis of the differences and to develop an in-depth discussion on the methodology adopted. The analysis proceeds by comparing the individual classes of the LC 2018 with the CLC 2018 classes that potentially correspond to them. In practice an intersection between the two datasets was performed with GIS tools and the results are showed in the Table 4.11 (ha) and 4.12 (%), while the Table 4.10 illustrates CLC nomenclature.

Artificial

It is expected, from a semantic point of view, that there is a correspondence between the artificial abiotic surfaces class and class 1 CLC. This correspondence has been verified for 48% of the areas classified as artificial abiotic surfaces by LC (Figure 4.6).

The artificial abiotic surfaces include for the remaining part (not included in class 1 CLC) isolated buildings, small groups of buildings with extension <25 ha (which corresponds to the MMU of the CLC) and the road network.

These areas are, instead, classified by the CLC as:

- 211 (Arable land).
- 242 (Complex cultivation patterns).
- 243 (Agri-cultivations with important natural spaces).

Considering also these 3 last classes, the 84.5% of the areas classified in LC as artificial abiotic surfaces have a correspondence with the CLC classes (1xx, 211, 242 and 243). Among the other CLC classes the most represented are: 223, 311, 221, 222, 231. The main correspondences between the classes are highlighted with coloured background in Table 4.12 which shows the percentages.

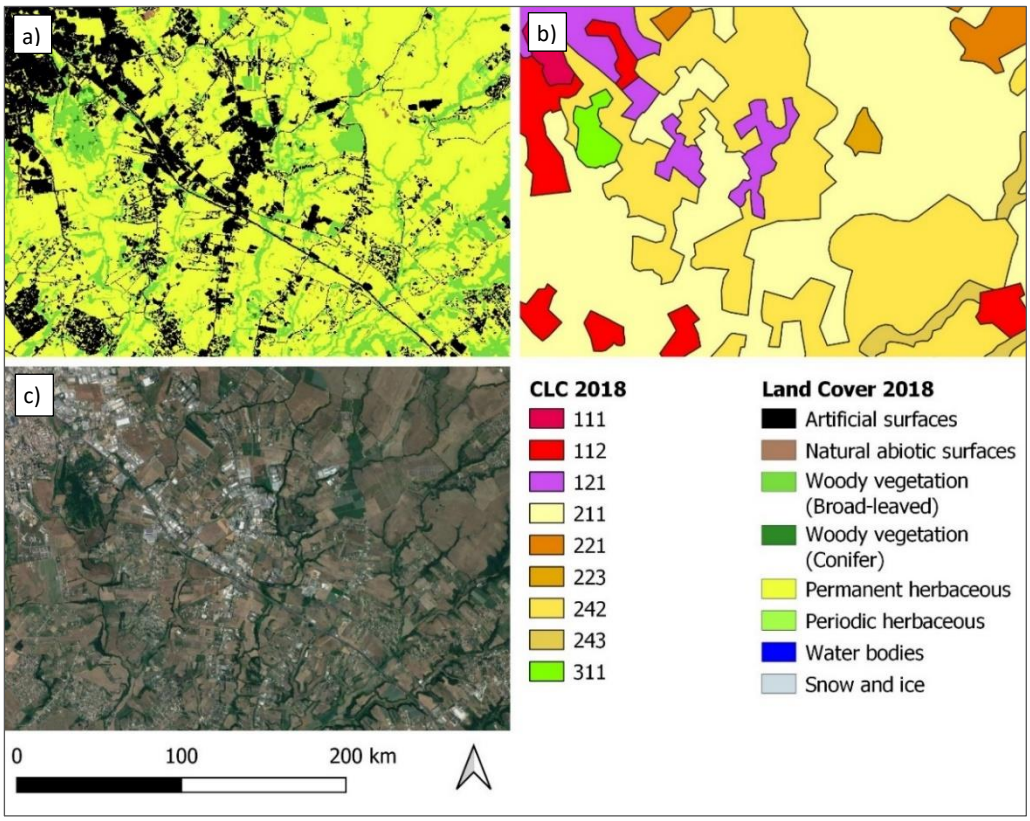

Figure 4.6 - Comparison CLC with LC map 2018.
(a) LC 2018, (b) CLC 2018, (c) high definition image from Google Earth 2018.

As can be seen in Figure 4.7, the polygons occupied by class 211 (Non-irrigated arable land) in the CLC 2018 map, correspond to classes belonging to urban, periodic herbaceous and broadleaf trees in the LC 2018 (a); these classes cannot be mapped in CLC map (b) due to the low resolution of the latter. The 242 CLC Class also includes significant portions of built areas or roadways.

Bare Soil

The natural class *Abiotic surfaces* has a plausible semantic correspondence with classes CLC 331 (dune and sand beaches), 332 (bare rocks, cliffs, outcrops), 333 (areas with sparse vegetation). 51.1% of natural abiotic surfaces coincide with these three CLC classes.

Since, natural abiotic surfaces include greenhouses and tilled land and in some particular situation also permanent crop, it is also possible to find this class within CLC 211, 221, 223 and 242.

Compared to CLC, the natural abiotic surface describes the geometry of rivers more accurately. The correspondence between the two data is greater near coastal beaches.

In periodic herbaceous falls also much of the class 231 CLC (Pastures), this is linked to the presence of snow, which in some periods of the year influences the reflectance of the area and the values of NDVI. In particular, the discontinuity registered in the values of NDVI leads these areas to have a behaviour more typical of the periodic herbaceous than the permanent vegetation. Herbaceous is also included in 323 (sclerophyll vegetation) and 333 (scattered vegetation).

Table 4.10 – CORINE nomenclature.

CORINE NOMENCLATURE				
Level 1		**Level 2**		**Level 3**
1 Artificial surfaces	11	Urban fabric	111	Continuous urban fabric
			112	Discontinuous urban fabric
	12	Industrial, commercial and transport units	121	Industrial or commercial units
			122	Road and rail networks and associated land
			123	Port areas
			124	Airports
	13	Mine, dump and construction sites	131	Mineral extraction sites
			132	Dump sites
			133	Construction sites
	14	Artificial, non-agricultural vegetated areas	141	Green urban areas
			142	Sport and leisure facilities
2 Agricultural areas	21	Arable land	211	Non-irrigated arable land
			212	Permanently irrigated land
			213	Rice fields
	22	Permanent crops	221	Vineyards
			222	Fruit trees and berry plantations
			223	Olive groves
	23	Pastures	231	Pastures
	24	Heterogeneous agricultural areas	241	Annual crops associated with permanent crops
			242	Complex cultivation patterns
			243	Land principally occupied by agriculture, with significant areas of natural vegetation
			244	Agro-forestry areas
3 Forest and semi natural areas	31	Forests	311	Broadleaved forest
			312	Coniferous forest
			313	Mixed forest
	32	Scrub and/or herbaceous vegetation associations	321	Natural grasslands
			322	Moors and heathland
			323	Sclerophyllous vegetation
			324	Transitional woodland-shrub
	33	Open spaces with little or no vegetation	331	Beaches, dunes, sands
			332	Bare rocks
			333	Sparsely vegetated areas
			334	Burnt areas
			335	Glaciers and perpetual snow
4 Wetlands	41	Inland wetlands	411	Inland marshes
			412	Peat bogs
	42	Maritime wetlands	421	Salt marshes
			422	Salines
			423	Intertidal flats
5 Water bodies	51	Inland waters	511	Water courses
			512	Water bodies
	52	Marine waters	521	Coastal lagoons
			522	Estuaries

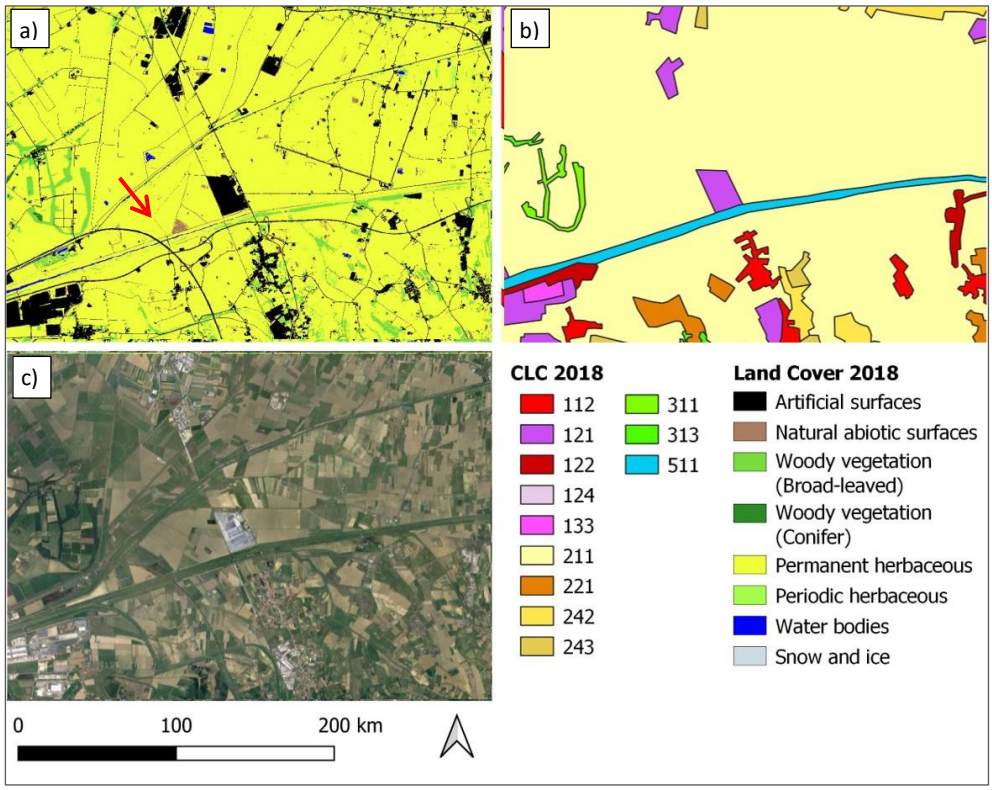

Figure 4.7 - Comparison CLC with LC map 2018. (a) LC 2018, (b) CLC 2018, (c) High definition image from Google Earth 2018. The arrow points to bare soil within agricultural fields; linear elements such as roads can be clearly distinguished, allowing the artificial to be precisely quantified.

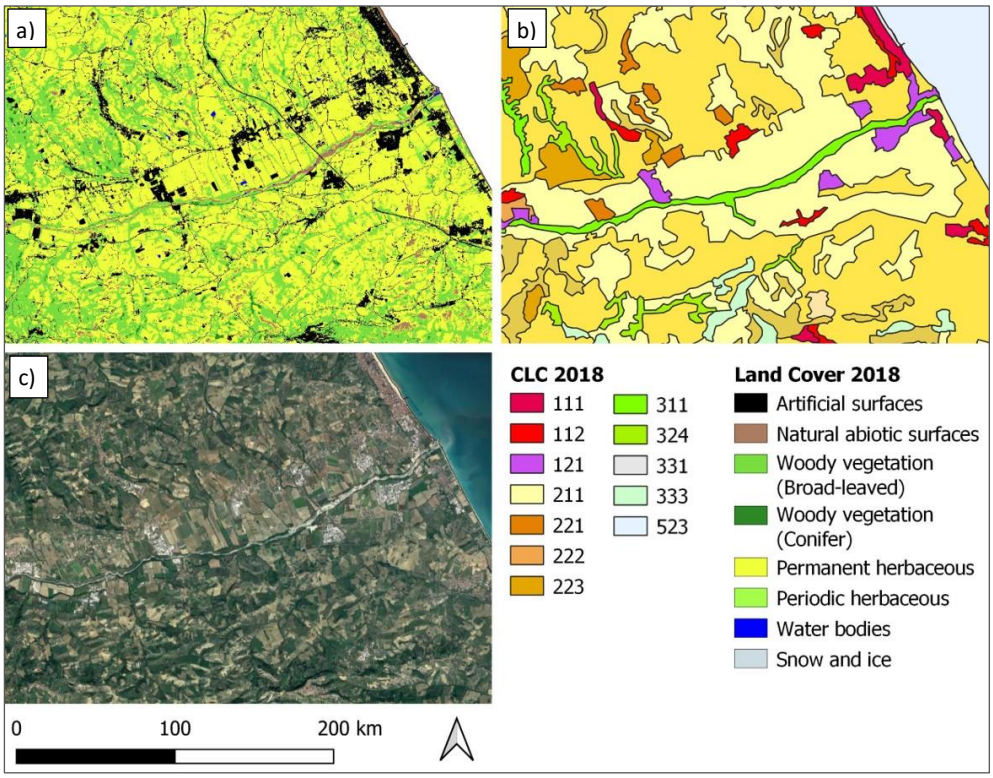

Figure 4.8 - Comparison CLC with LC 2018. (a) LC 2018, (b) CLC 2018, (c) High definition image from Google Earth 2018. CLC does not map minor water bodies since they are considered linear elements.

Table 4.11 - Cross tabulation between LC and CLC in ha.

CLC code	Forest harvest	Burnt areas	Artificial	Nat. Abiot.	Broadleaves	Needleaved	Periodic herb.	Permanent herb.	Water	Ice & Snow	Total
111	0.1	0.0	1292.2	56.2	74.4	2.0	153.9	0.6	1.5	0.0	1580.9
112	1.6	0.0	6129.9	384.4	1499.1	30.4	2227.0	51.2	12.3	0.1	10335.9
121	0.8	0.0	2131.0	104.3	252.1	3.4	576.0	10.5	4.4	0.0	3082.7
122	0.1	0.0	108.8	8.1	24.6	0.7	58.1	1.4	0.4	0.0	202.1
123	0.0	0.0	77.1	10.9	4.2	0.2	10.6	0.1	3.4	0.0	106.4
124	0.1	0.0	82.7	7.4	8.1	0.2	125.2	4.8	0.2	0.0	228.7
131	0.2	0.0	263.1	28.6	69.8	2.4	121.9	1.3	13.7	0.0	501.0
132	0.0	0.0	25.4	2.7	3.3	0.2	12.4	0.1	0.4	0.0	44.5
133	0.1	0.0	24.9	2.5	4.0	0.0	13.8	0.3	0.1	0.0	45.8
141	0.0	0.0	24.3	2.4	42.2	6.3	31.0	3.1	0.6	0.0	109.8
142	0.2	0.0	78.5	11.9	76.2	16.6	109.8	24.1	2.3	0.0	319.7
211	147.6	2.0	4162.6	1287.2	11101.0	79.7	61419.6	1218.5	84.1	0.1	79502.7
212	0.8	0.0	58.5	72.1	46.7	0.3	512.3	4.7	1.3	0.1	696.8
213	6.9	0.4	110.6	7.4	397.2	0.1	2410.1	6.4	3.6	0.0	2942.7
221	32.6	0.5	331.4	284.2	2698.2	11.3	2802.8	46.4	3.5	0.0	6211.0
222	27.5	0.4	244.5	67.9	2107.9	25.3	1254.8	26.6	4.2	0.0	3759.3
223	14.9	0.8	750.1	249.9	4911.9	82.3	5727.0	77.7	1.0	0.0	11815.7
231	10.7	0.2	234.6	37.9	1455.4	95.0	2144.6	150.8	6.1	0.0	4135.2
241	3.3	0.2	136.7	66.8	635.8	7.3	1436.9	13.0	0.4	0.0	2300.4
242	44.4	0.5	2347.2	474.5	7360.3	79.4	11337.0	316.6	15.1	0.1	21975.2
243	30.8	2.5	1272.0	188.8	11706.5	290.0	7646.4	218.8	19.4	0.0	21375.3
244	0.1	0.0	28.5	6.8	387.3	1.0	1244.9	22.8	0.8	0.0	1692.1
311	231.8	33.5	698.5	129.4	50158.3	1758.6	3272.9	63.7	25.9	5.2	56377.9
312	52.5	33.7	114.3	98.1	2271.6	8696.0	1588.2	11.3	15.1	0.7	12881.4
313	30.8	13.4	123.9	36.8	6052.4	2744.4	670.3	9.5	18.6	0.7	9700.8
321	30.2	1.7	72.9	158.0	2556.0	225.3	4574.4	24.9	5.7	6.4	7655.3
322	19.5	3.3	2.9	90.6	632.6	338.6	543.7	0.4	6.6	1.7	1639.8
323	7.6	2.0	108.4	226.8	4227.8	207.9	5167.7	46.5	7.6	0.2	10002.4
324	48.7	6.4	158.3	212.0	6312.8	1115.2	2383.8	25.0	15.0	1.6	10278.7
331	0.8	0.0	32.7	392.1	145.7	4.6	214.0	1.8	33.7	0.0	825.5
332	1.3	0.1	4.9	2950.1	90.9	12.8	592.5	0.2	15.6	681.9	4350.2
333	30.5	1.4	58.7	1555.0	2373.6	217.7	5645.0	11.9	15.9	98.1	10007.9
334	6.5	7.2	3.3	8.6	113.9	13.2	167.5	0.9	0.1	0.0	321.1
335	0.0	0.0	0.0	65.0	0.2	0.0	3.1	0.0	0.2	319.4	387.9
411	0.3	0.1	4.2	11.0	69.7	0.9	73.2	0.9	30.1	0.0	190.5
412	0.0	0.0	0.0	0.0	2.8	0.0	1.1	0.0	0.1	0.0	4.1
421	0.2	0.2	4.0	53.8	55.6	2.3	111.3	0.5	163.2	0.2	391.3
422	0.0	0.0	1.1	24.1	0.5	0.0	7.1	0.0	59.4	0.0	92.4
511	1.3	0.0	11.1	34.3	94.5	1.3	88.6	0.6	235.7	0.0	467.4
512	0.2	0.2	21.3	69.4	33.0	2.1	68.4	0.5	1557.9	0.9	1753.9
521	0.0	0.0	4.0	24.2	6.1	0.1	25.6	0.0	936.2	0.0	996.2
522	0.0	0.0	0.0	0.2	0.0	0.0	0.4	0.0	0.5	0.0	1.1
523	0.0	0.0	7.0	34.2	1.9	0.6	10.4	0.0	55.6	0.3	110.0
Total	784.9	111.1	21346.0	9536.6	120066.5	16075.9	126585.3	2398.4	3377.4	1117.7	301399.7

Table 4.12 - Cross tabulation between LC and CLC in %.

CLC code	Forest harvest	Burnt areas	Artificial	Nat. Abiot.	Broadleaves	Needleaved	Periodic herb.	Permanent herb.	Water	Ice & Snow	Total
111	0.0	0.0	6.1	0.6	0.1	0.0	0.1	0.0	0.0	0.0	0.5
112	0.2	0.0	28.7	4.0	1.2	0.2	1.8	2.1	0.4	0.0	3.4
121	0.1	0.0	10.0	1.1	0.2	0.0	0.5	0.4	0.1	0.0	1.0
122	0.0	0.0	0.5	0.1	0.0	0.0	0.0	0.1	0.0	0.0	0.1
123	0.0	0.0	0.4	0.1	0.0	0.0	0.0	0.0	0.1	0.0	0.0
124	0.0	0.0	0.4	0.1	0.0	0.0	0.1	0.2	0.0	0.0	0.1
131	0.0	0.0	1.2	0.3	0.1	0.0	0.1	0.1	0.4	0.0	0.2
132	0.0	0.0	0.1	0.0	0.0	0.0	0.0	0.0	0.0	0.0	0.0
133	0.0	0.0	0.1	0.0	0.0	0.0	0.0	0.0	0.0	0.0	0.0
141	0.0	0.0	0.1	0.0	0.0	0.0	0.0	0.1	0.0	0.0	0.0
142	0.0	0.0	0.4	0.1	0.1	0.1	0.1	1.0	0.1	0.0	0.1
211	18.8	1.8	19.5	13.5	9.2	0.5	48.5	50.8	2.5	0.0	26.4
212	0.1	0.0	0.3	0.8	0.0	0.0	0.4	0.2	0.0	0.0	0.2
213	0.9	0.4	0.5	0.1	0.3	0.0	1.9	0.3	0.1	0.0	1.0
221	4.2	0.5	1.6	3.0	2.2	0.1	2.2	1.9	0.1	0.0	2.1
222	3.5	0.4	1.1	0.7	1.8	0.2	1.0	1.1	0.1	0.0	1.2
223	1.9	0.8	3.5	2.6	4.1	0.5	4.5	3.2	0.0	0.0	3.9
231	1.4	0.2	1.1	0.4	1.2	0.6	1.7	6.3	0.2	0.0	1.4
241	0.4	0.2	0.6	0.7	0.5	0.0	1.1	0.5	0.0	0.0	0.8
242	5.7	0.5	11.0	5.0	6.1	0.5	9.0	13.2	0.4	0.0	7.3
243	3.9	2.3	6.0	2.0	9.8	1.8	6.0	9.1	0.6	0.0	7.1
244	0.0	0.0	0.1	0.1	0.3	0.0	1.0	1.0	0.0	0.0	0.6
311	29.5	30.1	3.3	1.4	41.8	10.9	2.6	2.7	0.8	0.5	18.7
312	6.7	30.4	0.5	1.0	1.9	54.1	1.3	0.5	0.4	0.1	4.3
313	3.9	12.0	0.6	0.4	5.0	17.1	0.5	0.4	0.5	0.1	3.2
321	3.8	1.5	0.3	1.7	2.1	1.4	3.6	1.0	0.2	0.6	2.5
322	2.5	3.0	0.0	1.0	0.5	2.1	0.4	0.0	0.2	0.2	0.5
323	1.0	1.8	0.5	2.4	3.5	1.3	4.1	1.9	0.2	0.0	3.3
324	6.2	5.7	0.7	2.2	5.3	6.9	1.9	1.0	0.4	0.1	3.4
331	0.1	0.0	0.2	4.1	0.1	0.0	0.2	0.1	1.0	0.0	0.3
332	0.2	0.1	0.0	30.9	0.1	0.1	0.5	0.0	0.5	61.0	1.4
333	3.9	1.3	0.3	16.3	2.0	1.4	4.5	0.5	0.5	8.8	3.3
334	0.8	**6.5**	0.0	0.1	0.1	0.1	0.1	0.0	0.0	0.0	0.1
335	0.0	0.0	0.0	0.7	0.0	0.0	0.0	0.0	0.0	28.6	0.1
411	0.0	0.1	0.0	0.1	0.1	0.0	0.1	0.0	0.9	0.0	0.1
412	0.0	0.0	0.0	0.0	0.0	0.0	0.0	0.0	0.0	0.0	0.0
421	0.0	0.2	0.0	0.6	0.0	0.0	0.1	0.0	4.8	0.0	0.1
422	0.0	0.0	0.0	0.3	0.0	0.0	0.0	0.0	1.8	0.0	0.0
511	0.2	0.0	0.1	0.4	0.1	0.0	0.1	0.0	7.0	0.0	0.2
512	0.0	0.2	0.1	0.7	0.0	0.0	0.1	0.0	46.1	0.1	0.6
521	0.0	0.0	0.0	0.3	0.0	0.0	0.0	0.0	27.7	0.0	0.3
522	0.0	0.0	0.0	0.0	0.0	0.0	0.0	0.0	0.0	0.0	0.0
523	0.0	0.0	0.0	0.4	0.0	0.0	0.0	0.0	1.6	0.0	0.0
Total	100.0	100.0	100.0	100.0	100.0	100.0	100.0	100.0	100.0	100.0	100.0

Water bodies

There is a direct correspondence of 84.5% between class 5 CLC and LC. In general LC maps the rivers more precisely thanks to a higher spatial resolution, while CLC polygons, related to rivers, are more limited in number and less accurate in geometry (Figure 4.8). Lakes are mapped with a similar degree of accuracy in both LC and CLC. In the *Water class* of LC also includes most wetlands, in particular salt pans (422).
In addition, CLC in situation maps the river as broadleaf, while in LC this class is classified as water and abiotic. An example is provided in Figure 4.8 (a) where it is possible to distinguish the tree component from the herbaceous component.

Ice and snows

There is a direct correspondence with class 335 CLC, in fact more than 98% of the areas classified as *Ice and snow* by the LC fall into classes CLC 335, 332 and 333. The correspondence of this class is mainly influenced by the period to which the data are referred: since the CLC is photo-interpreted on 2017 images and the coverage map is obtained from 2018 images. This difference is more evident in dynamic classes such as ice. In general, the class encompasses high altitude transition areas above the tree line near glaciers.

Trees vegetation

There is a direct correspondence between the *Needleaved* and *Broadleaved* classes of the LC Map (211 and 212) and the CLC classes 311 (89%), 312 (69%) and 313 (91%) (Figure 4.9).
There is also a correspondence with some mixed and heterogeneous CLC classes (such as 24 * and 32 *), this is due to the fact that the LC map distinguishes the tree component within them while CLC classes, in order not to lose this information, considers these classes as "mixed ", without spatially identifying the trees.

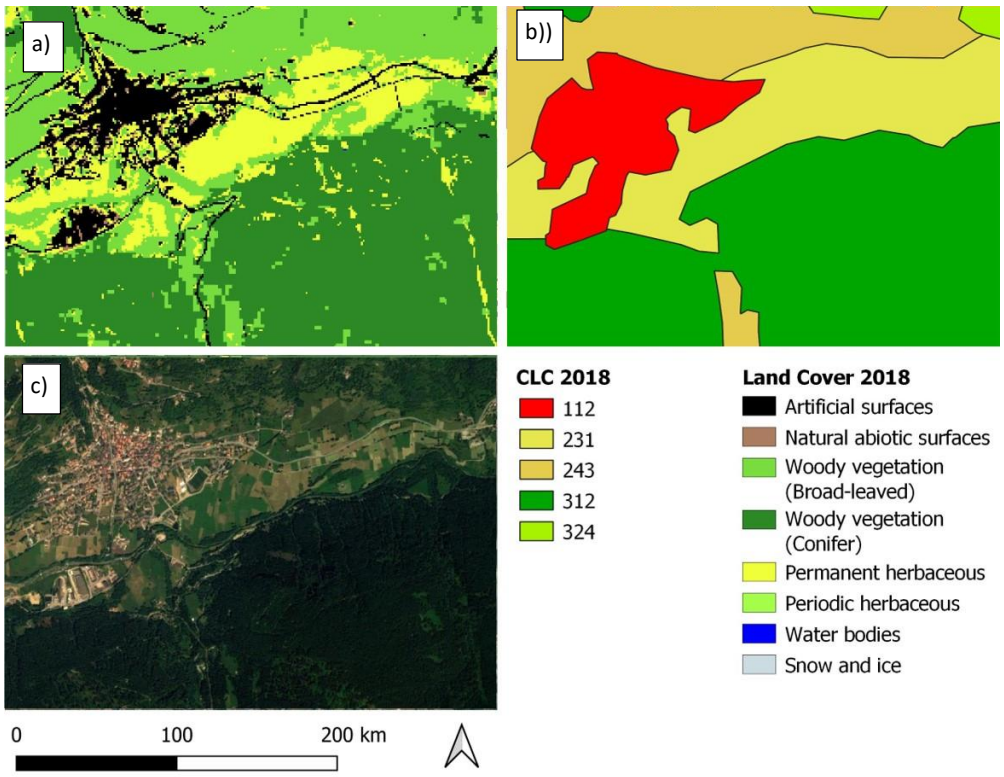

Figure 4.9 - - Comparison CLC with Land cover map 2018. (a) LC 2018, (b) CLC 2018, (c) High definition image from Google Earth 2018. Correspondence between the class Conifers in the two maps.

In correspondence with CLC 211 class, LC maps many areas with presence of woody vegetation and highlights the tunnels of trees around water bodies and canals, the rows of trees near roads and between the different properties and the small wooded areas in agricultural areas smaller than MMU of the CLC.
With reference to olive trees, the accuracy of the mapping is influenced by the density of the tree cover. In the presence of widely spaced trees, the underlying soil influences the spectral signature of the pixel, making it similar to that of a herbaceous tree. The broadleaf class of LC thus also includes CLC classes referring to permanent crops.
The identification of the vineyard, included in this class even though they are shrubs, is on the whole accurate but still requires refinement. The difficulties in identifying the class are linked to its spectral signature: it is similar to that of the sparse forest in the period of maximum vegetative phase, and to that of the herbaceous in the period of dormancy.

Herbaceous vegetation
There is a good correspondence between herbaceous classes and 21* and 24* CLC classes; 50.8% of the herbaceous LC falls in correspondence with arable CLC and 16% in correspondence with heterogeneous agricultural areas, of which the LC maps the herbaceous component. Sometimes the herbaceous class of LC is placed in correspondence of permanent crops CLC (as in the case of olive groves) this is due to the arrangement of the plants that influence the spectral signature of the pixels.
Due to a diversity in the definition of periodic and permanent herbaceous classes, it is not possible to establish a clear correspondence with CLC and LC classes. In the LC the classification system is related to the spectral signature of the classes over the year while in the CLC, the distinction is linked to criteria based on land use. In LC permanent herbaceous mainly correspond to 211, 243, 242 and 231 CLC classes. Due to the snow cover, which in certain periods of the year influences the reflectance of the area, a large part of the 231 CLC class is also covered by periodic grass. Thus, the discontinuity in NDVI values leads these areas to a more typical behaviour of periodic herbaceous than permanent. Important is the presence of herbaceous also in 323 (sclerophyllous vegetation) and 333 (scattered vegetation).

Burned areas
The figure recorded is consistent with that of the EFFIS (https://effis.jrc.ec.europa.eu/) and is equal to 11,106 ha. Since the CLC refers to 2017 images, it does not record fires that occurred between 2017 and 2018. In addition to the different reference period of the images, there is also a different minimum mapping unit that consequently don’t allow a significant direct correspondence between the LC fires and the corresponding CLC class (334).
The changes in tree vegetation affected a total of 89,596.38 ha (tab 2 and tab 3) and 12.40% (11,106 ha) were caused by fires, while 87.60% (78490 ha) had other causes (such as forest harvesting).

Other disturbances
The class "other disturbances" does not have a clear correspondence with the CORINE classes, not only because of the difficulties mentioned above in distinguishing exactly the tree cuts in the different Italian areas, but above all, as in the previous case, because of different reference year and different MMU of the CORINE, which does not identify small areas. In this case, therefore, the data was compared with some data coming from studies at regional level, showing a good correspondence (limited to these areas) (De Fioravante et al., 2021).

4.1.4 Discussion of land cover classification

Since the CLC is the only map that covers the entire national territory, it has been used to understand the criticalities of the system adopted and discuss the results.

The LC map has less thematic detail than the CLC, this is due to the difficulty of distinguishing well a large number of land cover classes on a large area, but especially on a heterogeneous territory such as Italy, using only satellite data.
The correspondences are influenced by three main aspects: the first is related to the minimum mappable unit which is 25 ha in the CLC while in the LC 2018 it is more detailed, mapping at the pixel level (10 m). This can also produce some errors and it is possible to find isolated pixels belonging to a certain class within a completely different CLC class (an example is the case of the built-up within agriculture).
The second aspect is linked to a semantic issue and to the differences between the two classification systems: this is the case of mixed classes or land use classes in the CLC nomenclature: for these classes it was not possible to make a comparison between the two classification systems used.
Finally, the third aspect concerns the lack of correspondence due to classification errors in the implemented methodology that leads to the incorrect classification of some pixels. In other situations, as in the forest disturbances class, the difficulties of comparing data lie in the different reference period considered in CLC for forest harvesting.
Regarding this last point related to classification, some critical issues emerged as regards the distinction between classes with very similar spectral signatures, such as the case of built-up area and bare soil (Nguyen et al., 2021), or the case of a precise di7u8.,[i]stinction of the different vegetation classes.
The separation between bare soil and urban areas using specific indices is commonly associated with low precision due to the high degree of homogeneity and confusion on the spectral characteristics as referred by several authors (X. Liu et al., 2018; Rasul et al., 2018). Max J. Steinhausen et alii (Steinhausen et al., 2018a) recognized the difficulty to distinguish them in their classification where rock and urban were among the classes with the lowest user accuracy and rock is the class with the weakest producer accuracy score. Several authors have proposed various indices (Pal & Antil, 2017; Rasul et al., 2018), but lack an analysis of their differentiation capacity between bare soil and urban cover and this aspect is still a challenging task. Valdiviezo et alii (Valdiviezo-N et al., 2018) analysed the potentiality and limitations of built-up indices, highlighting that their use is very conditioned by study area location, characteristics and seasonality of the satellite data.
In this research, the question related to similar spectral signatures was addressed exploiting SAR data considering that bare soil flat presents low backscatter and behaviour quite different from the urban region. In addition, the NDVI index was used to improve the accuracy of this latter class and better divide it from the barren land with a rough surface. Some problems have arisen from greenhouses which are covered for some periods by plastic materials that shows high brightness similar to the urban class. Further researches are therefore needed to obtain acceptable performance in particular to resolve the outstanding issues.
The combine use of vegetation indices based on optical Sentine-2 data and SAR Sentinel-1 data contributed to the classification performance since permitted to exploit different characteristics of remote sensing data. Even if a compared study wasn't conducted, the sole use of spectral signatures reduces the accuracy of results as demonstrated by several researches as (Joshi et al., 2016; Steinhausen et al., 2018b).
Other cases that posed some problems are related to the discrimination between *continuous* and *temporary herbaceous* vegetation. Figure 4.10 shows a *temporary herbaceous* vegetation class, in the example, the algorithm has well identified this class with agricultural fields, but in other situations, some limitations were identified for the exact separation of the two classes, producing a lower accuracy. The problem lies in the definition used that distinguishes periodic herbaceous class as a temporary transition from herbaceous vegetation to bare soil during the period of one year (cf. EAGLE) while in permanent herbaceous there must be no in which bare soil is present. The multi-temporal images can efficiently detect a short change of land cover, but in order to identify *periodic herbaceous* during the validation methodology step, it would have been necessary to use a time series (with high frequency and high spatial resolution), to understand if a period with bare soil had occurred: a data set of this type was not available for free. If the intention of EIONET was to distinguish permanent grassland from agricultural grassland (which during the year are

subject to periods with the presence of bare soil), a land use class would have been used (information which can be subsequently inserted), but the proposed methodology is based on the spectral response of the objects and can provide land cover and not land use information.

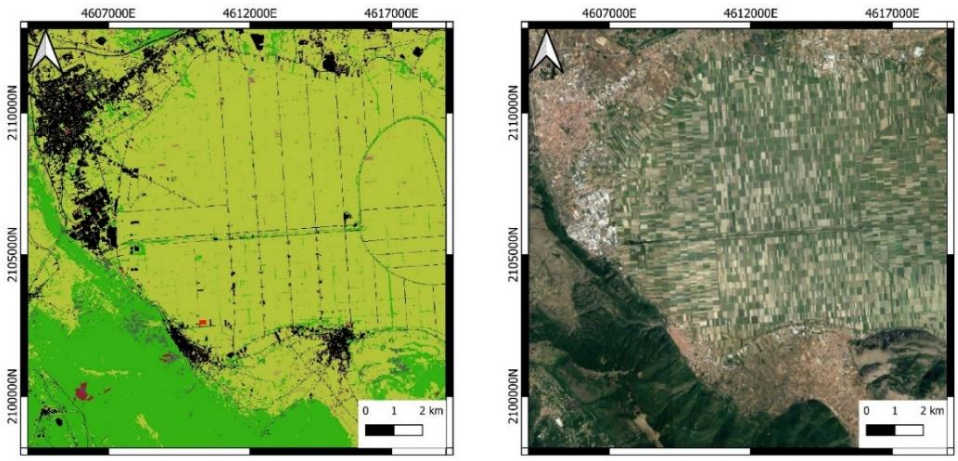

Figure 4.10 - Land cover map 2018 on the left, example of water class, (orthophoto on the right).

Good performances were obtained with regarding the distinction between conifers and broadleaved trees which provided results in line with other authors (Agrillo et al., 2021; Immitzer et al., 2019; Spadoni et al., 2020); many classifications have also tried to distinguish forest classes with greater detail, at the species level, with good results (Mickelson et al., 1998; Schriever & Congalton, 1995; X. Zhu & Liu, 2014), however, these are mainly tested in small areas (regional or sub-regional scale areas) or at a coarse spatial resolution, and their applicability over large areas would require careful analysis and an enormous amount of detailed data to be able to define the most important species. In addition, some tree species do not cover large enough areas for being detectable with 10 m resolution data, as are Sentinel-2 (Immitzer et al., 2019).
However, it is worth considering the question of the mixed woods and shrubs land covers: the Italian territory has several areas with mixed vegetation, i.e. characterized by both conifers and broadleaved trees: mixed class is included in one of them since it is not included the mixed typology in the proposed classification.
On the other hand, the introduction of the shrubs class to the classification system developed, would represent an added value since some accuracy errors are derived from the lack of a transition areas between woods and prairies, which often are covered with woody vegetation and in particular with shrubs. In addition, vineyards or other orchards classified, as previously specified, in the woody class, would be better defined as shrubs. The possibility therefore to improve the algorithm through the definition of a mixed class and, above all, of the shrubs class, represents further improvements, considering that repeat observations over time, the use of time-series and SAR data can help to capture the spectral variability and discriminating between more different land cover types.
Regarding forest disturbances classes, the importance of the NBR and NDVI indices for burned area detection is also highlighted by several studies that have provided good results both in Italy and in different areas of the world (Helman et al., 2015; Key & Benson, 1999, 2006; Parks et al., 2014; Pepe & Parente, 2018; Sobrino et al., 2019; Teodoro & Amaral, 2019). It was not possible to compare our data with those of CORINE because, as specified above, the changes refer to a different period; it was, however, possible to verify that the results obtained for the burned area class are in agreement with EFFIS (https://effis.jrc.ec.europa.eu/).
As noted above, the identification of other forest disturbances related to forest harvesting was more difficult. Different tree cutting systems in Italy depending on the areas and type of forests results in differences of spectral signature and in the need to define a specific algorithm to identify cutting areas.

Several systems have been developed for this purpose (White et al., 2017, 2018), but their applicability in Mediterranean forests presents some issues. This is due to the differences in the type of species, in the cultivation methods and in the edaphic conditions and to the rapid asexual regeneration of trees typical of these coppice forests in Italy (Chirici et al., 2020). Giannetti et al. (Giannetti et al., 2020) have implemented a system that exploits the properties of NDVI and NBR (using Landsat) obtaining good results for the Tuscan area. The results obtained in this study are comparable to those obtained by these authors, but for the reasons mentioned above, it provided some misclassifications in alpine areas where selective tree cutting is practiced or in small areas that are more difficult to locate. This problem has contributed to produce low accuracy for this class and requires the development of further systems to identify to better identify these areas.

The developed methodology is based on tree rules system using vegetation indices and backscatter values. This choice derives not only from tests performed in sample areas but also from previous studies evaluations that have shown the NDVI, NDWI or some specific bands such as NIR and SWIR bands effectiveness , particularly for vegetation classes (Bolyn et al., 2018; Immitzer et al., 2019; Persson et al., 2018b; Puletti et al., 2018). In addition, Grabska et al. (Grabska et al., 2019) pointed out the significance of the Red-Edge for mapping forest species or coniferous species according to Hościło and Lewandowska (Hościło & Lewandowska, 2019).

The use of decision rules has the advantage of being able to establish suitable rules for each land cover class, and of defining valid thresholds within a specific cover class group. An aspect that deserves more detail concerns the adaptation of the thresholds based on the characteristics of the territory, considering firstly the influence of hydrometeorological variables and seasonal climatic variations and the phenological evolution of vegetation to better characterize the different types of herbaceous classes and forest disturbances. Similar issues have been addressed by Spadoni et al. (Spadoni et al., 2020) in a case study applied to three Sentinel-2 granules in Italy.

The proposed system can be adopted to other European countries with a climate similar to Italy, adapting the thresholds and temporal ranges to local characteristics and vegetation phenology. In other climate situations the above assumptions would be not valid, therefore, could be necessary perform and test other thresholds before to implement this method.

These factors make the method easily modifiable and applicable to large. It must in fact be considered that large area as the Italian territory presents a strong heterogeneity from the morphological and climatic point of view that cannot be neglected. As highlighted in chapter two, many land cover classification methods have also achieved better accuracies than the methodology developed in this research, but they have all been applied to narrow study areas and many of these algorithms are sensitive to the number of training areas or to parameter settings and therefore take a long time when applied to large areas. Some products such as the Global Human Settlement Layer (Pesaresi et al., 2013), the Global Urban Foot-print (Esch et al., 2017) or the Global human-made Impervious Surface (Brown de Colstoun et al., 2017) are developed globally but are not very useful for monitoring since they are produced in specific periods of time. Nonetheless, good temporal and spatial resolution data represent a huge advantage for detailed studies and territorial analyses that require a frequently update of the map. This is also the direction indicated by the European Community within the Coperinicus programme which now requires individual states members to provide datasets with good spatial detail to be integrated with ancillary data already.

4.2 Spatial distribution of land consumption typologies

Since 2016 ISPRA has been mapping soil consumption with reference classification system based on three-level of detail. This system allows to describe the information not only in terms of presence-absence of soil consumption, but also to characterise the different typologies of soil consumption. A second level of detail distinguishes between reversible and permanent land consumption by defining:

Permanent land consumption: the part of the space that is covered with artificial constructions like a building or surfaces like a pavement. It includes buildings, paved roads, railways, airports (paved areas), ports (paved areas), other paved or sealed surfaces, waste dumps, paved greenhouses. It can be considered as Sealed Artificial Surfaces and Constructions. As defined in the Land Cover Component of the EAGLE Matrix class 1.1.1 (EAGLE, 2020).

*Reversible land consumption: a*ny process where natural surface material has been replaced by artificial material or where natural material has been removed from, forming a non-impervious and non-built-up surface as stated in the EAGLE class 1.1.2 Non sealed Artificial Surface (EAGLE, 2020). It includes soil compaction, excavation or temporary impervious coverage, unpaved roads, construction sites, courtyards or sports fields, permanent deposits of material, photovoltaic fields, quarries not yet restored.

The third level goes into more detail in the description of different subclasses (Table 4.13).

At the moment the 3rd level of classification does not consider the entire Italian territory and it is mainly applied to areas of new change as well as within the polygons drawn during the manual correction of omission errors. In this sense, the analyses performed in this research regard the changes occurred between 2016 and 2019. The study first covered the entire country, followed by an in-depth study on the distribution of land consumption (reversible and irreversible) in *high* and *very high* seismic and landslides hazard areas with a focus on a different typology of change.

Table 4.13 – Legend of different typologies of land consumption at third level of detail.

11	Permanent land consumption	12	Reversible land consumption
111	Buildings	121	Unpaved roads
112	Paved roads	122	Construction sites and other areas of compacted earth
113	Rail network	123	Non renaturalised mineral extraction sites
114	Airports	124	Quarry in ground water
115	Port areas	125	Photovoltaic systems on the ground
116	Other impermeable/paved areas, parking lots	126	Other artificial areas not related to agricultural activities, the removal of which restores the initial soil conditions
117	Permanent paved greenhouses		
118	Dumps sites		

4.2.1 The different typologies of land consumption in Italy

The level of land use classification that can be achieved depends on the images used for the photo-interpretation; the third level of classification can only be achieved if very high-resolution images of the area are available. If Sentinel-2 images are available, areas can be classified at most at the first or second level. More than 90% of the land consumption between 2016 and 2019 in Italy was mapped at the third classification level; in particular, 95.9% in 2016-2017, 90.8% in 2017-2018 and 94.5% in 2018-19 (Table 4.14). The area labelled only at the first level is 2.0% for 2016-2017, 6.4% for 2017-2018 and 0.2 for 2018-2019, while at the second level is 2.0% of changes (but not third level) for 2016-2017, 3.9% for 2017-2018 and the 5.3% for 2018-2019. It is important to note that areas that have been classified at level 3 also have level 2 and level 1. In the Table 4.14 the percentages are disaggregated. Figure 4.11 shows soil consumption reversible and permanent in Italy.

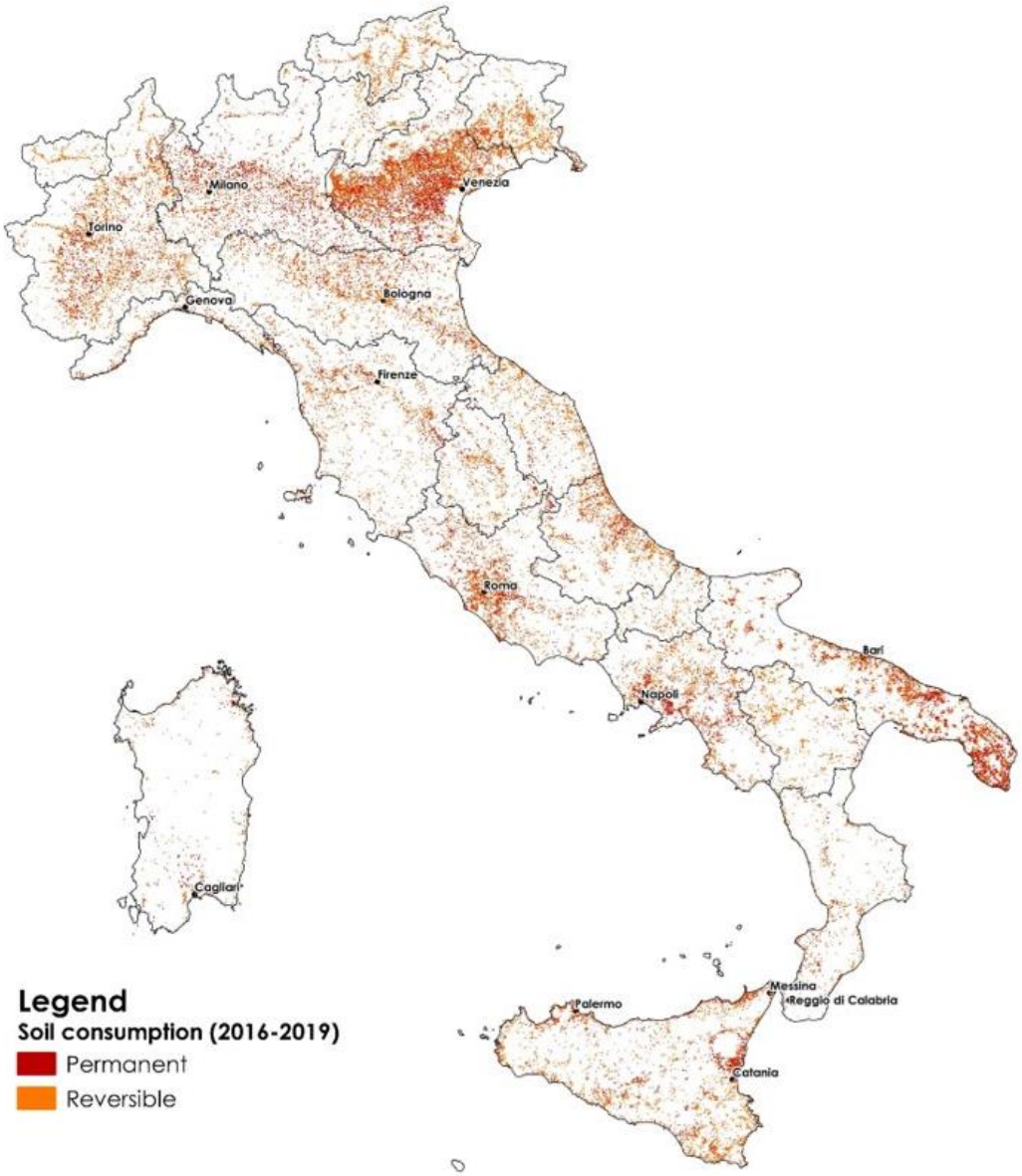

Figure 4.11 - Soil consumption reversible and permanent in Italy.

Table 4.14 - Areas classified at first, second and third level of detail expressed in % of total land consumption.

Level	16-17	17-18	18-19
1L	2.04	6.45	0.17
2L	2.01	3.9	5.33
3L	95.94	90.86	94.5

Taking into account the changes at the third level related to the transformation from natural (class 2) to artificial land cover, thus in terms of land consumption, it emerges that more than 60% of them fall under class 122 *'Construction sites and other earthen areas'*. Figures 4.12 and 4.13 show two examples of irreversible land consumption

a) 2016

b) 2019

c) Land consumption in 2019 in red

Figure 4.12 – Example of Land consumption

a) 2016

b) 2019

c) Land consumption in 2019 in red

Figure 4.13 - Land consumption in 2019 in red.

Analysing the areas with irreversible land consumption, class 111 (*Buildings*) has experienced the largest increase with about 1/6 of the new changes, although there has been a decrease in the observed period: from 947.4 ha (16.52% of the total) in the period 2016-17, to 733.9 ha in the period 2018-19 (or 13.52% of the total). It can be highlighted that other relevant contributions are those related to class 123 (*Mining)* for reversible (about 6% of the new land consumption in the observed period) and to class 116 (P*aved yards)*, just under 500 ha in the observed period, for irreversible land consumption.

In 2016-17 the percentage is 60.27% and in 2017-18 it increases to 63.87 and to 63.07% in 2018-19. In absolute terms, the highest value is in the period 2017-18 (3825 ha) with about 400 ha more than the periods 2016-17 and 2018-19 where the situation is similar: 3456 and 3423 ha respectively (Table 4.15).

Table 4.15 - Area and percentage of different typologies of land consumption in Italy during 16-17, 17-18 and 18-19.

Class	16-17		17-18		18-19	
	ha	%	ha	%	ha	%
111	947.39	16.52	820.59	13.7	733.9	13.52
112	157.66	2.75	117.61	1.96	96.81	1.78
113	0.67	0.01	1.35	0.02	0	0
114	6.75	0.12	2.55	0.04	17.48	0.32
115	1.08	0.02	7.56	0.13	4.21	0.08
116	493.9	8.61	476.19	7.95	472.61	8.71
117	26.89	0.47	7.56	0.13	8.73	0.16
118	28.54	0.5	7.69	0.13	8.33	0.15
121	123.54	2.15	170.52	2.85	126.96	2.34
122	3456.1	60.27	3825.89	63.87	3423.73	63.07
123	353.33	6.16	424.53	7.09	330.09	6.08
124	46	0.8	40.35	0.67	21.54	0.4
125	73.92	1.29	64.63	1.08	175.78	3.24
126	18.87	0.33	22.96	0.38	8.56	0.16
Tot	**5734.64**	**100**	**5989.98**	**100**	**5428.73**	**100.01**

In the next section the land use classified with a third level of detail in landslide and seismic hazard areas was analysed. The study was carried out by cross-referencing the dates of the hazard areas with the data related to soil consumption at the third level. In particular the transformations from reversible to permanent and vice-versa are considered alongside with the distribution of the main typologies of changes (classified at the third level) in the hazard areas of each region.

4.2.2 Land consumption in landslide hazard areas

The national mosaic of landslide hazard areas was compared with the land consumption for the production of new indicators and to study the trend in the periods 2016-2017, 2017-2018 and 2018-2019. The data referred to landslide derives from the national mosaic (Trigila A. et al., 2018) of the landslide hazard areas of Hydrogeological management Plans - PAI, carried out by ISPRA *for the monitoring, control and verification of the implementation and consistency with the planning of hydrogeological risk mitigation measures on the national territory*. The national mosaic of landslide hazard areas was necessary since each basin authority defines these areas on non-univocal criteria, therefore it is necessary to standardize the different areas at the national level analysing the classification of landslide hazard adopted by each Authority.

The whole national territory has therefore been subdivided into 5 hazard classes: very high P4, high P3, medium P2, moderate P1 and AA attention areas (those areas where are available information about hydrogeological instability but no class has been yet associated), based on the DPCM (Decree of the President of the Council of Ministers) 29 September 1998, in which methodologies and guidelines were suggested to limit and classify areas with different hydrological risk. The following analyses consider only the areas belonging to P3 and P4, i.e with dormant or active landslide phenomena, but characterized by medium to high probability of reactivation. The Table 4.16 shows the land use constraints and regulations in these two areas (Trigila A. et al., 2018).

Table 4.16 – Description of High and Very High landslide hazard areas.

Landslide hazard	Description
P3 High landslide hazard	It is possible, in addition to interventions allowed in areas of very high hazards, the interventions of expansion of existing buildings for the hygienic-sanitary adaptation and the realization of new treatment plants of wastewater and the extension of existing ones, after study of compatibility of the work with the state of existing instability.
P4 Very high landslide hazard	Only the following interventions are allowed: demolition interventions without reconstruction; interventions strictly necessary to reduce the vulnerability of existing buildings and to improve the protection of public safety, without increases in surface area or volume and without changes in intended use; reclamation works and accommodation of landslides; ordinary and extraordinary maintenance interventions; the construction of new linear and network infrastructures provided for by law, declared essential, not relocatable and without technically and economically sustainable design alternatives;…..

4.2.2.1 National landslides hazard

The landslide hazard areas P3 and P4 affect all Italian regions with variable values depending on the area: Emilia Romagna and Toscana are the regions in which the landslide hazard area P3 is greater, as a percentage of the total area P3 in Italy, with values equal to 14.8% and 18.5% (Table 4.17). Figure 4.14 shows the landslides hazards in ha of P3 and P4 in the Italian regions. If instead we consider the areas falling within class P4, Valle D'Aosta is the most affected. The regions with a smaller landslide area are Umbria, Veneto and Friuli Venezia Giulia where the sum of the areas classified as P3 and P4 does not exceed 20,000 ha.

Table 4.17 – Artificial surface in P3 and P4 (in 2019) and landslides hazards classes and their extension in Italy.

Region	Artificial in P3 hazard area (ha) in 2019	Artificial in P3 hazard area (%) in 2019	Artificial in P4 hazard area (ha) in (2019)	Artificial in P4 hazard area (%) in 2019	% of tot P3 in Italy	% of tot P4 in Italy	TOT P3 + P4 (ha)
Piemonte	2214	3.0	78338.21	2.6	5.19	8.87	153542.90
Valle d'A.	1237	1.0	155109.66	0.4	8.32	17.55	275750.51
Lombardia	1355	2.0	86172.03	1.3	3.68	9.75	139442.02
Trent. A.A.	1406	1.0	1566.76	1.6	8.65	0.18	126907.91
Veneto	259	4.5	10967.35	4.1	0.22	1.24	14100.88
Friuli V G.	198	5.4	17234.41	2.5	0.11	1.95	18801.17
Liguria	3110	4.5	6267.06	4.9	3.68	0.71	59537.04
Emilia R.	8207	3.6	122207.61	2.8	14.81	13.83	336854.32
Toscana	7221	2.8	43869.40	2.8	18.59	4.96	313352.85
Umbria	123	7.1	0.00	8.5	0.22	0.00	3133.53
Marche	1233	2.0	9400.59	2.5	4.22	1.06	70504.39
Lazio	294	4.2	57970.28	3.5	0.54	6.56	65804.10
Abruzzo	2047	2.1	53269.98	2.0	7.24	6.03	158243.19
Molise	861	1.8	21934.70	1.8	3.14	2.48	67370.86
Campania	5300	3.9	125341.14	3.9	8.65	14.18	250682.28
Puglia	1367	2.9	21934.70	4.6	3.14	2.48	67370.86
Basilicata	743	2.3	20367.94	2.6	2.27	2.30	53269.98
Calabria	973	4.8	6267.06	5.5	1.41	0.71	26634.99
Sicilia	618	4.1	17234.41	3.2	0.65	1.95	26634.99
Sardegna	1339	1.7	28201.76	2.7	5.30	3.19	104973.21
Italia	40104	2.7	883655.04	2.5	100.00	100.00	2332911.99

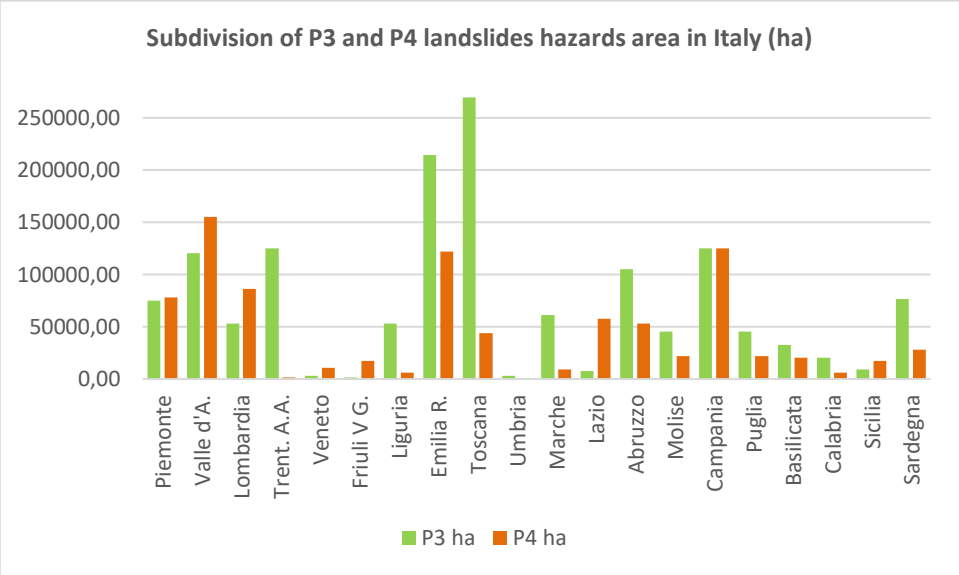

Figure 4.14 - Surface in ha of P3 and P4 landslides hazards area in the Italian regions

Land consumption in the areas classified as *High* (P3) and *Very high* (P4) shows values that ranging from 0.77% to 0.51%, between 2016 and 2017, from 1.46% to 0.44% between 2017 to 2018 and from 0.921% to 0.40% of between 2018 and 2019 compared to national one (Table 4.18).

Table 4.18 - Land consumption in P3 and P4 area in terms of hectares and percentages compared to national one.

Reference period	P3		P4		Italy	
	ha	%	ha	%	ha	%
16-17	41.41	0.78	27.42	0.51	5326.08	100
17-18	83.34	1.46	25.18	0.44	5694.28	100
18- 19	47.62	0.92	20.71	0.40	5186.39	100
Tot 16-19	**172.37**	**1.06**	**73.31**	**0.45**	**16206.75**	**100.00**

Considering the type of changes, most of Italian territory is classified at third level of detail but, in 2017-18 only 77% of the changes belonging to the class P3, and 78.9% belonging to the class P4, have this information (Table 4.19).

Table 4.19 – Land consumption mapped at 3rd level of detail in landslide hazard area.

Reference period	P3		P4	
	TOT 3rd level		TOT 3rd level	
	ha	%	ha	%
16-17	41.41	93.82	27.42	98.47
17-18	83.34	77.14	25.18	78.95
18- 19	47.94	100	20.71	99.57

Figure 4.15 shows land consumption at the second level, i.e. divided into permanent and reversible in terms of hectares and percentages. As it can be seen, the reversible land consumption prevails in both high and very high hazard areas in the three periods considered, while the irreversible one represents 20% of the new land consumption in the period 16-17 and remains below 15% (14% is the highest value during 18-19) in all areas in the following two periods. The analysis of changes in terms of land consumption, restoration and soil sealing shows that the changes are evenly distributed between the high and very high hazard areas,

although there is a slight prevalence in the P3 area. The 2017-2018 period is the one with the highest land consumption in both hazard areas, while the 2016-2017 and 2018-2019 periods are aligned.

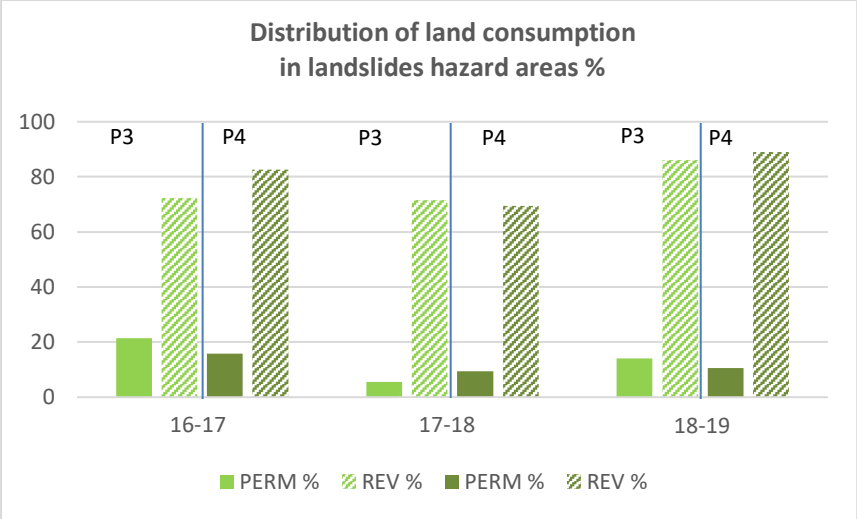

Figure 4.15 - Permanent and reversible land consumption in terms of hectares and percentages in P3 and P4 landslides hazard areas.

Table 4.20 - Table shows the transformation between classes 11 (irreversible land consumption) and 12 (reversible land consumption) in the different tree periods considered, in landslides hazard areas in ha.
Green areas represent transformations from built-up or reversible land consumption to natural areas (renaturation) while grey account for transitions from natural or reversible to built-up areas, i.e. irreversible land consumption.

P3 Landslides

	2017				
2016	1	11	12	2	Tot
1	-	4	12	0	**16**
11	0	-	1	0	**1**
12	0	1	-	15	**16**
2	3	9	45	-	**56**
Tot	**3**	**15**	**57**	**15**	**-**

	2018				
2017	1	11	12	2	Tot
1	-	0	3	0	**3**
11	0	-	0	1	**1**
12	0	4	-	16	**20**
2	19	5	75	-	**99**
Tot	**19**	**10**	**78**	**16**	**-**

	2019				
2018	1	11	12	2	Tot
1	-	0	0	0	**0**
11	0	-	1	0	**1**
12	0	8	-	8	**16**
2	0	7	49	-	**56**
Tot	**0**	**15**	**50**	**9**	-

P4 Landslides

	2017				
2016	1	11	12	2	Tot
1	-	8	7	0	**15**
11	0	-	1	0	**1**
12	0	2	-	3	**5**
2	0	4	26	-	**30**
Tot	**0**	**14**	**33**	**3**	**-**

	2018				
2017	1	11	12	2	Tot
1	-	1	1	1	**2**
11	0	-	0	0	**0**
12	0	2	-	6	**8**
2	6	2	23	-	**32**
Tot	**6**	**6**	**24**	**6**	**-**

	2019				
2018	1	11	12	2	Tot
1	-	0	0	0	**0**
11	0	-	0	0	**0**
12	0	2	-	7	**8**
2	0	2	25	-	**27**
Tot	**0**	**4**	**25**	**7**	**-**

The restorations almost exclusively affect the reversible consumed land, in line with national trends. Soil sealing is distributed evenly between new soil consumption on natural areas and soil sealing on reversible consumed soil, except in the period 2016-2017 in areas with hazard equal to P3. Table 4.20, in the previous page, shows Changes in terms of land consumption, restoration and soil sealing. Figure 4.16 shows soil consumption between 2016 and 2019 divided in permanent and reversible in P3 and P4 landslides hazard areas.

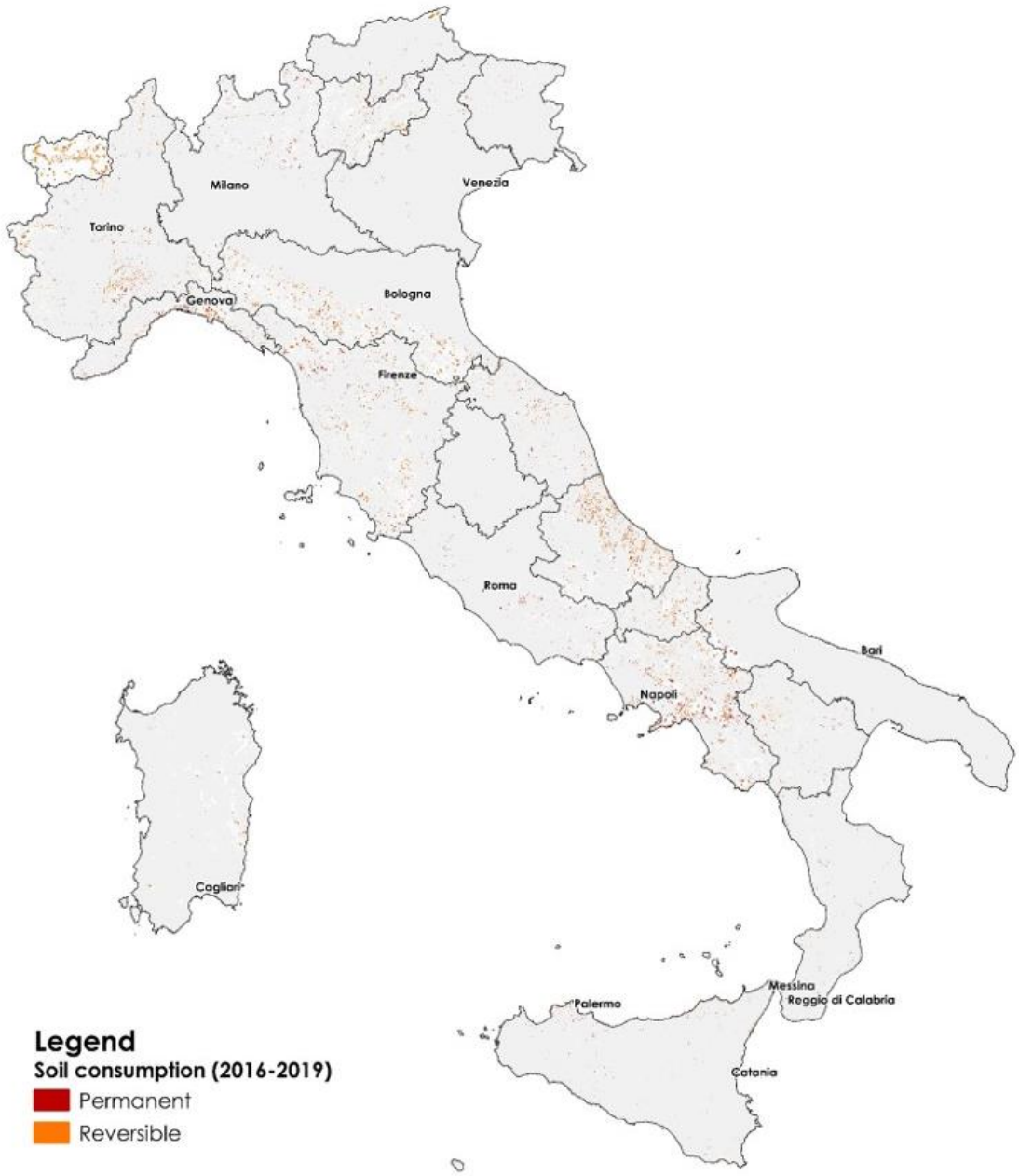

Figure 4.16 – Soil consumption between 2016 and 2019 divided in permanent and reversible in P3 and P4 landslides hazard areas.

Main typologies of change in landslides hazard area

The class of the third level in which the greatest number of changes is concentrated is class 122 (*building sites and other rammed-earth areas*) considering all the periods observed and with reference to both area

belonging to P3 and P4 hazard class. In particular, more than 60% of the changes related to class 122 have occurred in the periods 16-17 and 18-19, while in the period 17-18 most of the changes concerns the class 123, which present high values also in the other years. The strong variation of this class is the result of the dynamism of the quarry fronts. With reference to the permanent land consumption, the main classes are 111, which however undergoes a reduction over time in both hazard classes, and 116, for which there is not a clear trend (Table 4.21).

Table 4.21 - Trends of the different typologies of land consumption in areas P3 and P4 during 16-17, 17-18 and 18-19 periods.

	P3						P4					
	16-17		17-18		18-19		16-17		17-18		18-19	
Class code	ha	%	ha	%	ha	%	ha	%	ha	%	ha	%
111	3.4	9.4	2.3	3.7	1.7	3.7	1.8	6.8	1.0	5.4	0.6	2.7
112	1.7	4.6	-0.1	-0.2	0.8	1.7	0.4	1.5	0.4	2.0	0.1	0.6
113	0.0	0.0	0.0	0.0	0.0	0.0	0.0	0.0	0.0	0.0	0.0	0.0
114	0.0	0.0	0.0	0.0	0.0	0.0	0.0	0.0	0.0	0.0	0.0	0.0
115	0.0	0.0	0.0	0.0	0.0	0.0	0.2	0.8	0.0	0.0	0.0	0.0
116	2.9	8.1	2.2	3.6	4.2	9.1	1.5	5.5	1.0	5.5	1.5	7.4
117	0.0	0.0	0.0	0.0	0.0	0.0	0.0	0.0	0.0	0.0	0.0	0.0
118	0.0	0.0	0.0	0.0	0.0	0.0	0.0	0.0	0.0	0.0	0.0	0.0
121	2.4	6.5	3.4	5.5	1.7	3.7	1.5	5.6	2.3	12.6	2.6	12.9
122	29.4	81.3	25.1	40.3	34.3	75.0	20.6	78.0	6.2	33.6	16.3	79.3
123	-3.8	-10.4	29.0	46.7	2.9	6.2	0.5	1.7	7.5	41.0	-0.6	-2.9
124	0.0	0.0	0.0	0.0	0.0	0.0	0.0	0.1	0.0	0.0	0.0	0.0
125	0.0	0.0	0.0	0.0	0.0	0.0	0.0	0.0	0.0	0.0	0.0	0.0
126	0.2	0.5	0.3	0.4	0.3	0.7	0.0	0.1	0.0	0.0	0.0	0.0
Total	36.2	100	62.18	100	45.7	100	26.5	100	18.4	100	20.5	100

4.2.2.2 Regional landslide hazards

The analysis of the third level on regional scales are focused on the observation of the four main classes: 111 and 116 for permanent soil consumption and 122 and 123 for reversible soil consumption. With reference to the permanent soil consumption classes, the changes in high and very high hazard areas (Table 4.22 and 4.23) are small, often remaining below 1 ha in all regions (the only exception is Toscana, where 1.34 ha in class 116 in 2018-19). Considering the changes greater than 5 ha, it is possible to note that they are limited to class 122 in Emilia Romagna (for 2016-17), class 122 and 123 for Toscana (for 2017-18) and classes 122 and 123 for Piedmont, Abruzzo and the province of Trento (for 2018-19).

As can be seen from the analysis carried out, the most hazard classes (high P3 and very high P4) cover 8.4% of the national territory (5.4 and 3.4 respectively) (Trigila A. et al., 2018). In these areas, subject to the most restrictive land use constraints, the artificial surface is equal to 2.5% in P4 and 2.7 in P3 (referred to 2019). In the three years considered, the increase in these areas was 1% in P3 and 0,5 in P4 and, although this value is still lower than the national average, the data nonetheless show an increasing of land consumption, more marked in the regions Piemonte, Trentino Alto Adige and Toscana, mainly due to the construction of building *sites and other rammed-earth areas* (class 122).

Table 4.22 - Distribution of 111, 116, 122 and 123 classes in areas P3 in each Italian region during 16-17, 17-18 and 18-19 (ha).

	P3											
	16-17				17-18				18-19			
Region	111	116	122	123	111	116	122	123	111	116	122	123
Piemonte	-0.8	0.4	-1.2	0.0	0.3	0.3	4.2	0.1	0.1	0.5	9.9	0.0
Valle d'A.	0.0	0.0	4.1	0.6	0.2	0.2	2.3	0.0	0.0	0.0	-0.9	0.0
Lombardia	0.0	0.0	1.1	0.0	0.1	0.0	0.3	0.2	0.1	0.3	0.6	0.4
Trent. A.A.	0.2	0.4	2.7	2.6	0.0	0.0	1.1	-0.1	0.0	0.1	6.3	1.0
Bolzano	0.2	0.4	0.4	0.0	0.0	0.0	-0.1	0.1	0.0	0.0	0.1	1.0
Trento	0.0	0.0	2.3	2.6	0.0	0.0	1.1	-0.3	0.0	0.1	6.2	0.0
Veneto	0.1	0.0	0.8	0.0	0.1	0.0	-0.1	0.0	0.0	0.0	0.1	-0.5
Friuli V G.	0.0	0.0	0.0	0.0	0.0	0.0	0.0	0.0	0.0	0.0	0.0	0.0
Liguria	0.0	0.2	1.2	0.4	0.1	0.4	0.8	-1.5	0.0	0.4	1.4	0.7
Emilia R.	0.8	0.0	10.0	0.4	0.1	0.3	-1.9	0.0	0.1	0.2	1.1	-0.2
Toscana	0.3	0.4	4.0	-8.1	0.8	0.4	7.3	30.7	0.2	1.3	2.1	0.9
Umbria	0.0	0.0	0.0	0.0	0.0	0.0	0.0	0.0	0.0	0.0	0.0	0.0
Marche	0.2	0.0	3.2	0.0	0.0	0.0	1.8	0.0	0.1	0.1	1.4	0.0
Lazio	0.1	0.0	-0.6	0.0	0.0	0.0	0.3	-0.6	0.0	0.0	0.0	0.0
Abruzzo	0.0	0.8	0.9	0.0	0.0	0.0	2.2	0.0	0.2	0.4	5.5	0.0
Molise	0.2	0.1	0.9	0.0	0.0	0.0	0.3	0.0	0.0	0.0	0.3	0.3
Campania	0.8	0.4	1.8	0.3	0.6	0.3	4.7	0.3	0.3	0.6	2.4	0.0
Puglia	0.3	0.1	0.1	0.0	0.0	0.0	0.4	0.0	0.5	0.3	0.8	0.0
Basilicata	0.0	0.0	0.0	0.0	0.1	0.0	0.6	0.0	0.0	0.0	1.7	0.2
Calabria	0.0	0.0	0.1	0.0	0.1	0.0	-0.1	0.0	0.0	0.0	0.2	0.0
Sicilia	0.1	0.0	0.1	0.0	0.0	0.2	0.7	0.0	0.0	0.0	1.4	0.0
Sardegna	0.0	0.0	0.4	0.1	0.0	0.0	0.1	0.0	0.0	0.0	0.2	0.0
Italia	2.3	3.3	32.1	-1.2	2.3	2.2	26.2	28.9	1.7	4.2	40.5	3.9

Obviously it is not possible to establish from this study whether the increase is due to new buildings that comply with the constraints imposed by the legislation in these particularly delicate areas, the information extracted is however an information base of crucial importance as a support for local policies and the safeguarding of these areas.

It is important to underline that natural events linked to Landslides are very widespread throughout the Italian territory, and too often they turn into disasters due to human presence and activities: according to the Trigila et al. report (Trigila A. et al., 2018), 1.281970 inhabitants live in the most dangerous classes, equal to 2.2% of the population (P3 + P4).

In class P4, no area shows changes of more than 1 ha in size.

Table 4.23 - Distribution of 111, 116, 122 and 123 classes in areas P4 in each Italian region during 16-17, 17-18 and 18-19 (ha).

	P4											
	16-17				17-18				18-19			
Region	111	116	122	123	111	116	122	123	111	116	122	123
Piemonte	0.4	0.1	4.6	0.4	0.4	0.2	3.1	0.0	0.0	0.1	0.8	0.0
Valle d'A.	0.1	0.1	2.5	0.0	0.0	0.0	-0.1	0.0	0.0	0.0	-1.1	0.0
Lombardia	0.1	0.0	0.1	0.0	0.2	0.0	-0.4	0.0	0.0	0.7	2.7	0.5
Trent. A.A.	0.0	0.1	0.0	0.0	0.0	0.0	-0.6	0.2	0.0	0.0	0.0	0.0
Bolzano	0.0	0.1	0.0	0.0	0.0	0.0	-0.6	0.2	0.0	0.0	0.0	0.0
Trento	0.0	0.0	0.0	0.0	0.0	0.0	0.0	0.0	0.0	0.0	0.0	0.0
Veneto	0.0	0.0	5.0	0.1	0.0	0.0	-1.1	2.0	0.1	0.0	0.0	-3.2
Friuli V G.	0.0	0.0	0.1	0.0	0.0	0.0	0.1	0.0	0.0	0.0	0.0	0.0
Liguria	0.1	0.0	0.2	0.0	0.0	0.0	0.1	0.0	0.0	0.0	0.6	0.0
Emilia R.	0.3	0.0	2.6	-0.6	0.0	0.1	1.3	0.7	0.2	0.1	-0.2	0.0
Toscana	0.1	0.0	0.7	0.1	0.0	0.0	0.9	1.5	0.0	0.0	0.5	1.5
Umbria	0.0	0.0	0.0	0.0	0.0	0.0	0.0	0.0	0.0	0.0	0.0	0.0
Marche	0.0	0.0	0.0	0.0	0.1	0.0	-0.3	0.0	0.0	0.0	0.0	0.0
Lazio	0.4	0.2	1.0	0.1	0.0	0.0	0.3	0.6	0.0	0.0	2.8	0.0
Abruzzo	0.1	0.1	0.5	0.0	0.0	0.0	0.5	0.1	0.2	0.0	4.1	0.0
Molise	0.0	0.1	0.3	0.0	0.0	0.0	0.4	0.0	0.0	0.0	0.4	-0.1
Campania	0.3	0.5	2.6	0.2	0.2	0.7	2.6	2.5	0.1	0.3	2.6	0.0
Puglia	0.0	0.2	0.0	0.0	0.0	0.0	0.0	0.0	0.0	0.2	1.1	0.0
Basilicata	0.0	0.0	0.0	0.0	0.1	0.0	-0.1	0.0	0.0	0.0	0.1	0.7
Calabria	0.0	0.0	0.2	0.0	0.0	0.0	-1.0	0.0	0.0	0.0	1.0	0.0
Sicilia	0.0	0.0	0.2	0.0	0.1	0.0	0.3	0.0	0.0	0.1	0.9	0.0
Sardegna	0.0	0.0	0.0	0.0	0.0	0.0	0.0	0.0	0.0	0.0	0.0	0.0
Italia	1.8	1.5	20.7	0.5	1.0	1.0	5.6	7.7	0.6	1.5	16.3	-0.6

4.2.3 Land consumption in Italy in areas of seismic hazards

The seismic hazard classification of the national territory is based on the analysis of the probability that the territory will be affected in a certain time interval (generally 50 years) by an event exceeding a certain intensity or magnitude threshold. For the third-level analyses, only the areas classified as S1 and S2 were used. These areas were processed by ISPRA according to National Institute of Geophysics and Volcanology reference data[32] and SNPA and are based on reference peak ground acceleration (PGA) with a 10 percent probability of exceedance in 50 years as illustrated in Table 4.24.

Table 4.24 - Seismic areas processed by ISPRA.

Class	Description
S1	PGA > 0,25±0,025
S2	0,15 < PGA ≤ 0,25±0,025

[32] https://doi.org/10.13127/sh/mps04/ag

4.2.3.1 National seismic hazards

In Italy, about 123,216 km^2 of the surface is classified as seismically hazardous area belonging to S1 and S2[33] (Table 4.25 and Figure 4.17). Areas at high seismic hazard account for 34.7% and those at very high hazard for 6.1%. Observing the land consumption between 16 and 17 in the areas at high seismic hazard (S2) we have a figure of 33.4% while in those at very high seismic hazard (S1) we find a value of 4.09%; between 17 and 18 we have respectively 36.6% and 3.49% and between 18 and 19, 38.1% and 3.9% (Table 4.26). Figure 4.17 shows the surfaces in ha of S2 and S1 interested by land consumption both reversible and permanent.

Table 4.25 - Artificial surface in S2 and S1 (in 2019) and seismic hazards classes and their extension in Italy.

Region	Artificial in S2 hazard area (ha) in 2019	Artificial in S1 hazard area (%) in 2019	Artificial in S2 hazard area (ha) in (2019)	Artificial in S1 hazard area (%) in 2019	% of tot S2 in Italy	% of tot S1 in Italy	TOT S1 + S2
Piemonte	9	0.1	0	0.0	0.1	0.0	8106.5
Valle d'A.	0	0.0	0	0.0	0.0	0.0	0.0
Lombardia	13864	13.3	0	0.0	1.0	0.0	104357.3
Trent. A.A.	717	2.7	0	0.0	0.3	0.0	26534.2
Veneto	79956	12.2	525	2.9	6.2	1.0	672582.1
Friuli V G.	39630	7.9	4541	4.0	4.8	6.1	615964.6
Liguria	3035	3.5	0	0.0	0.8	0.0	85825.1
Emilia R.	137067	8.8	0	0.0	14.9	0.0	1555529.8
Toscana	32079	4.7	0	0.0	6.6	0.0	689744.3
Umbria	38928	5.7	1210	2.1	6.5	3.1	739117.2
Marche	64591	6.9	78	1.9	8.9	0.2	938243.5
Lazio	45767	7.6	2365	2.2	5.7	5.8	705928.7
Abruzzo	28616	5.3	11276	2.9	5.2	20.7	922275.1
Molise	10064	3.6	4485	3.8	2.7	6.4	401004.1
Campania	64992	10.4	13365	6.9	5.9	10.5	816721.2
Puglia	30006	4.1	0	0.0	7.0	0.0	733288.4
Basilicata	17395	3.4	4183	3.5	4.9	6.4	637042.2
Calabria	36751	4.4	34983	5.8	7.9	32.5	1427104.0
Sicilia	86245	7.8	7937	5.8	10.6	7.3	1242287.6
Sardegna	0	0.0	0	0.0	0.0	0.0	0.0
Italia	729711	7.0	84946	4.6	100.0	100.0	12321655.9

Table 4.26 - Land consumption in S1 and S1 classes of seismic hazard in terms of hectares and percentages compared to national one.

Reference period	S2		S1		Italy	
	ha	%	ha		ha	%
16-17	1780,5	33,43	217,8	4,09	5326,1	100,00
17-18	2089,7	36,70	199,0	3,49	5694,3	100,00
18-19	1981,2	38,20	203,1	3,92	5186,4	100,00

Almost all of the changes have a classification at level 3. In the period 2017-2018, 93.6% of the total land consumption in the S2 area and 72.02 in the S1 area was classified at level 3. This is the lowest value while

[33] Data elaborated from: http://zonesismiche.mi.ingv.it/

in the other two years the value is above 98% (Table 4.27). The Figures 4.18 and 4.19 show the soil consumption between 2016 and 2019 divided in permanent and reversible in S1 and S2 seismic hazard areas in Italy.

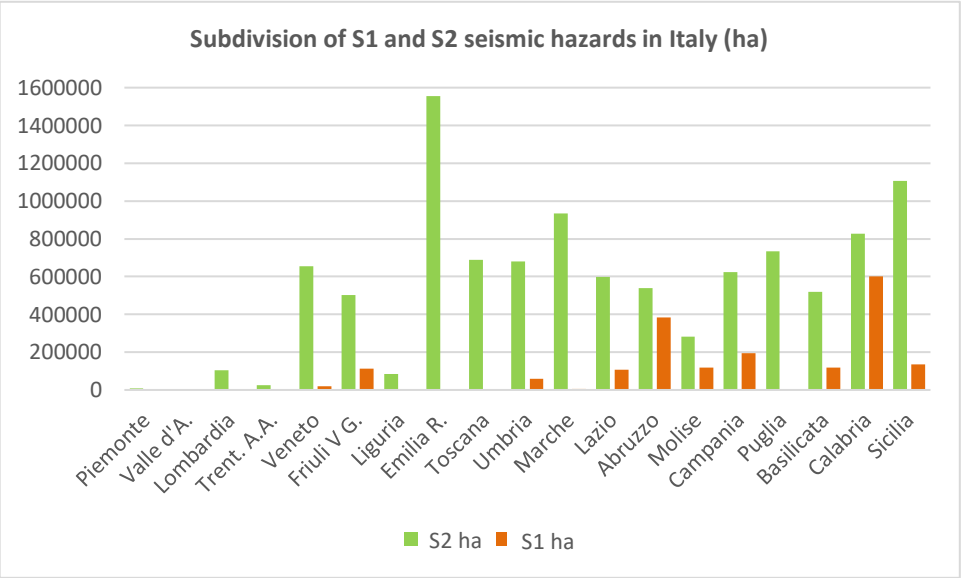

Figure 4.17- Surface in ha of S1 and S2 seismic hazards area in the Italian regions.

Table 4.27 - Land consumption mapped at 3rd level of detail in landslide hazard area.

Reference period	S2		S1	
	TOT 3rd level		TOT 3rd level	
	ha	%	ha	%
16-17	1780,54	98,38	217,75	99,71
17-18	2089,73	93,64	198,96	72,03
18-19	1981,17	99,82	203,14	99,85

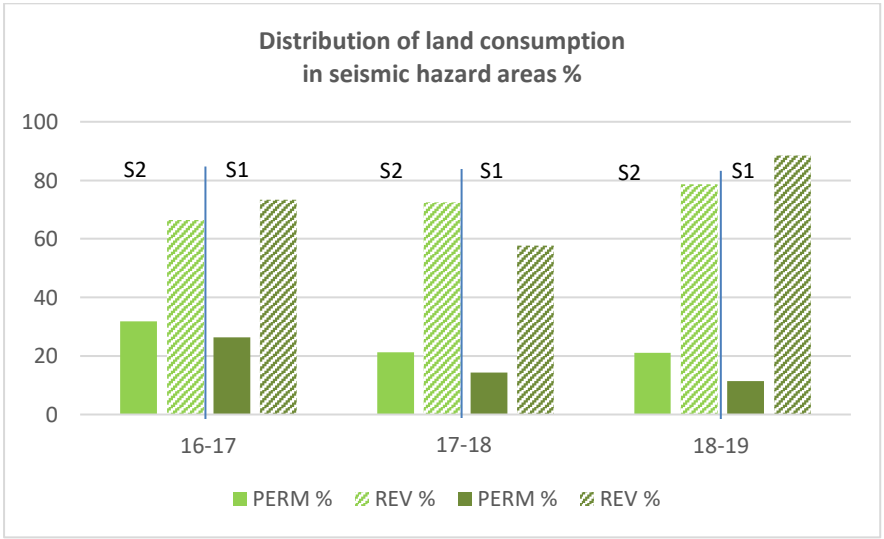

Figure 4.18 - Permanent and reversible land consumption in terms of hectares and percentages in S2 and S1 seismic hazard areas.

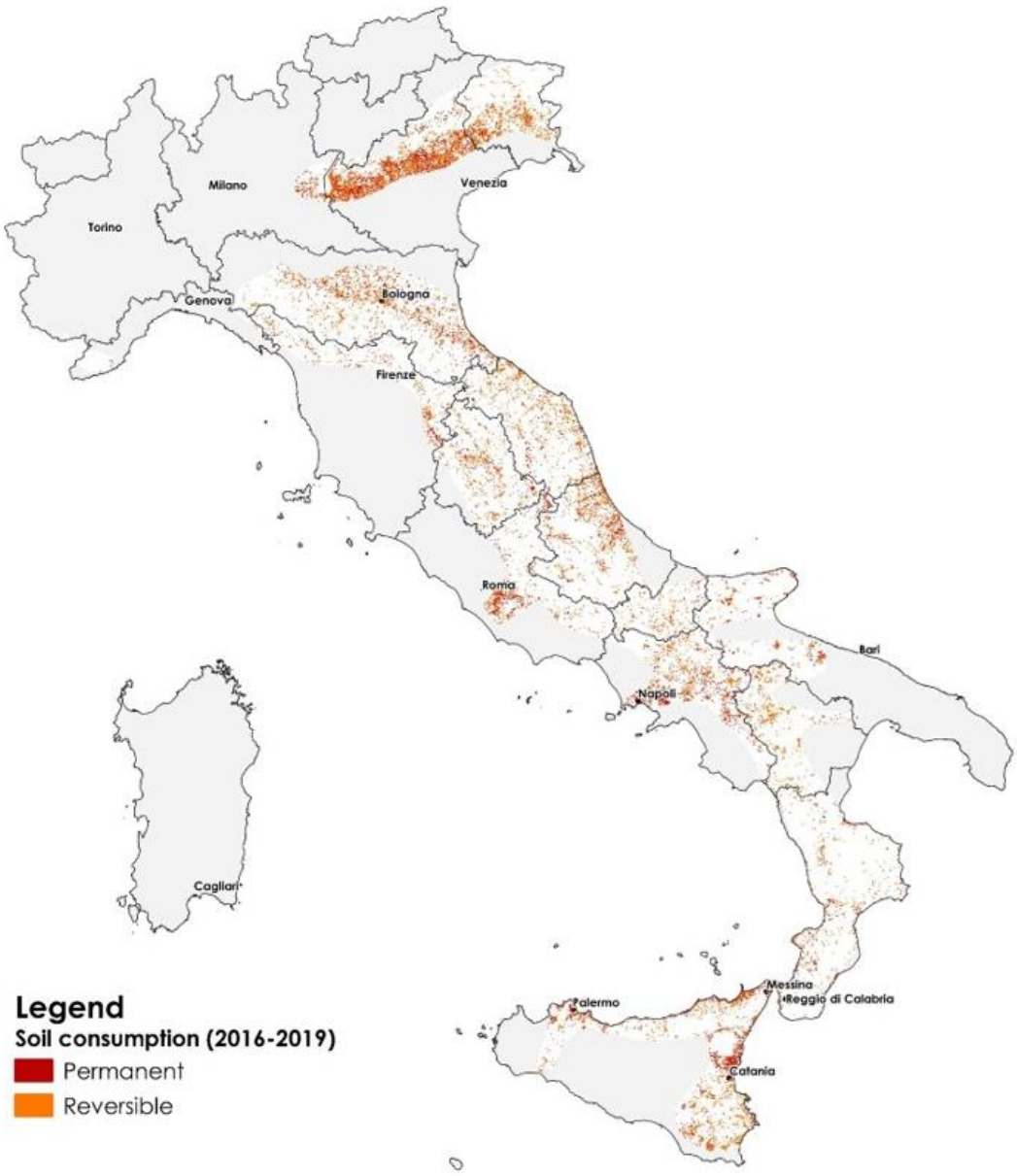

Figure 4.19 - Soil consumption between 2016 and 2019 divided in permanent and reversible in S1 and S2 seismic hazard areas.

The analysis of the transformations related to land consumption restoration and soil sealing shows how most of the changes occurred in the S2 hazard areas. The changes in these areas are over 10 times greater than those in the S1 range (Table 4.28).

The period 2017-2018 is the one with the greatest land consumption (black rectangles) in S2 zone, while for S1 areas, the land consumption remains fairly constant in the three observed periods. The restoration (green rectangles in Table 4.28) mainly affects the reversible land consumption in both hazard area, mainly due to the presence of construction site that are renaturalized at the end of the building activities. Soil sealing can take place in natural areas or in areas with reversible consumed soil: the first contribution is higher than the second in both areas and for all the years observed.

Table 4.28 - Table shows the transformation between classes 11 (irreversible land consumption) and 12 (reversible land consumption) in the different tree periods considered, in seismic hazard areas in ha.
Green areas represent transformations from built-up or reversible land consumption to natural areas (renaturation) while grey account for transitions from natural or reversible to built-up areas, i.e. irreversible land consumption.

S2 Seismic

	2017				
2016	1	11	12	2	Tot
1	-	161	152	8	321
11	0	-	88	7	95
12	1	149	-	198	347
2	37	575	1382	-	1994
Tot	**38**	**884**	**1622**	**214**	**-**

S1 Seismic

	2017				
2016	1	11	12	2	**Tot**
1	-	21	50	0	**71**
11	0	-	4	0	**4**
12	0	7	-	5	**12**
2	1	57	165	-	**223**
Tot	**1**	**85**	**219**	**5**	**-**

	2018				
2017	1	11	12	2	Tot
1	-	15	51	47	113
11	0	-	46	5	51
12	1	244	-	294	538
2	180	447	1808	-	2436
Tot	**181**	**707**	**1905**	**346**	**-**

	2018				
2017	1	11	12	2	**Tot**
1	-	2	1	1	**3**
11	0	-	1	0	**1**
12	0	17	-	13	**30**
2	57	29	127	-	**213**
Tot	**57**	**48**	**129**	**14**	**-**

	2019				
2018	1	11	12	2	**Tot**
1	-	0	0	0	**0**
11	0	-	18	3	**20**
12	0	365	-	253	**618**
2	4	422	1811	-	**2236**
Tot	**4**	**787**	**1829**	**255**	**-**

	2019				
2018	1	11	12	2	**Tot**
1	-	0	0	0	**0**
11	0	-	1	0	**1**
12	0	13	-	15	**28**
2	0	23	195	-	**218**
Tot	**0**	**36**	**196**	**15**	**-**

Main typologies of change in landslides hazard area

Table 4.29 shows the trends of the different typologies of land consumption in areas S1 and S2 during 16-17, 17-18 and 18-19 periods: the class 122 (*construction sites and other rammed-earth areas*) is the class in the third level of detail, where changes are most concentrated. More than 98% of the changes in S2 and more than three quarters of those in S1 fall into this class for all three periods observed. In the period 18-19 a large proportion of the S2 changes (17.2%) fall into class 121 (*dirt roads*). Class 111 (*buildings*) is significant in relation to permanent land use and is the second most important in all years and for both hazard areas, except for S2 area, in the period 18-19, where it is overtaken by dirt roads. It is significant that the extent of the areas affected by the appearance of new construction sites shows a downward trend, since in the period of reference it is reduced by one third in S2 and two thirds in S1 area.

4.2.3.2 Regional seismic hazards

Observing the regional distribution of changes in seismic zones, class 122 is characterised by the greatest extent of change in all regions, for all periods analysed and in both hazard areas.

Table 4.29 - Trends of the different typologies of land consumption in areas S3 and S4 during 16-17, 17-18 and 18-19 periods.

	S2						S1					
	16-17		17-18		18-19		16-17		17-18		18-19	
Class Code	ha	%	ha	%	ha	%	ha	%	ha	%	ha	%
111	258.46	15.06	216.22	11.50	200.66	11.03	28.8	13.7	13.0	9.3	10.8	5.3
112	72.19	4.21	38.39	2.04	27.00	1.48	1.5	0.7	5.6	4.0	1.1	0.5
113	0.16	0.01	0.13	0.01	0.00	0.00	0.0	0.0	0.4	0.3	0.0	0.0
114	0.62	0.04	0.03	0.00	16.62	0.91	4.8	2.3	0.0	0.0	0.0	0.0
115	0.08	0.00	0.00	0.00	2.91	0.16	0.2	0.1	0.0	0.0	0.0	0.0
116	202.84	11.82	174.01	9.25	160.64	8.83	19.9	9.4	9.6	6.9	10.1	5.0
117	13.75	0.80	3.34	0.18	7.30	0.40	2.2	1.0	0.1	0.1	0.0	0.0
118	3.17	0.18	2.74	0.15	0.04	0.00	0.0	0.0	0.0	0.0	1.1	0.6
121	38.72	2.26	80.83	4.30	26.35	1.45	4.0	1.9	8.3	6.0	31.0	15.3
122	1053.51	61.40	1279.21	68.01	1246.97	68.56	133.1	63.0	95.9	68.6	139.3	68.7
123	40.84	2.38	64.22	3.41	106.53	5.86	12.9	6.1	6.3	4.5	8.5	4.2
124	23.48	1.37	14.08	0.75	19.05	1.05	0.0	0.0	0.0	0.0	0.0	0.0
125	1.65	0.10	1.76	0.09	1.94	0.11	0.0	0.0	0.0	0.0	0.6	0.3
126	6.32	0.37	5.91	0.31	2.82	0.16	3.7	1.7	0.5	0.4	0.4	0.2
	1715.79	100.00	1880.87	100.00	1818.83	100.00	211.2	100.0	139.6	100.0	202.8	100.0

S2

The regions with the highest concentrations of changes are Sicily, Emilia Romagna and Veneto. Sicily and Emilia Romagna are in fact the two regions with the highest presence of territory in S2 class (respectively 10,57 and 14,8% of the total class) while in Veneto there is only 6,25% of the total surface classified as S2. However, it is the first region for land consumption with reference to class 111 in all three periods considered. Considering the periods 2016-17 and 2018-19, Veneto is ranked first for land consumption of class 122 and in 2016-2017 also for class 116. Although the trend is downward in S2 zone. Also significant is the increase in class 122 areas in Sicily, which more than tripled from 2016-17 to 2018-19, with values that increased from 84.5 ha to 267 ha (Table 4.30).

S1

Areas in class S1 are present in 11 of the 20 regions, but especially in Calabria (32.46%), Abruzzo (20.66%) and Campania (10.49%), where they account for almost two thirds of the total (Table 4.31). These three regions are particularly affected by the changes in relation to the three classes at the third level considered, in all three periods examined. In particular, Campania is the region with the largest area of land consumption in classes 116 and 122 between 2017 and 2019, although it has one third of its territory in class S1 compared to Calabria. In the latter there is a strong increase in land consumption in class 116, which more than tripled between 2016-17 and 2017-18. Looking at the growth values of class 111 they are high in Umbria between 2016 and 2018 and in Lazio in the period 2016-17 while the growth has drastically reduced in the last year. As evidence that the higher restrictions in these areas are effective, the changes in S1 are an order of magnitude lower than those in S2. Particularly in class 111, changes are low, indicating reduced building activity, although there are slight increases in 2016-17, presumably due to emergency activities following the earthquakes in central Italy. The highest values in this period in class 111 are indeed found in Lazio and Umbria but remain in any case limited to a few tens of hectares.

The analysis shows that, although the trend of increasing land consumption is below the national average, in these areas the construction and increase of both reversible and irreversible land consumption continues. The most affected classes are *Buildings*, *Other impermeable/paved areas, parking lots, squares, construction sites* and o*ther areas of compacted earth (sports fields, parking lots permanent storage of material, etc.),* which often turn into irreversible soil the following year. The map and the data produced can form the basis for further investigations in these areas that are subject to precise rules regarding new building.

Table 4.30 - Distribution of 111, 116, and 122 classes in areas S2 in each Italian region during 16-17, 17-18 and 18-19 (ha).

	16-17						17-18						18-19					
	111	111	116	116	122	122	111	111	116	116	122	122	111	111	116	116	122	122
Region	ha	%	ha	%	ha	%	ha	%	ha	%	ha	%	ha	%	ha	%	ha	%
Piemonte	0,0	0,0	0,0	0,0	0,0	0,0	0,0	0,0	0,0	0,0	0,0	0,0	0,0	0,0	0,0	0,0	0,0	0,0
Valle d'A.	0,0	0,0	0,0	0,0	0,0	0,0	0,0	0,0	0,0	0,0	0,0	0,0	0,0	0,0	0,0	0,0	0,0	0,0
Lombardia	6,1	2,4	0,2	0,1	5,8	0,5	4,3	2,0	5,7	3,3	6,7	0,5	14,4	7,2	3,7	2,3	35,2	2,8
Trent. A.A.	0,0	0,0	0,0	0,0	0,0	0,0	0,0	0,0	0,0	0,0	0,0	0,0	0,1	0,0	0,0	0,0	5,2	0,4
Veneto	99,8	38,6	89,5	44,1	304,4	28,9	54,7	25,3	33,5	19,3	260,3	20,3	44,1	22,0	8,8	5,5	110,2	8,8
Friuli V G.	14,9	5,8	5,1	2,5	68,6	6,5	8,7	4,0	3,5	2,0	107,8	8,4	9,7	4,8	5,4	3,4	74,5	6,0
Liguria	0,1	0,0	0,0	0,0	0,1	0,0	0,0	0,0	0,2	0,1	0,6	0,0	0,0	0,0	0,5	0,3	0,6	0,0
Emilia R.	42,9	16,6	18,9	9,3	169,6	16,1	51,1	23,6	24,0	13,8	223,5	17,5	38,6	19,3	24,3	15,1	170,5	13,7
Toscana	4,2	1,6	4,3	2,1	14,6	1,4	5,0	2,3	1,5	0,9	11,8	0,9	3,1	1,6	8,9	5,5	28,9	2,3
Umbria	5,1	2,0	3,9	1,9	70,4	6,7	4,1	1,9	9,0	5,2	49,4	3,9	4,8	2,4	4,3	2,7	37,6	3,0
Marche	13,4	5,2	14,8	7,3	44,0	4,2	13,9	6,4	3,0	1,7	147,0	11,5	16,4	8,2	13,4	8,4	166,8	13,4
Lazio	9,7	3,8	10,9	5,4	28,0	2,7	6,8	3,2	5,6	3,2	102,1	8,0	5,9	2,9	6,7	4,2	40,9	3,3
Abruzzo	11,3	4,4	9,2	4,5	60,3	5,7	4,1	1,9	3,3	1,9	48,3	3,8	8,4	4,2	11,2	7,0	108,6	8,7
Molise	1,3	0,5	0,7	0,3	16,2	1,5	1,6	0,8	1,3	0,7	11,4	0,9	1,2	0,6	1,9	1,2	8,6	0,7
Campania	14,3	5,5	16,5	8,1	76,2	7,2	10,2	4,7	17,1	9,8	47,9	3,7	7,8	3,9	17,0	10,6	46,6	3,7
Puglia	11,9	4,6	8,7	4,3	48,3	4,6	6,4	2,9	1,4	0,8	18,3	1,4	14,3	7,1	15,0	9,3	59,5	4,8
Basilicata	0,6	0,2	1,5	0,7	31,0	2,9	1,9	0,9	0,9	0,5	57,7	4,5	6,5	3,3	2,1	1,3	26,7	2,1
Calabria	2,1	0,8	2,0	1,0	31,4	3,0	4,3	2,0	2,4	1,4	38,8	3,0	3,4	1,7	1,7	1,0	59,7	4,8
Sicilia	20,7	8,0	16,6	8,2	84,9	8,1	39,1	18,1	61,7	35,5	147,8	11,6	21,7	10,8	35,9	22,4	267,0	21,4
Sardegna	0,0	0,0	0,0	0,0	0,0	0,0	0,0	0,0	0,0	0,0	0,0	0,0	0,0	0,0	0,0	0,0	0,0	0,0
Italia	258	100	203	100	1054	100	216	100	174	100	1279	100	201	100	161	100	1247	100

Table 4.31 - Distribution of 111, 116, and 122 classes in areas S4 in each Italian region during 16-17, 17-18 and 18-19 (ha).

	100	100	100	100	100	100	100	100	100	100	100	100	100	100	100	100	100	100
	16-17			**17-18**			**17-18**						**18-19**					
	111,0	111	116,0	116	122,0	122	111	111	116	116	122	122	111	111	116	116	122	122
Region	ha	%	ha	%	ha	%	ha	%	ha	%	ha	%	ha	%	ha	%	ha	%
Piemonte	0,0	0,0	0,0	0,0	0,0	0,0	0,0	0,0	0,0	0,0	0,0	0,0	0,0	0,0	0,0	0,0	0,0	0,0
Valle d'A.	0,0	0,0	0,0	0,0	0,0	0,0	0,0	0,0	0,0	0,0	0,0	0,0	0,0	0,0	0,0	0,0	0,0	0,0
Lombardia	0,0	0,0	0,0	0,0	0,0	0,0	0,0	0,0	0,0	0,0	0,0	0,0	0,0	0,0	0,0	0,0	0,0	0,0
Trent. A.A.	0,0	0,0	0,0	0,0	0,0	0,0	0,0	0,0	0,0	0,0	0,0	0,0	0,0	0,0	0,0	0,0	0,0	0,0
Veneto	0,0	0,0	0,0	0,0	0,1	0,1	0,0	0,1	0,0	0,4	1,2	1,2	0,0	0,0	0,0	0,0	0,1	0,1
Friuli V G.	0,9	3,2	0,8	3,8	5,1	3,8	0,7	5,3	0,0	0,0	5,0	5,2	0,0	0,4	0,0	0,0	3,0	2,2
Liguria	0,0	0,0	0,0	0,0	0,0	0,0	0,0	0,0	0,0	0,0	0,0	0,0	0,0	0,0	0,0	0,0	0,0	0,0
Emilia R.	0,0	0,0	0,0	0,0	0,0	0,0	0,0	0,0	0,0	0,0	0,0	0,0	0,0	0,0	0,0	0,0	0,0	0,0
Toscana	0,0	0,0	0,0	0,0	0,0	0,0	0,0	0,0	0,0	0,0	0,0	0,0	0,0	0,0	0,0	0,0	0,0	0,0
Umbria	7,9	27,2	0,1	0,4	15,1	11,3	5,4	41,4	1,9	19,8	5,2	5,4	0,2	2,1	0,0	0,0	1,1	0,8
Marche	0,1	0,3	10,0	50,3	0,0	0,0	0,0	0,0	0,0	0,0	2,2	2,3	0,0	0,0	0,0	0,0	0,0	0,0
Lazio	9,6	33,1	0,8	4,1	12,1	9,1	0,0	0,2	0,7	7,4	0,4	0,5	0,0	0,0	0,0	0,0	1,2	0,9
Abruzzo	2,1	7,4	0,8	4,0	14,0	10,5	0,1	0,9	0,0	0,0	16,5	17,2	2,9	26,9	0,6	5,9	14,6	10,5
Molise	1,0	3,3	0,0	0,0	6,2	4,6	0,3	2,0	0,1	1,5	4,0	4,2	0,9	8,7	0,5	5,0	5,4	3,9
Campania	2,6	8,9	2,9	14,7	20,4	15,3	1,6	12,4	4,8	50,1	20,0	20,9	0,9	8,2	4,8	47,6	32,1	23,1
Puglia	0,0	0,0	0,0	0,0	0,0	0,0	0,0	0,0	0,0	0,0	0,0	0,0	0,0	0,0	0,0	0,0	0,0	0,0
Basilicata	0,3	1,0	0,0	0,0	7,5	5,6	0,3	2,1	0,0	0,0	6,5	6,8	1,2	11,4	1,1	10,4	7,1	5,1
Calabria	3,8	13,1	3,5	17,6	37,3	28,0	4,1	31,5	1,4	14,9	17,1	17,8	3,8	35,7	1,0	9,7	40,5	29,0
Sicilia	0,7	2,5	1,0	5,2	15,5	11,6	0,6	4,3	0,6	5,9	17,8	18,5	0,7	6,6	2,2	21,4	34,2	24,6
Sardegna	0,0	0,0	0,0	0,0	0,0	0,0	0,0	0,0	0,0	0,0	0,0	0,0	0,0	0,0	0,0	0,0	0,0	0,0
Italia	28,8	100,0	19,9	100,0	133,1	100,0	13,0	100,0	9,6	100,0	95,9	100,0	10,8	100,0	10,1	100,0	139,3	100,0

4.3 Land consumption for Landslide Susceptibility Mapping

LSM is the representation of the spatial probability of landslide occurrence and it can be defined as a form of spatial prediction of landslide hazard based on the correlation between known landslide locations and the spatial arrangement of a set of predisposing factors (Corominas et al., 2003; Fell et al., 2008).
The scientific literature is rich of different methodologies to produce LSM (Reichenbach et al., 2018), ranging from simple bivariate statistical methods like frequency ratio (Chung & Fabbri, 2003; Kavoura & Sabatakakis, 2020; Yilmaz, 2009), logistic regression, discriminant analysis (Stephan Arnold, Barbara Kosztra, Gebhard Banko, Pavel Milenov et al., 1983), to complex machine learning algorithms like ANN (Ermini et al., 2005; Lee et al., 2004), RF (Catani et al., 2013; Xiao et al., 2020; Youssef et al., 2016). Of course, besides the statistical techniques used to perform the susceptibility assessment, also the input data are very important since their selection, their number and their parameterization can largely influence the quality of the results (Catani et al., 2013; Segoni et al., 2020).
Morphometric parameters are very used in landslide susceptibility studies such as slope gradient, curvature, aspect, terrain roughness, just to name a few; also vegetation indexes (e.g. the NDVI index) (Pradhan et al., 2010; Sezer et al., 2011) or land-use or land-cover thematic maps (Bălteanu et al., 2010; Shu et al., 2019), derived from remotely sensed data, constitute another series of important products in LSM.
Concerning land cover data, the CLC dataset has been representing for years the only complete and homogeneous mapping in Europe. Despite the undoubtful usefulness of CLC data in LSM and geographical studies in general, the classification system and the spatial resolution prevent from an optimal use in very detailed analysis, as pointed out in the previous section.

In particular a land consumption is widely acknowledged to have a connection with hydro-geomorphological hazards, because it can completely change the hydrological system of hillslopes and catchments (Acquaotta et al., 2019; Chen et al., 2013; Pistocchi, 2017); however, based on a deep analysis of literature, a statistical correlation with landslide susceptibility has never been attempted. The third objective of this thesis, developed as part of the monitoring of land degradation, is therefore to use, for the first time, the land consumption elaborated according to methodology presented in chapter 3, as an additional input parameter in a landslide susceptibility assessment. Different approaches to use land consumption were tested and quantitatively evaluated to define which is the most useful to improve landslide susceptibility assessments.

4.3.1 Variables used and test description

The test site is a 3100 km^2 area located in the Northern Toscana (Italy) and it was selected because of the availability of several high-quality datasets and because it is very prone to landslides (Battistini et al., 2017). The main landslide types affecting the area are rotational, translational and compound slides, slow earth flows, complex movements (mainly slides evolving into flows) and, to a lesser extent, debris flows. From a lithological point of view, the bedrock of the area is mainly composed by layered flysch rocks and by metamorphic rocks (phyllite and schists). The mountains are covered by forests and are sparsely urbanized, the main villages and cities are located in the valley floors and in the surrounding hills. The sectors of the area occupied by wide alluvial plains were excluded from the analyses because landslides are not a geomorphological process occurring in a similar setting.

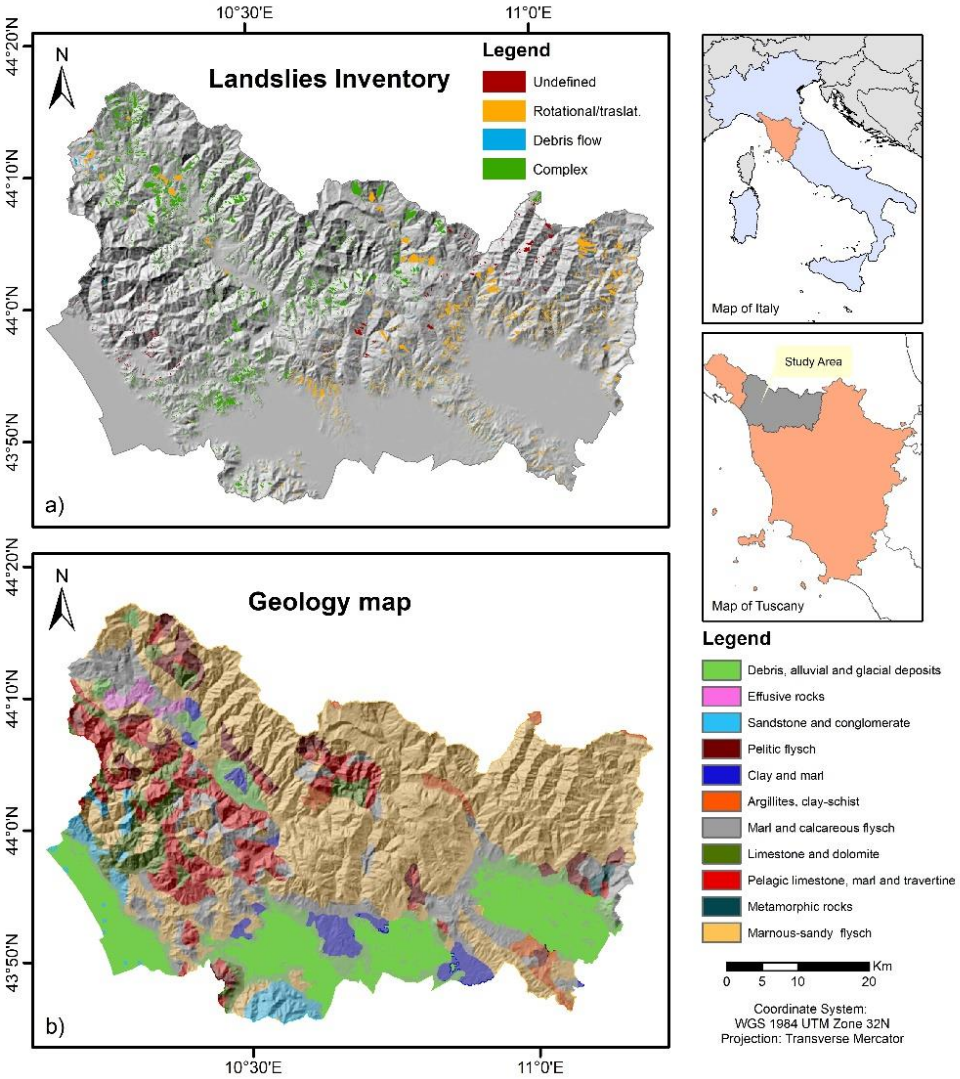

Figure 4.20 - Landslides inventory map (a), and geological map (b) showing the geographic location and main lithological units of the study area.

To carry out this analysis RF algorithm was used. RF can be used to solve classification and regression problems and it is a well-established technique in LSM because it is very flexible (Brenning, 2005; Catani et al., 2013; Xiao et al., 2020): it can use at the same time categorical and continuous numerical variables, it can better exploit complex information provided by many variables, it can handle multicollinearity and it is relatively robust with respect to overfitting issues. In RF model the trees are created by drawing a subset of training samples through replacement (a bagging approach). To create the dependent variable for the landslide susceptibility assessment, the catalogue of landslides IFFI (Inventory of landslides in Italy) published by ISPRA was used. A total of 7799 landslides were identified in the study area: most of them are mapped as complex movements (typically rotational/translational slides evolving into slow earthflows) or as rotational/translational slides and are classified according to Figure 4.20 (the figure shows also the main lithological units presents in the study area). The susceptibility analysis considers only these two typologies, as their triggering mechanism and causative factors are the same. Debris flows and landslides with unspecified typologies of movements were excluded from the analysis, since the objective of this study.

The production of a landslide susceptibility map requires the knowledge of the spatial distribution and interactions of various explanatory variables, which allow landslide-prone areas to be defined, independent of temporal controls, and indicate where landslides may be likely to occur in the future (Chacón et al., 2006). There is no consensus about which is the optimal set of explanatory variables to be used in susceptibility

studies and probably an optimal set is something very relative as it may vary according to the landslide type, to the characteristics of the study area and to the characteristics (e.g. spatial resolution or scale) of the available datasets. However, the main objective of this study is not the production of the best possible susceptibility map, but to explore the possibility to use a new explanatory variable derived from soil sealing monitoring data. As a consequence, a very limited set of parameters was used to define the base configuration of the susceptibility model: the "base parameters" were selected among the most used according to a literature review of general landslide studies (Reichenbach et al., 2018) and studies focused on the same test site (Segoni et al., 2016, 2018). The base parameters are Lithology (classified according the legend in Figure 4.20) Land use / land cover (derived from CLC and reclassified in 9 classes), Aspect, Elevation, Slope gradient, Planar curvature and Flow accumulation, all these data have a spatial resolution of 100 m. The Figure 4.21 summarise the main characteristic of methods used.

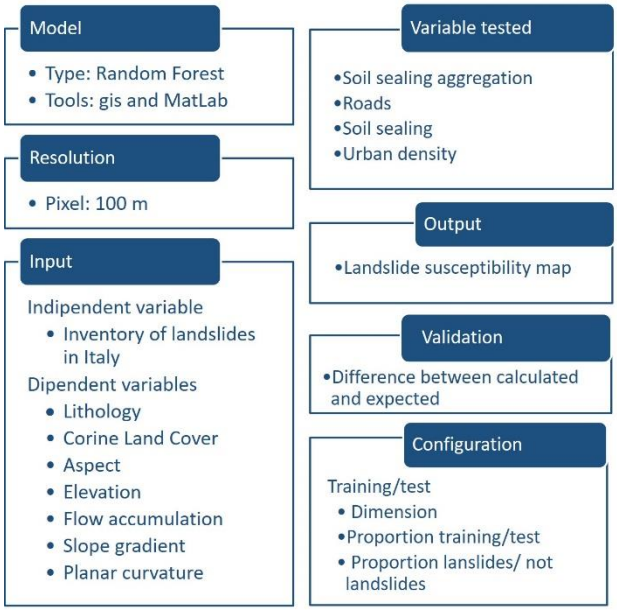

Figure 4.21 - Main characteristic of methods used.

This study aims to investigate whether soil sealing data can be conveniently used in landslide susceptibility mapping models. This variable is released by ISPRA through updating methodology as showed in previous section. The soil sealing is used as raw data to derive some parameters to be tested as explanatory variables in landslide susceptibility assessments. Indeed, the original soil sealing map contain very basic information (dichotomic classification between sealed and not-sealed soil) at high spatial resolution (10m) and some alternate approaches may be needed to convert this information into continuous variables, or to aggregate it at different pixel sizes. As instance, in this application it was decided to work at 100m spatial resolution, since this mesoscale has been acknowledged to be a good compromise in landslide susceptibility studies (Arnone et al., 2016; Catani et al., 2013) and the approach used to upscale the 10m original soil sealing map could influence the final results. The tested parameters are Soil sealing, Urbanization, Soil sealing aggregation (percentage of sealed soil) and Roads. Soil sealing (SS) is the most similar to the original land consumption: since the original raw data consists of a raster at a resolution of 10 m in which each cell can assume values 1 or 2; Urbanization (URB) represents a part of soil sealed, low-density urbanised areas, built areas with high density of urbanization; Soil sealing aggregation (SSA) was calculated using soil sealing high layer at 10 m resolution, where integer values in the range from 0 to 100, represent the percentage of soil sealed within each 100m pixel; Roads (ROA) considers the main and secondary communication routes, and practically all types of roads have been selected. As for SSA, the value of each cell represents the percentage of surface area affected by roads (asphalted and not) in relation to the area of the cell itself (1 ha). This

variable accounts for the disturbance of roads in the hillslope system. All these rasters were resampled to 100 m of resolution as the other data (Figure 4.22).

To train the susceptibility model 15557 randomly selected points were considered. The constraints for the random selection were set as follows: half of them were randomly sampled within landslide areas, the other half was sampled in areas outside landslide polygons.

The dataset was divided in a 70% subsample for model training and a 30% subsample for independent verification and testing. Within the subsamples, the balance between landslide and non-landslide conditions is kept at 50%-50%.

The validation of the susceptibility assessment is performed in terms of AUC (area under receiver-operator characteristic curves), a quantitative index widely used in landslide susceptibility studies to quantify the overall predictive effectiveness of a model (Fawcett, 2006; Frattini et al., 2010; Reichenbach et al., 2018). The relative importance of each parameter used within a model configuration is quantitatively expressed by the OOBE (out of bag error), an estimation of the relative error that the model would commit if a given parameter is omitted.

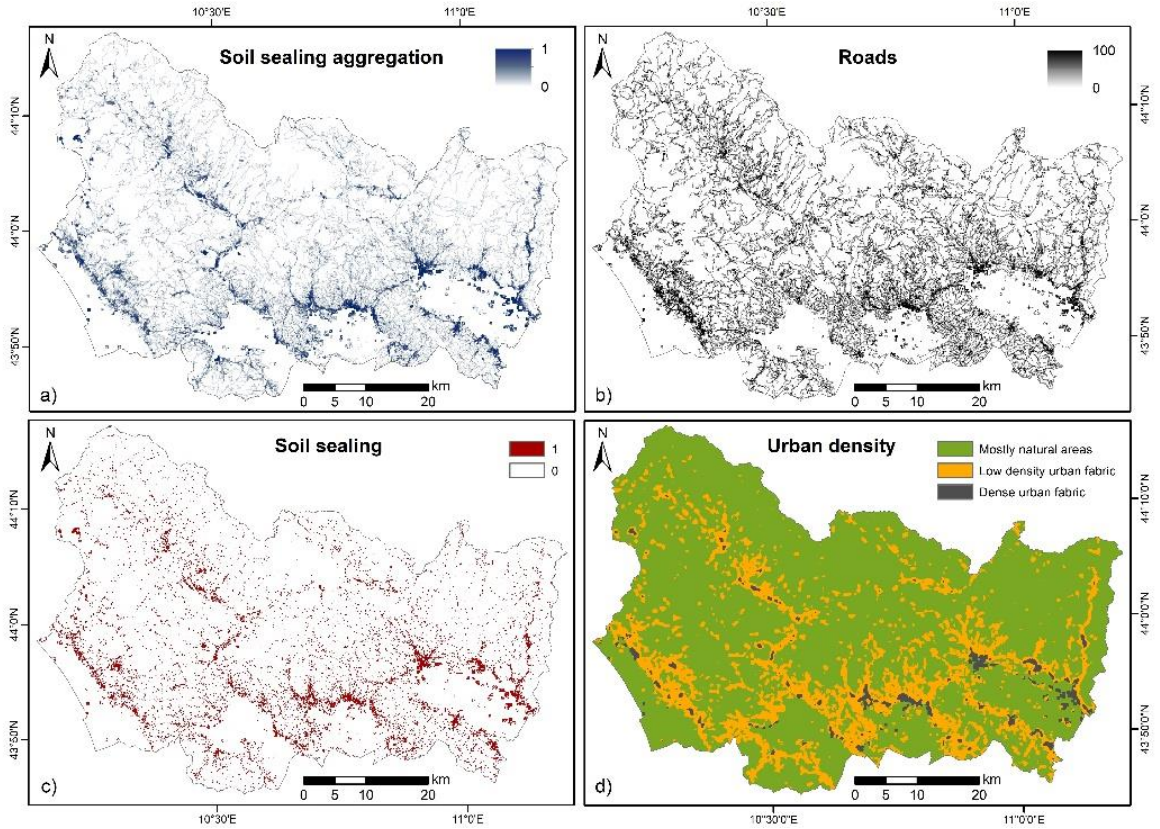

Figure 4.22 - Raster maps of the parameters derived from soil sealing and used as input parameters in landslide susceptibility analysis: (a) Soil sealing aggregation (SSA); (b) Roads (ROA); (c) Soil sealing (SS); (d) Urban density (URB).

A series of tests was conceived to assess whether soil sealing can provide a useful contribution in landslide susceptibility mapping and which soil sealing parameterization provides the best outcomes.

The first test was performed using only the basic parameters (base configuration), while a second test was carried out using all the basic parameters together with all the soil sealing parameters. The first test allows to analyse the performance of the model in a basic and standard configuration, establishing a benchmark for further comparisons with other sets of input parameters. The second one allowed to calculate the relative importance of each variable when all of them are considered together: the objective

of this test is to have a direct comparison of the importance of all the parameters, as expressed in terms of OOBE values.
The last group of tests was carried out adding to the base configuration each time a single soil-sealing-derived variable. For each configuration, the mean and maximum AUC was calculated, and the histogram of variables importance expressed in terms of OOBE was defined.

4.3.2 Results and landslides susceptibility map

The AUC values obtained by the validation of the different model configurations are showed in Figure 4.23. The base configuration reports the lowest accuracy (AUC = 0.65), thus indicating that soil sealing information has the potential to improve the accuracy of the susceptibility assessments. However, the results are very sensitive to the different parameterizations of soil sealing information: some of the soil sealing derived parameters produce only a very limited improvement to the performances of the model (SS, URB), while others bring a more marked contribution (ROA, SSA). The joint use of all the variables together returns intermediate results. The configuration that returned the best validation statistics is the one using the soil sealing aggregation (SSA) parameter, with an AUC of 0.74, showing that soil consumption can be used as an important feature in the landslide susceptibility mapping.
Another outcome of the test that can be used to investigate the impact of soil sealing derived parameters in the landslide susceptibility assessment is the comparison of OOBE values, which are indicators of the relative importance of each variable used. Figure 4.24 shows that the relative importance of the main morphometrical parameters is does not vary significantly from a configuration to another: slope gradient, elevation, curvature and flow accumulation are the most important parameters, followed by the categorical variables “lithology” and “land cover”.

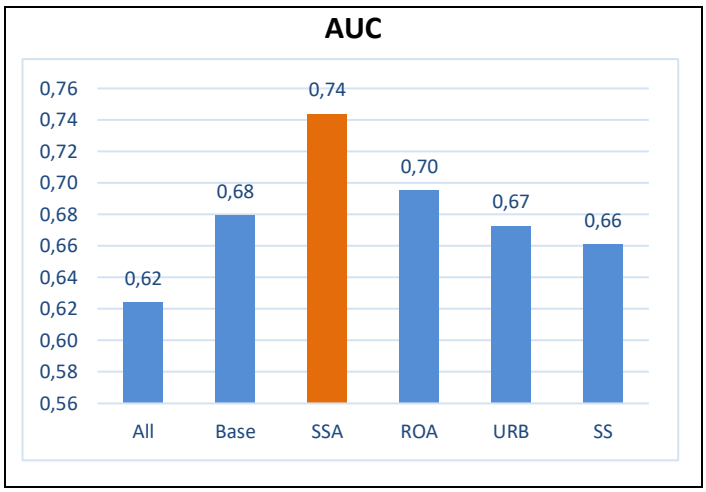

Figure 4.23 - Results of different tests.

The soil sealing derived parameters have a ranking (and a relative importance) that is clearly connected to the quality of the results observed with the AUC: the most effective parameter (SSA) has an OOBE value very close to lithology and land cover and markedly higher than the variable “aspect”. The parameter accounting on roads (ROA) has a ranking higher than aspect but the OOBE is lower than CLC and lithology. The other two soil sealing derived parameters are ranked as the least important parameters (thus, still with a positive impact on the modelling), and this is reflected by the low AUC values of the derived susceptibility assessments (but slightly higher than the base configuration).

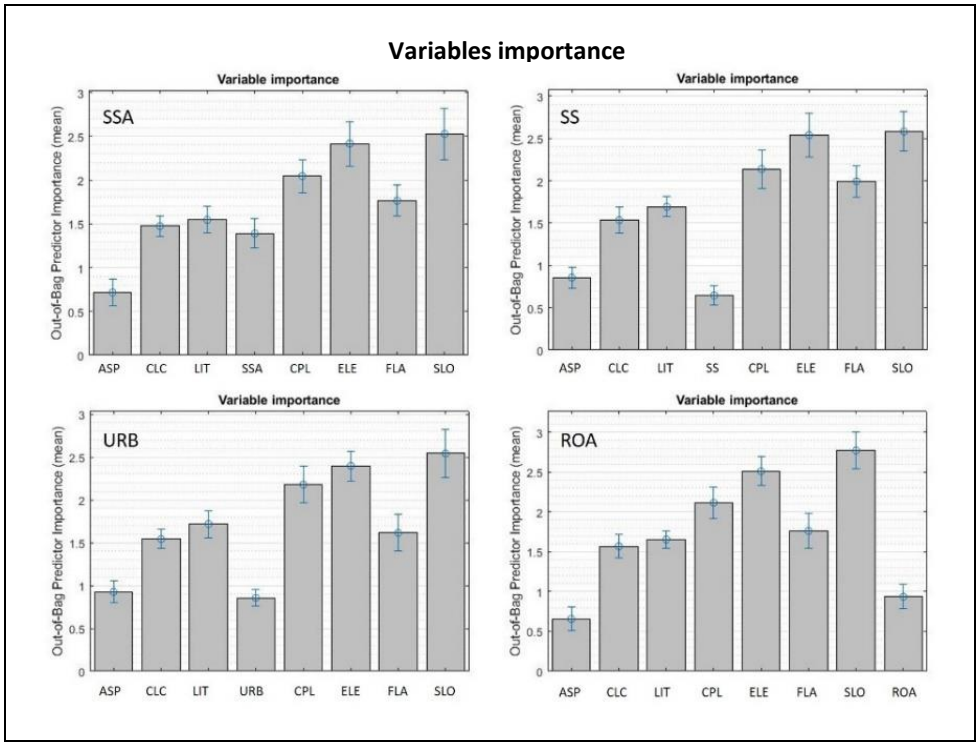

b)

Figure 4.24 – AUC values of different configurations.

Figure 4.25 shows the susceptibility map obtained using the best configuration (the one including the parameter "soil sealing aggregation").

The number of classes was set to 4, according to the Italian national regulation about landslide hazards, and the widely used by several authors (Aleotti & Chowdhury, 1999; Youssef et al., 2016). According to this classification, low susceptibility zones occupy the 32% of the study area and moderate, high and very high zones occupy the 32%, 27% and 10%, respectively.

4.3.3 Discussions

The outcomes of the analyses demonstrated that soil sealing information can have a positive influence in regional scale landslide susceptibility assessments, but the results are sensitive to the approach used to parametrize soil sealing.

Since in Italy soil sealing raw data are characterized by a very fine spatial resolution (10m pixels) and a coarse information (dichotomous classification in sealed and not-sealed pixels), the application to susceptibility models based on wider spatial units requires the derivation of parameters and many approaches could be pursued. In this study we introduced, tested and compared four approaches, based on four different soil-sealing-derived variables.

The best configuration corresponds to the one that uses the soil sealing aggregation variable, with an AUC value of 0.74 and higher ranking and OOBE value reached by SSA with respect to other soil sealing derived parameters.

Among the tested variables, SSA includes the most detailed information, with continuous values ranging from 0 to 100 representing the degree of sealing (and thus the degree of anthropogenic "disturbance") in each 100 m * 100 m cell used as spatial unit in the susceptibility analysis. It is worth highlighting that to create this variable the pixel size is upscaled from 10 m (the native resolution of the raw soil sealing map) to 100 m, but the coarser spatial resolution does not lead to a loss of effectiveness. This outcome is important as it leaves open other possibilities of application with different spatial units like basins or

geomorphic units, which, although less common (Reichenbach et al., 2018), are receiving a growing attention (Alvioli et al., 2016; Rossi et al., 2010; Van Den Eeckhaut et al., 2009).

The configuration encompassing SSA is the only one returning an AUC higher than 0.70 which is used by some authors as the limit to "good" results (Arabameri et al., 2019). Indeed, in the susceptibility mapping literature it is common to find even higher AUC values, but the main objective of this work is assessing the sensitivity to soil sealing parameterization and identifying some promising parameter derived by soil sealing products. For this reason, only a few morphological and thematic parameters have been used as explanatory variables of the susceptibility model, to avoid that the impact of soil sealing derived features would be shadowed. It is not excluded that other scholars could use the SSA parameter inside a more complex susceptibility model and to get better results in terms of AUC. For instance, other authors in the same test site obtained an AUC of 0.84 by using a RF model with 23 explanatory variables (Segoni et al., 2016).

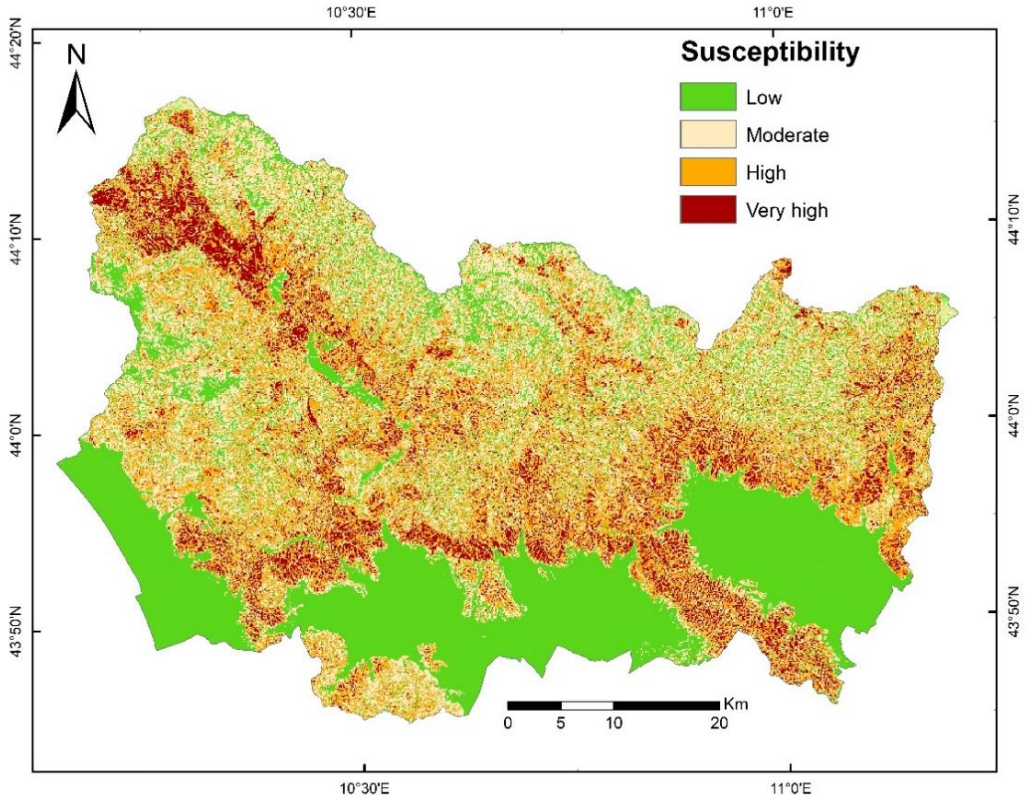

Figure 4.25 - Landslide susceptibility map using the soil sealing aggregation (SSA) variable, reclassified according to Jenks method, based on natural breaks.

The second-best result is given by the roads, with an AUC of 0.70 and a higher ranking and OOBE than SS and URB. ROA was structured as a continuous variable ranging from 0 to 1, each cell representing the percentage of area occupied by roads of every typology, from large highways to small paved roads. Conceptually, ROA is a subset of SSA: while the former quantifies the disturbance of roads on the hillslope system, the latter quantifies the disturbance driven by every human structure. Relatively to susceptibility mapping, in this study the latter seems to be more significant and to foster better results. This outcome should not be surprising since: roads are widely acknowledged as one of the most important human-related landslide predisposing factors, especially when built with cut-and-fill techniques, but the same can apply also to every other human asset, including buildings, as pointed out by a growing number of examples in literature (Mendes et al., 2018; Notti et al., 2015; Zhang et al., 2012). In this perspective, the use of road network is clearly only a partial information, while a good (i.e. spatially accurate and timely updated) soil

sealing map like the ones used in this research have the potential to hold a more complete information that can be conveniently used in landslide susceptibility mapping.
Another important test is the one using all soil sealing related parameters altogether (ALL model configuration). RF technique is acknowledged to be able to handle many parameters even if related each other and with collinearity issues. However, the joint use of SSA, SS, URB and ROA does not provide satisfactory results (AUC = 0.68). This outcome can be interpreted as an evidence of the effectiveness of SSA parameter.
Many scientific papers use Land Cover maps as an input variable, and the influence of this parameter is widely recognized. This is confirmed by our results, since land cover has a positive influence on the susceptibility assessment. However, it is important to remark that land cover is outperformed by soil sealing aggregation (higher ranking and OOBE value). Although CLC presents a good thematic detail, it is less effective in spatial resolution (25 ha minimum mappable unit) than soil sealing thematic maps, and this is probably the main reason of the lower forecasting effectiveness. Consequently, the possibility of using land consumption to improve landslide susceptibility assessments brings two advantages: a fine spatial resolution of 10 m of the raw data and a good temporal resolution as the soil sealing thematic layers in Italy and in other European countries is updated at an annual frequency. The latter point is particularly important also in the perspective of timely updates of hazard assessments.

4.4 Rapid change detection to monitor natural damages

Storm events are quite dangerous natural phenomena because they not only cause considerable economic damage and due to climate changes, these events are expected to increase in the future. To mitigate the impacts of extreme events and select the proper management actions, a rapid assessment of forest damages is fundamental for human security, for timber management, and for ecosystem conservation. The planning and execution of forest operations could take great advantage by the availability of rapid information from satellite data, in order to locate the sites and to estimate the extent of damages, since in this situations it is difficult to work in impacted and often remote forest areas.

4.4.1 Mapping changes after Vaia Storm

This case study was conducted in Northern Italy affected areas 29 October 2018 by VAIA storm with winds exceeding 200 km/h. Three regions: Friuli Venezia Giulia, Trentino Alto Adige, and Veneto have suffered substantial damage, estimated in about 42500 ha of forest resources destroyed (Figure 4.26).
The use of remote sensing data provides an excellent tool for the automatic identification of areas affected by the Vaia event in the north-east of Italy. The optical images, in fact, detect very well the presence/absence of vegetation caused by this type of event, moreover, the integration with SAR techniques allows to overcome the problem of cloud cover normally present in adverse weather conditions, such as the Vaia event.
The basic idea behind the use of SAR data is in the fact that the backscatter is not only influenced by the size, orientation and pattern of the trees, but also by the phenological change of the leaves in the case of broadleaved. Therefore, it is possible to identify changes in forest structure caused by storms. There are not yet many studies that exploit this potential. Few studies proved the value of SAR data in the context of detection of forest windthrows, including: a multi-sensor based research conducted by (Schwarz et al., 2003), who compared the results obtained with SAR data against those from optical data or the detection of area hits by storm events in Germany and Switzerland based on Sentinel 1 C-band data(Rüetschi et al., 2019).
The aim of this case study is to contribute to the development of knowledge to operationally exploit the complementary characteristics of free satellite data for mapping changes after a disaster event. To this end,

the potential of Sentinel 1 and Sentinel 2 data for the detection of areas impacted by the Vaia storm. was evaluated in the framework of rapid assessment of land processes.

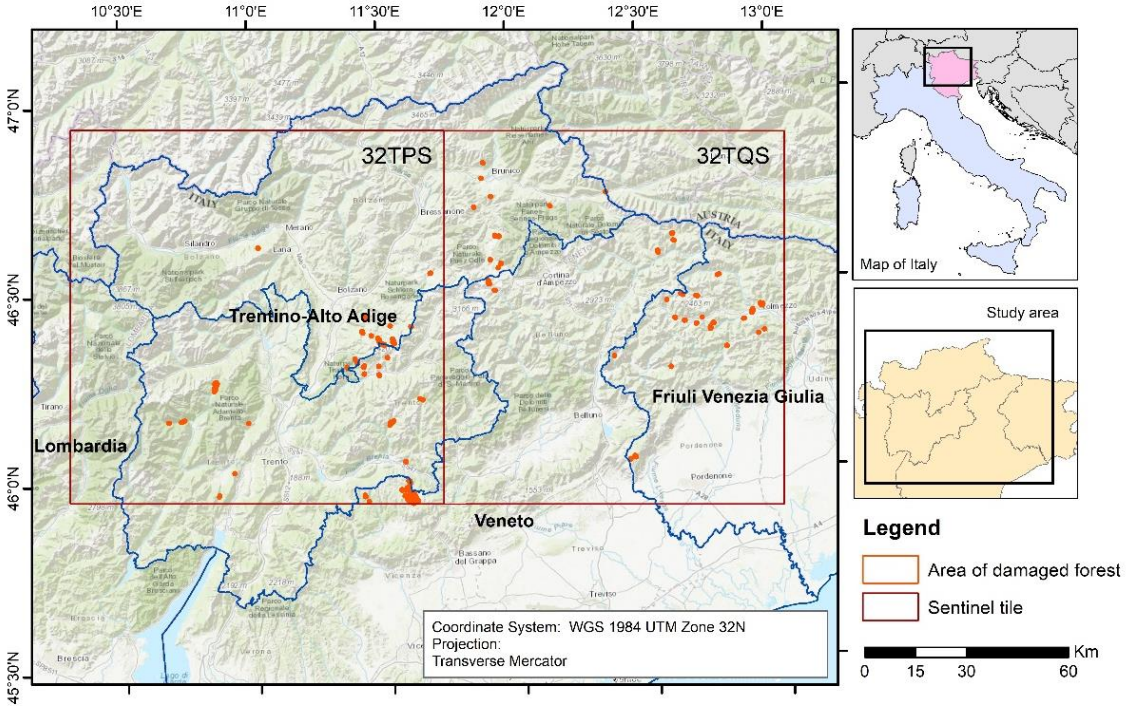

Figure 4.26 - Study area, Northern Italy; in red the 209 polygons used for training, cross validation and testing; in orange the rectangles of Sentinel 2 tiles.

Two different algorithms were considered for classification area hits by the storm event k-Nearest Neighbors approach, and RF evaluating the impact of algorithm choice on results.

The ground truth are polygons that identify the areas affected by the windthrow and they were provided by regional authorities. The polygon derived from regional dataset were filtered according to following criteria (i) polygons >2 ha, to include areas compatible with the spatial resolution -and thus the detection capability- of the remote sensing data used in this study; (ii) polygons in which the average terrain slope was below 20% in at least 85% of the surface, to exclude areas of distortion in SAR data; (iii) for the Veneto region only, polygons in which the amount of damaged trees resulted > 80% (representing more than 40% of the Veneto polygons).

The damage and not damage datasets included a total of 209 polygons, 104 from healthy forest stands, and 105 from damaged forest areas). Of this data, 90% were used as training area and the remaining 22 areas were used as independent test set for double assessment of the overall accuracy. The areas not affected by the storm were used in the classification; these polygons were manual photo-interpreted using high-definition Google Earth imagery.

Also, in this case the Google Earth Engine platform was used to process Sent1 images to generate a calibrated, ortho-corrected product at 10 m spatial resolution in dual-band cross polarization mode (VV – VH). Preprocessing included thermal noise removal, radiometric calibration, and terrain correction using a digital terrain model (SRTM 30 m). Free R software was used to calculate the vegetation indexes, to processes the single Sentinel 2 and to perform the classifications. Only bands at 10 - 20 m spatial resolution were used for tests (bands # 2, 3, 4, 5, 6, 7, 8, 8A, 11, 12), resampling at 10 m, the 20 m bands with a nearest neighbor approach.

Table 4.32 - List of vegetation indices used for tests.

Sensor	Index		Formula
Sentinel 2	NDVI	Normalized Difference Vegetation Index	(B8-B4)/(B8+B4)
	NBR	Normalized Burn Ratio	(B8 – B12)/(B8 + B12)
	NDVI2	Normalized Difference Vegetation Index 2	(B12-B8)/(B12+B8)
	SR	Simple Ratio	B8/B4
	ARI1	Anthocyanin Reflectance Index 1	1/B3-1/B5
	EVI	Enhanced Vegetation Index	2.5*(B8−B4)/(B8+ 6*B4−7.5*B2)+1000
	NDMI	Normal Difference Moisture Index	(B8−B11)/(B8+B11)
	MSI	Moisture Soil Index	B11/B8
	BAI	Burn Area Index	1/(0.1-B4)2 +(0.06-B8)2
	DVI	Difference Vegetation Index	B8-B4
	GDVI	Green Difference Vegetation Index	B8 – B3
	GARI	Green Atmospherically Resistant Index	B8-(B3- (B2-B4)/B8+(B3- (B2-B4)
	GRVI	Green Ratio Vegetation Index	B8/B3
	IPVI	Infrared Percentage Vegetation Index	B8/B8+B4
Sensor	**Bands or Index**		**Formula**
Sentinel 1	Bands		VH, VV
	Band ratios		VV/VH, VH/VV
	Normalized difference		(VV-VH)/(VV+VH), (VH-VV)/(VV+VH)

Four different combinations of variables were analyzed in 4 tests (named Set in Table 4.33): the first two tests used the Sentinel-2 post event bands and the vegetation indices indicated in Table 4.32 respectively. Test 3 used the Sentinel-1 and some indices always related to the post-event, and finally test 4 used the same data of test 3 and also the images acquired after the Vaia storm (Table 4.33), therefore considering the changes through the comparison before and after the event.

Table 4.33 - Predictors used in classification models.

Set	Predictors	Image date
Set1	Sentinel-2 (post event) bands	28/06/2019
Set2	Sentinel-2 (post event) Vegetation Indices	28/06/2019
Set3	Sentinel-1 (post event) Bands VH, VV	07-15/12/2018
	Sentinel-1 (post event) Band ratios VV/VH, VH/VV	07-15/12/2018
	Sentinel-1 (post event) Normalized difference (VV-VH)/(VV + VH), VH-VV/(VV + VH)	07-15/12/2018
Set4	Sentinel-1 (pre-post event difference) bands VH, VV	26/09- 03/10/2018 07-15/12/2018
	Sentinel-1 (post event difference) band ratios VV/VH, VH/VV	26/09- 03/10/2018 07-15/12/2018
	Sentinel-1 (pre-post event difference) normalized difference VV-VH, VH-VV	26/09- 03/10/2018 07-15/12/2018

Because of the few cloudless optical images for the period examined and the reflectance variations induced by different weather conditions and phenology, analysing the differences in spectral response between pre and post images (both in pixel values and post classification), would have led to greater uncertainty in the results. Therefore, it was preferred to work only on post-damage optical images using a binary classification

approach (healthy forest/damaged areas). The date of the Sentinels chosen refers to the first available cloudless image for the entire study area.
For the Sentinel-1, the data pre and post event scenes were used, because differently respect to the optical images, the SAR data are less affected by atmospheric condition and for this reason the use of differences between pre and post event was also evaluated to detect forest damaged areas.
The two classification algorithms used, RF and KNN, have already been briefly described in chapter 2. These methods need observations to optimize their parameters and a single procedure was applied to both of them using the training polygons (the different sets of predictors and the classification damaged or not damaged)(Vaglio Laurin et al., 2020). The optimization purpose is to calibrate the hyperparameters of RF and KNN, after this step, to avoid overfitting, one of the most common method is k-fold cross validation (k-fold CV). This method divides input data into k subsets of data (also known as fold). A model will train on all subsets except one (k-1) and then it will evaluate the model on the subset that was not used for training. This process is repeated k times, each time with a different subset reserved for evaluation (and excluded from training). At end of training, the performance on each of the k folds are evaluated in term of Overall Accuracy (OA), i.e. the percentage of cases where the classification as damaged or not damaged was correct. For both KNN and RF finally the hyperparameters combination with the greater OAcv was selected. As previously pointed out, an accuracy was also calculated using a data set equal to 10% of the polygons. This dataset was not used for the algorithm training.

4.4.2 Results and discussion of windthrown areas detection (Vaia event)

Table 4.35 shows the results obtained with a 9-fold cross validation procedure for the varions. Very similar results are obtained from the independent test or using the 9-fold cross validation models. The Figure 4.27 summarises the results obtained from different tests.
The methodologies used show a good match in the results with few differences compared to the tested approach. The accuracy shown in the Table 4.35 refers to the calculation based on the independent dataset, in terms of overall accuracy: the highest values are the same and equal to 0.86. The lowest accuracy refers to the accuracy obtained using SAR data showing a minimum (50%) in the case of KNN and Set 3 (i.e. bands and indexes referred to post-event) and a maximum for RF and Set 4 (difference of bands post-event). The results obtained using the independent test set are similar to those obtained with 9-fold CV but span over a slightly higher range, as expected considering the limited number of samples in the test set (n=22) (Vaglio Laurin et al., 2020).

Table 4.34 - Overall accuracy for classification models validated with 9-fold cross validation with producers and Users accuracy related to Healthy Forest and Damaged Areas.

Alghoritm	Predictors set	9-fold-cross validation %	Overall accuracy %	Producers Accuracy Healthy Forest %	Producers Accuracy Damaged Areas %	Users Accuracy Healthy Forest %	Users Accuracy Damaged Areas %
KNN	S2 Set1	82.00	86.00	100.00	78.57	72.73	100.00
	S2 Set2	85.00	82.00	88.89	76.92	72.73	90.91
	S1 Set3	71.00	50.00	50.00	50.00	45.45	54.55
	S1 Set4	66.00	64.00	61.54	66.67	72.73	54.55
RF	S2 Set1	83.00	82.00	88.89	76.92	72.73	90.91
	S2 Set2	84.00	86.00	90.00	83.33	81.82	90.91
	S1 Set3	66.00	64.00	63.64	63.64	63.64	63.64
	S1 Set4	66.00	68.00	64.29	75.00	81.82	54.55

Producer's accuracy of the damaged area provides the frequency in which areas affected by the Vaia storm on the ground were correctly classified as damaged areas on the map, in practice showing false negatives.

The user's accuracy of damaged forest shows high results indicating a few errors of commission. The values in this case vary from 90.9 to 100 for Sentinel-2 tests, while SAR data varies from 54.55 to 63.64 (with RF and Set3) for Sentinel-1. The values range from 76.92 to 83.33 using sentinel 2 and from 50 to 75 with Sentinel 1 dataset. The best performance was reached from RF algorithm while the best result linked to KNN in PA was 78.57 with Sentinel 2 bands. For a better reading of the data, the results are also shown in the diagram below (Figure 4.27).

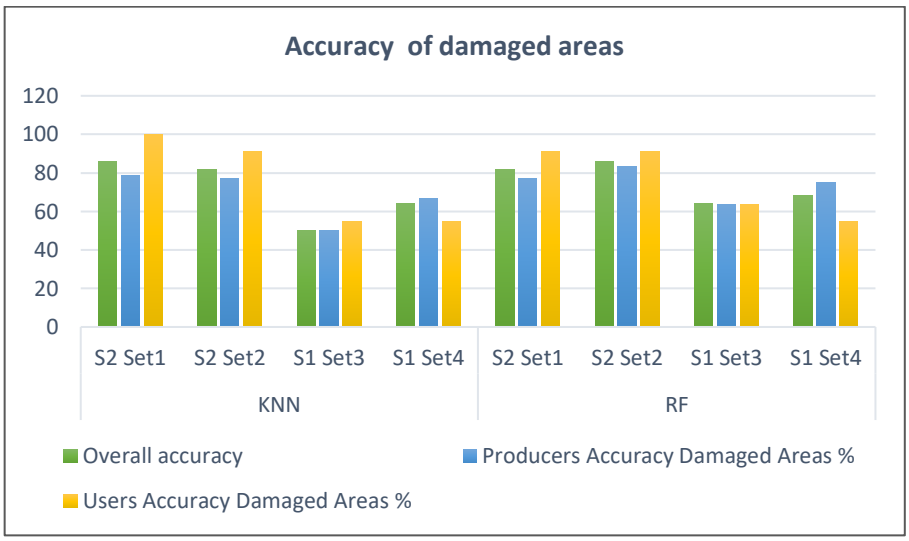

Figure 4.27 - Diagram of the results obtained for each tested configuration.

Regarding the use of the Sentinels, it is important to note that the images used refer to 7 months since all the previous images were covered with clouds. During this period the regrowth of vegetation has influenced the reflectance of the damaged areas with a consequent of reduction in the classification accuracy. The results are however in line with those obtained by other authors (Haidu et al., 2019) in Voges Mountain in France with 86% of accuracy or in United States and in European Russia with an OA of 75%, with more accurate results reported for larger areas (Baumann et al., 2014). At the time of the study there were not many studies using Sentinel-2 to detect changes related to forest windthrow detection, in 2020 a work on the same area using Sentinel-2 reported mapped the windthrows with an accuracy above 80% (Dalponte et al., 2020).

From this study it emerges that the vegetation indices provide the best results: this is probably because they tend to maximise sensitivity to vegetation characteristics while reducing disturbance factors such as atmospheric effects.

The SAR images generally gave worse results due, as Sentinel-2, to probably too much image acquisition distance compared to the event, which not only affects the reflectance, but also the backscattering.

The best scores are obtained using RF: 64% and 68% in OA with post-event data and pre-post event difference, respectively. With RF, the user's accuracy is low (54%) when using S1, pre-post event scenes differences, but the producer's accuracy is in line with the one obtained using the S2 data (75%). User's accuracies of damaged forest using shared data was not very high, but producer's accuracies provide values (75%) comparable to which obtained by Sentinel-2 when using S1 pre-post event scenes differences and RF algorithm. Also in this case previous studies conducted with C-band reached similar results (Schwarz et al., 2003; Ulander et al., 2005) while in others (Rüetschi et al., 2019) the authors obtained 88% in a German previous studies validation site, but the user's accuracy was only 21%.

However SAR has proven to plays an important role in the probability to obtain an image as soon as possible after a windthrow event due to a fast revisiting time and to the fact that this data is not influenced by

atmospheric condition; in addition the use of this data can provide valuable information since accuracy is acceptable (according to our methodology) for mapping changes liked to windthrows.

4.4.3 Mapping changes after Stromboli eruption

This paragraph presents the results achieved always in relation to the fourth objective, i.e. rapid land cover change detection after the fires. In particular, the efficiency of remote sensing images was analysed to evaluate the consequences caused in the summer of 2019 by some Stromboli eruptions: also in this case, the rapid identification of the damage is fundamental for the organisation of the interventions necessary to restore normal conditions and for the safety of people and things.

Stromboli is a volcanic island located in the Tyrrhenian Sea off the northern coast of Sicily, is characterized by intermittent explosions from three vent areas located in a summit crater that provides an example of the "Strombolian" types of eruption.

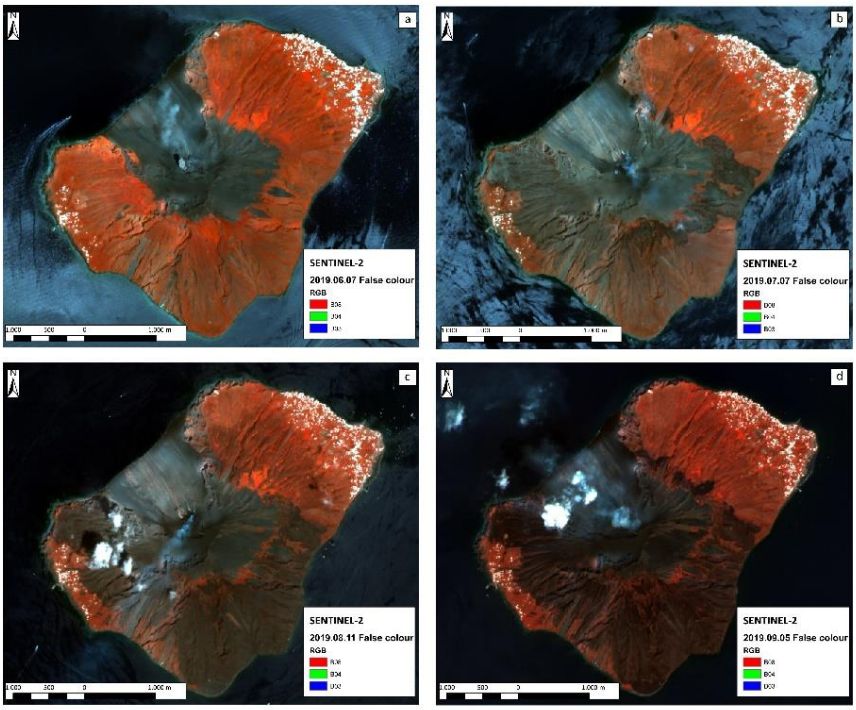

Figure 4.28 - Sentinel-2 image (false color) collected on: (a) 7 June 2019 (pre-eruption), (b) 7 July 2019,(c) 11 August 2019, (d) 5 September 2019[34].

Almost half of the island is covered with natural vegetation, represented mainly shrubs and Mediterranean bushes and for 13% by typically Mediterranean agricultural production like olive trees, vines. There are two villages on the island: Ginostra and Stromboli that constitute two built up areas (8% of island area) and finally bare soil covers 32% of island.

On 3rd July 2019, Stromboli was interested by a Strombolian paroxysm without long-term precursors. Followed in the subsequent months, by lava outpoured from a vent localized in the SW crater area, and sporadically from the NE one. On 28th August 2019, a new paroxysmal explosion occurred, with strong volcanic activity, and lava flow emitted from the SW-Central crater area (Turchi et al., 2020). In association with fire eruptions there are often fires caused by falling incandescent material that affect larger or smaller areas, depending on the case.

The Sentinel-2 dataset was used for the recognition of the impact on the Stromboli environment. Sentinel-2 images were acquired every 10 days. However, only a part of these images was used for this study because

[34] Source: Turchi et al., 2020

of high local cloud cover (Figure 4.28).NBR is one of the most widely used indices to perimeter the areas affected by fire and provide a qualitative assessment of the damage to different land cover classes.
This index has been calculated on two Sentinel-2 images acquired on different dates before and after the wildfire (after a not excessively high number of days, especially if the area affected by the fire consists mainly of pasture or low bush). As already highlighted in the methodological section, before a fire, healthy vegetation has very high near infrared reflectance and low infrared reflectance, after a fire the areas affected have relatively low near infrared reflectance and high reflectance in the short-wave infrared band. The behaviour of reflectance in NIR and SWIR can therefore be used to delimit areas of changes due to a fire, through the values of the NBR index. Since the area is small, the QGIS software was used to process the images and calculate the indices for the pre-fire and two post-fire periods according to the flow chart explained in the text below and shown in the Figure 4.29.

- *Image acquisition:*
  Multi-temporal Sentinel-2 images were used to detect the changes occurred after the volcanic explosion. In order to follow the monitoring of the events, several images were acquired, but for the calculation of the indexes, only the images that did not have cloud cover were selected.

Data acquisition pre- event:
- 07-06-2019

Data acquisition post- events:
- 07-07-2019
- 11-08-2019
- 05-09-2019

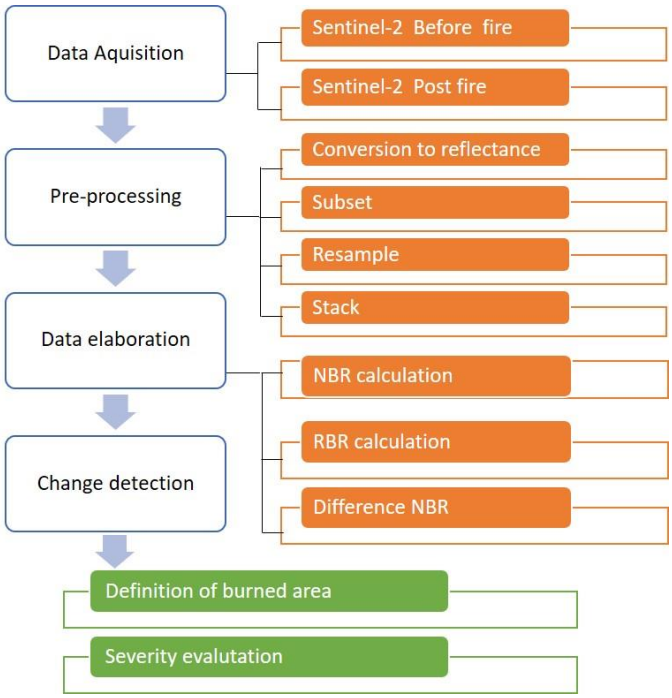

Figure 4.29 - Flowchart of the processing procedure for the wildfire impact and severity mapping.

- *Image pre-processing*:
  the image processing was performed using the free QGIS software, according to the following steps:
  1. Conversion the DN to Reflectance.
  2. Resample: In order to have the same spatial resolution, the images were resampled at 10 metres resolution.
  3. Subset: the images were clipped on the study area.
  4. Stack of image.

- *Calculation of NBR and RBR indices:*
    1. Index caluclation:
        - NBR is calculated for both images.
        - RBR calculation.
        - Difference between the index before and after the normalised event.

- *Identification of burned area:* i*ndex values are converted into levels in order to define burned limits:*
    1. Definition of burned area according to United States Geological Survey (USGS) classification
    2. Calculation of the classes of coverage affected by the fire

dNBR is calculated using the following equation for the Sentinel 2 satellite bands

$$\mathrm{dNBR} = \mathrm{NBR_{pre}} - \mathrm{NBR_{post}} \quad \text{where dNBR is} \quad \mathrm{NBR} = \frac{\mathrm{NIR\ (B8) - SWIR\ (B12)}}{\mathrm{NIR\ (B8) + SWIR\ (B12)}}$$

NIR and SWIR2 are respectively the reflectance value in the near infrared and the reflectance value in the short-wave infrared region; dNBR then gives the change in the NBR value of a given surface, before and after the fire. It is an absolute difference that can present a problem in areas with low vegetation cover because the absolute value of NBR before and after the event could be very small. In such situations the Relative Burn Ratio (RBR) value gives better results.

$$RBR = \frac{\mathrm{dNBR}}{\mathrm{NBRpre} + 1{,}001}$$

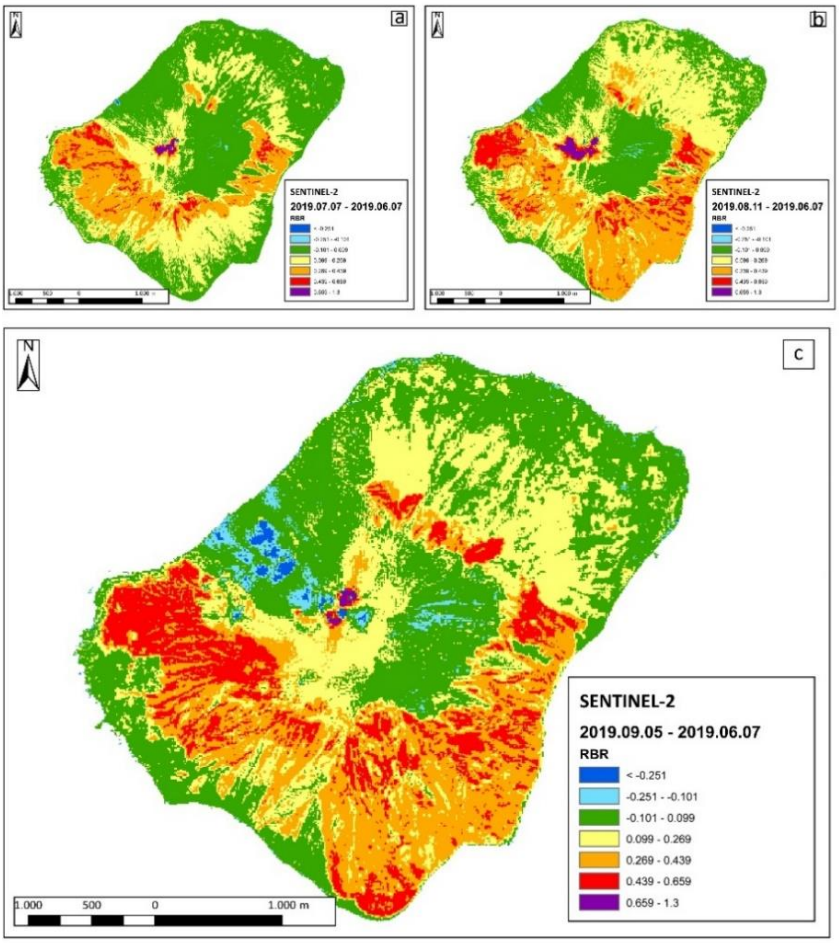

The Figure 4.30 - Relativized Burn Ratio (RBR) on: (a) 7 June 2019–7 July 2019, (b) 7 June 2019–11 August 2019, (c) 7 June 2019–5 September 2019.

The RBR values have been used to derive the map of the areas impacted by the wildfire produced by the 2019 paroxysmal explosions. The calculated values usually vary due to the different characteristics of the image and the acquisition conditions; however, the United States Geological Survey (USGS)(Key & Benson, 2006) has proposed a classification to interpret the severity of the fire (Figure 4.30). Areas with a value greater than 0.270 were considered burnt areas. In this study the thresholds proposed by the USGS were used to distinguish the burned/not burned areas. These thresholds were also tested to define the severity only to have an idea of the damage on the surfaces hit by the events, even if it was not the objective of the research. PLÉIADES optical images, field inspections, and eyewitness accounts have been used to validate the results.

Land cover map was (Figure 4.31) generated by manual photo-interpretation of the Pleiades with 0.5 m *0.5 m spatial resolution and collected on 13 June 2019 , 13 August 2019 and 8 October 2019 i.e. for the period before and after the fires (Turchi et al., 2020). Land cover map is very detailed, but for this research the original land use classes were aggregated in four land cover classes:

- *Abiotic*
- *Natural surface*
- *Agricultural surface*
- *Artificial surface*

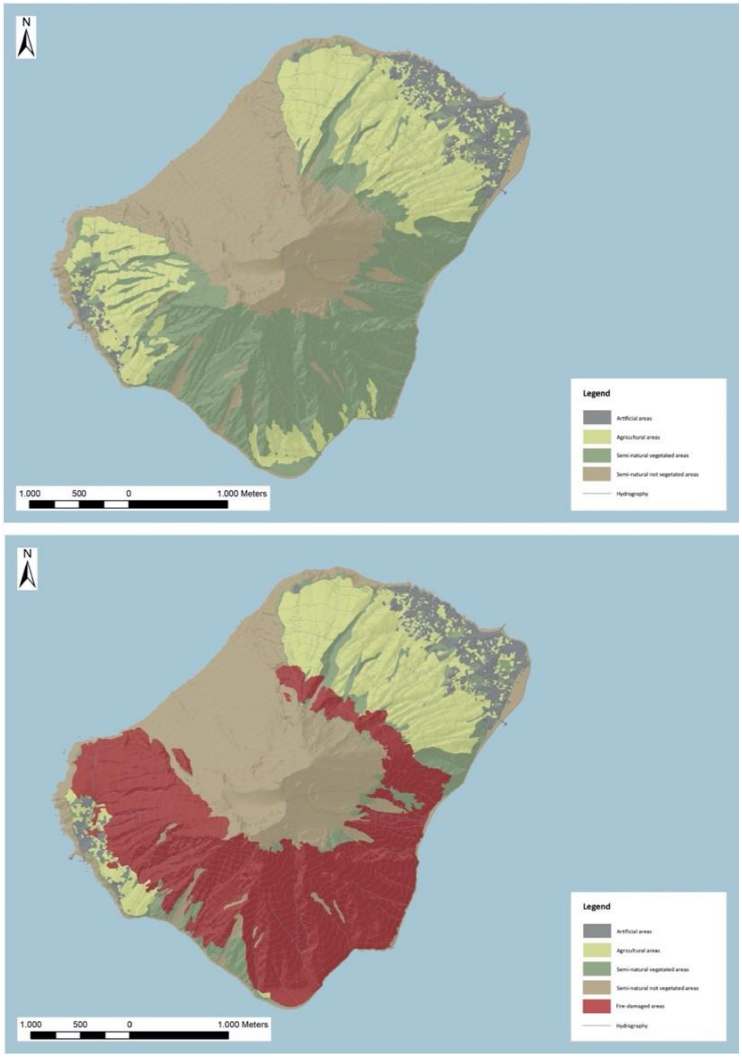

Figure 4.31 – Land cover map of Stromboli 2018 and 2019 post eruption.

4.4.4 Results and discussion of burned areas detection (Stromboli eruptions)

Sentinel-2 data images and Pleiades have permitted to monitor the increasing of the burnt surfaces and the progression of the fires on the agricultural and vegetated area. On the entire island of Stromboli, Sentinel-2 images were acquired every 10 days and some of these images were used for the analysis. For this reason, the integration between the results of the satellite data and ground field included interviews with the eyewitnesses, enabled to define well all the phenomena and to check the thresholds used.

The 3rd July 2019 eruption caused most of the fires in the island; a second fire broke out on 25th July 2019, but it was related to the incomplete reclamation of the burned areas on 3rd July 2019. Finally, on the 28th August 2019 explosion did not generate many wildfires, except for a small area in the north of the island. At the end of the summer period, the total area affected by fire was 496.47 ha, equal to 39.35% of the island surface.

The land cover most affected was the natural surface area with 352 ha equal to 27% of the total surface, followed by agriculture with 92 ha burned (7.28% of total area) and finally abiotic and artificial surface damaged only for a few hectares.

Apart from the worrying values in terms of lost hectares, the percentage change in agricultural and natural areas was considerable, with a decrease of 60% and 55% respectively.

A brief and speedy analysis was carried out with respect to the severity of the areas affected by the fire. The severity of the fire is defined as the degree of environmental change caused by the fire (Keeley, 2009; Veraverbeke et al., 2010). The intensity of the fire determines the severity of the damage, but the relationship is not necessarily constant, in fact, different ecological systems show varying degrees of sensitivity to fire. In this case, as previously mentioned, the severity values were used to perimeter the affected areas.

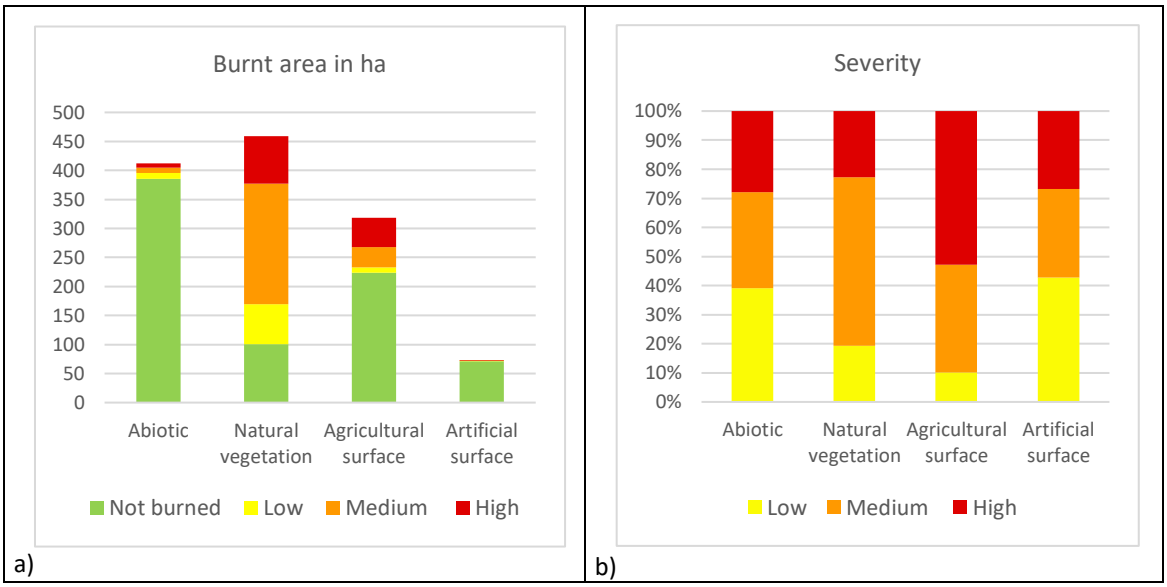

Figure 4.32 –Burnt area after the last eruption in ha (a) and percentage (b) according to the severity of damage.

Table 4.35 - Distribution of burnt area according to different land cover class in Stromboli.

Classes	Abiotic	Natural surface	Agricultural surface	Artificial surface	**Total**
ha burned	27,0	358,3	94,8	1,1	**481,1**
% burned	2,1	28,4	7,5	0,1	**38,1**

These values, proposed by the United States Geological Survey (USGS), which has provided good results in various situations, are used here to interpret the severity of the fire and to get an idea of the severity of the fire for each land cover class.
The severity values of burned area ranges between 0.27 and 0.66; most of the area is classified with a medium to high degree of severity, in particular 53% of the burned area is included in medium degree while 29% is included in high degree, for a total of about 251 and 140 ha respectively. The low severity category consists mainly of areas affected by the first event and subsequently interested by a modest vegetational regrowth. The "land cover" made it possible to analyse the distribution of the classes according to the different degree of severity. the graph in Figure 4.32 a) shows for each class of land cover, the hectares of land involved with respect to the severity of the fire, including the area outside the perimeter area, while Figure 4.32 b) displays only the damaged areas (whose values are summarized in the table 4.35) with the respective percentages of severity. The degree of severity of the fire has highlighted that some types of land cover as natural vegetation and agriculture suffered the most damage in particular the latter presents a high percentage of coverage in the high severity range. These vegetation classes are also those with the greatest extension in the area involved. Moreover the presence of shrubs formations has showed to be very susceptible to the passage of the fire also due to poor regeneration capacity (Frate et al., 2018); conversely, the least affected class is represented by artificial surfaces with the exception of industrial areas or public services, as evidenced by field surveys near photovoltaic power station in Ginostra village.

Chapter 5 Conclusions

5.1 Research finding and conclusions

This research investigated the potential of remote sensing to provide detailed spatial information of land cover and its transformation, suitable for multidisciplinary studies and applications and for different final users.

Remote sensing, considering recent technological advances in this sector, is a valid tool for monitoring the landscape and its evolution, as demonstrated in the last decade by numerous studies.

At European level, interest in remote sensing was affirmed with Regulation (EU) No 911/2010, which set up the Copernicus Earth observation programme. This programme has made available numerous cartographic products and Sentinel satellite images, both optical and radar, characterised by good spatial and temporal resolution. In the first part of this research, the European and Italian policies in the field of satellite monitoring were analysed with the aim of identifying the directions taken by the environmental policies in the field of monitoring and the needs required by the institutions at national and international level. The characteristics of currently available products were then analysed, highlighting, in each case, the fields of use and limitations.

Considering the conducted analysis, this research aimed to identify new ways to address the critical issues that have emerged and to respond to the request for updated data with high spatial resolution for monitoring land cover. Furthermore, this study intends to propose useful tools for the needs of institutions and research centres responsible safeguarding the territory.

The following specific objectives were set out (Figure 5.1):

1. Define an advanced operational methodology to extract land cover classes over very large areas using free satellite data.
2. Develop an efficient change detection strategy to improve the frequency and accuracy of land cover map with particular attention to land consumption and forest disturbance, by the means of an integrated use of free multi temporal optical and SAR image.
3. Improve the landslide susceptibility model by the use of soil sealing.
4. Contribute to the development of knowledge to assess the potential of free remote sensing data for rapid detection of environmental damages.

The study follows a multidisciplinary approach and takes into account different areas related to soil degradation, a phenomenon that is of considerable importance both at European and international level (as seen in the introductory chapters) since it influences the quality and quantity of land resources necessary for multiple ecosystem services. In addition to following a multidisciplinary approach, the developed themes

have the common goal to study the potential offered by the use of optical and radar data to produce land cover maps as tools for monitoring the territory.
The main results (discussed in the previous chapter) of this research in the field of land monitoring are highlighted here, and the positive aspects and the most important limits that have emerged, are summarized in relation to the set objectives.

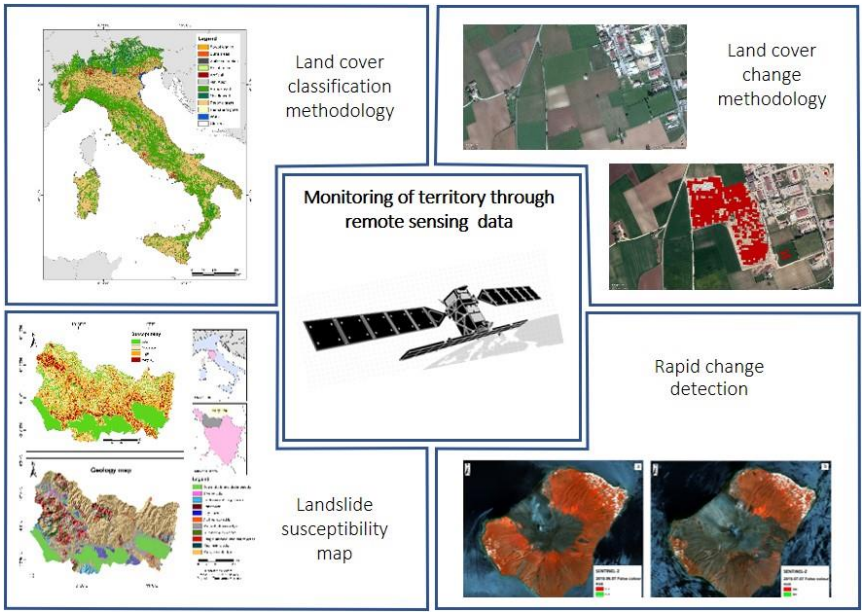

Figure 5.1 – Specific objectives of the research.

One of the main contributions of this research was the production of an innovative methodology for the classification of satellite images and a pixel based methodology for the updating the land cover mapping, choosing the entire national territory as study area. These procedures have some peculiar and innovative aspects which are described below.
The methodology as set out in detail exploits a decision rules method characterized by computational simplicity which allows a fast analysis of the large number of pixels which compose the images. This system is efficient in classifying large land cover areas since it is easy to use and interpret and can be applied to continuous variables like satellite images (Törmä, 2013). The system is based on the behaviour of some spectral indices and on the definition of thresholds for the discrimination of the different classes investigating the integrated use of multi-temporal Sentinel-1 (SAR) and Sentinel-2 (Optical) satellite data.
An advantage of the proposed method consists in the possibility of defining and modifying the thresholds or set rules, allowing the classification to be improved each time new information is acquired.
As described in Chapter 2, various techniques have been developed in recent years to monitor land changes using remote sensing along with semi-automatic classification processes. The main difficulty encountered by many of these techniques is that they provide good results in small areas but seem be poorly adaptable to large areas, not achieving the same level of accuracy due to the increased issues of spectral heterogeneity and complexity of land. These methodologies also require the management of a huge amount of training areas and the setting of various parameters, not allowing an easy interaction with the user. On the other hand, maps covering large areas often coincide with low to moderate resolution products, useful for a more limited number of applications.
One of the most important results of the developed methodology is the production of a map with a spatial resolution of 10 metres, an accuracy of 83% for the entire national territory and a minimum mappable unit of 100 m^2.

A similar procedure, which exploits the advantages of decision rules and the characteristics of optical and radar data, has been adopted to extract changes related to land consumption and forest disturbances. This therefore allows for the rapid updating of the map produced on an annual basis with the result of having an updated map of the entire Italian territory, capable of highlighting the changes that have occurred in the time period 2017-2018, with a soil consumption accuracy reaching 0.9.
Another advantage of the proposed method is that it uses completely free tools and data. The whole process was developed using the Google Earth Engine platform and open source GIS tools trying to take advantage of the free availability of sentinel-2 images provided by the Copernicus programme. All these aspects: the possibility to apply the methodology obtaining good results over large areas, the possibility to modify and improve the set rules, the use of free data, the high resolution and the possibility of annual updates make the procedure, and the derivable products, versatile and adaptable for different applications and economically sustainable. These factors are in line with the achievement of the first two objectives of this research.
Finally, a fundamental aspect that makes this methodology usable in various monitoring fields is the classification system, based on the EAGLE concept, which allows the produced data to be used and adapted to different needs. The system permits to add land use information, or specific land peculiarities while maintaining the characteristic of comparability with other land cover classes or other classification systems. This choice not only meets the requirements proposed at European level but also favours several different applications.
The products derived from this study have allowed the elaboration of a series of environmental indicators extended to the whole of the national territory, which have provided the possibility of performing analyses at different scales useful for understanding the transformations of the territory. The results also highlighted several critical issues for 'soil degradation': in Italy, land consumption continues to increase. Despite the agreement signed at European level to reach zero land consumption by 2030, figures continue to increase even in areas with hydraulic, landslide and seismic hazards. The analysis of changes at the third level made it possible to identify how much of the land consumption, in the last three years, is due mainly to the construction of new buildings and roads and how this is a trend in all Italian regions.
The comparison with the CLC data has highlighted some of the weaknesses of the system, first of all the impossibility of using the data for detailed analyses such as the indicators calculated for this study. The presence of mixed as well as land use classes and the minimum mappable units of the CLC data constitute a limitation for change detection analyses even over long periods.

One of the objectives identified was to understand whether the data on soil consumption produced in the methodology and three other variables related to soil sealing could improve the accuracy of landslide susceptibility assessments. A RF algorithm was used for the susceptibility analysis and seven conditioning factors were used as base variables (aspect, land cover, slope, elevation, lithology, planar curvature, and flow accumulation). The four-soil sealing derived variables were integrated in the susceptibility model, resulting in a series of tests (each variable alone, all variables together, none of them). For each test, the overall accuracy of the resulting map was evaluated in terms of AUC; in addition, the importance of each variable was evaluated in terms of the "out of bag error". The results of this analysis showed that: soil sealing data can be used to improve the effectiveness of landslide susceptibility assessments; among the tested variables, "soil sealing aggregation" was the most promising, leading to the highest AUC and showing a relative importance within the model higher than other widely used parameters like land cover. This result, in addition to improving the accuracy of susceptibility map, represents a novelty in studies of this type as soil sealing has never been tested as a predisposing factor for triggering landslides. In addition to the improved forecasting effectiveness, the use of soil sealing-derived parameters in landslide susceptibility studies seems promising because the original thematic layer is updated yearly, and this good temporal

resolution allows for a quick and constant update of susceptibility maps accounting for the modifications induced by human activity on hillslope systems.
The fourth objective stems from the impossibility of using the methodology in case of rapid changes as well as the need to understand the potential of the Sentinels in order to operationally evaluate the changes caused by a disaster event. In the case of areas affected by windthrow, the study showed the best performance using Sentinel-2 data even though Sentinel-1 data provided acceptable results; this represents an important finding considering that for events of this type, which often occur in the winter, the possibility of having optical images without clouds is poor. In this context the use of Sentinel-1 data, which do not depend on weather conditions and have a frequent revisiting time, may represent the only way to rapidly estimate damages or to know the areas to be explored. In the case-study of Stromboli, Sentinel-2 NIR and SWIR bands were used to calculate the NBR index. The choice of the index was motivated by the fact that it provided better results (Pepe & Parente, 2018). The USGS classification was used to identify the burned areas by recalibrating the values based on the data collected during field samples. This study made it possible to implement a rapid system for the recognition of burned areas through a simple index also used in the methodology for land cover and to precisely define thresholds for delimiting areas affected by fire. This process is therefore replicable in the future in case of similar situations. The results and the analysis conducted have allowed a greater understanding of the potential of Sentinel-2 images, improving knowledge in the field of rapid change detection after a disaster event, as in the intentions defined in the fourth objective. As in the previous case, the possibility of identifying burnt areas with radar data remain to be considered. This would favour all situations in which the availability of optical images is precluded by unfavourable weather conditions. In any case, when possible, the joint use of data should lead to better results as demonstrated by many studies that have tested this possibility (Joshi et al., 2016).
Some critical issues that appeared in this research are related to the ability of the proposed systems to optimally distinguish the different land cover classes. This is the case of the separation between temporary herbaceous vegetation and permanent herbaceous vegetation since the two classes have a quite similar behaviour throughout the year and the differences are related to seasonal fluctuations. A second problem, is then related to the EAGLE definition, as pointed out in the discussions, which is mainly based on the periods of non-cover in the case of temporary grassland and could create confusion to separate these two herbaceous classes.
The use of multi-temporal series has been an effective to precisely distinguish conifers from broadleaves and herbaceous class from trees. In all cases, the thresholds were studied in depth by analysing the temporal behaviour of the spectral responses of the different classes; then a strategy was set up based in many cases on training samples to calibrate the thresholds, and on a set of rules to extract as much information as possible from the combined use of satellite imagery.

5.2 Future developments

The topics covered in this thesis lay the foundations for several further investigations. Some possible insights into the proposed topics and possible applications are outlined below. One of the outstanding problems that may deserve further research is probably the definition of the class of shrubs. This would undoubtedly improve the thematic detail of the map and allow a more precise delimitation of the forest areas (and transition areas) or Mediterranean vegetation, characteristic of the Italian flora. Even the vineyards, which are currently included in the broadleaf class, would also be better placed in the shrubs class. This requires an in-depth analysis of the spectral behaviour of shrubs, which is easily confused with sparse trees on the one hand, and with herbaceous mixed with trees, on the other. The inclusion of this class would also prove useful for many applications (change detection studies) and for analyses of ecosystem transformation.
The main future development of this work, however, is undoubtedly the potential offered by the elaborated maps. Both at the national and international level, several land cover maps are produced at different scales, or covering different areas; other products covering the same area for different purposes, use different

classification system at different levels of detail and/or with different meanings for the same class name. It follows a very difficult exchange of land cover information between national Institutions and users, a reduced efficiency of the national database; a very difficult capacity to update the land cover information and mainly a series of different types of Land Cover dataset. This situation is common in many countries.
The only product available at national level is CLC which, as shown, in addition to not allowing detailed analysis, is updated every 6 years and has a minimum mappable unit of 25 ha. The other products available today in Italy cover regional surface; it is true that in some cases they present greater detail and also provide information on land use (useful for various applications), but they do not have adequate temporal resolution and are only available for partial areas of the Italian territory. Moreover, these products currently exist only for a few regions; the most updated ones are provided by Liguria and Lombardy and refer to 2018 (a layer for Liguria was rapidly updated to 2020) at the scale 1:10.00 and a minimum mappable unit of 1600m2. Other data are provided by Emilia Romagna (last available data to 2017) or Toscana (2016) always at the scale 1:10,000.
As highlighted in Chapter 2, soil monitoring through the production of a thematic map is one of the objectives of the 2030 Agenda for Sustainable Development at European level and is foreseen in the National Strategy for Sustainable Development (NSDS) approved by the CIPE in December 2017, with which Italy transposes these objectives and undertakes to implement monitoring through a system of indicators, including some specific ones on land consumption. The map obtained from the classification and updating methodology developed in this research falls within the requirements of the Space Economy Land Cover and Land Use Monitoring Service, which, in its "choice 4", foresees the production, among others, of data at a resolution of 10 metres, consistent with the EAGLE specifications.
The map is therefore intended to be a useful tool to check unauthorized building activities, to monitor the territory in the case of illegal forestry operations or to assess damage caused by natural events.
Existing land cover maps cannot be used because they do not meet the required specifications (in addition to having a partial extension). However, they can be useful to test the produced data, to provide training and control areas and to provide useful ancillary data.
The produced map can therefore be used in the future – as a geometric basis for various applications – or integrated with other data, such as many types of regional data, to form a product that meets the needs for rapid data updating, maintaining a spatial resolution of 10 metres but a better thematic detail.
Other suggested research is aimed at improving the accuracy of changes. These were derived through the decision rules algorithm described in Chapter 3, for the direct identification of changes in forestry and land consumption. By overlaying the changes on the land cover, it is possible to update the map produced on annual basis. It is known that even an error of a few percentage points can lead to a multiplication of the error when the map is updated, gradually producing an exponential increase in error. In land consumption, this problem virtually doesn't exist, since in photo-interpretation not only the new changes are identified, but also the old ones are rechecked on the entire previous series, thus avoiding the propagation of the error and always maintaining the accuracy at high levels.
In the case of changes related to forest disturbances, the difficulty in identifying clear-cuts is the result of several factors. In Mediterranean coppice forests, the recovery of vegetation activity takes place rapidly after cutting, therefore, to highlight these changes it is necessary to monitor them shortly after the cut (Chirici et al., 2020); moreover, the study of the spectral behaviour of coppice forests is very different from that of alpine forests where selective felling is applied. The same algorithm, therefore, in many cases is not able to identify disturbances of this type. The integration with recently published algorithms will allow to refine the data by overcoming many of the above-mentioned limitations (Giannetti et al., 2020).
Needless to say that for an optimal use of the algorithms for the identification of forest disturbances and in view of possible applications, the creation of a forest mask could be very useful; Copernicus also made an attempt but with little accuracy and at a spatial resolution of 20 m; this could be realised starting from the map produced within the framework of this research, improving the efficiency of some proposed thresholds,

but above all using images derived from hyperspectral sensors. The latter could improve the classification and lead to more accurate results in the future up area.

The present methodology could be useful for the improvement of large-scale operational services, with a high detailed spatial resolution, update frequency and in compliance with the main European Community requirements as EAGLE model. It constitutes an effective contribution in soil protection and environmental monitoring also in the context of European and international initiatives such as the space economy or the calculation of indicators related to United Nations SDGs.

List of publications

.

The following papers were published as part of this PHD:

1. Luti, T., Congedo, L., De Fioravante, P., Cavalli, A., Marinosci, I., Strollo, A., Riitano, N., Falanga, V. Mariani, L., Munafò, M. Land consumption monitoring with SAR data and multispectral indices. Remote Sens. 2021, 13, 1586.
2. De Fioravante, P., Luti, T., Cavalli, A., Giuliani, C., Dichicco, P., Marchetti, M., ... & Munafò, M. (2021). Multispectral Sentinel-2 and SAR Sentinel-1 Integration for Automatic Land Cover Classification. Land, 10(6), 611.
3. Segoni, S., Nocentini, N., Rosi, A., Luti, T., Pappafico, G., Munafò, M., Casagli, N., Catani, F. New explanatory variables to improve landslide susceptibility mapping: testing the effectiveness of soil sealing information and multi-criteria geological parameterization. IJEGE. 2020. Submitted
4. Luti, T.; Segoni, S.; Catani, F.; Munafò, M.; Casagli, N. Integration of Remotely Sensed Soil Sealing Data in Landslide Susceptibility Mapping. Remote Sens. 2020, 12, 1486.
5. Gaia Vaglio Laurin, Saverio Francini, Tania Luti, Gherardo Chirici , Francesco Pirotti , Dario Papale. Satellite open data to monitor forest damages caused by extreme climate-induced events: the case of the Vaia storm in Northern Italy. Forestry: An International Journal of Forest Research, 2020.
6. Segoni, S.; Pappafico, G.; Luti, T.; Catani, F. Landslide susceptibility assessment in complex geological settings: Sensitivity to geological information and insights on its parameterization. Landslides 2020, 1–11.
7. Turchi, A.; Di Traglia, F.; Luti, T.; Olori, D.; Zetti, I.; Fanti, R. Environmental Aftermath of the 2019 Stromboli Eruption. Remote Sens. 2020, 12, 994.
8. Munafò, M. (a cura di), 2020. Consumo di suolo, dinamiche territoriali e servizi ecosistemici. Edizione 2020, ISPRA, Report SNPA 15/2020. ISBN 978-88-448-1013-9
9. Munafò, M. (a cura di), 2019. Consumo di suolo, dinamiche territoriali e servizi ecosistemici. Edizione 2019. Report SNPA 08/19. ISBN 978-88-448-0964-5
10. L. Congedo, F. Assennato, R. Bruno, C. Ciocci, P. De Fioravante, M. Di Leginio, C. Giuliani, T. Luti, I. Marinosci, G. Milano, P. Pellegrino, S. Pranzo, M. Soraci, A. Strollo, A. Raudner, D. Trogu, M. Munafò (2018), “Il consumo di suolo e la crescita urbana”, ISPRA, pp14-36

References

Acquaotta, F., Faccini, F., Fratianni, S., Paliaga, G., Sacchini, A., & Vilímek, V. (2019). Increased flash flooding in Genoa Metropolitan Area: a combination of climate changes and soil consumption? *Meteorology and Atmospheric Physics*, *131*(4), 1099–1110. https://doi.org/10.1007/s00703-018-0623-4

Agrillo, E., Filipponi, F., Pezzarossa, A., Casella, L., Smiraglia, D., Orasi, A., Attorre, F., & Taramelli, A. (2021). Earth observation and biodiversity big data for forest habitat types classification and mapping. *Remote Sensing*, *13*(7), 1–29. https://doi.org/10.3390/rs13071231

Aleotti, P., & Chowdhury, R. (1999). Landslide hazard assessment: summary review and new perspectives. *Bulletin of Engineering Geology and the Environment*, *58*(1), 21–44.

Alvioli, M., Marchesini, I., Reichenbach, P., Rossi, M., Ardizzone, F., Fiorucci, F., & Guzzetti, F. (2016). Automatic delineation of geomorphological slope units with r. slopeunits v1. 0 and their optimization for landslide susceptibility modeling. *Geoscientific Model Development*, *9*(11), 3975.

Arabameri, A., Rezaei, K., Cerdà, A., Conoscenti, C., & Kalantari, Z. (2019). A comparison of statistical methods and multi-criteria decision making to map flood hazard susceptibility in Northern Iran. *Science of The Total Environment*, *660*, 443–458. https://doi.org/https://doi.org/10.1016/j.scitotenv.2019.01.021

Arnold, S., Kosztra, B., Banko, G., Smith, G., Hazeu, G., & Bock, M. (2013). The EAGLE concept – A vision of a future European Land Monitoring Framework. *EARSeL Symposium Proceedings 2013, Towards Horizon 2020*, 551–568.

Arnone, E., Francipane, A., Scarbaci, A., Puglisi, C., & Noto, L. V. (2016). Effect of raster resolution and polygon-conversion algorithm on landslide susceptibility mapping. *Environmental Modelling & Software*, *84*, 467–481.

Bălteanu, D., Chendeş, V., Sima, M., & Enciu, P. (2010). A country-wide spatial assessment of landslide susceptibility in Romania. *Geomorphology*, *124*(3), 102–112. https://doi.org/https://doi.org/10.1016/j.geomorph.2010.03.005

Ban, Y., Webber, L., Gamba, P., & Paganini, M. (2017). EO4Urban: Sentinel-1A SAR and Sentinel-2A MSI data for global urban services. *2017 Joint Urban Remote Sensing Event (JURSE)*, 1–4.

Ban, Y., & Yousif, O. (2016). Change detection techniques: a review. In *Multitemporal Remote Sensing* (pp. 19–43). Springer.

Battistini, A., Rosi, A., Segoni, S., Lagomarsino, D., Catani, F., & Casagli, N. (2017). Validation of landslide hazard models using a semantic engine on online news. *Applied Geography*, *82*, 59–65. https://doi.org/https://doi.org/10.1016/j.apgeog.2017.03.003

Baumann, M., Ozdogan, M., Wolter, P. T., Krylov, A., Vladimirova, N., & Radeloff, V. C. (2014). Landsat remote sensing of forest windfall disturbance. *Remote Sensing of Environment*, *143*, 171–179.

Belgiu, M., & Drăguţ, L. (2016). Random forest in remote sensing: A review of applications and future directions. *ISPRS Journal of Photogrammetry and Remote Sensing*, *114*, 24–31.

Bolyn, C., Michez, A., Gaucher, P., Lejeune, P., & Bonnet, S. (2018). Forest mapping and species composition using supervised per pixel classification of Sentinel-2 imagery. *Biotechnologie, Agronomie, Société et Environnement*, *22*(3), 16.

Bovolo, F., & Bruzzone, L. (2007). A split-based approach to unsupervised change detection in large-size multitemporal images: Application to tsunami-damage assessment. *IEEE Transactions on Geoscience and Remote Sensing*, *45*(6), 1658–1670.

Bovolo, F., Bruzzone, L., & Marconcini, M. (2008). A novel approach to unsupervised change detection based on a semisupervised SVM and a similarity measure. *IEEE Transactions on Geoscience and Remote Sensing*, *46*(7), 2070–2082.

Breiman, L, Friedman, J. H., Olshen, R. A., & Stone, C. J. (1984). Classification and regression trees. 1984. Wadsworth & Brooks. *Cole Statistics/Probability Series, Pacific Grove, Cal*.

Breiman, Leo. (2001). Random forests. *Machine Learning*, *45*(1), 5–32.

Brenning, A. (2005). Spatial prediction models for landslide hazards: review, comparison and evaluation. *Natural Hazards and Earth System Sciences*, *5(6)*, 853–862.

Brooner, W. (1976). Land-use map accuracy criteria. *Photogrammetric Engineering and Remote Sensing*, *42*(5), 671–677.

Brown de Colstoun, E. C., Huang, C., Wang, P., Tilton, J. C., Tan, B., Phillips, J., Niemczura, S., Ling, P.-Y., & Wolfe, R. E. (2017). *Global Man-made Impervious Surface (GMIS) Dataset From Landsat*. NASA Socioeconomic Data and Applications Center (SEDAC). https://doi.org/10.7927/H4P55KKF

Campbell, J. B., & Wynne, R. H. (2011). *Introduction to Remote Sensing, Fifth Edition*. Guilford Publications. https://books.google.it/books?id=NkLmDjSS8TsC

Camps-Valls, G., Tuia, D., Gómez-Chova, L., Jiménez, S., & Malo, J. (2011). Remote Sensing Image Processing. *Synthesis Lectures on Image, Video, and Multimedia Processing*, *5*(1), 1–192. https://doi.org/10.2200/S00392ED1V01Y201107IVM012

Catani, F., Lagomarsino, D., Segoni, S., & Tofani, V. (2013). Landslide susceptibility estimation by random forests technique: sensitivity and scaling issues. *Natural Hazards and Earth System Sciences*, *13*(11), 2815.

Celik, N. (2018). Change detection of urban areas in Ankara through Google Earth engine. *2018 41st International Conference on Telecommunications and Signal Processing (TSP)*, 1–5.

Chacón, J., Irigaray, C., Fernandez, T., & El Hamdouni, R. (2006). Engineering geology maps: landslides and geographical information systems. *Bulletin of Engineering Geology and the Environment*, *65*(4), 341–411.

Chen, L., Sela, S., Svoray, T., & Assouline, S. (2013). The role of soil-surface sealing, microtopography, and vegetation patches in rainfall-runoff processes in semiarid areas. *Water Resources Research*, *49*(9), 5585–5599.

Chirici, G., Giannetti, F., Mazza, E., Francini, S., Travaglini, D., Pegna, R., & White, J. C. (2020). Monitoring clearcutting and subsequent rapid recovery in Mediterranean coppice forests with Landsat time series. *Annals of Forest Science*, *77*, 1–14.

Chung, C.-J. F., & Fabbri, A. G. (2003). Validation of Spatial Prediction Models for Landslide Hazard Mapping. *Natural Hazards*, *30*(3), 451–472. https://doi.org/10.1023/B:NHAZ.0000007172.62651.2b

Cochran, W. G. (2007). *Sampling techniques*. John Wiley & Sons.

Cohen, W. B., Yang, Z., & Kennedy, R. (2010). Detecting trends in forest disturbance and recovery using yearly Landsat time series: 2. TimeSync—Tools for calibration and validation. *Remote Sensing of Environment*, *114*(12), 2911–2924.

Colditz, R. R. (2015). An evaluation of different training sample allocation schemes for discrete and continuous land cover classification using decision tree-based algorithms. *Remote Sensing*, *7*(8), 9655–9681.

Coluzzi, R., Imbrenda, V., Lanfredi, M., & Simoniello, T. (2018). A first assessment of the Sentinel-2 Level 1-C cloud mask product to support informed surface analyses. *Remote Sensing of Environment*, *217*, 426–443.

Commissione Europea. (2020). *Strategia dell'UE sulla biodiversità per il 2030 Riportare la natura nella nostra vita*. https://eur-lex.europa.eu/legal-content/EN/TXT/?qid=1590574123338&uri=CELEX%3A52020DC0380

Congalton, R. G. (1991). A review of assessing the accuracy of classifications of remotely sensed data. *Remote Sensing of Environment*, *37*(1), 35–46.

Congalton, R. G., & Green, K. (2019). *Assessing the accuracy of remotely sensed data: principles and practices*. CRC press.

Congedo, L. (2016). *Semi-Automatic Classification Plugin Documentation Release 4.8.0.1*. *October*. https://doi.org/10.13140/RG.2.2.25480.65286/1

Congedo, L., Sallustio, L., Munafò, M., Ottaviano, M., Tonti, D., & Marchetti, M. (2016). Copernicus high-resolution layers for land cover classification in Italy. *Journal of Maps*, *12*(5), 1195–1205. https://doi.org/10.1080/17445647.2016.1145151

Coppin, P., Jonckheere, I., Nackaerts, K., Muys, B., & Lambin, E. (2004). Review ArticleDigital change detection methods

in ecosystem monitoring: a review. *International Journal of Remote Sensing*, *25*(9), 1565–1596.

Corominas, J., Copons, R., Vilaplana, J. M., Altimir, J., & Amigó, J. (2003). Integrated Landslide Susceptibility Analysis and Hazard Assessment in the Principality of Andorra. *Natural Hazards*, *30*(3), 421–435. https://doi.org/10.1023/B:NHAZ.0000007094.74878.d3

Dalponte, M., Marzini, S., Solano-Correa, Y. T., Tonon, G., Vescovo, L., & Gianelle, D. (2020). Mapping forest windthrows using high spatial resolution multispectral satellite images. *International Journal of Applied Earth Observation and Geoinformation*, *93*, 102206.

De Fioravante, P., Luti, T., Cavalli, A., Giuliani, C., Dichicco, P., Marchetti, M., Chirici, G., Congedo, L., & Munafò, M. (2021). Multispectral Sentinel-2 and SAR Sentinel-1 Integration for Automatic Land Cover Classification. *Land*, *10*(6), 611.

Deng, J. S., Wang, K., Deng, Y. H., & Qi, G. J. (2008). PCA-based land-use change detection and analysis using multitemporal and multisensor satellite data. *International Journal of Remote Sensing*, *29*(16), 4823–4838.

Doula, M. K., & Sarris, A. (2016). Soil environment. In *Environment and development* (pp. 213–286). Elsevier.

Dozier, J. (1989). Spectral signature of alpine snow cover from the Landsat Thematic Mapper. *Remote Sensing of Environment*, *28*(1), 9–22.

EAGLE. (2020). *Explanatory Documentation of the EAGLE Concept*. https://land.copernicus.eu/eagle/files/explanatory-documentation/eagle-concept-explanatory-documentation-version-3-1-4-12-2020

EEA. (2019). *The European environment — state and outlook 2020 Knowledge for transition to a sustainable Europe* (European Environment Agency (ed.)). https://doi.org/10.2800/96749

Ehlers, M., Sofina, N., Filippovska, Y., & Kada, M. (2014). Automated techniques for change detection using combined edge segment texture analysis, GIS, and 3D information. In *Global urban monitoring and assessment through Earth observation* (pp. 346–373). CRC Press.

Ermini, L., Catani, F., & Casagli, N. (2005). Artificial Neural Networks applied to landslide susceptibility assessment. *Geomorphology*, *66*(1), 327–343. https://doi.org/https://doi.org/10.1016/j.geomorph.2004.09.025

Esch, T., Heldens, W., Hirner, A., Keil, M., Marconcini, M., Roth, A., Zeidler, J., Dech, S., & Strano, E. (2017). Breaking new ground in mapping human settlements from space – The Global Urban Footprint. *ISPRS Journal of Photogrammetry and Remote Sensing*, *134*, 30–42. https://doi.org/https://doi.org/10.1016/j.isprsjprs.2017.10.012

European Commission. (2002). Towards a Thematic Strategy for Soil Protection. *European Commission (EC) - COM(2002)179 Final*, 35.

European Commission. (2006a). Proposal for a Directive of the European Parliament and of the Council establishing a framework for the protection of soil and amending Directive 2004/35/EC. *Directive (COM (2006) 232)*, *0086*. https://doi.org/10.1017/CBO9781107415324.004

European Commission. (2006b). *Thematic strategy for soil protection, COM(2006)231* (Issue 11). http://onlinelibrary.wiley.com/doi/10.1002/cbdv.200490137/abstract%5Cnhttp://scholar.google.com/scholar?hl=en&btnG=Search&q=intitle:Thematic+strategy+for+soil+protection#1

European Commission. (2011). *European Commission: Roadmap to a Resource Efficient Europe - COM(2011) 571 final*.

European Commission. (2012). Soil sealing in-depht report. In *Science for Environment Policy. In-depth Report* (Issue March). https://doi.org/10.2779/75498

European Commission. (2019a). Reflection paper: Towards a Sustainable Europe by 2030. *Journal of Chemical Information and Modeling*, *53*(9), 1689–1699.

European Commission. (2019b). *Sustainable development in the European Union — Overview of progress towards the SDGs in an EU context — 2019 edition* (SDGs & me).

European Commission. (2019c). The European Green Deal, COM(2019) 640 final. In *European Commission*. https://doi.org/10.1017/CBO9781107415324.004

European Commission. (2020). *Roadmap, New Soil Strategy - healthy soil for a healthy life* (Issue 2020).

European Commission, Geneletti, D., Biasiolli, A., & Morrison-Saunders, A. (2016). No net land take by 2050 ? *Environmental Impact Assessment Review*, *67*(14), 117–123. https://doi.org/10.2779/537195

European Environment Agency. (2017). Landscapes in Transition. An account of 25 years of land cover change in Europe. *EEA Report*, *10*, 226. https://www.eea.europa.eu/publications/landscapes-in-transition

European Parliament, C. of the E. U. (2007). Directive 2007/2/EC of the European Parliament and of the Council of 14 March 2007 establishing an Infrastructure for Spatial Information in the European Community (INSPIRE). *Official Journal of the European Union*, *50*.

European Union. (2013). Decision No 1386/2013/EU of the European Parliament and of the Council of 20 November 2013 on a General Union Environment Action Programme to 2020 "Living well, within the limits of our planet." *Official Journal of the European Union*, *1600*, 171–200. http://eur-lex.europa.eu/legal-content/EN/TXT/PDF/?uri=CELEX:32013D1386&from=EN

Falkowski, M. J., Wulder, M. A., White, J. C., & Gillis, M. D. (2009). Supporting large-area, sample-based forest inventories with very high spatial resolution satellite imagery. *Progress in Physical Geography*, *33*(3), 403–423.

FAO. (2016). Map accuracy assessment and area estimation : a practical guide. *National Forest Monitoring Assessment Working Paper*, *E*(46), 69. http://www.fao.org/3/a-i5601e.pdf

Fawcett, T. (2006). An introduction to ROC analysis. *Pattern Recognition Letters*, *27*(8), 861–874. https://doi.org/https://doi.org/10.1016/j.patrec.2005.10.010

Fell, R., Corominas, J., Bonnard, C., Cascini, L., Leroi, E., & Savage, W. Z. (2008). Guidelines for landslide susceptibility, hazard and risk zoning for land use planning. *Engineering Geology*, *102*(3), 85–98. https://doi.org/https://doi.org/10.1016/j.enggeo.2008.03.022

Flores-Anderson, A. I., Herndon, K. E., Thapa, R. B., & Cherrington, E. (2019). *The SAR Handbook: Comprehensive Methodologies for Forest Monitoring and Biomass Estimation*.

Foody, G. M., & Mathur, A. (2006). The use of small training sets containing mixed pixels for accurate hard image classification: Training on mixed spectral responses for classification by a SVM. *Remote Sensing of Environment*, *103*(2), 179–189.

Formaggio, A. R., Epiphanio, J. C. N., & Simões, M. dos S. (2001). Radarsat backscattering from an agricultural scene. *Pesquisa Agropecuária Brasileira*, *36*(5), 823–830.

Frate, L., Fabrizio, M., Ciaschetti, G., & Spera, M. (2018). Analisi spaziale dell'incendio del Morrone nel Parco Nazionale della Majella mediante l'utilizzo di immagini satellitari. *Forest@-Journal of Silviculture and Forest Ecology*, *15*(1), 59.

Frattini, P., Crosta, G., & Carrara, A. (2010). Techniques for evaluating the performance of landslide susceptibility models. *Engineering Geology*, *111*(1), 62–72. https://doi.org/https://doi.org/10.1016/j.enggeo.2009.12.004

Frelih-Larsen, A., Bowyer, C., Albrecht, S., Keenleyside, C., Kemper, M., Nanni, S., Naumann, S., Mottershead, D., Landgrebe, R., Andersen, E., Banfi, P., Bell, S., Brémere, I., Cools, J., Herbert, S., Iles, A., Kampa, E., Kettunen, M., Lukacova, Z., … Vidaurre, R. (2017). *Updated Inventory and Assessment of Soil Protection Policy Instruments in EU Member States*. *February*, 462. https://www.ecologic.eu/14567

Gamba, P., Dell'Acqua, F., & Trianni, G. (2007). Rapid damage detection in the Bam area using multitemporal SAR and exploiting ancillary data. *IEEE Transactions on Geoscience and Remote Sensing*, *45*(6), 1582–1589.

Gardi, C., Panagos, P., Van Liedekerke, M., Bosco, C., & De Brogniez, D. (2015). Land take and food security: assessment of land take on the agricultural production in Europe. *Journal of Environmental Planning and Management*, *58*(5), 898–912. https://doi.org/10.1080/09640568.2014.899490

Ghosh, S., Roy, M., & Ghosh, A. (2014). Semi-supervised change detection using modified self-organizing feature map neural network. *Applied Soft Computing*, *15*, 1–20.

Giannetti, F., Pegna, R., Francini, S., McRoberts, R. E., Travaglini, D., Marchetti, M., Scarascia Mugnozza, G., & Chirici, G. (2020). A New Method for Automated Clearcut Disturbance Detection in Mediterranean Coppice Forests Using Landsat Time Series. *Remote Sensing*, *12*(22), 3720.

Goldblatt, R., Deininger, K., & Hanson, G. (2018). Utilizing publicly available satellite data for urban research: Mapping built-up land cover and land use in Ho Chi Minh City, Vietnam. *Development Engineering*, *3*, 83–99.

Gómez, C., White, J. C., & Wulder, M. A. (2016). Optical remotely sensed time series data for land cover classification: A review. *ISPRS Journal of Photogrammetry and Remote Sensing*, *116*, 55–72. https://doi.org/10.1016/j.isprsjprs.2016.03.008

Gorelick, N., Hancher, M., Dixon, M., Ilyushchenko, S., Thau, D., & Moore, R. (2017). Google Earth Engine: Planetary-scale geospatial analysis for everyone. *Remote Sensing of Environment*, *202*, 18–27. https://doi.org/10.1016/j.rse.2017.06.031

Grabska, E., Hostert, P., Pflugmacher, D., & Ostapowicz, K. (2019). Forest stand species mapping using the Sentinel-2 time series. *Remote Sensing*, *11*(10), 1197.

Gulácsi, A., & Kovács, F. (2020). Sentinel-1-imagery-based high-resolutionwater cover detection on wetlands, aided by google earth engine. *Remote Sensing*, *12*(10), 1–20. https://doi.org/10.3390/rs12101614

Haas, J., & Ban, Y. (2017). Sentinel-1A SAR and sentinel-2A MSI data fusion for urban ecosystem service mapping. *Remote Sensing Applications: Society and Environment*, *8*, 41–53.

Haidu, I., Furtuna, P. R., & Lebaut, S. (2019). Detection of old scattered windthrow using low cost resources. The case of Storm Xynthia in the Vosges Mountains, 28 February 2010. *Open Geosciences*, *11*(1), 492–504.

Hansen, M. C., & Loveland, T. R. (2012). A review of large area monitoring of land cover change using Landsat data. *Remote Sensing of Environment*, *122*, 66–74.

Hay, A. M. (1979). Sampling designs to test land-use map accuracy. *Photogrammetric Engineering and Remote Sensing*, *45*(4), 529–533.

He, C., Wei, A., Shi, P., Zhang, Q., & Zhao, Y. (2011). Detecting land-use/land-cover change in rural–urban fringe areas using extended change-vector analysis. *International Journal of Applied Earth Observation and Geoinformation*, *13*(4), 572–585.

Helman, D., Lensky, I. M., Tessler, N., & Osem, Y. (2015). A phenology-based method for monitoring woody and herbaceous vegetation in mediterranean forests from NDVI time series. *Remote Sensing*, *7*(9), 12314–12335. https://doi.org/10.3390/rs70912314

Holtgrave, A. K., Röder, N., Ackermann, A., Erasmi, S., & Kleinschmit, B. (2020). Comparing Sentinel-1 and -2 data and indices for agricultural land use monitoring. *Remote Sensing*, *12*(18). https://doi.org/10.3390/RS12182919

Hościło, A., & Lewandowska, A. (2019). Mapping forest type and tree species on a regional scale using multi-temporal Sentinel-2 data. *Remote Sensing*, *11*(8), 929.

Hussain, M., Chen, D., Cheng, A., Wei, H., & Stanley, D. (2013). Change detection from remotely sensed images: From pixel-based to object-based approaches. *ISPRS Journal of Photogrammetry and Remote Sensing*, *80*, 91–106.

Imhoff, M., Lahouari, B., Taylor, R., Colby, L., Robert, H., & William, L. (2004). Global patterns in human consumption of net primary production. *Nature*, *429*(6994), 867–870. https://doi.org/10.1038/nature02685.Published

Immitzer, M., Neuwirth, M., Böck, S., Brenner, H., Vuolo, F., & Atzberger, C. (2019). Optimal input features for tree species classification in Central Europe based on multi-temporal Sentinel-2 data. *Remote Sensing*, *11*(22). https://doi.org/10.3390/rs11222599

ISPRA. (2018). *TERRITORIO Processi e trasformazioni in Italia, Rapporti 296/2018* (ISPRA). Roma.

Johnson, R. D., & Kasischke, E. S. (1998). Change vector analysis: A technique for the multispectral monitoring of land cover and condition. *International Journal of Remote Sensing*, *19*(3), 411–426.

Joshi, N., Baumann, M., Ehammer, A., Fensholt, R., Grogan, K., Hostert, P., Jepsen, M. R., Kuemmerle, T., Meyfroidt, P., Mitchard, E. T. A., Reiche, J., Ryan, C. M., & Waske, B. (2016). A review of the application of optical and radar remote sensing data fusion to land use mapping and monitoring. *Remote Sensing*, *8*(1), 1–23. https://doi.org/10.3390/rs8010070

Karantzalos, K. (2015). Recent advances on 2D and 3D change detection in urban environments from remote sensing data. In *Computational Approaches for Urban Environments* (pp. 237–272). Springer.

Kavoura, K., & Sabatakakis, N. (2020). Investigating landslide susceptibility procedures in Greece. *Landslides*, *17*(1), 127–145. https://doi.org/10.1007/s10346-019-01271-y

Keeley, J. E. (2009). Fire intensity, fire severity and burn severity: a brief review and suggested usage. *International Journal of Wildland Fire*, *18*(1), 116–126.

Key, C. H., & Benson, N. C. (1999). The Normalized Burn Ratio (NBR): A Landsat TM radiometric measure of burn severity. *United States Geological Survey, Northern Rocky Mountain Science Center.(Bozeman, MT)*.

Key, C. H., & Benson, N. C. (2006). Landscape assessment: Remote sensing of severity, the Normalized Burn Ratio.

FIREMON: Fire Effects Monitoring and Inventory System. General Technical Report, RMRS-GTR-164-CD, 305–325. https://www.fs.fed.us/rm/pubs/rmrs_gtr164/rmrs_gtr164_13_land_assess.pdf

Kibblewhite, M. G., Jones, R. J. A., Montanarella, L., Baritz, R., Huber, S., Arrouays, D., Micheli, E., & Stephens, M. (2008). Environmental Assessment of Soil for Monitoring Volume VI: Soil Monitoring System for Europe. In *JRC Scientific and Technical Reports: Vol. EUR 23490*. https://doi.org/10.2788/95007

Kleeschulte, S., Banko, G., Smith, G., Arnold, S., Scholz, J., Kosztra, B., & Maucha, G. (2019). *Technical specifications for implementation of a new land-monitoring concept based on EAGLE D5: Design concept and CLC+ Backbone, technical specifications, CLC+ Core and CLC+ Instances draft specifications, including requirements review Version 5.4*. 0–78.

Koppel, K., Zalite, K., Voormansik, K., & Jagdhuber, T. (2017). Sensitivity of Sentinel-1 backscatter to characteristics of buildings. *International Journal of Remote Sensing*, *38*(22), 6298–6318. https://doi.org/10.1080/01431161.2017.1353160

Kotsiantis, S. B., Zaharakis, I., & Pintelas, P. (2007). Supervised machine learning: A review of classification techniques. *Emerging Artificial Intelligence Applications in Computer Engineering*, *160*(1), 3–24.

Lee, S., Ryu, J.-H., Won, J.-S., & Park, H.-J. (2004). Determination and application of the weights for landslide susceptibility mapping using an artificial neural network. *Engineering Geology*, *71*(3), 289–302. https://doi.org/https://doi.org/10.1016/S0013-7952(03)00142-X

Lefebvre, A., Sannier, C., & Corpetti, T. (2016). Monitoring urban areas with Sentinel-2A data: Application to the update of the Copernicus high resolution layer imperviousness degree. *Remote Sensing*, *8*(7), 606.

Li, Y., Martinis, S., & Wieland, M. (2019). Urban flood mapping with an active self-learning convolutional neural network based on TerraSAR-X intensity and interferometric coherence. *ISPRS Journal of Photogrammetry and Remote Sensing*, *152*, 178–191.

Liu, S., Du, Q., Tong, X., Samat, A., Bruzzone, L., & Bovolo, F. (2017). Multiscale morphological compressed change vector analysis for unsupervised multiple change detection. *IEEE Journal of Selected Topics in Applied Earth Observations and Remote Sensing*, *10*(9), 4124–4137.

Liu, X., Hu, G., Chen, Y., Li, X., Xu, X., Li, S., Pei, F., & Wang, S. (2018). High-resolution multi-temporal mapping of global urban land using Landsat images based on the Google Earth Engine Platform. *Remote Sensing of Environment*, *209*, 227–239.

Lu, D., Li, G., & Moran, E. (2014). Current situation and needs of change detection techniques. *International Journal of Image and Data Fusion*, *5*(1), 13–38.

Lu, D., Mausel, P., Brondizio, E., & Moran, E. (2004). Change detection techniques. *International Journal of Remote Sensing*, *25*(12), 2365–2401.

Ma, L., Liu, Y., Zhang, X., Ye, Y., Yin, G., & Johnson, B. A. (2019). Deep learning in remote sensing applications: A meta-analysis and review. *ISPRS Journal of Photogrammetry and Remote Sensing*, *152*, 166–177.

Mansaray, L. R., Huang, W., Zhang, D., Huang, J., & Li, J. (2017). Mapping rice fields in urban Shanghai, southeast China, using Sentinel-1A and Landsat 8 datasets. *Remote Sensing*, *9*(3). https://doi.org/10.3390/rs9030257

Mårtensson, U. (2011). Introduction to Remote Sensing and Geographical Information Systems. *Department of Physical Geography and Ecosystems Sciences*, 55.

Maxwell, A. E., Warner, T. A., Vanderbilt, B. C., & Ramezan, C. A. (2017). Land cover classification and feature extraction from national agriculture imagery program (NAIP) Orthoimagery: A Review. *Photogrammetric Engineering & Remote Sensing*, *83*(11), 737–747.

McFeeters, S. K. (2013). Using the normalized difference water index (ndwi) within a geographic information system to detect swimming pools for mosquito abatement: A practical approach. *Remote Sensing*, *5*(7), 3544–3561. https://doi.org/10.3390/rs5073544

McFEETERS, S. K. (1996). The use of the Normalized Difference Water Index (NDWI) in the delineation of open water features. *International Journal of Remote Sensing*, *17*(7), 1425–1432. https://doi.org/10.1080/01431169608948714

McRoberts, R. E. (2011). Satellite image-based maps: Scientific inference or pretty pictures? *Remote Sensing of Environment*, *115*(2), 715–724.

Mendes, R. M., de Andrade, M. R. M., Tomasella, J., de Moraes, M. A. E., & Scofield, G. B. (2018). Understanding shallow landslides in Campos do Jordão municipality-Brazil: disentangling the anthropic effects from natural causes in the disaster of 2000. *Natural Hazards & Earth System Sciences*, *18*(1).

Mickelson, J. G., Civco, D. L., & Silander, J. A. (1998). Delineating forest canopy species in the northeastern United States using multi-temporal TM imagery. *Photogrammetric Engineering and Remote Sensing*, *64*, 891–904.

Mitchell, T. (1997). Introduction to machine learning. *Machine Learning*, *7*, 2–5.

Montanarella, L., Scholes, R., & Brainich, A. (eds.). (2018). The IPBES assessment report on land degradation and restoration. *Intergovernmental Science-Policy Platform on Biodiversity and Ecosystem Services*, *May 2019*, 1–748. https://www.taylorfrancis.com/books/9781317275886/chapters/10.4324/9781315640051-105

Montero, E., Van Wolvelaer, J., & Garzón, A. (2014). The European urban atlas. In *Land use and land cover mapping in Europe* (pp. 115–124). Springer.

Moreira, A. (2013). Synthetic aperture radar (SAR): Principles and applications. *The 4th Advance Training Course in Land Remote Sensing*, 1–5.

Moser, G., & Serpico, S. B. (2006). Generalized minimum-error thresholding for unsupervised change detection from SAR amplitude imagery. *IEEE Transactions on Geoscience and Remote Sensing*, *44*(10), 2972–2982.

Munafò, M. (2019). *Consumo di suolo, dinamiche territoriali e servizi ecosistemici. Edizione 2019*. https://doi.org/978-88-448-0964-5

Munafò, M. (2020). *Consumo di suolo, dinamiche territoriali e servizi ecosistemici. Edizione 2019*. https://doi.org/978-88-448-0964-5

Naumann, S., Frelih-Larsen, A., Prokop, G., Ittner, S., Reed, M., Mills, J., Morari, F., Verzandvoort, S., Albrecht, S., Bjuréus, A., Siebielec, G., & Miturski, T. (2019). *Land Take and Soil Sealing—Drivers, Trends and Policy (Legal) Instruments: Insights from European Cities*. 83–112. https://doi.org/10.1007/978-3-030-00758-4_4

Nemmour, H., & Chibani, Y. (2006). Multiple support vector machines for land cover change detection: An application for mapping urban extensions. *ISPRS Journal of Photogrammetry and Remote Sensing*, *61*(2), 125–133.

Nezry, E. (2014). Adaptive speckle filtering in radar imagery. *Land Applications of Radar Remote Sensing; IntechOpen: London, UK*, 1–55.

Nguyen, C. T., Chidthaisong, A., Kieu Diem, P., & Huo, L.-Z. (2021). A Modified Bare Soil Index to Identify Bare Land Features during Agricultural Fallow-Period in Southeast Asia Using Landsat 8. *Land*, *10*(3), 231.

Notti, D., Galve, J. P., Mateos, R. M., Monserrat, O., Lamas-Fernández, F., Fernández-Chacón, F., Roldán-García, F. J., Pérez-Peña, J. V., Crosetto, M., & Azañón, J. M. (2015). Human-induced coastal landslide reactivation. Monitoring by PSInSAR techniques and urban damage survey (SE Spain). *Landslides*, *12*(5), 1007–1014. https://doi.org/10.1007/s10346-015-0612-3

Olofsson, P., Foody, G. M., Herold, M., Stehman, S. V., Woodcock, C. E., & Wulder, M. A. (2014). Good practices for estimating area and assessing accuracy of land change. *Remote Sensing of Environment*, *148*, 42–57. https://doi.org/10.1016/j.rse.2014.02.015

Olofsson, P., Foody, G. M., Stehman, S. V., & Woodcock, C. E. (2013). Making better use of accuracy data in land change studies: Estimating accuracy and area and quantifying uncertainty using stratified estimation. *Remote Sensing of Environment*, *129*, 122–131. https://doi.org/10.1016/j.rse.2012.10.031

Pal, M., & Antil, K. (2017). Comparison of Landsat 8 and Sentinel 2 data for Accurate Mapping of Built-Up Area and Bare Soil. *38th Asian Conference on Remote Sensing (ACRS 2017): Space Applications: Touching Human Lives Paper*, 137–140.

Parks, S. A., Dillon, G. K., & Miller, C. (2014). A new metric for quantifying burn severity: The relativized burn ratio. *Remote Sensing*, *6*(3), 1827–1844. https://doi.org/10.3390/rs6031827

Pepe, M., & Parente, C. (2018). Burned area recognition by change detection analysis using images derived from Sentinel-2 satellite: The case study of Sorrento Peninsula, Italy. *Journal of Applied Engineering Science*, *16*(2), 225–232.

Persson, M., Lindberg, E., & Reese, H. (2018a). Tree species classification with multi-temporal Sentinel-2 data. *Remote Sensing*, *10*(11), 1–17. https://doi.org/10.3390/rs10111794

Persson, M., Lindberg, E., & Reese, H. (2018b). Tree species classification with multi-temporal Sentinel-2 data. *Remote Sensing*, *10*(11), 1794.

Pesaresi, M., Corbane, C., Julea, A., Florczyk, A. J., Syrris, V., & Soille, P. (2016). Assessment of the added-value of sentinel-2 for detecting built-up areas. *Remote Sensing*, *8*(4), 299.

Pesaresi, M., Huadong, G., Blaes, X., Ehrlich, D., Ferri, S., Gueguen, L., Halkia, M., Kauffmann, M., Kemper, T., Lu, L., Marin-Herrera, M. A., Ouzounis, G. K., Scavazzon, M., Soille, P., Syrris, V., & Zanchetta, L. (2013). A global human settlement layer from optical HR/VHR RS data: Concept and first results. *IEEE Journal of Selected Topics in Applied Earth Observations and Remote Sensing*, *6*(5), 2102–2131. https://doi.org/10.1109/JSTARS.2013.2271445

Pimentel, D. (2006). Soil erosion: A food and environmental threat. *Environment, Development and Sustainability*, *8*(1), 119–137. https://doi.org/10.1007/s10668-005-1262-8

Pistocchi, A. (2017). Hydrological impacts of soil sealing and urban land take. *Urban Expansion, Land Cover and Soil Ecosystem Services*, 157–168.

Pradhan, B., Sezer, E. A., Gokceoglu, C., & Buchroithner, M. F. (2010). Landslide Susceptibility Mapping by Neuro-Fuzzy Approach in a Landslide-Prone Area (Cameron Highlands, Malaysia). *IEEE Transactions on Geoscience and Remote Sensing*, *48*(12), 4164–4177. https://doi.org/10.1109/TGRS.2010.2050328

Puletti, N., Chianucci, F., & Castaldi, C. (2018). Use of Sentinel-2 for forest classification in Mediterranean environments. *Ann. Silvic. Res*, *42*, 32–38.

Radke, R. J., Andra, S., Al-Kofahi, O., & Roysam, B. (2005). Image change detection algorithms: a systematic survey. *IEEE Transactions on Image Processing*, *14*(3), 294–307.

Rasul, A., Balzter, H., Ibrahim, G. R. F., Hameed, H. M., Wheeler, J., Adamu, B., Ibrahim, S., & Najmaddin, P. M. (2018). Applying built-up and bare-soil indices from Landsat 8 to cities in dry climates. *Land*, *7*(3), 81.

Reba, M., & Seto, K. C. (2020). A systematic review and assessment of algorithms to detect, characterize, and monitor urban land change. *Remote Sensing of Environment*, *242*(February). https://doi.org/10.1016/j.rse.2020.111739

Reichenbach, P., Rossi, M., Malamud, B. D., Mihir, M., & Guzzetti, F. (2018). A review of statistically-based landslide susceptibility models. *Earth-Science Reviews*, *180*, 60–91. https://doi.org/https://doi.org/10.1016/j.earscirev.2018.03.001

Rodriguez-Galiano, V. F., Ghimire, B., Rogan, J., Chica-Olmo, M., & Rigol-Sanchez, J. P. (2012). An assessment of the effectiveness of a random forest classifier for land-cover classification. *ISPRS Journal of Photogrammetry and Remote Sensing*, *67*, 93–104.

Rossi, M., Guzzetti, F., Reichenbach, P., Mondini, A. C., & Peruccacci, S. (2010). Optimal landslide susceptibility zonation based on multiple forecasts. *Geomorphology*, *114*(3), 129–142. https://doi.org/https://doi.org/10.1016/j.geomorph.2009.06.020

Rouse Jr, J. W. (1973). *Monitoring the vernal advancement and retrogradation (green wave effect) of natural vegetation*.

Ruby, E. (2005). How Urbanization Affects the Water Cycle. *CA WALUP Partnership Website*, 1–4. https://www.google.co.uk/?gws_rd=cr&ei=qIUdU4iVDoKqhAfK14CgCQ#q=pouplation+and+increasing+urbanization+effects+on+water+ycle

Rüetschi, M., Small, D., & Waser, L. T. (2019). Rapid detection of windthrows using sentinel-1 c-band sar data. *Remote Sensing*, *11*(2), 115.

Saha, S., Bovolo, F., & Bruzzone, L. (2019). Unsupervised deep change vector analysis for multiple-change detection in VHR images. *IEEE Transactions on Geoscience and Remote Sensing*, *57*(6), 3677–3693.

Salvati, L., Bajocco, S., Ceccarelli, T., Zitti, M., & Perini, L. (2011). Towards a process-based evaluation of land vulnerability to soil degradation in Italy. *Ecological Indicators*, *11*(5), 1216–1227. https://doi.org/10.1016/j.ecolind.2010.12.024

Scalenghe, R., & Ajmone-Marsan, F. (2009). The anthropogenic sealing of soils in urban areas. *Landscape and Urban Planning*, *90*(1–2), 1–10. https://doi.org/10.1016/j.landurbplan.2008.10.011

Schneider, A. (2012). Monitoring land cover change in urban and peri-urban areas using dense time stacks of Landsat satellite data and a data mining approach. *Remote Sensing of Environment*, *124*, 689–704.

Schriever, J. R., & Congalton, R. G. (1995). Evaluating seasonal variability as an aid to cover-type mapping from Landsat

Thematic Mapper data in the Northeast. *Photogrammetric Engineering and Remote Sensing*, *61*(3), 321–327.

Schwarz, M., Steinmeier, C., Holecz, F., Stebler, O., & Wagner, H. (2003). Detection of windthrow in mountainous regions with different remote sensing data and classification methods. *Scandinavian Journal of Forest Research*, *18*(6), 525–536.

Segoni, S., Pappafico, G., Luti, T., & Catani, F. (2020). Landslide susceptibility assessment in complex geological settings: sensitivity to geological information and insights on its parameterization. *Landslides*. https://doi.org/10.1007/s10346-019-01340-2

Segoni, S., Tofani, V., Lagomarsino, D., & Moretti, S. (2016). Landslide susceptibility of the Prato–Pistoia–Lucca provinces, Tuscany, Italy. *Journal of Maps*, *12*(sup1), 401–406. https://doi.org/10.1080/17445647.2016.1233463

Segoni, S., Tofani, V., Rosi, A., Catani, F., & Casagli, N. (2018). Combination of rainfall thresholds and susceptibility maps for dynamic landslide hazard assessment at regional scale. *Frontiers in Earth Science*, *6*, 85.

Sezer, E. A., Pradhan, B., & Gokceoglu, C. (2011). Manifestation of an adaptive neuro-fuzzy model on landslide susceptibility mapping: Klang valley, Malaysia. *Expert Systems with Applications*, *38*(7), 8208–8219. https://doi.org/https://doi.org/10.1016/j.eswa.2010.12.167

Shu, H., Hürlimann, M., Molowny-Horas, R., González, M., Pinyol, J., Abancó, C., & Ma, J. (2019). Relation between land cover and landslide susceptibility in Val d'Aran, Pyrenees (Spain): Historical aspects, present situation and forward prediction. *Science of The Total Environment*, *693*, 133557. https://doi.org/https://doi.org/10.1016/j.scitotenv.2019.07.363

Singh, A. (1989). Review article digital change detection techniques using remotely-sensed data. *International Journal of Remote Sensing*, *10*(6), 989–1003.

Skirvin, S. M., Kepner, W. G., Marsh, S. E., Drake, S. E., Maingi, J. K., Edmonds, C. M., Watts, C. J., & Williams, D. R. (2004). Assessing the accuracy of satellite-derived land-cover classification using historical aerial photography, digital orthophoto quadrangles, and airborne video data. *Remote Sensing and GIS Accuracy Assessment*, *9*, 115–131.

Sobrino, J., Llorens, R., Fernández, C., Fernández-Alonso, J., & Vega, J. (2019). Relationship between Soil Burn Severity in Forest Fires Measured In Situ and through Spectral Indices of Remote Detection. *Forests*, *10*(5), 457. https://doi.org/10.3390/f10050457

Spadoni, G. L., Cavalli, A., Congedo, L., & Munafò, M. (2020). Analysis of Normalized Difference Vegetation Index (NDVI) multi-temporal series for the production of forest cartography. *Remote Sensing Applications: Society and Environment*, *20*(August). https://doi.org/10.1016/j.rsase.2020.100419

Stehman, Stephen V., & Foody, G. M. (2019). Key issues in rigorous accuracy assessment of land cover products. *Remote Sensing of Environment*, *231*(June), 111199. https://doi.org/10.1016/j.rse.2019.05.018

Stehman, Stephen V., Olofsson, P., Woodcock, C. E., Herold, M., & Friedl, M. A. (2012). A global land-cover validation data set, II: Augmenting a stratified sampling design to estimate accuracy by region and land-cover class. *International Journal of Remote Sensing*, *33*(22), 6975–6993. https://doi.org/10.1080/01431161.2012.695092

Stehman, S V, & Czaplewski, R. L. (1998). Design and Analysis for Thematic Map Accuracy Assessment - an application of satellite imagery. *Remote Sensing of Environment*, *64*(January), 331–344. http://www.ingentaconnect.com/content/els/00344257/1998/00000064/00000003/art00010%5Cnhttp://dx.doi.org/10.1016/S0034-4257(98)00010-8

Steinhausen, M. J., Wagner, P. D., Narasimhan, B., & Waske, B. (2018a). Combining Sentinel-1 and Sentinel-2 data for improved land use and land cover mapping of monsoon regions. *International Journal of Applied Earth Observation and Geoinformation*, *73*, 595–604.

Steinhausen, M. J., Wagner, P. D., Narasimhan, B., & Waske, B. (2018b). Combining Sentinel-1 and Sentinel-2 data for improved land use and land cover mapping of monsoon regions. *International Journal of Applied Earth Observation and Geoinformation*, *73*(April), 595–604. https://doi.org/10.1016/j.jag.2018.08.011

Stephan Arnold, Barbara Kosztra, Gebhard Banko, Pavel Milenov, G. S., Gerard Hazeu Revised by: Stephan Arnold, Geoff Smith, Michael Bock, G., & Hazeu, Barbara Kosztra, Christoph Perger, M. C. (1983). *Multivariate models for landslide hazard evaluation*. Ogy. https://doi.org/10.1007/BF01031290

Stephan Arnold, Barbara Kosztra, Gebhard Banko, Pavel Milenov, G. S., Gerard Hazeu Revised by: Stephan Arnold, Geoff Smith, Michael Bock, G., & Hazeu, Barbara Kosztra, Christoph Perger, M. C. (2021). *Explanatory Content*

Documentation of the EAGLE Concept [2021, version 3.1]. https://land.copernicus.eu/eagle/content-documentation-of-the-eagle-concept/manual/eagle-explanatory-documentation-v3-1-version-2021

Strollo, A., Smiraglia, D., Bruno, R., Assennato, F., Congedo, L., De Fioravante, P., Giuliani, C., Marinosci, I., Riitano, N., & Munafò, M. (2020). Land consumption in Italy. *Journal of Maps*, *16*(1), 113–123.

Sun, Z., Xu, R., Du, W., Wang, L., & Lu, D. (2019). High-resolution urban land mapping in China from sentinel 1A/2 imagery based on Google Earth Engine. *Remote Sensing*, *11*(7), 752.

Teodoro, A., & Amaral, A. (2019). A statistical and spatial analysis of portuguese forest fires in summer 2016 considering landsat 8 and sentinel 2A data. *Environments - MDPI*, *6*(3). https://doi.org/10.3390/environments6030036

Tewkesbury, A. P., Comber, A. J., Tate, N. J., Lamb, A., & Fisher, P. F. (2015). A critical synthesis of remotely sensed optical image change detection techniques. *Remote Sensing of Environment*, *160*, 1–14.

Thanh Noi, P., & Kappas, M. (2018). Comparison of random forest, k-nearest neighbor, and support vector machine classifiers for land cover classification using Sentinel-2 imagery. *Sensors*, *18*(1), 18.

Thonfeld, F., Feilhauer, H., Braun, M., & Menz, G. (2016). Robust Change Vector Analysis (RCVA) for multi-sensor very high resolution optical satellite data. *International Journal of Applied Earth Observation and Geoinformation*, *50*, 131–140.

Trigila A. et al. (2018). *Dissesto idrogeologico in Italia: pericolosità e indicatori di rischio - edizione 2018. ISPRA, Rapporti 287/2018*. ISPRA.

Turchi, A., Di Traglia, F., Luti, T., Olori, D., Zetti, I., & Fanti, R. (2020). Environmental Aftermath of the 2019 Stromboli Eruption. *Remote Sensing*, *12*(6), 994.

Ulander, L. M. H., Smith, G., Eriksson, L., Folkesson, K., Fransson, J. E. S., Gustavsson, A., Hallberg, B., Joyce, S., Magnusson, M., & Olsson, H. (2005). Mapping of wind-thrown forests in southern Sweden using space-and airborne SAR. *Proceedings. 2005 IEEE International Geoscience and Remote Sensing Symposium, 2005. IGARSS'05.*, *5*, 3619–3622.

UNCCD. (2016). *Achieving Land Degradation Neutrality at the country level*. https://knowledge.unccd.int/topics/land-degradation-neutrality

UNCCD. (2017). *The Global Land Outlook* (First edit). Bonn, Germany.

United Nations. (2015). *Transforming our World: The 2030 Agenda for Sustainable Development, A/RES/70/1.* Washington, DC, USA. https://sustainabledevelopment.un.org/content/documents/21252030 Agenda for Sustainable Development web.pdf

United Nations. (2018). World Urbanization Prospects. In *Demographic Research* (Vol. 12). https://population.un.org/wup/Publications/Files/WUP2018-Report.pdf

Vaglio Laurin, G., Francini, S., Luti, T., Chirici, G., Pirotti, F., & Papale, D. (2020). Satellite open data to monitor forest damage caused by extreme climate-induced events: a case study of the Vaia storm in Northern Italy. *Forestry: An International Journal of Forest Research*.

Valdiviezo-N, J. C., Téllez-Quiñones, A., Salazar-Garibay, A., & López-Caloca, A. A. (2018). Built-up index methods and their applications for urban extraction from Sentinel 2A satellite data: discussion. *JOSA A*, *35*(1), 35–44.

Van Den Eeckhaut, M., Reichenbach, P., Guzzetti, F., Rossi, M., & Poesen, J. (2009). Combined landslide inventory and susceptibility assessment based on different mapping units: an example from the Flemish Ardennes, Belgium. *Natural Hazards and Earth System Sciences*, *9*(2), 507–521.

Veraverbeke, S., Lhermitte, S., Verstraeten, W. W., & Goossens, R. (2010). The temporal dimension of differenced Normalized Burn Ratio (dNBR) fire/burn severity studies: The case of the large 2007 Peloponnese wildfires in Greece. *Remote Sensing of Environment*, *114*(11), 2548–2563.

Volpi, M., Tuia, D., Bovolo, F., Kanevski, M., & Bruzzone, L. (2013). Supervised change detection in VHR images using contextual information and support vector machines. *International Journal of Applied Earth Observation and Geoinformation*, *20*, 77–85.

Warner, T. A., Almutairi, A., & Lee, J. Y. (2009). Remote sensing of land cover change. *The SAGE Handbook of Remote Sensing, SAGE, London*, 459–472.

Weng, Q. (2013). *Remote Sensing of Natural Resources* (Q. W. Guangxing Wang (ed.); 1st Editio). CRC Press.

https://doi.org/https://doi.org/10.1201/b15159

White, J. C., Saarinen, N., Kankare, V., Wulder, M. A., Hermosilla, T., Coops, N. C., Pickell, P. D., Holopainen, M., Hyyppä, J., & Vastaranta, M. (2018). Confirmation of post-harvest spectral recovery from Landsat time series using measures of forest cover and height derived from airborne laser scanning data. *Remote Sensing of Environment*, *216*, 262–275. https://doi.org/https://doi.org/10.1016/j.rse.2018.07.004

White, J. C., Wulder, M. A., Hermosilla, T., Coops, N. C., & Hobart, G. W. (2017). A nationwide annual characterization of 25years of forest disturbance and recovery for Canada using Landsat time series. *Remote Sensing of Environment*, *194*, 303–321. https://doi.org/https://doi.org/10.1016/j.rse.2017.03.035

Wulder, M. A., White, J. C., Magnussen, S., & McDonald, S. (2007). Validation of a large area land cover product using purpose-acquired airborne video. *Remote Sensing of Environment*, *106*(4), 480–491.

Wunder, S., Kaphengst, T., & Frelih-Larsen, A. (2018). Implementing Land Degradation Neutrality (SDG 15.3) at National Level: General Approach, Indicator Selection and Experiences from Germany. In H. Ginzky, E. Dooley, I. L. Heuser, E. Kasimbazi, T. Markus, & T. Qin (Eds.), *International Yearbook of Soil Law and Policy 2017* (pp. 191–219). Springer International Publishing. https://doi.org/10.1007/978-3-319-68885-5_11

Xiao, T., Segoni, S., Chen, L., Yin, K., & Casagli, N. (2020). A step beyond landslide susceptibility maps: a simple method to investigate and explain the different outcomes obtained by different approaches. *Landslides*, *17*(3), 627–640. https://doi.org/10.1007/s10346-019-01299-0

Ye, S., Chen, D., & Yu, J. (2016). A targeted change-detection procedure by combining change vector analysis and post-classification approach. *ISPRS Journal of Photogrammetry and Remote Sensing*, *114*, 115–124.

Yilmaz, I. (2009). Landslide susceptibility mapping using frequency ratio, logistic regression, artificial neural networks and their comparison: A case study from Kat landslides (Tokat—Turkey). *Computers & Geosciences*, *35*(6), 1125–1138. https://doi.org/https://doi.org/10.1016/j.cageo.2008.08.007

Youssef, A. M., Pourghasemi, H. R., Pourtaghi, Z. S., & Al-Katheeri, M. M. (2016). Landslide susceptibility mapping using random forest, boosted regression tree, classification and regression tree, and general linear models and comparison of their performance at Wadi Tayyah Basin, Asir Region, Saudi Arabia. *Landslides*, *13*(5), 839–856. https://doi.org/10.1007/s10346-015-0614-1

Zanotta, D. C., Bruzzone, L., Bovolo, F., & Shimabukuro, Y. E. (2015). An adaptive semisupervised approach to the detection of user-defined recurrent changes in image time series. *IEEE Transactions on Geoscience and Remote Sensing*, *53*(7), 3707–3719.

Zhang, F., Liu, G., Chen, W., Liang, S., Chen, R., & Han, W. (2012). Human-induced landslide on a high cut slope: a case of repeated failures due to multi-excavation. *Journal of Rock Mechanics and Geotechnical Engineering*, *4*(4), 367–374. https://doi.org/https://doi.org/10.3724/SP.J.1235.2012.00367

Zhou, T., Pan, J., Zhang, P., Wei, S., & Han, T. (2017). Mapping winter wheat with multi-temporal SAR and optical images in an urban agricultural region. *Sensors (Switzerland)*, *17*(6), 1–16. https://doi.org/10.3390/s17061210

Zhu, X. J. (2005). *Semi-supervised learning literature survey*. University of Wisconsin-Madison Department of Computer Sciences.

Zhu, X., & Liu, D. (2014). Accurate mapping of forest types using dense seasonal Landsat time-series. *ISPRS Journal of Photogrammetry and Remote Sensing*, *96*, 1–11.

Zhu, Z. (2017). Change detection using landsat time series: A review of frequencies, preprocessing, algorithms, and applications. *ISPRS Journal of Photogrammetry and Remote Sensing*, *130*, 370–384.

Zhu, Z., & Woodcock, C. E. (2014). Continuous change detection and classification of land cover using all available Landsat data. *Remote Sensing of Environment*, *144*, 152–171.

Acknowledgements

University of Florence and ISPRA are kindly acknowledged for assistance and support in this research.

I would like to thank Professor Gherardo Chirici, the University researchers Samuele Segoni and Federico Di Traglia and Dr. Agnese Turchi and Saverio Francini for their technical advises and for fruitful research collaboration.

My deep appreciation goes out to Dr Luca Congedo, Ines Marinosci and all the research group of the Ispra who were always so helpful and provided me with their assistance and suggestions for improvement of this thesis. I am especially grateful to Paolo De Fioravante for his invaluable advice and feedback on my research and for always being available and so supportive in numerous ways during all PHD stages.

I would like to extend my thanks to Pasquale Dichicco, Marco Luti Locchi and Emanuele Sbaffi for their assistance in improving some images.

A very special thanks to my great friends Alessandro Buccilli, Sonia Folin and Silvia Martorelli for helping me enormously, in the mammoth task of English revision, made even more difficult by the distance imposed by the lockdown period. Their excellent work has made an invaluable contribution to my PhD.

Finally, I would like to express my sincere gratitude to my mum, dad and my sister Valentina, my close friends for always believing in me and encouraging me to follow my projects, especially during this challenging period and in particular a heartfelt thanks to my children Matteo and Alice and to Emanuele who have been by my side supporting and helping in whatever way they could throughout this PhD with their joy and enthusiasm.